Dynamic Modelling of Emulsion Polymerization for the Continuous Production of Nitrile Rubber

By

Ian David Washington

A thesis
presented to the University of Waterloo
in fulfillment of the
thesis requirement for the degree of
Master of Applied Science
in
Chemical Engineering

Waterloo, Ontario, Canada, 2008

I hereby declare that I am the sole author of this thesis. This is a true copy of the thesis, including any required final revisions, as accepted by my examiners.

I understand that my thesis may be made electronically available to the public.

Abstract

Commodity and specialty-grade rubbers, such as styrene-butadiene (SBR) or nitrile-butadiene (NBR), are industrially produced in large trains of continuous reactors using an emulsion polymerization process. Both SBR and NBR systems are largely unstudied. Furthermore, the studies that have been published on NBR have been typically limited to issues concerning the characteristics of the product behaviour (i.e. oil/fuel resistance, tensile strength, hardness, compression set).

In this work a detailed mathematical model has been developed in order to simulate the industrial production of NBR via emulsion copolymerization of acrylonitrile (AN) and butadiene (Bd) in batch, continuous and trains of continuous reactors. Model predictions include monomer conversion, polymerization rate, copolymer composition, number- and weight-average molecular weights, tri- and tetra-functional branching frequencies, and the number and average size of polymer latex particles. NBR is typically produced at low temperatures (5 to 10^oC) using a redox initiation system to generate free radicals. The system is typically composed of three phases, water, polymer particles, and monomer. Surfactants and electrolytes are used to stabilize the particle and monomer phases as polymerization proceeds. Of particular industrial importance, in today's world of tailor-made products, is detailed control over the polymerization reaction. Such control requires a deep understanding of the influence of various reactant feed rates and reactor operating conditions on the process response. In particular, policies to minimize copolymer composition drift and to control molecular weight, polydispersity and chain branching at desirable levels.

The model is cast in a dynamic form using ordinary differential equations to describe the change of each species, the average number of particles, total average polymer volume, and the first three leading moments of the molecular weight distribution. With a multiphase system it is necessary to determine the concentration of each component in each phase. For this, a constant partition coefficient approach was adopted, as opposed to a purely thermodynamic approach. Particle generation was modelled considering both micellar and homogeneous mechanisms. Model parameters were obtained from the open literature or arrived at after sensitivity analysis. Simulations starting the reactors full of water, feeding all ingredients to the first reactor and using an average residence time of 60 minutes revealed considerable copolymer drift starting in the forth reactor (33% conversion), and heightened molecular weights and chain branching once the monomer phase disappeared (50% conversion). Further simulations revealed that both copolymer drift and the growth of molecular weight and branching could be controlled through additional feed streams of AN and chain transfer agent to downstream reactors. Furthermore, polymer productivity could be increased by appropriately splitting the total monomer feed between the first couple of reactors in the train.

Acknowledgements

I wish to express my thanks to professors T.A. Duever and A. Penlidis for their supervision, guidance, patience, and financial support throughout this project.

Further appreciation goes to fellow group and lab members for their assistance, fruitful discussions, and friendship throughout this work.

Finally, I would thank my parents for their support and encouragement.

Contents

List of Tables **ix**

List of Figures **xii**

Nomenclature **xiii**

1 Introduction **1**
1.1 Process Description . . . 1
1.2 Project Objectives & Scope . . . 2
1.3 Thesis Organization . . . 2

2 Literature Review **3**
2.1 Nitrile Rubber Production Fundamentals . . . 3
2.1.1 Chemistry . . . 3
2.1.2 Properties of NBR . . . 4
2.1.3 Manufacture . . . 5
2.2 Polymerization Fundamentals & Background . . . 7
2.2.1 Emulsion Polymerization . . . 7
2.3 Acrylonitrile/Butadiene Polymerization . . . 13
2.3.1 Butadiene Homopolymerization . . . 13
2.3.2 Acrylonitrile Homopolymerization . . . 15
2.3.3 AN/Bd Copolymerization . . . 17
2.4 Emulsion Polymerization Process Modelling Survey . . . 20

3 Process Model Development **22**
3.1 Reaction Mechanism . . . 22
3.1.1 Aqueous Phase Reactions . . . 23
3.1.2 Particle Phase Reactions . . . 28
3.2 Particle Nucleation . . . 34
3.2.1 Nucleation Rates . . . 35
3.3 Radical Concentrations . . . 37
3.3.1 Aqueous Phase . . . 37
3.3.2 Particle Phase . . . 39
3.4 Monomer Partitioning . . . 39
3.4.1 Thermodynamic Approach . . . 40
3.4.2 Critical Conversion Approach . . . 42
3.4.3 Constant Partition Coefficient Approach . . . 43
3.5 Radicals per Particle . . . 46

3.6 Radical Desorption . . . 49
3.7 Molecular Weights & Chain Branching . . . 51
3.8 Material / Energy / Population Balances . . . 53
3.8.1 Mass Balances . . . 53
3.8.2 Heat Balance . . . 55
3.9 Summary of Model Assumptions . . . 56
3.10 Model Database . . . 58
3.10.1 Kinetic Rate Constants . . . 58
3.10.2 Nucleation Parameters . . . 62

4 Model Testing **66**
4.1 Model Trend Verification for NBR Simulations . . . 66
4.1.1 Baseline Model Simulations . . . 67
4.1.2 Influence of Emulsifier & Initiator on Particle Nucleation . . . 73
4.1.3 Influence of Impurities on Polymerization Rate . . . 76
4.1.4 Effect of CTA on Molecular Weight & Branching Frequency . . . 84
4.1.5 Influence of Radical Desorption on Polymerization . . . 87
4.1.6 Continuous Reactor Start-Up . . . 92
4.2 Model Validation with Literature Data . . . 95
4.2.1 Simulation of NBR Data . . . 95
4.2.2 Simulation of Emulsion Bd Data . . . 103
4.3 Concluding Remarks . . . 110

5 Simulation Case Studies **111**
5.1 Reactor Train Simulations . . . 111
5.1.1 Baseline Simulations . . . 112
5.1.2 Comparison to Simulations of Minari et al. . . . 118
5.1.3 Effect of Impurities in a Reactor Train . . . 122
5.1.4 Reactor Train Start-up Procedures . . . 124
5.2 Simulation Studies on Polymerization Optimization Scenarios . . . 126
5.2.1 Copolymer Composition Control . . . 126
5.2.2 Molecular Weight and Chain Branching Control . . . 129
5.2.3 Particle Size Control . . . 132
5.3 Reactor Operation Studies for Maximizing Polymer Production . . . 135
5.3.1 Maximizing Particle Nucleation in the 1st Reactor . . . 135
5.3.2 Splitting Feed Streams Between 1st & Downstream Reactors . . . 136
5.4 Concluding Remarks . . . 140

6 Concluding Remarks & Recommendations **141**
6.1 General Summary/Contributions . . . 141
6.2 Concluding Remarks . . . 142
6.3 Recommendations . . . 143
6.4 Future Work . . . 145

References **146**

Appendices **159**

A Process Model **160**

B Model Implementation **179**

C Model Parameters **184**

D Model Troubleshooting **190**

List of Tables

2.1 NBR property relation to AN content [74] . . . 5
2.2 Typical nitrile rubber polymerization recipes . . . 7
2.3 Smith-Ewart limiting cases . . . 12
2.4 Species partitioning literature . . . 12
2.5 Butadiene emulsion polymerization literature . . . 13
2.6 Butadiene propagation & termination rate constants . . . 15
2.7 Butadiene transfer rate constants . . . 15
2.8 Acrylonitrile emulsion polymerization literature . . . 17
2.9 Acrylonitrile propagation & termination rate constants . . . 17
2.10 Acrylonitrile transfer rate constants . . . 17
2.11 Reactivity ratios for AN/Bd copolymerization . . . 18
2.12 Acrylonitrile & butadiene emulsion copolymerization literature . . . 19
2.13 NBR process modelling literature . . . 20
2.14 Emulsion polymerization modelling literature . . . 21

3.1 Aqueous phase phenomena involving radicals . . . 23
3.2 Particle phase phenomena involving radicals . . . 28
3.3 Transfer to monomer rate constant comparison . . . 30
3.4 Comparison of NBR kinetic rate constants . . . 60
3.5 CTA & impurity rate constant approximations . . . 61
3.6 Transfer to CTA (mercaptan) coefficient comparison . . . 62
3.7 Baseline nucleation parameters for micellar and homogeneous mechanisms . . . 64

4.1 NBR base case batch recipes . . . 67
4.2 Summary of batch reactor simulation properties . . . 71
4.3 Influence of monomer soluble impurities on final polymer properties in a batch reactor . . . 81
4.4 Influence of water soluble impurities on final molecular properties in a batch reactor . . . 83
4.5 Cold NBR emulsion recipe in Vega et al. [171] . . . 96
4.6 Model parameters used to fit data of Vega et al. [171] . . . 97
4.7 Cold NBR emulsion final product properties - comparison between measurement and simulation results . . . 97
4.8 Hot NBR emulsion recipe (PARACRIL) . . . 100
4.9 Model parameters used to fit data of Dube et al. [33] . . . 100
4.10 Butadiene emulsion recipe from Weerts [184] . . . 103
4.11 Model parameters used to fit the data of Weerts [184] . . . 104
4.12 Industrial butadiene emulsion recipe from Pallaske et al. [133] . . . 106
4.13 Model parameters used to fit the data of Pallaske et al. [133] . . . 107

5.1 NBR process recipes . . . 113
5.2 Final simulated properties for baseline batch and continuous processes . . . 114
5.3 Comparison of final simulated properties for the continuous process of Minari et al. [105] . . . 119
5.4 Comparison of final simulated properties for the continuous process using AN additions to control $\overline{F}_{AN}$ . . . 129

C.1 Acrylonitrile database items . . . 185
C.2 Butadiene database items . . . 186
C.3 AN/Bd copolymer database items . . . 187
C.4 Water database items . . . 187
C.5 Dresinate database items . . . 187
C.6 Tamol database items . . . 187
C.7 Sodium Oleate database items . . . 188
C.8 Hydroquinone database items . . . 188
C.9 Dissolved oxygen database items . . . 188
C.10 *para*-Menthane hydroperoxide database items . . . 188
C.11 Potassium persulfate database items . . . 188
C.12 *tert*-Dodecyl mercaptan database items . . . 189
C.13 *tert*-Butyl catechol database items . . . 189
C.14 Sodium formaldehyde sulfoxylate database items . . . 189
C.15 Ferrous sulfate database items . . . 189

List of Figures

2.1 Chemical structure of AN and Bd 4
2.2 Nitrile rubber polymerization - continuous process 5
2.3 Nitrile rubber polymerization - batch process 6
2.4 Harkin's concept of micellar nucleation 9
2.5 Representation of the homogeneous nucleation mechanism 10

3.1 Monomer concentrations in each phase - constant partition coefficients 45
3.2 Instantaneous copolymer composition of AN as a function of the mole fraction of AN in the feed (i.e. particle phase) (Mayo-Lewis Equation) 61
3.3 Cumulative copolymer composition of AN as a function of conversion 63
3.4 Parameter sensitivity for ε & k_{cp} - influence on N_p 64
3.5 Parameter sensitivity for ε & k_{cp} - influence on $\overline{d}_p$ (top) & $\bar{n}$ (bottom) 65

4.1 Batch (a,c) & continuous (b,d) reactor simulation - conversion and composition for cold NBR 68
4.2 Batch (a,c) & continuous (b,d) - particle number & diameter for cold NBR 69
4.3 Batch (a,c) & continuous (b,d) - molecular weights & branching frequencies for cold NBR . 70
4.4 Batch reactor simulation - average number of radicals per particle & termination rate constant for cold NBR 72
4.5 Batch reactor simulation - particle number for different levels of emulsifier and initiator . . . 74
4.6 Continuous reactor simulation - particle number versus mean residence time at different levels of emulsifier & initiator 75
4.7 Batch reactor simulation - effect of $[MSI]$ on conversion & polymerization rate 77
4.8 Continuous reactor simulation - effect of $[MSI]$ on conversion & polymerization rate 78
4.9 Batch (top) & CSTR (bottom) reactor simulation - effect of $[MSI]$ on particle number & diameter 79
4.10 Batch reactor simulation - effect of k_{fmsi} for 100 ppm MSI 80
4.11 Batch reactor simulation - effect of $[WSI]$ on conversion & polymerization rate 82
4.12 Continuous reactor simulation - effect of $[WSI]$ on conversion & polymerization rate 83
4.13 Batch reactor simulation - effect of $[CTA]$ on molecular weight and chain branching 85
4.14 Batch reactor simulation - molecular weight sensitivity to k_{fcta} 86
4.15 Batch reactor simulation - effect of R_{des} on conversion, polymerization rate, radical capture rate 87
4.16 Average number of radicals per particle as a function of α' and m 89
4.17 Batch reactor simulation - effect of R_{des} on particle number & size 89
4.18 Batch reactor simulation - comparison of desorption models - conversion & desorption rate . 91
4.19 Continuous reactor simulation - start-up policies - conversion, particle number & diameter for $\theta = 60$ minutes 93

4.20 Continuous reactor simulation - start-up policies - molecular weight & branching frequency for $\theta = 60$ minutes . . . 94
4.21 Continuous reactor simulation - start-up policies - conversion & particle number for $\theta = 30, 60, 80$ minutes . . . 94
4.22 Batch reactor simulation - comparison to industrial data from Vega et al. [171] - conversion, copolymer composition, particle number & average diameter . . . 98
4.23 Batch reactor simulation - comparison to industrial data from Vega et al. [171] - molecular weight & branching frequencies . . . 99
4.24 Batch reactor simulation - comparison to pilot plant data (recipe 1) - percent solids & particle diameter . . . 101
4.25 Batch reactor simulation - comparison to pilot plant data (recipe 2) - percent solids & particle diameter . . . 102
4.26 Batch reactor simulation - comparison to experimental data of Weerts [184] (recipe 1) - conversion & particle diameter . . . 105
4.27 Batch reactor simulation - comparison to experimental data of Weerts [184] (recipe 2) - conversion . . . 105
4.28 Batch reactor simulation - comparison to industrial data of Pallaske et al. [133] (recipe 1) - conversion and particle diameter . . . 108
4.29 Batch reactor simulation - comparison to industrial data of Pallaske et al. [133] (recipes 2 & 3) - conversion and particle diameter . . . 109

5.1 Continuous reactor train simulation - continuous recipe 1 - conversion, copolymer composition, particle number & diameter . . . 115
5.2 Continuous reactor train simulation - continuous recipe 1 - number-, weight-average molecular weights & tri-, tetra-functional branching frequencies . . . 116
5.3 Comparison between batch and steady-state reactor train property profiles - conversion, CCC, particle number, diameter, molecular weight & branching frequencies . . . 117
5.4 Continuous reactor train simulation - continuous recipe 2 - conversion & copolymer composition . . . 120
5.5 Continuous reactor train simulation - continuous recipe 2 - particle number, diameter, and molecular properties . . . 121
5.6 Continuous reactor train simulation - impurity effects - conversion, polymer production rate, particle number & diameter . . . 123
5.7 Continuous reactor train simulation - reactor startup (recipe 1, Table 5.1) - conversion, particle number, diameter & molecular weight . . . 125
5.8 Continuous reactor train simulation - copolymer composition control . . . 128
5.9 Continuous reactor train simulation - molecular weight control . . . 131
5.10 Semi-batch reactor simulation - particle size control through emulsifier additions . . . 133
5.11 CSTR reactor simulation - effect of emulsifier pulse additions . . . 134
5.12 Continuous reactor train simulation - maximizing particle nucleation in the 1^{st} reactor . . . 136
5.13 Continuous reactor train simulation - monomer feed policies for maximizing polymer production . . . 137
5.14 Continuous reactor train simulation - monomer feed policies for maximizing polymer production - resulting latex properties . . . 139

D.1 Batch simulation - phase/monomer volumes & concentrations . . . 191
D.2 CSTR Train Simulation - phase/monomer volumes & concentrations . . . 192
D.3 Batch Simulation - number of particles via homogeneous & micellar nucleation . . . 193

D.4 Batch simulation - number of particles via homogeneous & micellar nucleation - sensitivity to j_{cr} 193
D.5 CSTR train simulation - average number of radicals per particle 194

Nomenclature

Symbol	Description
A_1, A_2, A_3	Parameters for the termination rate constant expression $[-]$
A_d	Total surface area of monomer droplets $\left[dm^2\right]$
A_m	Total free micellar area $\left[dm^2\right]$
A_p	Total surface area of particles $\left[dm^2\right]$
A	Rate of decrease of termination rate parameter in free-volume model $[-]$
$\overline{BN}_3$	Number of tri-functional branches per chain [#]
$\overline{BN}_4$	Number of tetra-functional branches per chain [#]
B	Rate of decrease of propagation parameter in free-volume model $[-]$
$[CTA]_p$	Concentration of chain transfer agent in the particle phase $[mol/L]$
$\hat{C}_{p_i}$	Specific heat capacity of species i $[cal/g/K]$
C_i	Transfer coefficient of species i $[-]$
d_p	Monodisperse diameter of polymer particles $[dm]$
D_p	Diffusivity of monomer radicals in the particle phase $\left[dm^2/min\right]$
D_w	Diffusivity of monomer radicals in the aqueous phase $\left[dm^2/min\right]$
f	Initiator efficiency $[-]$
f_{i_k}	Mole fraction of monomer i in phase k, $(k = p,a)$ $[-]$
f_{msi_j}, f_{z_j}	Mole fraction of impurity (MSI, WSI) j $[-]$
F	Radical capture efficiency $[-]$
$\overline{F}_{i_k}$	Cumulative copolymer composition of monomer i (mole fraction of monomer i bound in copolymer in phase k) $[-]$
F_{i_k}	Instantaneous copolymer composition of monomer i (mole fraction of monomer i bound in copolymer in phase k) $[-]$
$F_{i_{in}}$	Molar flow of species i into the reactor $[mol/min]$
$F_{p_{in}}$	Particle flow into the reactor $[\#/min]$
F_i	Molar flow of species i out of the reactor $[mol/min]$
F_p	Particle flow out of the reactor $[\#/min]$
$\left[Fe^{+2}\right]$, $\left[Fe^{+3}\right]$	Total concentration of iron ions $[mol/L]$
ΔG_i^k	Molar Gibb's free energy of monomer i in phase k $[cal/mol]$
$\hat{H}$, $\overline{H}$	Specific $[cal/g]$ and molar Enthalpy $[cal/mol]$
H	Homogeneous nucleation grouping term as per Equation 3.68
$\Delta\overline{H}_p$	Heat of polymerization $[cal/mol]$
$[I]_a$	Concentration of initiator in the aqueous phase $[mol/L]$
j_{cr_i}	Critical chain length at which radical ending in monomer i precipitates from solution [#]

Symbol	Description
j_{cr}	Overall critical chain length at which radicals precipitate from solution [#]
k_1, k_2	Iron oxidation & reduction rate constant $[L/mol/min]$
k_d	Initiator decomposition rate constant $\left[min^{-1}\right]$
k_{cm}	Micelle radical capture rate constant $[dm/min]$
k_{cp}	Particle radical capture rate constant $[dm/min]$
k_{cd}	Droplet radical capture rate constant $[dm/min]$
k_{des}	Radical desorption rate constant $\left[min^{-1}\right]$
k_{p_k}	Overall propagation rate constant in phase k $[L/mol/min]$
$k_{p_{ij_k}}$	Rate constant for propagation of radicals ending in monomer i with radicals ending in monomer j in phase k $[L/mol/min]$
k_{t_k}	Overall termination rate constant in phase k $[L/mol/min]$
$k_{t_{ij_k}}$	Rate constant for termination of radicals ending in monomer i with radicals ending in monomer j in phase k $[L/mol/min]$
k_{t_o}	Termination rate constant at zero conversion $[L/mol/min]$
k_{td}	Rate constant for termination by disproportionation $[L/mol/min]$
k_{tc}	Rate constant for termination by combination $[L/mol/min]$
k_{fm}	Overall rate constant for transfer to monomer $[L/mol/min]$
$k_{fm_{ij}}$	Rate constant for transfer to monomer j from a radical ending in monomer i $[L/mol/min]$
k_{fp}	Overall rate constant for transfer to polymer $[L/mol/min]$
$k_{fp_{ij}}$	Rate constant for transfer to monomer j on dead polymer from a radical ending in monomer i $[L/mol/min]$
k_p^*	Rate constant for reaction with terminal double bonds $[L/mol/min]$
k_p^{**}	Rate constant for reaction with internal double bonds $[L/mol/min]$
k_{fcta}	Overall rate constant for transfer to chain-transfer agent $[L/mol/min]$
k_{fcta_i}	Rate constant for transfer to chain-transfer agent from a radical ending in monomer i $[L/mol/min]$
k_{fmsi}	Overall rate constant for transfer to monomer-soluble impurity $[L/mol/min]$
k_{fmsi_i}	Rate constant for transfer to monomer-soluble impurity from a radical ending in monomer i $[L/mol/min]$
k_z	Overall rate constant for reaction with water-soluble impurity $[L/mol/min]$
k_{z_i}	Rate constant for reaction with water-soluble impurity i $[L/mol/min]$
k_h, k_{h_o}	Rate constant for homogeneous nucleation $\left[min^{-1}\right]$
$K_i^{a/p}$	Partition coefficient for monomer i between the aqueous and particle phases $[-]$
$K_i^{d/a}$	Partition coefficient for monomer i between the droplet and aqueous phases $[-]$
K_{cta}	Partition coefficient for chain-transfer agent between the droplet and particle phases $[-]$
K_{msi}	Partition coefficient for monomer-soluble impurity between the droplet and particle phases $[-]$
K_o	Rate of diffusion of radicals leaving the particle phase $\left[min^{-1}\right]$
K_3	Parameter in Free-volume model $[-]$
$K_{3,test}$	Parameter in Free-volume model used to determine onset of diffusion-controlled termination $[-]$

Symbol	Description
L	Critical average diffusion path length of a free radical in the aqueous phase before precipitation occurs $[dm]$
l_o	RMS monomer length (mean root distance per square root of the number of monomer units in a segment) $[Angstroms]$
l_j	Lennard-Jones Diameter (equivalent sphere diameter for a monomer unit) $[Angstroms]$
$[M]_k$	Total concentration of monomer in phase k $[mol/L]$
$[M_i]_k$	Concentration of monomer i in phase k $[mol/L]$
$[M]_a^{sat}$	Aqueous phase monomer saturation concentration $[mol/L]$
$[MIC]_a$	Concentration of micelles in the aqueous phase $[mol/L]$
$[MSI]_p$	Concentration of monomer soluble impurity in the particle phase $[mol/L]$
$\overline{M}_w$, $\overline{MW}_w$	Cumulative weight-average molecular weight
$\overline{M}_n$, $\overline{MW}_n$	Cumulative number-average molecular weight
M_{eff}	Effective molecular weight of a hypothetical average copolymer unit
MW_i	Molecular weight of species i $[g/mol]$
MW_{mi}	Molecular weight of monomer i $[g/mol]$
M_{pol}	Mass of total polymer $[g]$
M_T	Total mass of reactor contents $[g]$
M_s	Mass of solvent $[g]$
M_{m_i}	Mass of monomer i $[g]$
M_{emul_i}	Mass of emulsifier i $[g]$
$\dot{m}_c$	Mass flow of cooling-jacket coolant $[g/min]$
m_d	Partition coefficient for monomeric radicals between particle and aqueous phase $[-]$
m_{ij}	Molar volume ratio $\left(\overline{V}_i/\overline{V}_j\right)$ $[-]$
m	Parameter in Free-volume model $[-]$
$\overline{n}$	Average number of radicals per particle $[\#/\#]$
N_A	Avogadro's number $[\#/mol]$
N_j	Total number of moles of species j $[mol]$
N_{j_k}	Number of moles of species j in phase k $[mol]$
N_p	Total number of particles $[\#]$
N_{mic}	Number of particles formed by micellar nucleation $[\#]$
N_{hom}	Number of particles formed by homogeneous nucleation $[\#]$
n	Parameter in Free-volume model $[-]$
$q_{T_{in}}$	Total volumetric flow rate into the reactor $[L/min]$
q_T	Total volumetric flow rate out of the reactor $[L/min]$
$q_{k_{in}}$	Volumetric flow rate of phase k into the reactor $[L/min]$
q_k	Volumetric flow rate of phase k out of the reactor $[L/min]$
$q_{pol_{in}}$	Volumetric flow rate of polymer into the reactor $[L/min]$
q_{pol}	Volumetric flow rate of polymer out of the reactor $[L/min]$
Q_o, Q_1, Q_2	Zeroth, first, and second moments of the molecular weight distribution $[-]$
$\dot{Q}_{Rx}$	Rate of heat generated by polymerization $[cal/min]$
$\dot{Q}_{jacket}$	Rate of heat transfer to the cooling jacket $[cal/min]$
$\dot{Q}_{loss}$	Rate of heat transfer (loss) to the surroundings $[cal/min]$

Symbol	Description
r_{mic}	Average micelle radius $[dm]$
r_p	Average swollen monodisperse particle radius $[dm]$
r_i	Monomer reactivity ratio $[-]$
R	Universal gas constant $[cal/mol/K]$
R_I	Rate of radical initiation $[mol/L/min]$
R_{I_c}	Rate of initiator consumption $[mol/L/min]$
R_{RA}	Rate of reducing-agent consumption $[mol/L/min]$
$R_{Fe^{+2}}$, $R_{Fe^{+3}}$	Rate of iron ion consumption $[mol/L/min]$
$R_{z_{i_a}}$	Rate of reaction of water soluble impurity i in the particle phase $[mol/L/min]$
$R_{msi_{i_p}}$	Rate of reaction of monomer soluble impurity i in the particle phase $[mol/L/min]$
$R_{cta_{i_p}}$	Rate of reaction of chain transfer agent i in the particle phase $[mol/L/min]$
R_{cm}	Rate of radical capture by micelles $[mol/L/min]$
R_{cp}	Rate of radical capture by particles $[mol/L/min]$
R_{cap}	Total rate of radical capture (micelles and particles) $[mol/L/min]$
R_{p_k}	Rate of polymerization in phase k $[mol/L/min]$
$R_{p_{i_k}}$	Rate of polymerization of monomer i in phase k $[mol/L/min]$
R_{Q_i}	Rate of moment generation of the i^{th} moment $[mol/L/min]$
$R_{\overline{BN}_i}$	Rate of branch formation ($i = 3,4$ - tri/tetra) $[mol/L/min]$
$[R^{\cdot}]_a$	Total concentration of radicals in the aqueous phase $[mol/L]$
$\left[R^{\cdot}_k\right]_a$	Total concentration of radicals in the aqueous phase of length k $[mol/L]$
$\left[R^{\cdot}_{k,i}\right]_a$	Concentration of radicals in the aqueous phase of length k ending in monomer i $[mol/L]$
$[R^{\cdot}]_a^{cap}$	Total concentration of radicals in the aqueous phase capable of being captured $[mol/L]$
$[R^{\cdot}]_a^{mic}$	Concentration of radicals in the aqueous phase capable of being captured by micelles $[mol/L]$
$[R^{\cdot}]_a^{par}$	Concentration of radicals in the aqueous phase capable of being captured by particles $[mol/L]$
$[R^{\cdot}]_a^{hom}$	Concentration of radicals in the aqueous phase capable of undergoing homogeneous nucleation $[mol/L]$
$[RA]_a$	Concentration of reducing agent in the aqueous phase $[mol/L]$
S_{a_i}	Surface area covered by one molecule of emulsifier i $\left[dm^2/molecule\right]$
$[S]_{CMC}$	Critical micelle concentration $[mol/L]$
$[S]_t$	Total concentration of emulsifier $[mol/L]$
T_r	Temperature of the reactor $[K]$
T_j	Temperature of the reactor cooling jacket $[K]$
T_g	Glass transition temperature $[K]$
ν_p	Average volume of each particle (V_p/N_p) $\left[dm^3\right]$
V_k	Volume of phase k ($k = a,p,d$) $\left[dm^3\right]$
V_{pol}	Volume of polymer $\left[dm^3\right]$
V_i	Volume of species i $\left[dm^3\right]$
V_i^k	Volume of monomer i in phase k $\left[dm^3\right]$
V_{i_o}	Initial total volume of monomer i $\left[dm^3\right]$
$V_{f_{cr}}$	Critical free-volume for propagation $[L]$

Symbol	Description
$[WSI]_a$	Total concentration of water-soluble impurities (inhibitors) in the aqueous phase $[mol/L]$
$\dot{w}$	Total mass flow $[g/min]$
X	Total conversion of monomer (mass basis) $[-]$
X_i	Conversion of monomer i $[-]$
X_{seed}	Conversion of monomer in seed particles $[-]$
x_c	Conversion at the end of interval II in emulsion polymerization $[-]$
Y_o, $[R^{\cdot}]_p$	Total radical concentration in the particle phase $[mol/L]$
$[Z]$	Total water-soluble impurity concentration $[mol/L]$

Greek Letters

Symbol	Description
α	Dimensionless grouping term representing radical entry into polymer particles $[-]$
α	Free-volume expansion coefficient for monomer or polymer $[-]$
α	Fraction of the critical chain-length ($j_{critical}$) where radical capture begins $[-]$
β	Molecular weight contribution due to termination by combination $[-]$
β_i	Probability that monomeric radicals react in the aqueous phase by propagation or termination $[-]$
γ	Fraction of termination by disproportionation $[-]$
δ	Lumped monomeric radical diffusion coefficient
δ_i	Solubility parameter for monomer or homopolymer i $\left[\left(cal/dm^3\right)^{1/2}\right]$
δ	Segmental diffusion $[L/g]$
ε	Ratio of radical capture (radical absorption) between particles and micelles (k_{cp}/k_{cm}) $[-]$
μ	Ratio of the rate constants for homogeneous and micellar nucleation (k_{ho}/k_{cm}) $\left[dm^{-1}\right]$
ρ_i	Density of species i $[g/L]$
ρ_{m_i}	Density of monomer i $[g/L]$
ρ_{des} , R_{des}	Rate of radical desorption $[mol/L/min]$
ρ_{des}^{mic} , R_{des}^{mic}	Rate of re-absorption of desorbed radical into micelles $[mol/L/min]$
σ	Surface tension $\left[cal/dm^2\right]$
τ	Molecular weight contribution due to termination by disproportionation and transfer to small molecules $[-]$
ϕ_i^k	Volume fraction of monomer i in phase k $[-]$
$\phi_{i,sat}^a$	Volume fraction of monomer i in the aqueous phase at its saturation level $[-]$
ϕ_p^k	Volume fraction of copolymer in phase k $[-]$
$\phi_{i_k}^{\cdot}$	Mole fraction of radicals ending in monomer i in phase k $[-]$
ϕ_{wall}	Walling termination factor $[-]$
χ_{ij}	Flory-Huggins interaction parameter between monomers i and j $[-]$
χ_{ip}	Flory-Huggins interaction parameter between monomer i and copolymer $[-]$
λ	As per Equation 3.117 $[-]$
ξ	As per Equation 3.118 $[-]$
η	As per Equation 3.87
φ	As per Equation 3.90 $(\varphi \geq 1)$ $[-]$
ζ	Monomer solubility $[g/100gwater]$

Abbreviations

Symbol	Description
AA	Acrylic Acid
AN	Acrylonitrile
Bd	Butadiene
BA	Butyl Acrylate
CCC	Cumulative copolymer composition
CSBR	Chloro-Styrene Butadiene Rubber
DIBHP	Diisobutyl hydroperoxide
HYQ	Hydroquinone
IP	Isoprene
PMHP	*para*-menthane hydroperoxide
PVC	Polyvinyl Chloride
MA	Methyl Acrylate
MMA	Methyl Methacrylate
NBR	Nitrile Butadiene Rubber
SAN	Styrene Acrylonitrile
SBR	Styrene Butadiene Rubber
Sty	Styrene
SFS	Sodium formaldehyde sulfoxylate
VAc	Vinyl Acetate
VDC	Vinylidene Chloride
VCl	Vinyl Chloride

Sub/Superscripts

Symbol	Description
a	Aqueous phase
p	Particle phase or simply polymer
pol	Corresponds to total polymer
d	Droplet phase
j, i	Corresponds to monomer (AN or Bd) or multiple CTA, emulsifier, impurity species
k	Corresponds to the phase
m	Corresponds to monomer

Chapter 1

Introduction

The use of mathematical models to simulate a desired process is common practice in almost all fields of science and engineering. Nowadays, with the increasing computational power of the personal computer, the application of models to predict real time information is becoming ever more practical. The polymer manufacturing industry is one example, where the use of powerful predictive models can aid in reducing product development time, improve process monitoring, control and optimization abilities, and inherently reduce process costs. With these common goals in mind, it is the purpose of this thesis to present a mechanistic model that can be used to predict the process behaviour during the manufacture of nitrile rubber.

Typical model predictions will include conversion, polymerization rate, copolymer composition, number- and weight-average molecular weights, tri- and tetra-functional branching characteristics, and the number and average size of the polymer latex particles. Using the model predictions, physical properties of the resulting rubber (i.e. Mooney viscosity, elasticity, swelling resistance, etc.) can be estimated by correlating the model response (i.e. reaction variables) to experimental and/or plant data.

1.1 Process Description

Nitrile rubber is a synthetic polymer made from the copolymerization of acrylonitrile (AN) and butadiene (Bd) using a free radical mechanism. Emulsion polymerization is the predominant method of manufacture and, on an industrial scale, a continuous process, rather than a batch process, is used to produce rubber in large volumes. The product of emulsion polymerization is a latex based polymer. Subsequent processes are further used to coagulate the polymer from the latex and vulcanize it to a usable rubber form. Depending on customer specific requirements, many different grades of rubber can be produced that are generally distinguishable by their molecular properties, performance (i.e. chemical and temperature resistance) and intended end use (e.g. seals, shoe soles, tubing).

1.2 Project Objectives & Scope

The objective of this project is to develop a detailed mechanistic mathematical model in order to simulate isothermal or non-isothermal emulsion copolymerization of AN-Bd in batch, continuous, and trains of continuous reactors (CSTR's). The overall goal is to develop a practical tool to predict polymer production rate and product quality (molecular weight averages and branching characteristics) on an industrial scale. The scope of this initial phase of the project is to develop a computer model, use the model to simulate various reaction scenarios of AN-Bd copolymerization and assess the model validity/performance when compared to literature and plant data.

1.3 Thesis Organization

This thesis is organized as follows:

Chapter 2 provides a review of relevant literature on NBR that focusses on reaction engineering aspects. A brief discussion on rubber production and polymerization fundamentals is given. Theoretical aspects of emulsion and copolymerization theories are touched on with reference to important articles found in the literature. A thorough review on AN, Bd, and AN-Bd homo- and co-polymerization is provided. This is followed by a review of relevant papers on modelling techniques used for emulsion systems.

In Chapter 3, general mechanistic mathematical techniques are presented which are commonly used for emulsion polymerization. As well, the mathematical model used in this study to simulate AN-Bd emulsion copolymerization is discussed. Attention is given to the detailed development (i.e. specific equations used) with relation to existing techniques used in the literature.

Model simulations and testing are carried out in Chapter 4 using batch, continuous and trains of continuous reactors. The influence of important parameters on various model responses is assessed. Model checks that verify trends in various "internal" variables are carried out. Model comparisons to AN, Bd and AN-Bd homo- and co-polymerization data are also performed.

The use of the model to simulate various reactor operation scenarios is presented in Chapter 5. Reactor train studies are carried out to assess the model response to additions of various recipe ingredients along the train (e.g. CTA, monomer, emulsifier).

Chapter 6 restates the important conclusions found in this study and provides recommendations for further study. Finally, several appendices are attached which restate the process model, elaborate on the details of the model algorithms, list all model parameters, and provide additional model simulation profiles.

Chapter 2

Review of Process Fundamentals & Previous Modelling Efforts

The purpose of this chapter is to discuss theoretical concepts, mechanisms, and modelling approaches that have been previously used in the literature. General aspects of emulsion polymerization are discussed. A review of acrylonitrile and butadiene homo- and co-polymerization is given. Finally, a review of emulsion process modelling is provided, with reference to key sources that were found useful.

2.1 Nitrile Rubber Production Fundamentals

This section briefly discusses the chemical makeup of NBR, the copolymer properties that influence the final rubber product characteristics, industrial methods of manufacture from a reaction perspective, and typical reactant species that are used to produce the NBR copolymer.

2.1.1 Chemistry

Nitrile rubber (NBR) is a synthetic polymer produced by polymerizing acrylonitrile (AN) and butadiene (Bd) monomers using a free radical mechanism in an emulsion system. The basic chemical structures can be seen in Figure 2.1.

Butadiene can be incorporated into the copolymer in several isomeric configurations, cis-, trans-, and vinyl, and depending on the AN composition, the percentage of each isomer can vary. At high AN levels the trans- configuration is dominant (92%), while at low levels (15% AN) the cis- isomer increases to approximately 5%. The relative percentage of each isomer and the sequence in which each monomer combines in the polymer chain are reflected in the underlying properties of the polymer. Typical properties and the influence of AN content is further discussed in section 2.1.2.

NBR made from the chain addition of AN and Bd often contains many unsaturated double bonds. These highly reactive sites can undergo further reaction and degradation within the rubber product. Thus, to prevent

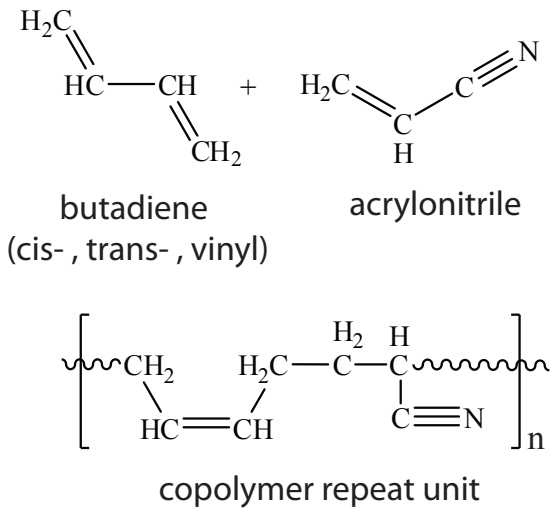

Figure 2.1: Chemical structure of AN and Bd

this, antioxidants are typically added to protect the rubber during shipping and storage. Another common modification to enhance rubber stability involves the chemical modification through hydrogenation. In this process coagulated rubber is dissolved in a solvent and, using a catalyst, hydrogenated to saturate most of the copolymer structure. Apart from hydrogenation, polymerization with small amounts of a tertiary monomer and blends of NBR with other homo- and copolymers are commonly used to enhance rubber properties. A further discussion on modified rubber grades can be found in Mackey and Jorgensen [93].

2.1.2 Properties of NBR

The main indicators for product quality are the polymer molecular weight, degree of chain branching and level of bound AN in the copolymer. The molecular weight can be quite high ranging from $2.5x10^5$ to $6x10^5$ with varying degrees of polydispersity (e.g. 2 to 6). The chain structure can vary widely, ranging from mainly linear chains to highly branched chains (i.e. tri- and tetra-functional branching). The level of bound AN can be varied (e.g. 15 to 50%) depending on a number of desired properties (e.g. oil/fuel resistance, tensile strength, heat resistance, resilience, flexibility). Table 2.1 summarizes the influence of bound AN on various measurable rubber properties.

Other important product quality properties, due to their relation to molecular weight and chain branching, are Mooney viscosity and gel content. Hence, controlling Mooney and gel, in the rubber product, requires the direct control of molecular weight and chain branching within the reactor. Mooney measurements are typically taken prior to compounding in order to provide an indication of the processability of the polymer. Depending on the processing method, Mooney can range from 30 to 50 for injection molding applications and 60 to 80 for an extrusion process. The units of Mooney viscosity are arbitrary and dependent on the test method used.

Table 2.1: NBR property relation to AN content [74]

Lower AN Content		Higher AN Content
	oil/fuel resistance improves	$\longrightarrow$
	rate of curing increases	$\longrightarrow$
	tensile strength increases	$\longrightarrow$
	abrasion resistance improves	$\longrightarrow$
	heat resistance improves	$\longrightarrow$
$\longleftarrow$	compression set decreases	
$\longleftarrow$	hysteresis	
$\longleftarrow$	resilience improves	
$\longleftarrow$	low temperature flexibility improves	
$\longleftarrow$	gas permeability decreases	

2.1.3 Manufacture

For large scale production of rubber, a continuous process is employed, while a batch process is typically used for smaller quantities of varying products. In the continuous process, many reactors are connected in series to form a train with the output flow from the previous reactor entering the next reactor as an input. Raw materials are typically charged to the first reactor where polymerization initiates and, depending on the recipe, are often fed to downstream reactors to control specific polymer properties. Figure 2.2 gives a general process flow schematic.

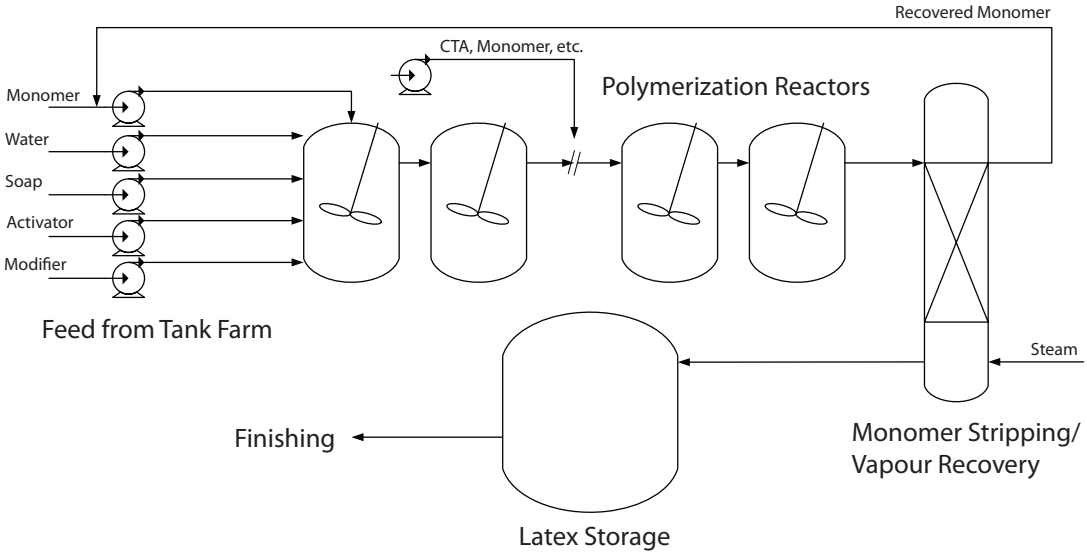

Figure 2.2: Nitrile rubber polymerization - continuous process

In a batch process material is charged to each reactor separately, and once the reaction is complete the latex is transferred to one or two holding tanks before the residual monomer is stripped and the resulting latex is further processed. Figure 2.3 illustrates the batch process.

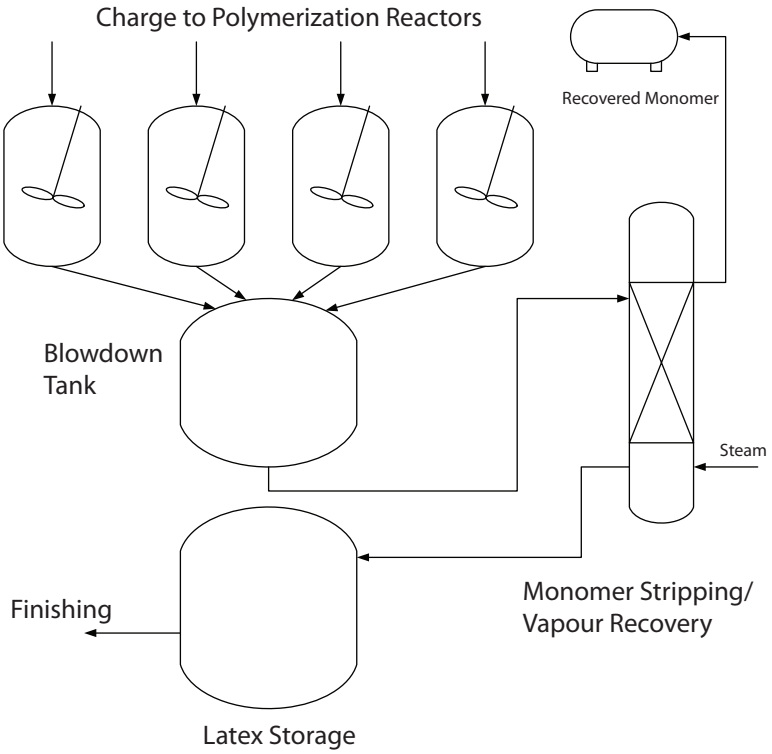

Figure 2.3: Nitrile rubber polymerization - batch process

Nitrile rubber recipes are formulated based on the temperature at which the polymerization takes place (hence, the terms 'cold' and 'hot' recipes). Cold recipes are those that use a redox radical initiation mechanism with temperatures in the range of 5^oC to 15^oC. Hot recipes employ peroxidic initiators that thermally decompose to free radicals in the range of 30^oC to 50^oC. A typical example of both recipe types can be seen in Table 2.2.

The ratio of AN to Bd can vary depending on the desired final rubber properties, Table 2.1. The amount of water can also vary; however, this is primarily dependent on the heat generated by polymerization and the available heat transfer capacity of the reactor cooling system. Electrolytes are often used to help control and maintain the colloidal stability of the polymer particles. Typically potassium and sodium salts are used (e.g. Na_2CO_3 or K_2CO_3). Polymerization initiator systems used are mainly water soluble and are designed to generate a continuous supply of free radicals. The choice of emulsifier is dependent on the monomers, polymerization conditions (i.e. temperature, latex stabilization capability), and the influence on the final product. Typically more than one emulsifier with differing functionality are used to control and stabilize particle formation and growth. A detailed discussion on the functionality of each recipe ingredient can be found in Hofmann [74].

Table 2.2: Typical nitrile rubber polymerization recipes

	Parts per Hundred Monomer (PPHM)	
Material	**Cold Polymerization**	**Hot Polymerization**
Acrylonitrile	32	32
Butadiene	68	68
Water	180 - 200	180 - 200
Electrolyte	0.3	0.3
Hydroperoxide	0.04	-
Persulfate	-	0.25
Iron chelate [a]	0.005	-
Reducing agent	0.03	-
Primary Emulsifier	2.8	2.8
Secondary emulsifier	0.5 - 1.25	0.5 - 1.25
Chain transfer agent	0.4	0.4

[a] e.g. $FeSO_4 \cdot 7H_2O$

2.2 Polymerization Fundamentals & Background

Emulsion polymerization is considered to be one of the most complex polymerization processes, due to its heterogeneous nature and complex nucleation and kinetic mechanisms. Since the 1980's there has been a significant increase in the number of publications discussing the modelling of emulsion systems and the complex phenomena occurring at the micro- and macro-scale of the reaction/reactor system. The purpose of this section is not to discuss in detail the entire process, mechanisms and kinetics of emulsion polymerization, but instead to give a flavour of these aspects, point to articles of particular importance, and to discuss typical recipe ingredients and their functionality within the emulsion system. For further details on the mechanistic aspects refer to Gilbert [58], while further information on the ingredients can be found in Bovey et al. [13].

2.2.1 Emulsion Polymerization

Emulsion polymerization is widely used in industry to manufacture synthetic rubber, latex paints, adhesives, and coatings. The process incorporates free radical polymerization, colloidal reaction sites and an aqueous dispersion medium. Due to the inherent nature of this process, several advantages are offered. First, the dispersion medium is water, which can be easily recycled back to the system. As well, the use of water allows for a less viscous environment which promotes heat transfer away from the reaction sites and between the cooling medium. Along with the inherent process advantages, a water medium has several environmental and economic advantages. From the environmental side, a water based process eliminates the release of VOC's to the atmosphere and reduces the water treatment required before release to the sewer. Economically, using water as a main ingredient eliminates the use of expensive solvents, as well as the added process expenses to recover organic solvents. A second advantage to using emulsion polymerization, as opposed

to solution or bulk, is the ability to simultaneously achieve higher reaction rates and molecular weights. This realization is made possible due to the compartmentalization of reaction sites (i.e. particles) within the aqueous medium, which prevents radical termination between adjacent sites [135]. Disadvantages of an emulsion system are generally found in post reactor stages, during latex coagulation, separation, and cleaning of the polymer from undesired ingredients.

Polymer Particle Formation & Growth

Perhaps the most important aspect of emulsion polymerization is the particle formation mechanism. In general, particle nucleation is considered to occur by one or a combination of the following nucleation mechanisms: micellar nucleation, homogeneous nucleation, coagulative nucleation, and monomer droplet initiation.

The degree to which one or a combination of these mechanisms operate is highly dependent on the nature of recipe ingredients (e.g. monomer water solubility, emulsifier type ionic/nonionic, initiator type redox/thermal), amount of each ingredient (e.g. emulsifier concentration), and reactor operation (e.g. temperature, agitation).

Micellar nucleation was conceptually introduced in 1947 by Harkins [72], and subsequently quantified in 1948 by Smith & Ewart [154]. Since its inception, the conceptual aspect proposed by Harkins has remained; however, the original theory was based on ionic surfactants, and monomers with low or negligible water solubility and high solubility in their own polymer [35]. Thus, much of the quantitative theory of Smith & Ewart has been modified and extended to give a more general picture of the kinetic and mechanistic aspects of micellar nucleation. For further details refer to the review articles of Ugelstad and Hansen [165] and Nomura [119, 125]. In general micellar nucleation begins when emulsifier accumulates in the dispersion medium above a critical concentration forming the so called micelles, whereby a small amount of monomer solubilizes (in the micelles). Free radicals initiated in the aqueous phase subsequently sting these monomer swollen micelles forming polymer particles. Conceptually this process is separated into three distinct stages as illustrated in Figure 2.4.

During the first stage, also known as the nucleation or seed stage, micelles form from the emulsifier, radicals grow in the aqueous phase until they are captured by micelles and/or particles, and particles are formed (from micelles upon radical entry or from homogeneous nucleation). Once radicals begin to grow within the particles much of the remaining emulsifier, in the form of micelles, is used to stabilize the growing particles. Once all the micelles have been consumed and particle generation ceases, stage one is complete.

A thermodynamic equilibrium exists between monomer droplets and growing polymer particles. As monomer is incorporated into the growing polymer chain within the particles, monomer from the droplets rapidly diffuses through the aqueous medium and into the particles. During this stage, particles remain saturated with monomer and a constant volumetric swelling ratio between monomer droplets and polymer particles is maintained. The end of the growth stage occurs when the separate droplets disappear.

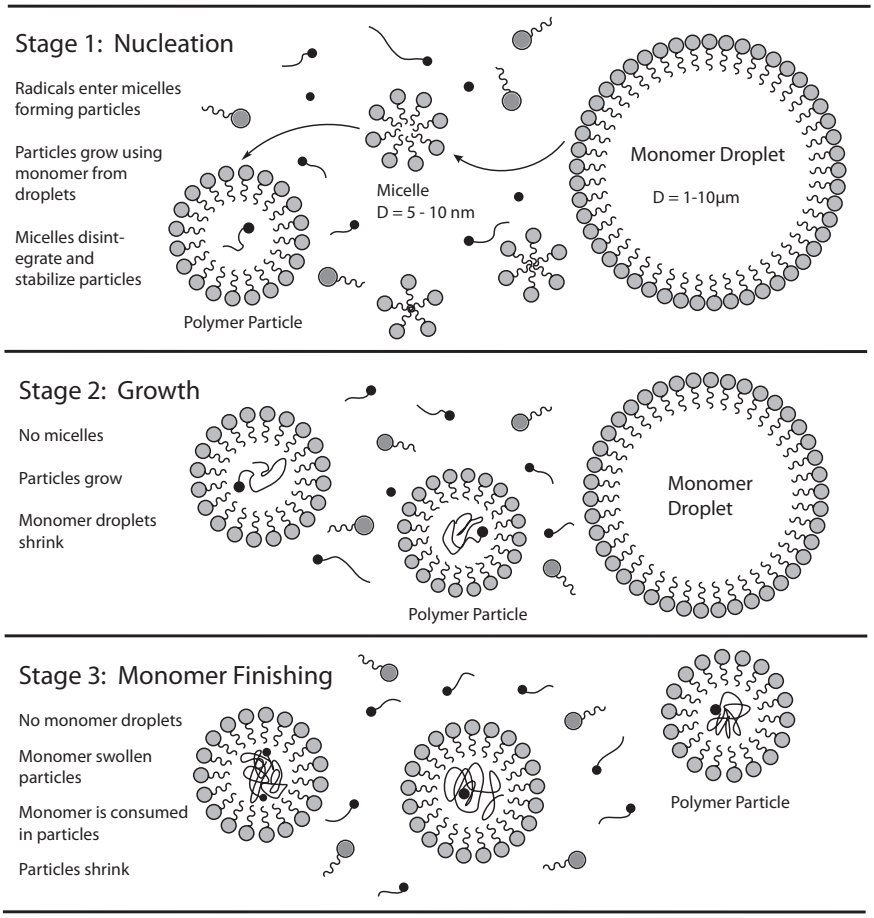

Figure 2.4: Harkin's concept of micellar nucleation

The final stage (stage 3 of Figure 2.4) proceeds by consuming the remaining monomer inside the polymer particles. During this time fresh monomer is not being supplied to the particles, thus, since the polymer density is greater than the monomer density, the particles shrink. Also during this stage, the extent of gelation becomes of significant importance due to the diffusional limitations placed on the free radical mechanism (e.g. radical termination and propagation in the particles).

The concept of homogeneous nucleation was initially developed to handle particle nucleation when micelles were not present (i.e. emulsifier concentration is below the CMC) and the monomer is moderately soluble in the aqueous phase. The restriction that the concentration be below a critical value for nucleation to occur was later proven to be unnecessary [147]. These ideas were further refined and cast into a qualitative framework by Fitch and Tsai [42], and then extended further by Hansen and Ugelstad [70]. Further reviews were provided by both Fitch [41] and Hansen and Ugelstad [71] that compare, contrast and quantify their ideas with other nucleation theories (i.e. micellar, coagulative, droplet). The combination of these ideas has since been termed "HUFT" theory [69].

The process of homogeneous nucleation initiates when free radicals are generated in the aqueous phase. These radicals react with monomer units dissolved in the water phase (the is always a finite, even if small,

solubility) and propagate until a point where they become insoluble and precipitate to form particles that are quickly stabilized by either absorbing emulsifier, coagulating with other particles, or by a combination of the aforementioned methods. This process is illustrated in Figure 2.5, where the symbols $+M$, α, and $j_{critical}$ represent the growing monomer chain, fraction of the critical chain-length where capture begins (i.e. $\alpha < 1$), and the critical chain-length where precipitation occurs.

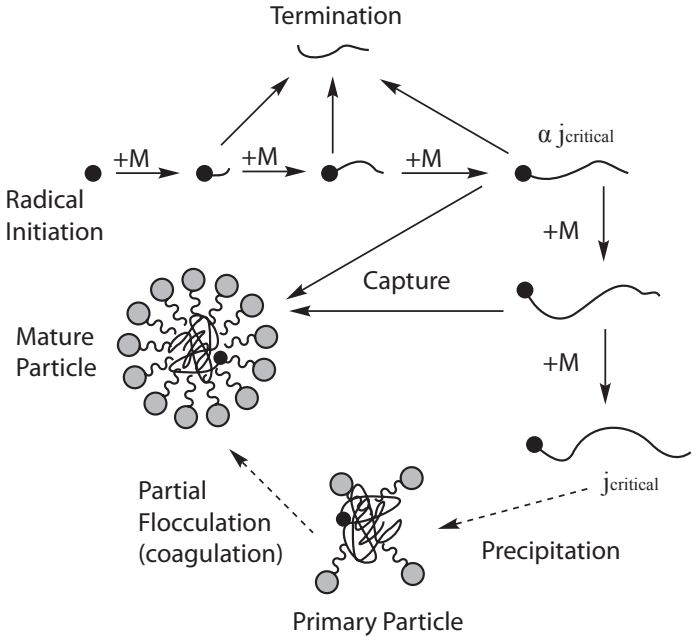

Figure 2.5: Representation of the homogeneous nucleation mechanism

According to HUFT theory, soluble oligomeric radicals propagate in the aqueous phase to a point where their path diverges taking on two possible fates. Radicals either continue to grow to a point where they ultimately become insoluble in the aqueous phase, or are captured by existing particles. Although this theory is capable of quantifying primary particle formation, it does not account for particle coagulation, which is considered by many researchers to exist for particles to become colloidally stable. The extension of the HUFT model to include coagulation was made by Feeny et al. [39] who have, among others (Song and Poehlein [155]), since confirmed their initial models [108]. Further details can be found in a recent review from the Gilbert group [160], who give an up-to-date discussion on the current beliefs of particle nucleation.

The remaining nucleation method to briefly mention is droplet initiation. Typically in emulsion polymerization the monomer droplets serve only as a reservoir for the supply of monomer to the growing particles. However, if the monomer droplets become considerably small, then there is greater competition for the capture of oligoradicals from the aqueous phase. In the chance that a radical is captured, a new particle is formed. In order to achieve the required conditions for droplet nucleation, particular emulsifiers and stabilizers must be used along with high agitation rates. Two modes of polymerization that employ droplet nucleation are mini- and micro- emulsion polymerization. Details can be found in a recent review by Schork

et al. [152].

Emulsion Polymerization Kinetics

The most distinguishing attribute that separates emulsion polymerization from bulk or solution polymerization is radical compartmentalization. When radicals are segregated in different particles, propagation can proceed further before termination occurs. Thus, radical compartmentalization leads simultaneously to a higher propagation rate and polymer molecular weight. This can be seen directly through the defining rate and molecular weight (number-average degree of polymerization - r_N) definitions below.

Emulsion	Bulk/Solution
$R_p = k_p [M]_p \frac{\bar{n} N_p}{N_A}$	$R_p = k_p [M] \left(\frac{R_I}{k_t}\right)^{1/2}$
$\frac{1}{r_N} = \frac{R_t}{R_p} \sim \frac{R_I}{R_p}$	$\frac{1}{r_N} = \frac{R_t}{R_p}$

For the emulsion case, the rate of polymerization, in stages 1 and 2, is primarily dependent on the product of the number of particles times the average number of radicals per particle. This is contrary to bulk or solution polymerization, where increasing the initiator concentration increases the rate of polymerization, but decreases the molecular weight. In emulsion polymerization, increasing the number of particles (i.e. adding emulsifier) at a constant initiator level increases both the polymerization rate and molecular weight.

Classical Smith-Ewart theory is often used to classify different emulsion systems into three limiting cases listed in Table 2.3. These three cases can be deduced from the early works of O'Toole [131] and Ugelstad and Hansen [165] as shown by Penlidis [135], who demonstrates the coupling of a balance on radicals entering and exiting the aqueous phase with a population balance on particles with "n" radicals in order to obtain an expression for the average number of radicals per particle. Further details are given in section 3.5.

For Case I systems the rate of radical desorption dominates the rate of radical capture, giving rise to an average number of radicals per particle that is much less than 0.5. Examples of monomers falling into this category are vinyl acetate and vinyl chloride. In Case II systems, the average number of radicals adheres to 0.5, as the rate of desorption is negligible compared to the rate of radical capture. Typically in these systems radical termination is instantaneous when a radical enters a particle already containing one radical; however, as the conversion increases the polymer chains become highly entangled creating a diffusion-controlled environment which results in the so called gel-effect. This in turn causes the number of radicals per particle to increase beyond 0.5 and to shift from Case II kinetics and approach Case III. Examples of systems conforming to Case II kinetics (with a later potential transition to Case III kinetics) are styrene, methyl methacrylate, and butadiene.

Table 2.3: Smith-Ewart limiting cases

Limiting Case	**Characteristics**	$\bar{n}$	**Limiting Equation**[a]
Case I	Small particles ($d_p < 100$nm) Large number of particles Radical desorption Water soluble monomers	$\bar{n} \ll 0.5$	$\bar{n} = R_I^{1/2}/N_p \left(\frac{V_p}{2k_t} + \frac{N_p}{2k_{des}}\right)^{1/2}$
Case II	Fast bimolecular termination Relatively small particles ($d_p < 200$nm)	$\bar{n} = 0.5$	-
Case III	Large particles ($d_p > 200$nm) Important gel-effect	$\bar{n} \gg 0.5$	$\bar{n} = \left(\frac{V_p R_I}{2k_t N_p^2}\right)^{1/2}$

[a] other similar expressions have been proposed [10, 89]

Phase Distribution of Reaction Species

The partitioning of different species between the aqueous, monomer droplet and particle phases is a characteristic of the emulsion process that distinguishes it from solution or bulk processes. While some authors consider the presence of micelles as a separate phase, many often lump them in as part of the particle phase creating three phases of interest. In order to properly capture the physical behaviour of the system in a model, appropriate methods are required for determining the distribution of species between these three phases. Methods that are currently used are based on either purely thermodynamic or semi-empirical expressions. Table 2.4 summarizes selective relevant literature sources on monomer partitioning.

Table 2.4: Species partitioning literature

Source	**Method**	**Comments**
Guillot [63]	Thermodynamic	Development of thermodynamic equations
Armitage et al. [5]	Thermodynamic	Algorithm to solve thermodynamic equations
Gugliotta et al. [60]	Partition Coefficients	Comparison between thermodynamic and empirical approaches
Penlidis [136]	Critical Conversion	Development using x_c parameter for homo/co-polymer systems
Omi et al. [126]	Empirical Model	Development using empirical relations

In the thermodynamic case, an equilibrium balance that relates the free energy of mixing of monomer into its polymer to the interfacial free energy between the particle, droplet or aqueous phase is used to obtain volume factions of monomer in each phase. Partition coefficients are defined as a ratio of the volume fraction of monomer (or other species) between two particular phases. Using proper estimates of these coefficients, a mass balance can be written and the phase concentrations determined. For the critical conversion approach, mass balances are used in conjunction with a parameter that signals when the monomer droplets disappear (i.e. end of stage 2). Again volume fractions of monomer in each phase can be calculated and in turn the corresponding concentrations obtained. Empirical expressions are derived in a similar manner, using mass balances; however, these expressions typically do not rely on a single parameter, which may make them less

convenient to use. Section 3.4 is devoted to discussing partitioning techniques in more depth, and the reader is referred there for further information.

2.3 Acrylonitrile/Butadiene Polymerization

Despite the long history of industrial production of NBR, very little has been published in the open literature on the reaction engineering aspects of the process. Much of the existing literature focusses on the processing and resulting rubber properties. This section aims to review important literature relating to the emulsion polymerization of AN and Bd separately as homopolymers and together as a copolymer. Of particular interest to this work are the rate constants for propagation, transfer to monomer, transfer to chain transfer agent (mercaptan), termination, and crosslinking. As well, representative reaction data sources for emulsion homo- and copolymerization of the respective monomers are referenced, which will subsequently be used for model testing/validation.

2.3.1 Butadiene Homopolymerization

In the 1990's, the kinetic aspects of the emulsion polymerization of butadiene received considerable attention compared to what was originally published in the 1950's. A listing of open literature sources on mechanistic and kinetic aspects of butadiene emulsion polymerization can be seen in Table 2.5.

Table 2.5: Butadiene emulsion polymerization literature

Source	Remarks
Meehan [100]	Estimation of x_c using pressure-conversion measurements
Morton et al. [110, 111]	Propagation & chain transfer rate constants. Conversion-time data
Minhas [107]	Batch conversion data at different initiator & emulsifier levels
Pallaske et al. [133][a]	Data on conversion, diameter, and percent solids
Weerts et al. [185–189][a]	Data on conversion, particle size & number
Deibert et al. [29]	Rate constants for propagation, termination, transfer to monomer
Verdurmen et al. [175–180]	Radical transfer, termination, desorption rate coefficients

[a] Data used for model comparisons

Much of the early work on butadiene polymerization in emulsion systems has been derived from research on synthetic rubber sponsored by the US government during WWII. This work was later summarized by Bovey et al. [13], which is a classic reference on synthetic rubber, particularly SBR.

The first to present details on the kinetic aspects of propagation, transfer, and crosslinking was Morton et al. [111]. Their experiments were conducted at fairly low temperatures, 0^oC to 30^oC, characteristic of a cold rubber recipe, using a peroxide-amine initiator/chain transfer system, as opposed to a persulfate-mercaptan system. The reasoning for this choice was that the rate of polymerization was found to be invariant to such variables as emulsifier and CTA levels and was only influenced by temperature. Thus, rate constants could be estimated, with limited confounding effects from initiator or emulsifier. As well,

the system was found to fall under the Case II regime of Smith & Ewart, where the average number of radicals per particle remained around 0.5. As a result, the propagation rate constant estimated was said to be representative of the butadiene system.

The kinetics of polybutadiene were revisited to a greater extent in the late 1980's to early 1990's when Weerts et al. [185] performed several studies on the influence of initiator, emulsifier, and CTA type and concentration on particle growth rate, number and size. Experiments were conducted at a higher temperature than those of Morton, at roughly 60^oC. The reaction kinetics were found to be independent of initiator type, while radical capture was found to be weakly dependent on initiator concentration. Limited particle coagulation was evident, which extended to approximately 40% conversion; however, the effect on polymerization rate was said to be minimal, since the average number of radicals increased with particle size. On comparing emulsifiers sodium dodecyl sulfate (SDS) and Dresinate 214 (rosin acid soap), SDS was found to have a greater particle stabilizing effect. During stages 1 and 2, from Harkin's theory, it was observed that the average radical number remained below 0.5.

In order to remove or lessen the effect of particle size dispersity and coagulation on the reaction kinetics, and in an attempt to estimate better rate coefficients, Verdurmen et al. [175] performed seeded experiments. The average number of radicals per particle was found to fall between the Case I and II regimes (i.e. $\bar{n} \leq 0.5$), which was dependent on particle diameter (i.e. above 200 nm $\bar{n}$ remained around 0.5). Further work was performed in order to characterize the effect of persulfate initiator and mercaptan chain transfer agent on particle growth and the events responsible for radical entry and exit from the particles. Radical desorption was found to be independent of persulfate concentration, while t-DDM was found to minimize desorption in the presence of fatty-acid emulsifiers. These observations were justified based on the so-called promoting effect of the mercaptan [180]. Radicals were shown to exit the particles and then to re-enter (eventually remaining in the particles). Estimates of the desorption coefficient were correlated to the size of the growing particles by a power relationship, ($k_{des} \propto r_p^{\alpha}$), were α was said to be highly uncertain with a variance greater than its mean value, which would make this correlation highly unreliable.

Around the same time, Deibert et al. [29] performed solution polymerization experiments with butadiene in chlorobenzene in order to deduce the propagation rate coefficient. Using their estimate, comparisons were made to that of Weerts et al. [187], which revealed good agreement. As well, $\bar{n}$ was estimated and compared well to the results of Weerts. In a further attempt to estimate termination and transfer rate constants, Deibert and Bandermann [28] performed experiments using free-radical solution polymerization of butadiene in chlorobenzene. Arrhenius expressions were presented for transfer to monomer and solvent and for radical termination and propagation. An important note was that the experiments were conducted at low conversion levels and not over the entire range. Therefore, the rate constant estimates can only be considered accurate at low conversions and molecular weights. As well, attached to the termination rate constant estimate was a variance of about 42% of the mean value, while the propagation and transfer to monomer had lesser variances of about 10% and 18%. Though these errors seem large, they are quite reasonable given the experimental difficultly in determining a precise value.

Tables 2.6 and 2.7 summarize available rate constants for butadiene, which were reported in the articles

listed in Table 2.5 and in the polymer handbook [14]. Comparisons were made at a temperature of 60^oC, since many of the reported values where given at this temperature.

Table 2.6: Butadiene propagation & termination rate constants

k_p (L/mol/min) [a]		k_t (L/mol/min)		Source
$7.2 \times 10^9 exp(-9300/RT)$	5700	-	-	Morton et al. [111]
-	12000	-	-	Weerts et al. [187]
-	$19200 \pm 16\%$	-	4.2×10^{11}	Verdurmen et al. [175]
$4.83 \times 10^9 exp(-8531/RT)$	12200	$6.78 \times 10^{11} exp(-1412.76/RT)$	8.02×10^{10}	Deibert and Bandermann [28] [b]

[a] Arrhenius expression and value at $T = 60^oC$
[b] Solution polymerization in chlorobenzene

Table 2.7: Butadiene transfer rate constants

k_{fm} (L/mol/min) [a]		k_{fcta} (L/mol/min)		Source
-	-	$3.06 \times 10^8 exp(-6400/RT)$	19360	Morton et al. [111]
-	6	-	-	Weerts et al. [187]
-	0.6 - 6	-	-	Verdurmen et al. [175]
$2.532 \times 10^8 exp(-10213.18/RT)$	50.5	-	-	Deibert and Bandermann [28]

[a] As in Table 2.6

Prior to the kinetic studies of Weerts and Verdurmen, a paper on the modelling and subsequent validation of the emulsion polymerization of butadiene was published by Pallaske et al. [133]. Pilot plant experiments were carried out in a 40 L reactor under batch and continuous operation. Model predictions on conversion-time, average particle diameter, particle size distribution, and percent solids agreed reasonably well with the experimental results. A rather surprising finding was that during CSTR experiments oscillations were observed under certain conditions (i.e. low emulsifier feed flow rate). The model appeared to adequately capture this behaviour. Unfortunately, no model parameters were divulged, presumedly due to the proprietary nature of the work, but an adequate amount of data was shown under batch operation that reveals the behaviour of the process from which model parameters could be estimated.

2.3.2 Acrylonitrile Homopolymerization

Compared to butadiene, the emulsion polymerization of acrylonitrile has not nearly received the same attention. A listing of the literature on acrylonitrile along with some brief comments can be seen in Table 2.8.

A number of early studies that were carried out in emulsion focussed on characterizing the polymerization mechanism with respect to the role of various recipe ingredients (i.e. locus of polymerization) [79, 85, 162, 163]. Of these studies, only one reported on an expression of the propagation rate constant, Thomas and Webb [161]. Shortly after Thomas, a number of kinetic studies were performed by Dainton et al. [25] who provided estimates of the propagation and termination rate constants, albeit under solution polymerization conditions. Another study that explored different recipe formulations was that of Tazawa

et al. [159]. Their work focussed on investigating the rate of polymerization and in turn the mechanistic aspects of polymerization. They further postulated that the major locus for polymerization was on the surface of the particles, which is in agreement to prior findings by Izumi [79] who stated that the locus is on and in the particle as well as in the aqueous phase. Furthermore, Tazawa et al. cite a considerable amount of their experimental data along with estimates of the critical conversion (i.e. conversion where droplets disappear). The studies of Tazawa where extended to the semi-batch regime by Omi et al. [128]. There experiments where carried out by feeding the monomer so that droplets did not form in a separate phase (i.e. starve-fed) and the aqueous phase remained at its saturation limit. In doing so, they were able to successfully model the system by developing a relation to express the partitioning of the monomer between aqueous and particle phases. They also compared two different models; one in which propagation occurs on the surface of the particles and the other by the conventional approach where monomer diffuses into the particles and propagates. The surface propagation model was found to resemble the experimental data more closely, which was presumably due to a low monomer concentration combined with the fact that acrylonitrile does not like its own polymer.

In the mid to late 1980's the kinetic and mechanistic aspects of AN emulsion polymerization were revisited by McCarthy et al. [96]. In their studies, seeded experiments were carried out in order to remove any ambiguous effects that may be present during particle formation, which would certainly affect the rate constant estimates. Their findings were in accord with previous claims that the locus of polymerization is on the particle surface, and consequently considerable deviation from the typical Smith & Ewart Case II kinetic regime was observed (i.e. $\bar{n} \gg 0.5$). Compared to previous rate constant estimates, established from other solution and emulsion polymerization experiments, the values obtained from seeded emulsion experiments were considerably lower. With respect to previous emulsion experiments [161], the assumption of a Case II kinetic regime (i.e. $\bar{n} = 0.5$) was stated as the most likely reason for the high rate constant estimates. Soon after McCarthy et al., Sarkar et al. [150] performed persulfate initiated aqueous polymerizations (i.e. emulsifier-free), and provided estimates of termination rate constants for both aqueous and particle phases. These estimates were based on the propagation rate constant estimate provided by Dainton and Eaton [22]. The reason given for not using the estimates of McCarthy et al. was that they did not consider the interaction between the persulfate ion (initiator) and the monomer, and thus no induced decomposition of the persulfate initiator, which evidently was not supported by the findings of Sarkar. Clearly, there still seems to be some discrepancies between the different rate constant estimates available and the influences that various mechanistic aspects have on the kinetics of the system.

Many of the previous studies on AN polymerization have been related to mechanistic and kinetic characteristics under batch and semi-batch operation. In order to elucidate the polymerization behaviour under continuous operation, Nishida et al. [116] performed experiments in a CSTR. Their findings confirm others, in that, under emulsifier-free polymerization, oligoradicals precipitate from solution forming a particle phase where polymer continues to grow. They also demonstrate that unseeded polymerization causes the conversion to oscillate, which is typical with many systems under CSTR operation (e.g. VAc, VCl). In order to dampen the oscillatory behaviour a tubular pre-reactor was implemented, which acted as nucleating reactor to seed the CSTR. This configuration successfully produced a stable latex while achieving a steady-state

Table 2.8: Acrylonitrile emulsion polymerization literature

Source	Remarks
Uchida [163, 164]	Batch studies. Influence of inhibitors on conversion
Thomas et al. [162]	Batch studies on mechanism & kinetics and the influence of recipe ingredient level
Dainton et al. [22–25]	Kinetic studies using solution polymerization. Propagation and termination rate constants
Kiuchi [85]	Batch studies on polymerization mechanism
Izumi [79]	Batch studies on mechanistic aspects of polymerization
Tazawa et al. [159][a]	Batch experiments. Data on conversion, particle number & polymer yield
Omi et al. [128]	Semi-batch experiments & modelling. Data on polymer yield
McCarthy et al. [96]	Kinetic study under seeded conditions. Propagation rate constant estimation
Elbing et al. [36, 37]	Seeded study on the polymerization mechanism
Nishida et al. [116]	PFR, CSTR & tube-CSTR experiments. Data on conversion
Boguslavsky et al. [12]	Batch experiments. Data on conversion and particle size

[a] Data used for model comparisons

conversion.

A listing of available rate constants can be seen in Tables 2.9 and 2.10. An Arrhenius expression is stated along with a comparison at 50^oC.

Table 2.9: Acrylonitrile propagation & termination rate constants

k_p (L/mol/min) [a]		k_t (L/mol/min)		Source
-	1.2×10^6 [b]	-	-	Thomas and Webb [161]
$1.8 \times 10^9 exp(-4100/RT)$	3.04×10^6	$1.98 \times 10^{12} exp(-5400/RT)$	4.4×10^{11}	Dainton and Eaton [22][c]
-	1.8×10^4 - 7.2×10^4	-	-	McCarthy et al. [96]
$6.282 \times 10^9 exp(-7278.38/RT)$ [d]	7.5×10^4	-	-	Garcia-Rubio et al. [56]
-	-	-	2.3×10^9 [e]	Sarkar et al. [150]

[a] Arrhenius expression and value at $T = 50^oC$
[b] Estimated at 40^oC
[c] Aqueous solution polymerization
[d] Estimated in conjunction with styrene as a copolymer
[e] Particle phase estimate, for the aqueous phase $k_t = 3.6 \times 10^{12}$

Table 2.10: Acrylonitrile transfer rate constants

k_{fm} (L/mol/min) [a]		k_{fT} (L/mol/min)		Source
$(0.3 \times 10^{-4}$ - $1.0 \times 10^{-4}) \times k_p$	2.2 - 7.5 [b]	$0.73 \times k_p$ [c]	5.5×10^4	Brandrup et al. [14]

[a] As in Table 2.6
[b] Using k_p of Garcia-Rubio et al. [56] at 50^oC
[c] Transfer to n-Docecanethiol (n-DDM) which is considered more reactive then t-DDM [167]

2.3.3 AN/Bd Copolymerization

Since the first use of butadiene and acrylonitrile in emulsion polymerization in the 1930's, the main application has been the production of synthetic rubber. Only a few studies have appeared on these two monomers

concerning the kinetic aspects of the copolymerization. A summary of these studies along with some other related studies with similar monomers (i.e. Sty/AN, Sty/Bd, IP/Bd) can be seen in Table 2.12.

Much of the early work relating to the copolymerization of AN and Bd has been with respect to composition [38, 183]. These studies report data on the change in copolymer composition with conversion and in turn provide estimates on the reactivity ratios according to the well-known Mayo-Lewis equation. Further studies on reactivity ratio estimation were performed by Vialle et al. [181], where instead of the typical terminal model, a penultimate model was used. They claimed that the varying degrees of different estimates present in the literature, may have been due to underlying penultimate effects (i.e. the penultimate unit of the growing radical chain affects its reactivity) that were previously not considered. They conclude by stating that one reactivity ratio is sufficient for radicals ending in a acrylonitrile unit, while penultimate effects are likely present with butadiene, and that the reactivity ratio must be estimated considering several different possible reactions (i.e. polarity effects, different reactivities of 1,2- and 1,4- butadiene, and charge transfer complexes between monomers). A later report by the same group [65], demonstrated the use of a terminal model where the reactivities of 1,2- and 1,4- butadiene are considered different. Under these conditions, r_B could be represented as a function of four different ratios that account for the effect of different butadiene conformations. In doing so, an estimate of r_B was able to be made, which when used in the derived model (i.e. composition based model similar to Mayo-Lewis equation) gave good agreement with experimental results. A listing of reactivity ratios from the sources just mentioned can be seen in Table 2.11.

Table 2.11: Reactivity ratios for AN/Bd copolymerization

$r_A = k_{p_{AA}}/k_{p_{AB}}$	$r_B = k_{p_{BB}}/k_{p_{BA}}$	**T** (^oC)	**Source**
0.1 ± 0.059 [a]	0.452 ± 0.023	50^oC	Wall et al. [183]
0.02	0.28	5^oC	Embree et al. [38]
0.04	0.30	5^oC	Guyot et al. [65]
0.05	0.35	-	Brandrup et al. [14]

[a] ratios were re-estimated from data of Wall according to Brandrup et al. [14]

In order to obtain rubbers with a desired set of final properties, Poddubny and Rabinerzon [140] studied the influence of chain transfer agents on the molecular weight distribution. Their results suggested that desirable molecular weight distributions and corresponding polymer properties are achieved with the use of modifiers with relatively low transfer constants (e.g. $C_x = k_{fT}/k_p \sim 1.0$) in combination with an optimum feed policy (i.e. under batch operation a single charge of CTA is insufficient). Further studies were performed by Uraneck and Burleigh [167] on the efficiency of various types of modifiers to achieving a desired molecular weight. Their findings show a number of interesting results: normal mercaptans are inefficient in nitrile systems, the transfer constant (C_x) decreases as the nitrile content increases and as the modifier's molecular weight increases, and tertiary mercaptans were the most efficient at low temperatures. Apart from the discussion in Bovey et al. [13], which was mainly concerned with SBR, the study of Uraneck is probably the only source on NBR which provides numerous data of the effect of different modifier types and concentrations on various physical-mechanical properties of the resulting rubber.

Attempts to further quantify the rate of crosslinking within butadiene systems have been made by Burnett et al. [17, 18, 19]. Apart from the previous estimate provided by Morton for homo-Bd and respective of the fact that Burnett's estimate was from an SBR system, this newer estimate is probably the closest value to describing the kinetic behaviour of crosslinking in an NBR system.

Table 2.12: Acrylonitrile & butadiene emulsion copolymerization literature

Source	**Polymer System(s)**	**Remarks**
Wall et al. [183]	NBR, CSBR	Data on conversion and bound AN
Embree et al. [38]	NBR	Data on bound AN & reactivity ratio estimation
Orr and Breitman [130]	NBR, SBR, MMA/Bd	Properties of various emulsifiers (i.e. CMC, S_a)
Poddubny and Rabinerzon [140]	NBR, SBR	Study of the influence of CTA on the MWD
Hofmann [74]	NBR	Comprehensive review of NBR processing
Uraneck and Burleigh [167]	NBR, SAN	Experimental data for X & effect of CTA on Mooney
Burnett et al. [17–19]	SBR	Rate constant information for crosslinking
Vialle et al. [181]	NBR	Reactivity ratio estimation (Penultimate model)
Guillot [63]	SAN	Modelling & experimental studies on partitioning
Lin et al. [91]	SAN	Batch modelling & experimental validation
Guyot [64], Guyot et al. [65]	SAN, AN/BA, NBR	Composition control, reactivity ratio estimation
Hoffman [73]	SAN	Batch modelling & experimental validation
Omi et al. [127]	SAN	Semi-batch modelling & experimental data on yield
Shvetsov [153]	NBR, IP/AN	Batch reactor experimental data on Np, X, PSD
Filho et al. [40]	SBR	Batch modelling & experimental validation

Experiments on acrylonitrile/butadiene emulsion copolymerization systems that report on both kinetic and mechanistic aspects are scarce. A discussion along with limited data on monomer-polymer ratio, particle number, particle size distribution, and rate of polymerization is provided by Shvetsov [153]. However, his studies were based on micro-emulsions (i.e. droplet nucleation) and the influence of different types and doses of activator over the course of the polymerization. Due to the lack of direct experimental information on NBR systems, related systems must be looked at for insight into effective modelling approaches. For example, styrene/acrylonitrile (SAN) and styrene/butadiene (SBR) are two systems that can provide insight. Modelling studies combined with experimentation that use emulsion polymerization to produce SAN and SBR have been performed by a number of groups (Table 2.12). Guillot [63] applied a thermodynamic approach to model the monomer partitioning, which gave satisfactory agreement with experimental results. On the other hand, Lin et al. [91] used an experimental approach to monomer partitioning (i.e. x_c approach), while Hoffman [73] and Omi et al. [127] used partition coefficients based on experimental evidence. While these approaches are more empirical than that of Guillot, good model predictions were obtained nonetheless. Models for predicting the production of SBR have also been presented by Broadhead [15], Wong [190] and Gugliotta et al. [61].

Based on the aforementioned studies, recent efforts to model NBR have been carried out using similar techniques. A listing of sources on NBR process modelling and related industrial process control applications can be seen in Table 2.13.

Table 2.13: NBR process modelling literature

Source	Remarks
Dube et al. [33]	Batch model development & comparison to limited industrial data
Mutha [113]	Model-based process control applications
Vega et al. [171]	Batch/semi-batch model development & comparison to industrial data
Gugliotta et al. [62]	On-line state estimation studies
Rodriguez et al. [146]	Model development to include chain-length distributions
Vega et al. [172, 173]	On-line control studies based on state estimation
Minari et al. [104–106]	Simulation studies of CSTR train. Optimal grade change strategies

2.4 Emulsion Polymerization Process Modelling Survey

Generalized approaches to the detailed mechanistic modelling of emulsion polymerization did not begin to appear in the literature until the 1970's. Earlier models were typically situation dependent and limited by differing theories of the process mechanism. A listing of some of the notable modelling approaches has been summarized in Table 2.14. This table outlines the reactor system considered, the approach to modelling the particle size, other aspects that were modelled, and the polymer system(s) that was considered. A detailed account of each of these studies will not be given here, instead only a selected few will be mentioned depending on the relevance to the work in this thesis.

The articles that were found most useful in the development of the model in this work were those of Broadhead et al. [16], Hamielec et al. [68], Gugliotta et al. [61], Dube et al. [33, 34], and Gao and Penlidis [53]. These articles provide a thorough review on many techniques used for emulsion polymerization modelling, more specifically particle nucleation, molecular weight, chain branching (tri-functional), crosslinking (tetra-functional), species partitioning, and diffusion-controlled kinetics. These techniques will be discussed to a necessary extent during the derivation of the model in Chapter 3.

Table 2.14: Emulsion polymerization modelling literature

Source	Reactor System	Model Level[a]	Other Attributes[b]	Polymer System(s)[c]
Min and Ray [101, 102]	Batch/CSTR	PB	-	MMA
Kiparissides et al. [83]	CSTR	ADA	-	VAc
Hamielec and MacGregor [66, 67]	CSTR	ADA, RTA, MA	CLD, MWA, LCB	SBR, SAN
Kanetakis et al. [82]	SS-CSTR train[d]	RTA	MWA, LCB	SBR
Wong [190]	SS-CSTR train	RTA	MWA, LCB	SBR
Broadhead et al. [16]	Dyn-CSTR	ADA, MA	MWA, LCB	SBR
Omi et al. [126, 129]	Semi-batch	MA	CLD, MWA	SAN, AN/VDC, MMA/BA
Dougherty [31, 32]	Batch/semi-batch	PB	MWA	Sty/MMA
Penlidis et al. [138]	CSTR	PB	IMP	PVC, VCM/VAc
Hamielec et al. [68]	Batch/CSTR	ADA, MA	LCB, MWA	G
Chen and Wu [21]	Batch	PB	-	Sty/MMA, SBR
Rawlings and Ray [143, 144]	Batch/CSTR	PB	-	MMA, Sty, VAc
Mead and Poehlein [97, 98]	SS-CSTR	ADA	-	SAN, Sty/MMA
Richards et al. [145]	Batch/CSTR	PB	CN	Sty, Sty/MMA
Storti et al. [158]	Batch	PB	TP	SAN, AN/Sty/MMA
Nomura et al. [124]	Batch	MA		Sty/MMA
Forcada and Asua [45, 46]	Batch	MA	RD, MWA	Sty/MMA
Fontenot and Schork [44]	Batch	MA	RD, DN	G
Gugliotta et al. [61]	CSTR	PB	MWA, LCB	SBR
Dube et al. [33, 34]	Batch/semi-batch	MA	MWA, LCB	NBR
Vega et al. [171]	Batch/semi-batch	MA	MWA, LCB, IMP	NBR
Saldivar et al. [149]	Batch/semi-batch/CSTR	PB	MWA, LCB	MA/VAc, Sty/MMA
Rodriguez et al. [146]	Batch	PB	MWA, CLD, LCB	NBR
Gao and Penlidis [53]	Batch/semi-batch	MA, PB	MWA, LCB, RD, IMP	G
Zeaiter et al. [191]	Semi-batch	PB	MWA	Sty
Immanuel et al. [78]	Semi-batch	PB	CN, RD	VAc/BA
Casella et al. [20]	Batch	MA	RD	Sty, BA, VAc
Meadows et al. [99]	Semi-batch	PB	CN, RD	Sty
Zubitur et al. [192, 193]	Semi-batch	MA	MWA, RD, IMP, TP	Sty/Bd/AA
Fortuny et al. [48]	Batch	PB	CN	BA/MMA
Vale and McKenna [168]	Batch/semi-batch/CSTR	PB	-	G
Park et al. [134]	Batch	PB	MWA, CLD	BA/VAc
Alhamad et al. [2]	Batch/semi-batch	PB	MWA	Sty/MMA
Srour et al. [156]	Batch/semi-batch	PB	MWA, TP	Sty/MMA/MA

[a] PB - population balance, ADA - age distribution analysis, RTA - residence time approximation, MA - monodisperse approximation

[b] MWA - molecular weight averages, LCB - long-chain branching, CLD - chain length distribution, RD - radical desorption, IMP - impurities, DN - droplet nucleation, TP - terpolymerization, CN - coagulative nucleation

[c] G - general system, check Nomenclature for other abbreviations

[d] Steady-state (SS) model

Chapter 3

Emulsion Polymerization Modelling for NBR Systems

This chapter provides a description of the modelling approaches used in the development of the model in the thesis, clearly outlines all modelling assumptions, and provides some insight into the parameters used in the model. Apart from the typical approaches to modelling free-radical polymerization, the following details inherent to emulsion polymerization are discussed: particle nucleation, monomer partitioning, average number of radicals per particle, radical desorption from particles, molecular weight, and chain branching. Each section in this chapter is divided and laid out in a modular fashion that aims to build up the model by starting with the fundamental underlying mechanism and progressing towards the reactor material balances. A detailed listing of all the equations in the model, as well as specific algorithms for computer implementation, are provided in Appendices A & B.

3.1 Reaction Mechanism

In this section the free-radical reaction mechanism will be discussed and the kinetic rate constants and reaction rates derived. The mechanistic aspects considered in this model are: initiation, propagation, termination, transfer to monomer, polymer and CTA, reaction with impurities, and reaction with internal and terminal double bonds. These reactions will be discussed by considering the aqueous and particle phases separately, as radicals are assumed to only exist in these two phases.

Individual species rate constants can be given in general as an Arrhenius expression; however, with polymer systems the overall rate constants vary not only with temperature, but also with composition, polymer weight, monomer conversion and radical chain length. To capture these other dependencies the pseudo-kinetic rate constant method is employed, along with semi-empirical expressions to account for diffusion-controlled reactions.

3.1.1 Aqueous Phase Reactions

Radicals are initiated in the aqueous phase and, for fairly water-soluble monomers, may propagate and terminate according to a typical free radical mechanism. The different possible fates of radicals in the aqueous phase are summarized in Table 3.1, and further discussed in the sections that follow.

Table 3.1: Aqueous phase phenomena involving radicals

Process	**Comments**
Radicals entering the aqueous phase	
Initiation	Radical generation from water soluble initiator
Desorption	Radical exit from particles due to chain transfer to monomer
Reactions involving radicals	
Radical propagation	Radicals propagate with dissolved monomer (oligomerization)
Reaction with Impurities	Radicals are consumed by water impurities causing an induction period
Radical termination	Radicals may terminate through a bimolecular reaction
Radicals leaving the aqueous phase	
Capture by micelle	Radicals are captured by micelles forming particles (i.e. $A_m > 0$)
Capture by Particle	Radicals are captured by (pre)existing particles
Precipitation of oligoradicals	Radicals propagate to a critical length and then form particles

Radical Initiation

Free-radical initiators used in the production of rubber are typically water soluble. Thus, radical initiation is only considered to occur in the aqueous phase and modelled accordingly. Two commonly used initiation methods are employed. The first, redox initiation, is used for the production of "cold" rubber, where the reactor is operated in a temperature range from 5^oC to 15^oC. The second, proceeds by typical thermal decomposition of the initiator, and is employed in the production of "hot" rubber at temperatures ranging from 30^oC to 50^oC.

The redox approach requires a reducing agent in a stoichiometric oxidation/reduction cycle in order to generate free-radicals. Following Broadhead et al. [16], Dube et al. [33] and Vega et al. [171], the mechanism of Andersen and Proctor [4] is used to describe redox initiation and can be written in general as follows:

$$I + Fe^{2+} \xrightarrow{k_1} R^{\cdot}_{in} + Fe^{3+} + Y^- \tag{3.1}$$

$$Fe^{3+} + RA \xrightarrow{k_2} Fe^{2+} + RA^+ \tag{3.2}$$

$$R^{\cdot}_{in} + M_j \xrightarrow{k'_{p_{ja}}} R^{\cdot}_{1,j} \tag{3.3}$$

where, I represents the initiator (i.e. persulfate or peroxide); Y^- is the reduction product (e.g. OH^- for peroxide or SO_4^{2-} for persulfate); RA is the reducing agent, often called the activator; RA^+ is the oxidation product of RA; $R^{\cdot}_{in}$ is the primary initiator fragment and $R^{\cdot}_{1,j}$ denotes a radical of unit chain length ending in monomer j. The iron ions are introduced in the form of ferrous sulfate heptahydrate ($FeSO_4 \cdot 7H_2O$) and are

chelated with ethylene diamine tetrasodium acetate (EDTA) in order to reduce the effective concentration of Fe^{2+} which prevents undesirable side reactions. The reaction proceeds with the initiator reacting with Fe^{2+} generating free-radicals and Fe^{3+}. The reducing agent then reduces Fe^{3+} back to Fe^{2+} and the process continues until the initiator is fully consumed. The free radicals generated from the initiator, $R_{in}^{\cdot}$, propagate with monomer forming primary radicals. Redox systems employ many different types of peroxide based initiators, which depend on many different factors (i.e. rate of initiation to cost of initiator). In this work, the main redox initiator employed for demonstration purposes is *para*-menthane hydroperoxide (PMHP), while for thermal initiation potassium persulfate (KPS) is used. The reducing agent used is sodium formaldehyde sulfoxylate (SFS).

The rate constants used to describe the oxidation and reduction steps, k_1 and k_2, are to be considered as effective rate constants, as there may very well be side reactions occurring but are neglected for simplicity. Estimates for these kinetic parameters using an PMHP initiated system are listed in Appendix C. The primary radical propagation rate constant, $k_{p_{ja}}^{'}$, is usually of higher value than the rate constant of radicals with greater chain length. However, for simplicity $k_{p_{ja}}^{'}$ is set equal to $k_{p_{ja}}$, where 'a' designates the aqueous phase. Further assumptions on radical propagation will be stated shortly. Note that it is unnecessary to consider diffusional effects during radical initiation, as the aqueous phase remains mainly as water with only minor amounts of monomer and oligoradicals. This is in contrast to bulk or solution polymerization, where the viscosity can become quite high.

The rate of redox initiation can be written as a first order reaction with respect to initiator and oxidizing agent, according to Equation 3.4.

$$R_I = k_1 [I] \left[Fe^{2+}\right] \tag{3.4}$$

Thermal initiation follows a simpler mechanism of homolytic cleavage of the $-O-O-$ bond in the persulfate or peroxide initiator. The commonly accepted overall mechanism is as follows:

$$I \xrightarrow{k_d} 2R_{in}^{\cdot} \tag{3.5}$$

$$R_{in}^{\cdot} + M_j \xrightarrow{k_{p_{ja}}^{'}} R_{1,j}^{\cdot} \tag{3.6}$$

Though written in a fairly simple form, many unwanted side reactions occur that consume initiator fragments limiting the number of primary radicals formed. Collectively, these reactions are known as the so-called "Cage" effect, and to account for this an efficiency factor is included when defining the thermal decomposition rate constant. The efficiency factor is a positive value that is less than one, in practice typically ranging from 0.65 to 0.85. The rate of thermal initiation can be written as a pseudo first order expression according to Equation 3.7

$$R_I = 2fk_d [I] \tag{3.7}$$

The overall rate of radical initiation can be written in a form that considers the influence of both redox and thermal initiation together. The two previous expressions can be combined according to Equation 3.8. Under low temperature conditions this new equation reduces back to the previous redox expression, since the influence of thermal decomposition will be negligible, while for simulations at higher temperatures a reducing

agent is not used, thus the overall equation reduces back to the thermal decomposition expression.

$$R_I = k_1 [I] \left[Fe^{2+}\right] + 2 f k_d [I] \tag{3.8}$$

Apart from radical initiation, reaction rates for initiator, reducing agent, Fe^{2+}, and Fe^{3+} consumption are necessary when performing a mass balance on the system. Note that there is a slight difference between the rate of radical initiation and the consumption rate of initiator. The rate of initiator consumption is not concerned with the successful formation of radicals, only that the initiator has been converted to some other product (i.e. efficiency is of no interest). Also, the rate of total iron consumption is considered zero, as iron is not consumed. The consumption and generation rates of Fe^{2+}, and Fe^{3+} are assumed to be of equal magnitude. An expression for the reaction rate of each of the aforementioned species is as follows:

$$R_{I_c} = k_1 [I] \left[Fe^{2+}\right] + k_d [I] \tag{3.9}$$

$$R_{RA} = k_2 [RA] \left[Fe^{3+}\right] \tag{3.10}$$

$$R_{Fe^{2+}} = k_1 [I] \left[Fe^{2+}\right] - k_2 [RA] \left[Fe^{3+}\right] \tag{3.11}$$

Note that $[I]$, $[RA]$, $\left[Fe^{2+}\right]$ and $\left[Fe^{3+}\right]$ represent the concentrations of initiator, reducing agent, ferrous ions and ferric ions in the system, respectively. These rate expressions are used explicitly in Equations A.105 to A.109 in Appendix A. A further discussion on redox initiation, as it applies to the modelling of cold rubber production, can be found in Broadhead [15].

Radical Propagation

Once radicals are initiated, propagation can proceed with monomer according to the following mechanism:

$$R^{\cdot}_{n,i} + M_j \xrightarrow{k_{p_{ija}}} R^{\cdot}_{n+1,j} \tag{3.12}$$

where, $R^{\cdot}_{n,i}$ represents a radical of length n ending in monomer species i, M_j is a monomer unit of species j, and $k_{p_{ija}}$ is the rate coefficient for the propagation of radicals of type i with monomer j. Note that, for lack of evidence to the contrary, the chemically-controlled propagation rate constant is considered to be of equivalent value in both aqueous and particle phases.

In order to develop a tractable expression for the rate of polymerization a number of assumptions are employed. They are listed as follows:

1. The propagation rate constant is chain-length independent (equal-reactivity assumption (ERA)).
2. The reaction of monomer in reactions other than propagation is negligible. Thus the rate of propagation can be considered equivalent to the rate of polymerization (long-chain approximation of type I (LCA-I)).
3. The rate of propagation of radical i with monomer j is approximately equal to that of radical j with monomer i. In other words, in the long run the number of times monomer j follows monomer i is

approximately equivalent to monomer i following monomer j (long-chain approximation of type II (LCA-II)).

Taking into consideration the aforementioned assumptions, the overall rate of polymerization (total monomer consumption) can be defined. In general, this can be written as follows:

$$R_p = k_p [M] [R^{\cdot}] \tag{3.13}$$

To generalize Equation 3.13 to multicomponent systems, pseudo rate constants can be used according to Equation 3.14.

$$k_p = \sum_{j}^{N} \sum_{i}^{N} k_{p_{ij}} f_j \phi_i^{\cdot} \tag{3.14}$$

In the above two equations, $[M]$ is the total monomer concentration, $[R^{\cdot}]$ is the total radical concentration, f_j is the mole fraction of monomer j, and $\phi_i^{\cdot}$ is the fraction of radicals ending in monomer i. The radical and monomer concentrations, in each phase, are discussed in subsequent sections of this chapter.

Radical Termination

Radicals may terminate through a bimolecular reaction either by a combination of radical chains or by disproportionation, according to the following mechanism.

$$R_{n,i}^{\cdot} + R_{m,j}^{\cdot} \xrightarrow{k_{t_{ija}}} P_{(m+n)} \text{ or } P_n + P_m \tag{3.15}$$

For acrylonitrile, only limited information is available from Sarkar et al. [150] on the rate of termination in the aqueous phase. In contrast to developing an expression for the total rate constant using the pseudo method and considering that butadiene is quite insoluble in water, the total rate constant for radical termination is approximated by the rate constant for AN termination.

$$k_{t_a} \simeq k_{t_{a_{AN}}} \tag{3.16}$$

In addition to mutual radical termination, radicals can react with water impurities, such as oxygen or hydroquinone, forming dead molecules. A representative mechanism is as follows:

$$R_{n,i}^{\cdot} + Z_j \xrightarrow{k_{z_{ij}}} P_i \tag{3.17}$$

where, P_i is a dead oligoradical, Z_j represents a molecule of water impurity of type j, and $k_{z_{ij}}$ is the rate constant for reaction of radical i with impurity j. Information on the reactivity of impurities towards different monomers is often difficult to obtain. Thus, it is assumed that reaction with water-soluble impurities (WSI) is independent of the monomer type and only dependent on the impurity type.

The total rate of radical consumption by WSI's can be stated according to Equation 3.18:

$$R_z = k_z [Z]_a [R^{\cdot}]_a \tag{3.18}$$

where, $[Z]_a$ and $[R^{\cdot}]_a$ are the concentrations of impurities and radicals in the aqueous phase, respectively, and k_z is the overall WSI rate constant written as follows:

$$k_z = \sum_{j}^{N_z} k_{z_j} f_{z_j} \tag{3.19}$$

As previously mentioned, WSI's consume aqueous phase radicals very quickly (i.e. $R_z \gg R_{p_a}$), which leads to an induction period at the beginning of the polymerization until all the impurities have been consumed. This is shown in detail in Chapter 4 during model testing.

Radical Absorption/Desorption

Most modelling efforts assume that radicals are capturable from the point of initiation [70], while newer approaches consider that radicals must first achieve a certain chain length before capture [33, 160]. The approach of this work follows Dube et al. [33] and approximates the critical chain length for radical capture (z) based on what is known about the critical chain length for radical precipitation (j_{cr}) (i.e. $1 < z < j_{cr}$). A further discussion on this assumption is given in section 3.2.

The capture of radicals by micelles is known as micellar nucleation, and can be described through a radical diffusion or collision process. The main difference is that the rate of capture using the diffusional approach is proportional to a diffusivity coefficient, while when considering the collision process the rate is proportional to the total micelle surface area. The approach used in this work to model radical capture follows the collision process. In fact, both collision and diffusion theories become equivalent when the particle or micelle surface to volume ratio is high. The rate of capture by micelles can be stated according to Equation 3.20.

$$R_{cm} = k_{cm} A_m [R^{\cdot}]_a^{mic} / V_a \tag{3.20}$$

The rate of radical capture by existing particles is described using a similar equation to that used for capture by micelles. The expression can be written as:

$$R_{cp} = k_{cp} A_p [R^{\cdot}]_a^{par} / V_a \tag{3.21}$$

where, k_{cm} and k_{cp} are mass transfer coefficients for radical capture by micelles and particles, respectively, A_m is the free micellar surface area, A_p is the particle surface area, V_a is the volume of the aqueous phase, $[R^{\cdot}]_a^{mic}$, is the concentration of radicals in the aqueous phase that are capable of being captured by micelles, and $[R^{\cdot}]_a^{par}$ is a similar radical concentration for capture by particles. These concentrations are defined in section 3.2.

Radical desorption occurs when small molecules diffuse out of existing particles and back into the aqueous phase. Typically, this is a result of radical transfer to monomer or chain transfer agent. In the case of CTA, large molecules are generally used which are too bulky to desorb and therefore its contribution to desorption is usually not considered. The overall rate at which radicals desorb from the particle phase can be stated as follows:

$$R_{des} = k_{des}\left[R^{\cdot}\right]_p V_p / V_a \tag{3.22}$$

where, $\left[R^{\cdot}\right]_p$ is the total concentration of radicals in the particle phase, V_p is the total volume of the particle phase, and k_{des} is an apparent desorption rate constant in units of min^{-1}. Section 3.6 is dedicated to the explanation of radical desorption, so the reader is referred there for further information.

3.1.2 Particle Phase Reactions

Once radicals have traversed the aqueous phase into the particles, reactions proceed in the particles in the presence of a much higher concentration of polymer than in equivalent bulk polymerization conditions. The different possible fates considered for radicals in the particle phase are summarized in Table 3.2, and discussed further in the sections that follow.

Table 3.2: Particle phase phenomena involving radicals

Process	**Comments**
Reactions leading to active radicals	
Propagation	Radical chain propagation
Transfer to monomer	Radical transferred to a monomer unit (may lead to desorption)
Transfer to CTA	Radical transferred to a transfer agent
Reactions leading to chain branching	
Transfer to dead polymer	Re-activation of dead polymer (leads to tri-functional branching)
R_{xn} with internal or pendant double bonds	Leads to tetra-functional branching (i.e. cross-linking)
R_{xn} with terminal or residual double bonds	Leads to tri-functional branching (i.e. long-chain branching)
Reactions leading to inactive radicals	
R_{xn} with impurities	Radical consumption by monomer impurities (i.e. reduces $\bar{n}$)
Radical termination	Mutual termination by combination or disproportionation

Propagation

As is the case in the aqueous phase, radicals propagate with monomer according to the following mechanism:

$$R^{\cdot}_{n,i} + M_j \xrightarrow{k_{p_{ij_p}}} R^{\cdot}_{n+1,j} \tag{3.23}$$

For copolymerization systems, the cross propagation rate constants are defined from the reactivity ratios, which when considering the terminal model, can be defined as:

$$r_A = \frac{k_{p_{AA}}}{k_{p_{AB}}} \tag{3.24}$$

$$r_B = \frac{k_{p_{BB}}}{k_{p_{BA}}} \tag{3.25}$$

The general assumptions for particle phase radical propagation are the same as explained with aqueous phase propagation. In developing a polymerization rate expression, pseudo rate constants can be used to generalize the derivation, as previously explained; however, in the particle phase the appropriate radical concentration must be used. In the case of copolymerization, the general expression for the rate of polymerization given previously (Equation 3.13) can be restated for monomer j (where $j = A, B$) as follows:

$$R_{p_{j_p}} = \sum_i^N k_{p_{ij}} f_j \phi_i^{\cdot} [M]_p [R^{\cdot}]_p = \frac{k_{p_{AA}} k_{p_{BB}} \left(r_j [M_j]_p^2 + [M_A]_p [M_B]_p \right)}{k_{p_{BB}} r_A [M_A]_p + k_{p_{AA}} r_B [M_B]_p} [R^{\cdot}]_p \tag{3.26}$$

This equation demonstrates the transition from the multi-monomer case using pseudo rate constants to the more specific case of copolymerization expressed using only homo- and cross-propagation rate constants. If there are no diffusional limitations, the rate constants in the particle and aqueous phases are assumed to be the same, with the only obvious difference being the radical concentration (to be discussed later).

The fraction of radicals, used above, can be derived using the LCA-II as previously mentioned. After some algebraic manipulation a general expression can be derived as follows:

$$\phi_i^{\cdot} = \frac{\sum_{j;j\neq i}^N k_{p_{ji}} f_i}{\sum_s^N \sum_{t;t\neq s}^N k_{p_{ts}} f_s} \tag{3.27}$$

which, for the copolymerization case, it reduces to:

$$\phi_A^{\cdot} = \frac{k_{p_{BA}} f_A}{k_{p_{BA}} f_A + k_{p_{AB}} f_B} \tag{3.28}$$

$$\phi_B^{\cdot} = 1 - \phi_A^{\cdot} \tag{3.29}$$

The mole fraction of monomer j is derived, as usual, from the moles of each monomer in the particle phase. It should be clear from the above derivations that the rate of polymerization is dependent on both the monomer and radical concentrations in each particular phase.

Chain Transfer

Apart from propagating, radicals can transfer their activity to other surrounding species. The reactions considered here are listed in Table 3.2, and will be discussed in sequence. Note that transfer to emulsifier

and solvent, as well the phenomenon of radical back-bitting (i.e. intramolecular transfer leading to short-chain branching) were all considered negligible in an NBR system.

Radicals may undergo chain transfer to monomer according to the following mechanism:

$$R_{n,i}^{\cdot} + M_j \xrightarrow{k_{fm_{ij}}} P_{n,i} + R_{1,j}^{\cdot} \tag{3.30}$$

In the above reaction the radical centre is transferred from the growing radical chain to a single monomer unit, thus producing a dead polymer chain and a radical of unit chain length. Radicals of such a small length can easily diffuse through the polymer mass and potentially desorb from the polymer particle. Therefore, transfer to monomer is of considerable importance when assessing if a particular system will exhibit radical desorption. Typically systems involving butadiene show very little desorption (i.e. case II kinetics), while systems of vinyl acetate (VAc) show considerable desorption ($\bar{n} \ll 0.5$). Table 3.3 gives an indication of the transfer to monomer rate coefficient comparing AN, Bd and VAc. These rate constants are for transfer to like monomers (i.e. radicals ending in AN to AN monomer). Notice that the k_{fm} for VAc dominates Bd, and is only slightly larger than that of AN at low temperatures. This might lead one to think that transfer to AN is important; however CTA plays a dominant role in AN/Bd systems and when considering the rate of transfer to CTA, it is considerably greater than for transfer to monomer. As well, there is no experimental evidence to suggest that transfer to monomer leads to radical desorption for an AN system.

In an attempt to reduce the number of uncertain parameters, radical transfer to an unlike monomer was neglected in the model development (i.e. $k_{fm_{AB}} \simeq 0$ and $k_{fm_{BA}} \simeq 0$). A similar approximation was made by Broadhead [15], while Vega et al. [172] assume that transfer from like and unlike radicals to the same monomer is approximately equivalent (i.e. $k_{fm_{AA}} \simeq k_{fm_{BA}}$). This assumption is explored further in section 4.1.5.

Table 3.3: Transfer to monomer rate constant comparison

	Transfer to Monomer - k_{fm} (L/mol/min) [a]		
T ^oC	AN	Bd	VAc
60	4.14	1.58	3.6 [b]
10	0.22	0.05	0.26
5	0.15	0.03	0.19

[a] as calculated from the Arrhenius expressions given in Appendix C
[b] calculated from $k_{fm} = 1.117 \times 10^7 \exp(-9895/RT)$ L/mol/min [55]

As alluded to above, transfer to CTA plays an important role in NBR/SBR systems. More specifically, CTA is designed to regulate the polymer molecular weight by promoting chain-transfer. The transfer reaction proceeds when a radical chain abstracts a labile hydrogen molecule from a CTA molecule (e.g. mercaptan) producing a dead polymer molecule and a new radical composed of the CTA molecule. The CTA is specifically designed to be a large molecule in order to prevent the possibility of radical desorption.

The reaction mechanism can be stated as follows:

$$R^{\cdot}_{n,i} + CTA \xrightarrow{k_{fcta_i}} P_{n,i} + CTA^{\cdot} \tag{3.31}$$

where, k_{fcta_i} is the individual CTA rate constant for reaction with monomer i. The overall pseudo rate constant can be derived to give:

$$k_{fcta} = \sum_{i}^{N} k_{fcta_i} \phi^{\cdot}_i \tag{3.32}$$

A further discussion on the transfer coefficient for transfer to CTA will be given in section 3.10.

In addition to radical transfer to small molecules, radical activity can transfer to large polymer molecules. The general mechanism can be represented as follows:

$$R^{\cdot}_{n,i} + P_{m,j} \xrightarrow{k_{fp_{ij}}} P_{n,i} + R^{\cdot}_{m,j} \tag{3.33}$$

In the above reaction, transfer occurs when a hydrogen atom is abstracted from the polymer backbone. This leads to an internal radical that further propagates forming a tri-functional branch point. The relative number of these branch points is indicative of the overall degree of long-chain branching (LCB) within the polymer. Moreover, as branching increases, so does the weight-average molecular weight, and when observing the entire molecular weight distribution a distinct shouldering effect becomes evident.

As noted by Dube et al. [33], chain-branching in styrene-acrylonitrile (SAN) systems is not typically observed in practice. This suggests that AN units within the dead polymer molecule are not likely to give up a hydrogen atom, due to the limited electron withdrawing effect of the cyano- group whereby the hydrogen atoms remain fairly stable. Therefore, it is assumed that transfer to polymer will only involve butadiene units within the polymer chain (i.e. $k_{fp_{BA}} \simeq 0$ and $k_{fp_{AA}} \simeq 0$). However, one may find that including these parameters provides a better fit to molecular weight data. Thus, these parameters can be used as an extra degree of freedom for model fitting.

In general, the overall pseudo-rate constant for transfer to polymer is:

$$k_{fp} = \sum_{i}^{N} \sum_{j}^{N} k_{fp_{ij}} \phi^{\cdot}_i \overline{F}_j \tag{3.34}$$

Notice here that each individual rate constant is now weighted by the cumulative copolymer composition and not the monomer composition.

Besides chain branching from transfer to polymer, radicals may react directly with an internal or terminal double bond within the dead polymer. Reactions with terminal double bonds lead to the formation of internal radicals that propagate to form tri-functional branch points and eventually lead to long-chain branches. By comparison, reactions with internal double bonds lead to tetra-functional branching, otherwise known as cross-linking. The mechanism for both reactions can be written as follows:

$$R^{\cdot}_{n,i} + P^{i=}_{m,j} \xrightarrow{k^{**}_{p_{ij}}} R^{\cdot}_{n+m} \tag{3.35}$$

$$R_{n,i}^{\cdot} + P_{m,j}^{t=} \xrightarrow{k_{p_{ij}}^{*}} R_{n+m}^{\cdot} \tag{3.36}$$

In theory, reactions could occur with both internal and terminal double bounds; however, in practice reactions with terminal double bonds are not typically observed with rubber systems. This is apparent from a minimal change in the number-average molecular weight with increasing conversion under isothermal batch conditions. Based on these observations, the rate constants for terminal double bond polymerization are assumed to be negligible for an NBR system. A similar approach was taken by Dube et al. [33] and Vega et al. [171] for NBR and by Broadhead et al. [16] and Gugliotta et al. [61] for SBR.

In a similar manner to k_{fp}, the overall pseudo-rate constant for internal double-bond polymerization (k_p^{**}) is defined as:

$$k_p^{**} = \sum_{i}^{N}\sum_{j}^{N} k_{p_{ij}}^{**} \phi_i \overline{F}_j \tag{3.37}$$

where, for obvious reasons (i.e. AN units do not contribute to internal double bond formation), $k_{p_{AA}}^{**} = 0$ and $k_{p_{BA}}^{**} = 0$.

Termination

Radical termination can occur through a mutual radical-radical interaction or from a reaction with monomer impurities. As is the case in the aqueous phase, mutual termination occurs when two radicals collide and terminate through a combination or disproportionation mechanism, represented as follows:

$$R_{n,i}^{\cdot} + R_{m,j}^{\cdot} \xrightarrow{k_{tc_{ij}}} P_{(m+n)} \tag{3.38}$$

$$R_{n,i}^{\cdot} + R_{m,j}^{\cdot} \xrightarrow{k_{td_{ij}}} P_m^{t=} + P_n \tag{3.39}$$

where, k_{tc} and k_{td} are the termination rate constants for combination and disproportionation; $P_{(m+n)}$ represents polymer formed from radical combination; $P_m^{t=}$ corresponds to polymer with a terminal double bond and P_m signifies a dead polymer chain. The two termination rate constants, k_{tc} and k_{td}, are defined through the overall termination rate constant, k_t, and the ratio, γ, that describes the fraction of termination by disproportionation occurring in the system. These are defined as follows:

$$\gamma = k_{td}/k_t \tag{3.40}$$

$$k_t = k_{tc} + k_{td} \tag{3.41}$$

In order to use these relations, an appropriate method must first be used to describe the overall termination rate constant, k_t. As polymerization proceeds, the polymer chains grow and become more entangled making it more difficult for radicals to diffuse through the reaction medium (i.e. polymer mass). In emulsion polymerization, the particles contain a significant amount of polymer (e.g. greater than 30% by volume), from the onset of particle nucleation. The high concentration of polymer creates a viscous environment that diffusion-

ally limits the movement of radicals. In order to properly model this behaviour, diffusion-controlled effects must be considered. The two common approaches used to describe diffusional limitations are either based on free-volume theory or are simply empirical in nature. Free-volume theory requires knowledge of numerous parameters (thermodynamic and physical properties) that may not be readily known nor easily estimated. For this reason, the more practical approach, and the approach used in this thesis, is the development of a semi-empirical expression. In general, termination can pass through three different regimes of diffusion-controlled behaviour: segmental-diffusion (low conversion, mainly chemically controlled), translational-diffusion (moderate to high conversion), and reaction-diffusion (high conversion). The conversion during the production of NBR is typically not allowed to go beyond 80%, thus reaction-diffusion is typically not observed. Segmental and translational diffusion can be adequately taken into account using a polynomial expression where k_t is described as a function of conversion, according to the following expression:

$$k_t = k_{t_o} \exp(A_1 X + A_2 X^2 + A_3 X^3) \tag{3.42}$$

$$X = \begin{cases} x_c & \text{if } V_d > 0 \\ x & \text{otherwise} \end{cases}$$

where, A_1, A_2, and A_3 are adjustable parameters, k_{t_o} is the chemically-controlled termination rate constant, and X is conversion. When monomer droplets exist, the conversion is set to a constant value of x_c, whereas after the droplets disappear the conversion is set to its actual value for the remainder of the reaction. Using this methodology, k_t will remain constant (somewhere below k_{t_o}) until the droplets disappear, after which point the value will steadily decrease as conversion increases. As stated by Dube et al. [33], this approach is probably the only practical way of handling k_t in multicomponent industrial polymerization systems.

The chemically-controlled rate constant, seen above, can be determined by the usual pseudo-approach, as follows:

$$k_{t_o} = \sum_i^N \sum_j^N k_{t_{o_{ij}}} \phi_i^{\cdot} \phi_j^{\cdot} \tag{3.43}$$

where, termination between like radicals is described through an Arrhenius expression, while termination between unlike radicals can be expressed as follows:

$$k_{t_{o_{ij}}} = \phi_{wall} \left(k_{t_{o_{ii}}} k_{t_{o_{jj}}} \right)^{1/2} \tag{3.44}$$

For the interested reader, details on free-volume theory have been reviewed by Hamielec et al. [68] and Dube et al. [34]. A recent discussion on semi-empirical approaches to modelling k_t through the different regimes of diffusion-controlled behaviour has been provided by Hutchinson and Penlidis [76].

In addition to mutual radical termination, radicals can terminate by reacting with monomer-soluble impurities (MSI) that enter the system with the monomer feedstock, from the recycle of residual monomer, or from a number of other possible routes within an industrial process. Monomer impurities reside mainly in the organic phase and diffuse into the particles alongside the monomer. Typical impurities in rubber systems

are 4-t-butyl catechol (TBC), vinyl acetylene, hydroquinone (HYQ), and dissolved oxygen. On an industrial level, TBC and vinyl acetylene usually enter the system from impure monomer feedstock; HYQ is added as a short-stop to terminate the polymerization ($\sim 70\%$ conversion), and in reactor trains, HYQ is added to the final reactor and subsequently recycled back to the monomer feedstock, after latex stripping, creating further contamination; oxygen enters from the reactor headspace, due to poor or nonexistent evacuation. A representative reaction for radical consumption by monomer impurities is as follows:

$$R_{n,i}^{\cdot} + MSI_j \xrightarrow{k_{fmsi_{ij}}} P_i \tag{3.45}$$

where, MSI_j and P_i signify impurity and dead polymer. The overall pseudo-rate constant that accounts for multiple impurities with different monomer reactivities can be written as follows:

$$k_{fmsi_p} = \sum_{i}^{N} \sum_{j}^{N_{msi}} k_{fmsi_{ij}} \phi_i^{\cdot} f_{msi_j} \tag{3.46}$$

In general, very little is known on the individual impurity rate constants with respect to each monomer. It is often more convenient to assume equal monomer reactivity, thereby reducing the expression above to only a function of each MSI. This reduction is as follows:

$$k_{fmsi_p} = \sum_{j}^{N_{msi}} k_{fmsi_j} f_{msi_j} \tag{3.47}$$

Monomer impurities can have a dramatic effect on the rate of polymerization that affects particle nucleation, growth and molecular weight. Thus, careful consideration must be given when assessing industrial or lab scale polymerization data.

3.2 Particle Nucleation

The overall number of particles nucleated can be determined by considering all possible mechanisms that produce or consume particles within the reactor. Typically micellar and homogeneous mechanisms are used to model monomer systems where one or more of the monomers is water soluble [33]. However, coagulative nucleation has been suggested to be an intimate part of the homogeneous mechanism and thus in some cases should be considered [59]. The decision to further complicate the model by considering aspects of coagulation should be based on whether any improvement is made by doing so. When considering a monodisperse particle size, as is the case in this work, coagulation tends not be as important when compared to modelling the entire distribution. Thus, coagulation will not be discussed here.

An overall balance on the number of particles that enter, leave, and are generated within a continuous reactor can be given as follows:

$$\frac{dN_p}{dt} = F_{p_{in}} - F_p + (R_{mic} + R_{hom}) V_a \tag{3.48}$$

where, $F_{p_{in}}$ and F_p are the particle flow rates, and R_{mic} and R_{hom} are the rates of nucleation by micellar and homogeneous mechanisms.

3.2.1 Nucleation Rates

The rate of micellar nucleation, R_{mic}, has in the past been modelled using the well known theory of Smith and Ewart [154]. The rate of homogeneous nucleation, R_{hom}, was first introduced by Fitch and Tsai [42]. Since these initial theories of Smith & Ewart and Fitch & Tsai, methods to describe micellar and homogeneous nucleation have advanced to describe a more detailed picture of particle formation. Such modifications put forth, are those by Nomura [121], and Hansen and Ugelstad [70]. Using aspects from these most recent theories, Hamielec et al. [68], Penlidis and Dube [137] and Dube et al. [33, 34] have described methods for particle nucleation, which will now be examined in further detail.

Micellar Nucleation

Micellar nucleation occurs when a radical is absorbed into a micelle forming a polymer particle. The process can be described using radical collision or diffusion theories. General expressions for radical capture can be given as:

$$R_{cap} = \frac{k_{cm} A_m}{V_a} [R^{\cdot}]_a N_A \tag{3.49}$$

$$R_{cap} = 4\pi r_{mic} D_w F [R^{\cdot}]_a N_A \tag{3.50}$$

where, k_{cm} is a mass transfer coefficient for radical capture, D_w is the diffusivity of radicals in the aqueous phase, and F is an efficiency factor. A review of these approaches can be found in Gao and Penlidis [53]. In this work the collision process for radical capture will be used (Equation 3.49).

The rate of micellar nucleation describes the rate at which particles are formed when a radical in the aqueous phase is captured by a micelle. An expression for this rate and hence the rate of nucleation can be given by Equation 3.51 [137].

$$R_{mic} = \left(R_{des}^{mic} + \frac{k_{cm} [R^{\cdot}]_a^{mic}}{r_{mic}} \right) N_A \tag{3.51}$$

where, R_{des}^{mic} accounts for the rate at which desorbed radicals are recaptured by micelles, thus creating new particles (see Equation A.42 in Appendix A), and the second portion of this equation accounts for the usual capture of radicals formed from the initiator, where k_{cm} is the rate constant for radical capture by micelles (i.e. mass-transfer coefficient), $[R^{\cdot}]_a^{mic}$ represents the concentration of radicals in the aqueous phase that are capable of becoming captured by micelles, and r_{mic} is the radius of a micelle.

In this development, it is assumed that micelles are monodisperse with a constant radius. As well, only a fraction of the radicals initiated can become captured by micelles, while the remaining are captured

by particles or undergo homogeneous nucleation. It is important that in developing a rate expression for micellar nucleation all three of these processes be considered, especially if homogeneous nucleation is of major influence. Expressions that ignore homogeneous nucleation are much more straightforward. For example, Broadhead et al. [16] modelled an SBR system where homogeneous nucleation was ignored, and their rate expression was derived considering a direct proportion to the radical concentration formed from initiator. In other words, all radicals formed from the initiator are capable of being captured by a micelle. Excluding the radical re-capture term in Equation 3.51, their expression was as follows:

$$R_{mic} = R_I \left(\frac{A_m}{A_m + \varepsilon A_p} \right) N_A \tag{3.52}$$

where, R_I is the rate of initiation, A_m and A_p are the free emulsifier area and polymer particle surface area, respectively, and ε is the capture efficiency for particles relative to micelles.

In developing an expression for radicals capturable by micelles and particles, a similar approach to Equation 3.52, where a capture efficiency is considered, is used. Further details are given in section 3.3.

Homogeneous Nucleation

Homogeneous nucleation occurs when radicals grow in the aqueous phase to a length at which they become insoluble and precipitate forming polymer particles. The particle formation process considered in this work uses HUFT theory, where the aqueous phase radical concentration is determined by performing a population balance on radicals of chain length less than their critical value (j_{cr}).

In general, the rate of homogeneous nucleation can be written as follows [70]:

$$R_{hom} = k_{p_a} \left[R^{\cdot}_{j_{cr}-1} \right]_a [M]_a N_A \tag{3.53}$$

This equation reflects that a particle is formed (at a length of j_{cr}) when a radical of chain length $(j_{cr}-1)$ reacts with a monomer unit, thus causing the radical to precipitate from solution. In some cases, radicals can precipitate before they reach their theoretical stability limit. For example, if monomer B (butadiene) adds to a radical ending in A (acrylonitrile) this may cause the polymer to become so hydrophobic that precipitation occurs immediately. Thus, to generalize Equation 3.53, the following re-formulation can be performed [33]:

$$R_{hom} = k_h \left[R^{\cdot} \right]_a^{hom} V_a N_A \tag{3.54}$$

As the number of particles increases, the homogeneous nucleation rate constant (k_h) decreases quite quickly, eventually dying off completely and signaling the end of homogeneous nucleation. The fundamental basis for k_h comes from Fitch and Tsai [42], who defined it in terms of one adjustable parameter (k_{h_o}) as follows:

$$k_h = \begin{cases} k_{h_o} \left(1 - \frac{LA_p}{4V_a} \right) & \text{if } LA_p < 4V_a \\ 0 & \text{otherwise} \end{cases} \tag{3.55}$$

where, L represents the average distance a radical travels before precipitation, which is believed to be around 10^{-4} dm in magnitude. Though L is usually set as a parameter, it can be calculated from Einstein's diffusion law as:

$$L = \left(\frac{2D_w j_{cr}}{k_p [M]_a^{sat}} \right)^{1/2} \tag{3.56}$$

k_{h_o}, on the other hand, represents the initial rate constant at zero conversion, and is often set indirectly by specifying an efficiency factor that is defined as the fraction of radicals formed by homogeneous to micellar nucleation (μ). This fraction is given as follows:

$$\mu = k_{h_o}/k_{cm} \tag{3.57}$$

3.3 Radical Concentrations

Free radicals are generated in the aqueous phase from either a redox reaction or thermal decomposition of the initiator. In the case of water soluble monomers, initiator fragments propagate with monomer units (i.e. they form oligoradicals) until they are captured by micelles, particles, react with water impurities, or terminate through mutual radical termination. In this section expressions for the overall average radical concentration in aqueous and particle phases are derived.

3.3.1 Aqueous Phase

The concentration of radicals in the aqueous phase is determined by considering all possible fates that a radical may have. In general, radical balances can be written to track the consumption and generation of radicals. An example is as follows:

$$\frac{d[R_{in}^{\cdot}]_a}{dt} = R_I - k_{p_a}^{'}[R_{in}^{\cdot}]_a[M]_a - k_z[R_{in}^{\cdot}]_a[Z]_a \tag{3.58}$$

$$\frac{d[R_1^{\cdot}]_a}{dt} = R_{des} + k_{p_a}^{'}[R_{in}^{\cdot}]_a[M]_a - k_{p_a}[R_1^{\cdot}]_a[M]_a - k_z[R_1^{\cdot}]_a[Z]_a - k_{t_a}[R_1^{\cdot}]_a[R^{\cdot}]_a \tag{3.59}$$

$$\frac{d[R_k^{\cdot}]_a}{dt} = k_{p_a}[R_{k-1}^{\cdot}]_a[M]_a - k_{p_a}[R_k^{\cdot}]_a[M]_a - k_z[R_k^{\cdot}]_a[Z]_a - k_{t_a}[R_k^{\cdot}]_a[R^{\cdot}]_a - R_{cm} - R_{cp} \tag{3.60}$$

The above balances assume that radicals of any size can be captured by micelles or particles. However, it is more commonly accepted that radicals must first reach a certain size before they can become irreversibly absorbed. For an AN/Bd system, previous modelling efforts [33, 137] assumed that radicals of chain length greater than $j_{cr}/2$ are capturable, Bd radicals precipitate at a length of $j_{cr}/2$, and AN radicals precipitate at j_{cr} unless a Bd unit is added at which point the radical immediately precipitates to form a particle. Therefore, Equation 3.60 can be rewritten in pseudo form for two cases: chain lengths $k = 2$ to $j_{cr}/2$ and $k = j_{cr}/2+1$ to $j_{cr}-1$.

For $k = 2$ to $j_{cr}/2$:

$$\frac{d\left[R_k^{\cdot}\right]_a}{dt} = k_{p_a}\left[R_{k-1}^{\cdot}\right]_a[M]_a - k_{p_a}\left[R_k^{\cdot}\right]_a[M]_a - k_z\left[R_k^{\cdot}\right]_a[Z]_a - k_{t_a}\left[R_k^{\cdot}\right]_a[R^{\cdot}]_a \tag{3.61}$$

For $k = j_{cr}/2+1$ to $j_{cr}-1$:

$$\frac{d\left[R_k^{\cdot}\right]_a}{dt} = k_{p_a}\left[R_{k-1}^{\cdot}\right]_a[M]_a - k_{p_a}\left[R_k^{\cdot}\right]_a[M]_a - k_z\left[R_k^{\cdot}\right]_a[Z]_a - k_{t_a}\left[R_k^{\cdot}\right]_a[R^{\cdot}]_a - R_{cm} - R_{cp} \tag{3.62}$$

At $k = j_{cr}$:

$$\frac{d\left[R_{j_{cr}}^{\cdot}\right]_a}{dt} = k_{p_a}\left[R_{j_{cr}-1}^{\cdot}\right]_a[M]_a - R_{cm} - R_{cp} \tag{3.63}$$

Typically equations 3.58 to 3.63 are not solved in their dynamic form. Instead they are approximated using the steady-state hypothesis (SSH) and solved as a system of algebraic equations. The SSH has been proven to be a valid assumption beyond the first 10 seconds of initiation where transient effects die out [70]. Notice as well, that radical in and out flow terms are neglected in the previous balances, as these terms are assumed to be of a small and equal magnitude and therefore have negligible contribution to the overall aqueous phase radical concentration. Also, Equation 3.63 represents the hypothetical radical concentration at j_{cr}, where radicals can either undergo homogeneous nucleation, or be captured by micelles or particles.

By applying the SSH to the previous balances, the total radical concentration can be obtained by summing up all radicals of length k ending in monomer unit i, as follows:

$$[R^{\cdot}]_a = [R_{in}^{\cdot}]_a + \sum_{i=1}^{N}\sum_{k=2}^{jcr-1}\left[R_{k,i}^{\cdot}\right]_a \tag{3.64}$$

The steady-state concentration of radicals that may be captured by micelles, $[R^{\cdot}]_a^{mic}$, can be determined by considering all radicals of chain-length greater than $j_{cr}/2$. An expression can be written as follows:

$$[R^{\cdot}]_a^{mic} = \sum_{k=jr/2+1}^{jcr-1}[R_k^{\cdot}]_a\left(\frac{A_m}{A_m+\varepsilon A_p}\right) + \left[R_{jcr}^{\cdot}\right]_a\left(\frac{A_m}{A_m+\varepsilon A_p+\mu H}\right) \tag{3.65}$$

In a similar manner, the concentration of radicals that may be captured by particles, $[R^{\cdot}]_a^{par}$, can be given as:

$$[R^{\cdot}]_a^{par} = \sum_{k=jr/2+1}^{jcr-1}[R_k^{\cdot}]_a\left(\frac{\varepsilon A_p}{A_m+\varepsilon A_p}\right) + \left[R_{jcr}^{\cdot}\right]_a\left(\frac{\varepsilon A_p}{A_m+\varepsilon A_p+\mu H}\right) \tag{3.66}$$

Furthermore, the concentration of radicals that may undergo homogeneous nucleation, $[R^{\cdot}]_a^{hom}$, can be written as:

$$[R^{\cdot}]_a^{hom} = \left[R_{jcr}^{\cdot}\right]_a\left(\frac{\mu H}{A_m+\varepsilon A_p+\mu H}\right) \tag{3.67}$$

where H, in the above expression, corresponds to the fraction homogeneous nucleation occurring in the

system and is defined as:

$$H = \frac{k_h}{k_{h_o}} V_a \tag{3.68}$$

Further details on the above equations can be found in Appendix A, as well as in Dube et al. [34].

3.3.2 Particle Phase

In the particle phase the concentration of radicals can be defined in terms of the total number of particles and the average number of radicals per particle. Some approaches consider the entire particle size distribution where each radical of type i and length l is accounted for within each particle of volume V at time t [149], while other approaches assume a monodisperse size distribution where all particles are nucleated at the same time and grow at the same rate. Regardless of the approached used, the general expression for the total radical concentration can be stated as follows:

$$[R^{\cdot}]_p = \frac{\bar{n} N_p}{V_p N_A} \tag{3.69}$$

where, in the case of a polydisperse distribution each particle j of a different class V (i.e. $N_p = \sum_j N_{p,j}(V,t)$) and the total average number of radicals i in each particle class j (i.e. $\bar{n} = \sum_j \sum_i n_{i,j} N_{p,j}(V,t) / \sum_j N_{p,j}(V,t)$) would have to be accounted for. The model in this work will not calculate the entire PSD, as at this point partial information on the distribution will suffice. Thus, for the time being an approximate monodisperse particle size distribution will be used, and if the need presents itself at a later time approximate information of the PSD can be readily obtained with only minor modifications to the current model [15, 136].

3.4 Monomer Partitioning

Besides particle nucleation, monomer partitioning is of great importance in an emulsion system in order to properly determine the rate of polymerization, copolymer composition, conversion, and molecular weights. In a multiphase system, monomer partitions between each phase depending on its relative phase solubility. As well, the rate of monomer mass transfer is typically much higher than the rate of polymerization, thus a thermodynamic equilibrium of the monomer between each phase exists while each of the three phases are present. Considering these aspects, much of the theoretical work on monomer partitioning has been on establishing accurate thermodynamic models, based on Flory-Huggins theory, to estimate the concentration of monomer in each phase [94, 112, 166].

Assuming negligible volume change from mixing and immiscibility of water in the monomer or particle

phase, the following general balances can be written for monomer i in each phase:

$$V_a = \sum_i^N V_i^a + V_w \tag{3.70}$$

$$V_p = \sum_i^N V_i^p + V_{pol} \tag{3.71}$$

$$V_d = \sum_i^N V_i^d \tag{3.72}$$

$$\sum_i^N V_i = \sum_i^N \left(V_i^a + V_i^p + V_i^d \right) \tag{3.73}$$

Using these general balances, a number of different partitioning models can be defined to determine the individual monomer volumes and concentrations in each phase.

Morton et al. [112] was the first to propose a quantitative theory for partitioning based on Flory-Huggins thermodynamic theory that considered monomer saturated particles (i.e. stage II). Vanzo et al. [169] extended Morton's model to include partial swelling of the polymer particles (i.e. stage III). A detailed review of these models considering multicomponent systems was given by Ugelstad et al. [166]. Extensions were further made by Maxwell et al. [94, 95], Noel et al. [117, 118], and Schoonbrood et al. [151] who developed semi-empirical relations that removed the dependence on the Flory-Huggins interaction parameters present in the Morton/Vanzo equations. Kiparissides et al. [83] propose an empirical approach to determining the monomer concentration in the particle phase based on a parameter to signal when the droplets disappear (i.e. x_c), while Dougherty [31] used a similar approach with the inclusion of a second parameter to allow for monomer water solubility. Hamielec and MacGregor [67] and Omi et al. [129] developed an empirical approach based on constant partition coefficients and an overall mass balance, in order to determine the monomer concentrations in each phase over the entire course of polymerization.

In this section, three particular partitioning methods will be discussed: the thermodynamic approach (theoretical), the critical conversion approach (empirical), and the constant partition coefficient approach (semi-empirical). More emphasis will be given to the latter method as this is the approach implemented in the model of this thesis.

3.4.1 Thermodynamic Approach

Much of what is known on the thermodynamic partitioning of monomers stems from the early works of Morton et al. [112] and Vanzo et al. [169]. Since these early publications, the theory has been refined to account for multiple monomers under conditions of both saturated particles (i.e. stage I and II when droplets exist) and partially saturated particles (i.e. stage III when the droplets have disappeared). The development shown here will highlight some key ideas of the thermodynamic approach; however, for further details the reader is referred to the papers of Liu et al. [92] and Gao and Penlidis [53], as well as to recent discussions by Leiza and Meuldijk [87] and Fortuny et al. [47].

At equilibrium, the molar free energies (ΔG) of monomer j in each phase are equal. In stage I and II the following balances can be written:

$$\left(\frac{\Delta G}{RT}\right)_j^p = \left(\frac{\Delta G}{RT}\right)_j^a \tag{3.74}$$

$$\left(\frac{\Delta G}{RT}\right)_j^p = \left(\frac{\Delta G}{RT}\right)_j^d \tag{3.75}$$

$$\left(\frac{\Delta G}{RT}\right)_j^a = \left(\frac{\Delta G}{RT}\right)_j^d \tag{3.76}$$

while, in stage III the droplet phase is no longer present and Equations 3.74 and 3.75 are removed from the model. The thermodynamic relations for the above chemical potentials can be written as follows:

$$\begin{aligned}\left(\frac{\Delta G}{RT}\right)_j^p &= \ln\phi_j^p + (1-m_{ji})\,\phi_i^p + \phi_p^p + \chi_{ji}\left(\phi_i^p\right)^2 + \chi_{jp}\left(\phi_p^p\right)^2 \\ &\quad + \phi_i^p\phi_p^p\left(\chi_{ji}+\chi_{jp}+\chi_{ip}m_{ji}\right) + \frac{2\sigma_j\overline{V}_j}{r_pRT}\end{aligned} \tag{3.77}$$

$$\left(\frac{\Delta G}{RT}\right)_j^d = \ln\phi_j^d + (1-m_{ji})\,\phi_i^d + \chi_{ji}\left(\phi_i^d\right)^2 \tag{3.78}$$

$$\left(\frac{\Delta G}{RT}\right)_j^a = \ln\left(\frac{\phi_j^a}{\phi_{j,sat}^a}\right) \tag{3.79}$$

where, Equation 3.77 describes the chemical potential of monomer j in the particle phase, which can be considered the most general form of the chemical potential regardless of the phase. Equation 3.78 describes the chemical potential in the droplet phase assuming negligible free-energy contribution from large monomer droplets. Equation 3.79 provides an approximation for the free-energy in the aqueous phase. Furthermore, ϕ_i^k represent the volume fraction of monomer i or j ($i \neq j$) in phase k; m_{ij} represents the ratio of molar volumes ($\overline{V}_j$) of monomers i and j; χ_{ij} corresponds to the monomer-monomer or monomer-polymer Flory-Huggins interaction parameters; σ_j represents the interfacial tension of monomer j; finally, r_p represents the monomer-swollen particle radius. Symbols not described here are shown in the nomenclature.

Combining the mass balance equations for each monomer in each phase (i.e. Equations 3.70-3.73) with the equilibrium balances above (i.e. Equations 3.74-3.76), a system of non-linear equations can be solved for each volume fraction (e.g. ϕ_i^k and ϕ_p^p). As pointed out by Gao and Penlidis [53], the solution of this system (i.e. convergence to a unique solution) is highly dependent on the initial guesses used for the ϕ's (i.e. solution variables of the system), and can be quite sensitive to small changes in the ϕ's (i.e. the system can be quite stiff). As an alternative to solving the system through a gradient based method (i.e. Newton-Raphson, which often requires excellent initial guesses, or a conjugate-gradient based minimization problem), Armitage et al. [5] have proposed an approximate iterative algorithm, using a particular formulation of the aforementioned equations, that was proven to provide adequate partitioning results [53, 60]. A detailed version of this

algorithm is provided in Appendix B.

Besides having to provide fairly good initial guesses, another drawback to solving the thermodynamic equations in the above form is the limited availability of decent estimates of the Flory-Huggins interaction parameters (χ_{ij}). Poor estimates can, and usually will, lead to very poor predictions of the volume fractions, which propagates through to the respective monomer concentrations. Furthermore, to employ Equation 3.77 the particle radius must be known, which can be determine from Equation 3.80; however, this requires the fraction of polymer in the particle phase (ϕ_p^p), which is initially unknown (since V_p is unknown) and must be guessed and iterated upon until convergence in V_p.

$$r_p = \left(\frac{3V_{pol}}{4\pi N_p \phi_p^p} \right)^{1/3} \tag{3.80}$$

3.4.2 Critical Conversion Approach

The so-called critical conversion approach tries to correlate the point in time when the monomer droplets disappear through the use of a parameter called x_c. This requires a considerable amount of experimental data to properly estimate the critical conversion, and as pointed out by Dube et al. [34], the approach in general is only really practical when simulating the reactor under a narrow range of operability.

For a homopolymer system, the volume fraction of polymer in the particle phase can be derived from a mass balance to give the following expression:

$$\begin{aligned} \phi_m^p &= \frac{(1-x)}{1-x\left(1-\frac{\rho_m}{\rho_p}\right)} \\ x &= \begin{cases} x_c & \text{if } X \leq x_c \\ X & \text{otherwise} \end{cases} \end{aligned} \tag{3.81}$$

where, X corresponds to the conversion a time t and x_c represents the critical conversion parameter.

If the monomer is insoluble in the aqueous phase then the fraction in the droplet phase can easily be obtained by taking the difference between the total monomer in the system and the amount in the particle phase. On the other hand, if the monomer is moderately soluble in the aqueous phase then this must be accounted for either through a modification of the above expression [31], or by assuming a saturation concentration based on the solubility.

An extension of the above equation to copolymer systems has been derived and discussed by Penlidis

[136]. In its final form, ϕ_i^p for monomer i where $i = 1,2$, can be expressed as follows:

$$\begin{aligned} \phi_i^p &= \frac{(1-x_i)}{1-x_i\left(1-\frac{\rho_i}{\rho_p}\right)+\left(1-x_j\left(1-\frac{\rho_j}{\rho_p}\right)\right)\frac{V_{jo}}{V_{io}}} \\ x_i &= \begin{cases} x_{c_i} & \text{if } X_i \leq x_{c_i} \text{ and } i \neq j \\ X_i & \text{otherwise} \end{cases} \end{aligned} \tag{3.82}$$

where, two parameters are now required to signal the disappearance of each monomer (x_{c_1} and x_{c_2}), and a weighting term (V_{j_o}/V_{i_o}) is included that places a dependence on the ratio of each monomer in the initial reactor charge.

Both of the above relations, for homo- and copolymerization, provide a rather simple approach to determining approximate monomer concentrations in each phase. However, due to differing monomer/ polymer/water solubilities, establishing estimates for the critical conversion in a copolymer system can be quite difficult and may not necessarily correspond to those determined from each individual homopolymer system. Thus, as the number of monomers increases the critical conversion approach becomes less attractive and essentially implausible beyond two monomers.

3.4.3 Constant Partition Coefficient Approach

A more practical method compared to the x_c-approach and a much simpler method computationally speaking compared to the thermodynamic approach, is the constant partition coefficient model. In this approach, the fraction of monomer in each respective phase (or concentration) is defined in terms of partition coefficients, which are assumed to remain constant over the course of polymerization. The coefficients are determined from experimental or industrial data through typical parameter estimation procedures.

The coefficient describing the equilibrium partitioning of monomer between the droplet and aqueous phases can be related to the respective monomer volume fractions or concentrations as follows:

$$K_i^{d/a} = \frac{\phi_i^d}{\phi_i^a} = \frac{[M_i]_d}{[M_i]_a} \tag{3.83}$$

where, ϕ_i^k corresponds to the volume fraction of monomer i in phase k, which can be easily related to the monomer concentration. By combining the above definition with a mass balance on each monomer within each phase (e.g. Equation 3.73, assuming constant monomer density), the monomer concentration in each phase can be determined. For example, the concentration in the particle phase can be written as:

$$[M_i]_p = \frac{N_i}{K_i^{d/a}K_i^{a/p}V_d + K_i^{a/p}V_a + V_p} \tag{3.84}$$

where, N_i is the total moles of monomer i in the system, and V_k is the volume of each phase ($k = d,a,p$). The remaining monomer concentrations can be obtained using Equation 3.84 and the corresponding partition

coefficients as follows:

$$[M_i]_a = K_i^{a/p}[M_i]_p \tag{3.85}$$

$$[M_i]_d = K_i^{d/a}[M_i]_a \tag{3.86}$$

In the above development, two partition coefficients are required to determine the concentrations in each phase. The approach used in the model of this thesis is slightly different than what is presented above. First, only one partition coefficient is used that describes the particle and aqueous phase monomer distribution. Second, a balance is written on the monomer in the aqueous phase where the concentration is assumed to remain at the saturation limit until the droplet phase disappears. Once the droplets are depleted, the transfer of monomer from the aqueous phase into the particle phase is assumed to occur at a rate proportional to the rate of monomer consumption. Thus, the concentration of monomer in the aqueous phase decreases from its saturation limit according to the rate of polymerization (this will be discussed again later after Equation 3.90). A mass balance can thus be written as:

$$\frac{dN_{i_a}}{dt} = F_{i_{a_{in}}} - F_{i_a} - \eta \tag{3.87}$$

$$\eta = \begin{cases} 0 & \text{if } V_d > 0 \\ R_{p_{i_a}} V_a & \text{otherwise} \end{cases}$$

where, $F_{i_{a_{in}}}$ and F_{i_a} represent the molar in/out flows of monomer i dissolved in the aqueous phase, and $R_{p_{i_a}}$ corresponds to the rate of polymerization in the aqueous phase which, in this situation, represents the rate of monomer transfer from the aqueous to the particle phase. The differential equation is initialized at the monomer saturation limit based on water solubility. For example, if the solubility is defined in terms of grams of monomer per 100 grams of water then, assuming there is water and monomer initially present in the reactor, the initial moles of dissolved monomer can be set as:

$$N_{i_a} = \frac{M_{w_o}\zeta}{100} MW_i \tag{3.88}$$

where, M_{w_o} is the initial mass of water charged to the reactor and ζ represents the monomer water solubility at standard conditions (i.e. standard temperature and pressure). Note that in the model herein a constant solubility value was used and temperature dependence was neglected.

Equations 3.85 and 3.87 can now be combined to determine the moles (or concentration) of monomer in the droplet phase by taking the difference from the total moles of monomer in the system and the moles of monomer in the aqueous and particle phases defined through the aforementioned equations. This can be written as follows:

$$N_{i_d} = N_i - N_{i_a} - N_{i_p} \tag{3.89}$$

Once the droplet phase is consumed (i.e. stage III), the partition coefficient is no longer used, as the aqueous

and particle phases are no longer at equilibrium; instead, the number of moles of monomer in the particle phase is determined by taking the difference between the total moles in the system and the moles in the aqueous phase described through the differential equation above. For a batch reactor, the use of the partition coefficient method, according to what has been described above, can be seen in Figure 3.1.

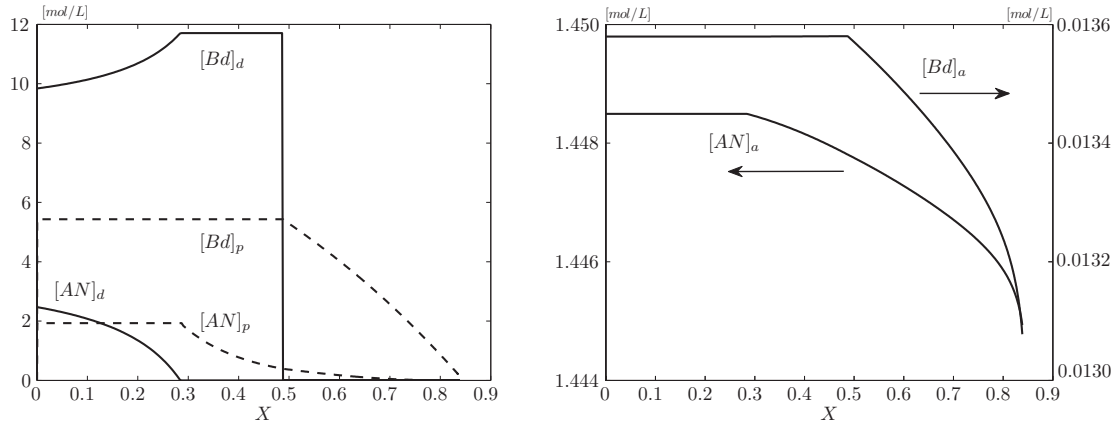

Figure 3.1: Monomer concentrations in each phase - constant partition coefficients

Notice that the particle and aqueous phase concentration profiles for each monomer remain constant at equilibrium, according to the partition coefficient, while monomer droplets exist. Once the droplets are depleted the concentrations decline, as monomer is consumed in the particle and is transferred from the aqueous phase into the particle phase. In Figure 3.1b, the concentrations appear to only slightly decrease from their saturation limit. This behaviour is a result of the method of formulation seen in Equation 3.87, where the rate of diffusion of monomer into the particle phase was approximated by the rate of polymerization in the aqueous phase, which is quite low relative to the particle phase. The actual degree of departure from the saturation limit is difficult to know without performing experiments. However, one would think that unless the monomer concentration in each particle became less than the concentration in the surrounding aqueous phase, then minimal mass transfer would occur. For AN-Bd copolymerization, consumption of AN in the particle phase occurs quite quickly into the reaction (i.e. $< 30\%$ conversion), hence this causes the AN in the aqueous phase to rapidly diffuse into the particle phase until it is fully consumed. To model this behaviour Equation 3.87 would require slight modification to increase the rate of monomer depletion from the aqueous phase. The simplest modification would be to include a proportionality constant in front of the rate of polymerization, as follows:

$$\frac{dN_{i_a}}{dt} = F_{i_{a_{in}}} - F_{i_a} - \varphi R_{p_{i_a}} V_a \tag{3.90}$$

where, φ is a constant greater than or equal to one (Dube et al. [33], for instance, used $\varphi = 1$). Another method to capture the depletion of AN from the aqueous phase once the droplets disappeared, would be to assume monomer transfers into the particle phase from the aqueous phase at a rate equivalent to the rate of polymerization in the particle phase, $R_{p_{i_p}}$, as opposed to the polymerization rate in the aqueous phase as

shown in Equation 3.87. This approach would eliminate introducing the parameter φ shown in Equation 3.90, which was introduced for simply increasing the rate of transfer of monomer from the aqueous phase. The approach taken in this thesis was to set the rate of AN transfer to the particle phase equal to the rate of polymerization in the aqueous phase, according to Equation 3.87.

The use of constant partition coefficients is clearly a much easier approach to partitioning when compared to the thermodynamic approach; however, use of constant coefficients is only an approximation of the more theoretically sound thermodynamic approach, and at the very least should be compared to the different variants of the thermodynamic approach in order to establish an idea of the relative differences. Gugliotta et al. [61] use the thermodynamic approach in their model for SBR in a continuous reactor train, and show that the coefficients (i.e. $K_i^{a/p} = \phi_i^a/\phi_i^p$) can drift up to 30%, compared to assuming constant coefficients, for the more water soluble monomer (butadiene in this case, which by any standard is only slightly water soluble). In a further study, Gugliotta et al. [60] compared the thermodynamic and constant coefficient approaches, and suggested that for water soluble monomers (e.g. AN) and moderate solids content (e.g. 30%) a thermodynamic approach may provide greater accuracy. Unfortunately, the studies performed were not with respect to AN or Bd, so it is difficult to speculate on which model is more appropriate. Nevertheless, the thermodynamic approach can be quite difficult to implement due to the lack of proper parameter estimates (i.e. monomer/monomer, monomer/polymer interaction constants) and information on particle size, which make the constant coefficient approach more attractive. This is presumably why Vega et al. [171] resort back to the constant coefficient approach in their NBR model. Clearly further experimental work needs to be performed using the AN/Bd copolymer system in order to shed more light on monomer partitioning, and irrespective of the modelling approach used, process and/or experimental data are necessary in order to properly estimate the partitioning parameters.

Noting the potential flaws in using constant coefficients (i.e. variation with temperature and the amount of dissolved emulsifier in the aqueous phase [47]), the method has proven to be effective for an NBR system, at least on an industrial scale, at providing adequate predictions of the process response [171] (see Chapter 4, section 4.2). Therefore, for the model presented in this thesis, constant partition coefficients are used.

3.5 Radicals per Particle

The average number of radicals per particle ($\bar{n}$) is a key factor when determining the rate of polymerization. In general, $\bar{n}$ can be defined as a function of both time and volume, which will give the entire distribution of particles of size V containing n number of radicals. This definition can be expressed as:

$$\bar{n} = \frac{\sum_{n=1}^{\infty} nN_n(V,t)}{\sum_{n=0}^{\infty} N_n(V,t)} \tag{3.91}$$

In this form, partial differential equations would need to be solved for the entire size distribution of particles containing n radicals (i.e. size dependent population balances). Since a monodisperse size distribution is assumed in the model presented in this thesis, the volume dependence in the above equation will be ignored,

and the population balances solved according to radical entry and exit from the particles.

There have been may different variations for formulating and solving both steady-state and transient expressions of $\bar{n}$, all with the aim of capturing the complex mechanistic and kinetic features of emulsion polymerization [9, 75, 89, 123, 131, 154, 157, 165]. The approach that is used in this work, follows that of Huo et al. [75], which is based on a steady-state approximation and accounts for monomer impurities.

In general, to determine the average number of radicals in each particle, $\bar{n}$, two population balances must be written. The first, a radical balance on the aqueous phase; the second, a balance on radicals entering and exiting the particles. Typically, the stationary-state hypothesis is applied which assumes the following for each balance:

1. The rate of radical flow into the aqueous phase equals the flow out of the aqueous phase
2. The rate of formation of radicals (in particles containing n radicals) equals the rate of consumption

Considering each balance and applying each assumption in sequence, the first balance on the aqueous phase can be written as follows:

$$\underbrace{R_I + R_{des}}_{\text{flow into aqueous phase}} = \underbrace{R_{cm} + R_{cp} + k_{t_a}\left[R^{\cdot}\right]_a^2 + k_{z_a}\left[R^{\cdot}\right]_a\left[Z\right]_a}_{\text{flow out of aqueous phase}} \tag{3.92}$$

where, the left side represents the appearance of radicals in the aqueous phase (i.e. initiation and desorption), and the right side represents the disappearance from the aqueous phase (i.e. radical capture by micelles and particles, water-phase termination, and reaction with water-soluble impurities).

The second balance looks at the distribution of radicals among particles by assuming a steady-state between appearance and disappearance of radicals within any class of particles containing n radicals. A balance can be written as follows:

$$\begin{aligned} &\tfrac{R_{cm}+R_{cp}}{N_p}\left[N_{n-1}\right] + \left(k_{des} + k_{fmsi_p}\left[MSI\right]_p\right)(n+1)\left[N_{n+1}\right] + \tfrac{k_{tp}}{\nu_p}(n+1)(n+2)\left[N_{n+2}\right] \\ &\quad = \left(\tfrac{R_{cm}+R_{cp}}{N_p} + \left(k_{des} + k_{fmsi_p}\left[MSI\right]_p\right)n + \tfrac{k_{tp}}{\nu_p}(n-1)\,n\right)\left[N_n\right] \end{aligned} \tag{3.93}$$

Equations 3.92 and 3.93 can be re-written in dimensionless form to allow for an easier presentation of the solution. From Equation 3.92, the following rearrangement can be given:

$$\alpha = \alpha' + m\bar{n} - Y\alpha^2 - W\alpha \tag{3.94}$$

where, the above terms are dimensionless groupings defined as:

$$\alpha = \frac{(R_{cm}+R_{cp})\,\nu_p V_a N_A^2}{k_{t_p} N_p} \qquad Y = \frac{k_{t_p} k_{t_a} N_p}{k_{ab}^2 \nu_p V_a N_A^2}$$
$$\alpha' = \frac{R_I \nu_p V_a N_A^2}{k_{t_p} N_p} \qquad W = \frac{k_{z_a}[Z]_a}{k_{ab}}$$
$$m = \frac{k_{des}\nu_p N_A}{k_{t_p}}$$

In a similar manner, Equation 3.93 can be written using dimensionless terms, which yields the following recursive equation:

$$\alpha\,[N_{n-1}] + p\,(n+1)\,[N_{n+1}] + (n+1)\,(n+2)\,[N_{n+2}] = (\alpha + pn + (n-1)\,n)\,[N_n] \tag{3.95}$$

where, α is defined as before and p is defined as:

$$p = \frac{\left(k_{des} + k_{fmsi_p}\,[MSI]_p\right)\nu_p N_A}{k_{t_p}} \tag{3.96}$$

The general solution of Equation 3.95, originally proposed by O'Toole [131], for a monodisperse particle size distribution can be written in terms of a modified Bessel function to give $\bar{n}$ as follows:

$$\bar{n} = \left(\frac{a}{4}\right)\frac{I_p(a)}{I_{p-1}(a)} \tag{3.97}$$

where, $a = \sqrt{8\alpha}$. An approximate solution to Equation 3.97 was proposed by Ugelstad and Hansen [165], and can be written as a partial fraction expansion:

$$\bar{n} = \cfrac{\alpha}{p + \cfrac{2\alpha}{p+1+\cfrac{2\alpha}{p+2+\cdots}}} \tag{3.98}$$

As mentioned by Dube et al. [34], Equation 3.98 was found to require approximately 10 levels of fractions to obtain adequate convergence in $\bar{n}$.

When the rate of desorption is greater than zero (i.e. $m > 0$), then α becomes a function of $\bar{n}$. In this case, Equations 3.94 and 3.98 must be solved in an iterative manner, to obtain a solution for $\bar{n}$. A detailed algorithm has been provided in Appendix B.

Other methods for solving $\bar{n}$, considering steady- and unsteady-state regimes, are those of Ballard et al. [9], Abusleme and Giannetti [1], and Li and Brooks [89]. Those that account for a polydisperse particle size distribution have been given by Lichti et al. [90], Min and Ray [102], and Giannetti [57].

The approach to determining $\bar{n}$ presented above (i.e. the application of Equation 3.98 in combination with Equations 3.94 and 3.96) was deemed sufficient enough to describe the approximate kinetics of an

NBR system, while providing a desirable level of computational efficiency. Thus, the alternative methods just mentioned were not implemented nor explored to a significant extent; however, the results of Li and Brooks [89] provide a vary similar steady-state expression for $\bar{n}$ to that shown in Equation 3.98, as well as a transient expression that deserves future consideration.

3.6 Radical Desorption

In general, radical desorption occurs when radicals transfer to small molecules, which subsequently diffuse from the particle phase into the aqueous phase. It is commonly accepted that this only occurs with monomeric radicals (i.e. radicals of unit length), as a result of transfer to monomer, impurity, or chain transfer agent. However, if relatively large chain-transfer agents are used, desorption is not likely to occur from transfer to CTA. In order to effectively describe radical desorption, researchers have focussed on developing rate constant expressions that combine radical transfer kinetics and radical diffusion theory. A number of different expressions have been proposed in the literature that attempt to capture the complex behaviour of radical desorption. A general discussion of these expressions has been given by Dube et al. [34] and Gao and Penlidis [53]. A detailed review will not be repeated here; instead only the approaches deemed sufficient for modelling potential radical desorption in an NBR system will be discussed.

In the following development, radicals are assumed only to desorb from transfer to monomer, as the CTA used in a NBR system (t-dodecyl mercaptan) is a large and water insoluble molecule. As well, radicals that react with monomer-soluble impurities are assumed to remain in the particle phase. Two approaches will be considered in the model of this thesis; the first was proposed by Nomura [121], and the second by Asua et al. [8]. As shown by Asua, under the assumptions just mentioned, both approaches result in a similar rate constant expression. Nomura's expression can be stated, in its simplest form, as follows:

$$k_{des} = k_{fm}\left[M\right]_p \frac{K_o}{K_o\bar{n} + k_p\left[M\right]_p} \tag{3.99}$$

where, K_o represents the rate of diffusion of monomeric radicals out of the particle phase, and can be defined as:

$$K_o = \frac{12D_w\delta}{m_d d_p^2} \tag{3.100}$$

where, D_w is the diffusivity of radicals in the aqueous phase, m_d is the partition coefficient for radicals between the particle and aqueous phases (i.e. $K^{p/a}$), d_p is the swollen particle diameter, and δ is the ratio of external particle surface (i.e. film) mass-transfer resistance to the overall resistance of radicals through the particle/aqueous phase interface, given as:

$$\delta = \left(1 + \frac{\psi D_w}{m_d D_p}\right)^{-1} \tag{3.101}$$

where, D_p is the diffusivity of radicals in the particle phase, and depending on the approximations used to arrive at δ, ψ can range from 2 to 6. For further details on this derivation, refer to Nomura [121]. An

important note is that Nomura assumed that particles contain at most one radical, instantaneous termination occurs when another radical enters a particle already containing a radical, and the re-absorption of desorbed radicals, and aqueous phase termination or propagation reactions are negligible. Clearly at higher conversions, when $\bar{n}$ can increase considerably (due to the gel effect), or when the monomer is fairly water soluble, some of these assumptions can break down. Asua et al. [8] developed an expression that accounted for both termination and propagation in the aqueous phase, and re-entry of desorbed radicals, while not being restricted to instantaneous termination in the particle phase.

Asua's expression can be stated in a similar form to that of Nomura's:

$$k_{des} = k_{fm}\left[M\right]_p \frac{K_o}{\beta K_o + k_p\left[M\right]_p} \tag{3.102}$$

where, β is the probability that a monomeric radical reacts in the aqueous phase by either termination or propagation, and can be expressed as:

$$\beta = \frac{k_{p_a}\left[M\right]_a + k_{t_a}\left[R^{\cdot}\right]_a}{k_{p_a}\left[M\right]_a + k_{t_a}\left[R^{\cdot}\right]_a + k_{cm}A_m/V_a + k_{cp}A_p/V_a} \tag{3.103}$$

Note that β will always be between zero and one, and under the assumptions of Nomura's model $\bar{n}$ is also considered to be between zero and one. Thus, when β and $\bar{n}$ are of the same magnitude, both models will provide a comparable prediction for the rate of desorption. However, when $\bar{n}$ increase beyond one, Nomura's approach underpredicts k_{des}, while when the monomer is significantly water soluble (i.e. aqueous phase termination and propagation) and transfer to monomer is important, k_{des} increases causing $\bar{n}$ to decrease to a point where it eventually diverges causing k_{des} to increase further. Upon comparing both approaches to experimental data, Asua et al. [8] have shown that their model provides more accurate predictions. Thus, considering these findings and the general nature of Asua's model, it seems like a favourable choice for implementation into the model of this work.

In a more general form, Asua's expression can be modified to allow for multiple monomers and water impurities. Forcada and Asua [45] demonstrate this modification for a copolymer system, and using these ideas, as well as those shown in Gao and Penlidis [53], a general formulation of the desorption rate constant that considers the possibility of multiple monomers desorbing into the aqueous phase, as well as the influence of water-soluble impurities, can be given as follows:

$$k_{des_i} = \sum_j^N k_{fm_{ji_p}}\phi_{j_p}^{\cdot}\left[M_i\right]_p \frac{K_{o,i}}{\beta_i K_{o,i} + \sum_j^N k_{p_{ij_p}}\left[M_j\right]_p} \tag{3.104}$$

where, k_{des_i} corresponds to the individual rate constant for monomer i. Using a similar analogy, the monomeric aqueous phase reaction probabilities can be expressed as follows:

$$\beta_i = \frac{\sum_j^N k_{p_{ij_a}}\left[M_j\right]_a + \sum_j^N k_{t_{ij_a}}\left[R^{\cdot}\right]_a}{\sum_j^N k_{p_{ij_a}}\left[M_j\right]_a + \sum_j^N k_{t_{ij_a}}\left[R^{\cdot}\right]_a + k_{z_{i_a}}\left[Z\right]_a + k_{cm}A_m/V_a + k_{cp}A_p/V_a} \tag{3.105}$$

where, it is assumed that desorbed monomeric radicals propagate, terminate, react with impurities, and may be re-absorbed into particles or into micelles. Taking the sum of each individual rate constant provides an overall rate constant, as follows:

$$k_{des} = \sum_{i}^{N} k_{des_i} \tag{3.106}$$

As previously noted by Dube et al. [33], and as found through simulations in this study, desorption in an NBR system may be quite minimal having a negligible influence on the latex properties (e.g. conversion, N_p, d_p, etc.). Further comments on the influence of radical desorption and whether including it may improve the model predictive capabilities will be given in the forthcoming chapters.

3.7 Molecular Weights & Chain Branching

The development of expressions to describe polymer molecular weight when considering the possibility of nonlinear polymerization can be quite involved. Nonlinear polymerization occurs when a radical chain grows by intermolecular chain transfer to polymer (i.e. radical propagation with dead polymer), polymerization with terminal or internal double bonds that may be due to the presence of multifunctional monomers, a result of transfer to monomer, or termination by disproportionation. In developing equations to describe average molecular weight ($\overline{M}_n$ and $\overline{M}_w$) and chain branching ($\overline{BN}_3$ and $\overline{BN}_4$), both transfer reactions and termination reactions need to be considered. Mathematical modelling of these reactions is typically carried out using population balances to account for all active and inactive polymer chains. However, for nonlinear polymerization, it can often be very difficult or near impossible to describe the entire molecular weight distribution by a closed form equation. Thus a more practical method is to capture partial information of the distribution through the first few leading moments; however, this approach only describes average quantities. Moment concentrations for dead polymer and live radical distributions can be defined as follows:

$$Q_i = \sum_{r=2}^{\infty} r^i \left[P_r\right] \tag{3.107}$$

$$Y_i = \sum_{r=1}^{\infty} r^i \left[R_r^{\cdot}\right] \tag{3.108}$$

The method of moments tracks the rate of change of Q_i and Y_i, which are just like any other state variable in the model. For the first few moments a physical meaning can be attached; the zeroth dead polymer moment, Q_o, is the concentration of dead polymer, while the first dead polymer moment, Q_1, is the concentration of monomer units bound in the dead polymer. Similar meanings are attached with live radicals, Y_o and Y_1.

In the case of emulsion polymerization, the concentration of live radicals in the polymer particles is negligible compared to dead polymer and is often neglected when developing the moment equations (i.e. $[P_r] \gg [R_r^{\cdot}]$). The first three leading moments of the dead polymer distribution can adequately describe the

cumulative number- and weight-average molecular weights, which can be defined as follows:

$$\overline{M}_n = MW_{eff}\frac{Q_1}{Q_0} \tag{3.109}$$

$$\overline{M}_w = MW_{eff}\frac{Q_2}{Q_1} \tag{3.110}$$

The first step in developing tractable expressions for Q_i, is to properly formulate balances on active and inactive radical chains that account for all consumption and generation reactions. Using these balances along with the definition of the dead polymer moment (Equation 3.107), the rate of generation of the leading moments of the dead polymer chains can be derived. Details on these aspects will not be given here, as the derivation is quite lengthy. The reader is directed to the recent articles of Hutchinson and Penlidis [76] and Barandiaran et al. [10] for further details on these aspects, as well, for a rigorous discussion on the method of moments (mathematical development and numerical comparison to other methods) refer to Iedema and Kolhapure [77]. What will be given here are the rates of generation of the first three leading moments, tri-functional branching, and tetra-functional branching. The balances were formulated by considering the following assumptions: negligible initiator in the particle phase; transfer to monomer, polymer, CTA, and reaction with impurities (MSI); and contribution from radical termination.

The rates of moment generation for Q_o, Q_1, and Q_2 can be defined as follows:

$$R_{Q_o} = \left(\tau + \frac{\beta}{2} - C_{p^{**}}\frac{Q_1}{[M]_p} - C_{p^*}\frac{Q_o}{[M]_p}\right) k_p [M]_p [R^{\cdot}]_p \tag{3.111}$$

$$R_{Q_1} = \gamma k_p [M]_p [R^{\cdot}]_p \tag{3.112}$$

$$R_{Q_2} = \left(\gamma + 2\left(1 + \frac{C_{p^*}Q_1 + C_{p^{**}}Q_2}{[M]_p}\right)\frac{\xi}{\lambda} + \beta\left(\frac{\xi}{\lambda}\right)^2\right) k_p [M]_p [R^{\cdot}]_p \tag{3.113}$$

where several group terms can be defined, for convenience and compactness, as follows:

$$\tau = \frac{k_{td}[R^{\cdot}]_p}{k_p[M]_p} + C_{fm} + C_{fcta}\frac{[CTA]_p}{[M]_p} + C_{fmsi}\frac{[MSI]_p}{[M]_p} \tag{3.114}$$

$$\beta = \frac{k_{tc}[R^{\cdot}]_p}{k_p[M]_p} \tag{3.115}$$

$$\gamma = 1 + C_{fm} + C_{fcta}\frac{[CTA]_p}{[M]_p} + C_{fmsi}\frac{[MSI]_p}{[M]_p} \tag{3.116}$$

$$\lambda = \tau + \beta + (\gamma - 1) + C_{fp}\frac{Q_1}{[M]_p} \tag{3.117}$$

$$\xi = \gamma + C_{p^*}\frac{Q_1}{[M]_p}(C_{fp} + C_{p^{**}})\frac{Q_2}{[M]_p} \tag{3.118}$$

The transfer and reaction constants are defined as:

$$C_i = \frac{k_i}{k_p} \tag{3.119}$$

where $i = fm, fcta, fmsi, fp, p^*, p^{**}$, for transfer to monomer, transfer to CTA, reaction with MSI, transfer to polymer, reaction with terminal double bonds, and reaction with internal double bonds.

As previously mentioned, the moments act as state variables that are tracked over time, as material enters and leaves the reactor. Defined in terms of moles ($V_p Q_i$), a material balance can be written for each moment as follows:

$$\frac{d\left(V_p Q_i\right)}{dt} = Q_{i_{in}} q_{p_{in}} - Q_i q_p + R_{Q_i} V_p \tag{3.120}$$

The generation rates for tri-functional branching (i.e. long-chain branching) and tetra-functional branching (i.e. cross-linking) can be expressed as follows:

$$R_{\overline{BN}_3} = \left(C_{fp} Q_1 + C_{p^*} Q_o\right) k_p \left[R^{\cdot}\right]_p \tag{3.121}$$

$$R_{\overline{BN}_4} = C_{p^{**}} Q_1 k_p \left[R^{\cdot}\right]_p \tag{3.122}$$

In a similar manner to the moments, the average branching frequencies can be tracked according to the following balance:

$$\frac{d\left(V_p Q_o \overline{BN}_i\right)}{dt} = \left(Q_o \overline{BN}_i\right)_{in} q_{p_{in}} - Q_o \overline{BN}_i q_p + R_{\overline{BN}_i} V_p \tag{3.123}$$

3.8 Material / Energy / Population Balances

Balances can be performed on each component within the system by writing differential equations to describe the accumulation or consumption of each species. Typically ordinary differential equations are adequate to describe the change in free monomer, bound monomer, emulsifier, and other components; however, if information over the entire particle size or molecular weight distribution is required, then partial differential equations are needed. Typically a population balance approach is taken where balances are written for the change in a particular property within an elemental volume over a certain time period. The approach taken in this work does not use population balances, instead appropriate approximations are made in order to capture "average" information on the particle and molecular weight distributions.

3.8.1 Mass Balances

A typical balance on the number of moles of species i in a volume element V can be stated as follows:

$$\frac{dN_i}{dt} = F_{i_{in}} - F_i - R_i V \tag{3.124}$$

where, F represents the molar flow and R_i the overall rate of reaction.

For a multiphase system, species are present in different phases in all of which a reaction can occur. Thus, the reaction term in Equation 3.124 can be generalized as follows:

$$R_i V = \sum_{k}^{P} \sum_{i}^{N} R_{i_k} V_k \tag{3.125}$$

where, k corresponds to the phase where the reaction takes place.

To account for the flow rate of material out of the reactor, a constant overflow approach is taken. This avoids introducing a controller to maintain a particular level within the reactor, which for the purpose of this work was deemed unnecessary. The total outflow of each component in the reactor can be described in the usual way for liquid phase reactions. A general expression, considering each phase k, can be written as follows:

$$F_i = \sum_{k}^{P} [i]_k \, q_k \tag{3.126}$$

where, $[i]_k$ is the concentration of component i and q_k is the hypothetical volumetric flow rate of phase k, which can be related to the total volumetric flow rate out of the reactor as follows:

$$q_k = \frac{V_k}{V_T} q_T \tag{3.127}$$

At the overflow point, the total volumetric flow rate out of the reactor can be defined by the total flow rate into the reactor less the overall organic phase shrinkage due to polymerization, Equation 3.128.

$$q_T = q_{T_{in}} - \underbrace{\sum_{i}^{N} MW_{m_i} \left(R_{p_{i_a}} V_a + R_{p_{i_p}} V_p \right) \left(\frac{1}{\rho_{m_i}} - \frac{1}{\rho_p} \right)}_{\text{polymer shrinkage}} \tag{3.128}$$

Material inflow to the reactor train only needs to be specified for the first reactor, since all downstream reactors take previous outflows as inflows. Inflows can be specified by defining the mass flow of each individual species, or by defining the total inflow rate along with each component composition (i.e. mass, mole, volume fractions). Further details on these specifications can be found in Appendix A.

In order to track the change in total particle phase volume two separate equations can be written depending on the stage of polymerization. During stages I & II, monomer droplets are present, thus it is assumed that monomer is continuously supplied to the particles at a rate which maintains a constant equilibrium between droplets and particles. The onset of stage III occurs when all the droplets have been consumed. At this point monomer concentration in the particle phase decreases, with only minimal monomer diffusing from the aqueous phase, thus, due to the density difference between monomer and polymer, the particles start to shrink causing the total particle phase volume to decrease. The total average particle phase volume under each of the aforementioned regimes (i.e. Equation 3.129 when droplets exist and Equation 3.130 otherwise)

can be described according to the following two equations:

$$\frac{dV_p}{dt} = q_{p_{in}} - q_p + \frac{\sum_i^N MW_{m_i}\left(R_{p_{i_a}}V_a + R_{p_{i_p}}V_p\right)}{\phi_p^p \rho_p} \tag{3.129}$$

$$\frac{dV_p}{dt} = q_{p_{in}} - q_p + \frac{\sum_i^N MW_{m_i}R_{p_{i_a}}V_a}{\rho_p} + \sum_i^N MW_{m_i}R_{p_{i_p}}V_p\left(\frac{1}{\rho_{m_i}} - \frac{1}{\rho_p}\right) \tag{3.130}$$

where, $q_{p_{in}}$ and q_p are the volumetric flow rates of particles in and out of the reactor, and ρ corresponds to the density of monomer or polymer. In order to properly account for the copolymer density, ρ_p, the individual homopolymer densities must be weighted according to the cumulative copolymer composition. This can be written as follows:

$$\rho_p = \sum_i^N \rho_{p_i}\overline{F}_i \tag{3.131}$$

3.8.2 Heat Balance

Including an energy balance within the model can provide information on the reactor heat removal required when different operation policies are considered. In general, the change in overall enthalpy can be stated as:

$$\frac{d\hat{H}}{dt} = \dot{w}_{in}\hat{H}_{in} - \dot{w}\hat{H} + \dot{Q}_{Rx} + \dot{Q}_{jacket} + \dot{Q}_{stir} + \dot{Q}_{loss} \tag{3.132}$$

where, $\dot{w}_{in}\hat{H}_{in}$ is the flow of enthalpy into the reactor, $\dot{w}\hat{H}$ is the flow out of the reactor, $\dot{Q}_{Rx}$ is the heat generated due to reaction (i.e. polymerization), $\dot{Q}_{jacket}$ is the heat transferred to the cooling jacket, $\dot{Q}_{stir}$ is the work done on the reaction mixture by the agitator, and $\dot{Q}_{loss}$ is the heat loss to the surroundings.

From here, several appropriate approximations can be made in order to arrive at the more familiar balance describing the change in reactor temperature [30, 142]. This can be written as:

$$\sum_k^P \sum_j^N V_j^k \rho_j \hat{C}_{p_j} \frac{dT_r}{dt} = \dot{w}_{in}\hat{H}_{in} - \dot{w}\hat{H} + \dot{Q}_{Rx} + \dot{Q}_{jacket} + \dot{Q}_{loss} \tag{3.133}$$

where, the flow of enthalpy in and out of the reactor can be approximated as:

$$\dot{w}_{in}\hat{H}_{in} = \sum_j^N \dot{w}_{j_{in}}\hat{C}_{p_j}\left(T_{in} - T_{ref}\right) \tag{3.134}$$

$$\dot{w}\hat{H} = \sum_j^N \dot{w}_j\hat{C}_{p_j}\left(T_r - T_{ref}\right) \tag{3.135}$$

The heat of reaction, considering both aqueous and particle phase as a locus of polymerization, can be defined as:

$$\dot{Q}_{Rx} = \sum_k^P \sum_j^N R_{p_{j_k}} V_k \left(-\Delta\overline{H}_{p_j}\right) \tag{3.136}$$

where, $R_{p_{j_k}}$ is the rate of polymerization of monomer j in phase k, and $-\Delta\overline{H}_{p_j}$ is the heat of polymerization of monomer j.

In addition to a balance on the reactor (Equation 3.133), a balance must be written on the cooling jacket in order to properly track T_{jacket} as a state variable. This equation can be written as follows:

$$m_c\hat{C}_{p_c}\frac{dT_{jacket}}{dt} = F_c MW_c\hat{C}_{p_c}\left(T_{jacket_{in}} - T_{jacket}\right) - \dot{Q}_{jacket} + \dot{Q}_{jacket_{loss}} \tag{3.137}$$

where the heat transfer to the jacket, ($\dot{Q}_{jacket}$), can be written as:

$$\dot{Q}_{jacket} = -UA_{jacket}\left(T_r - T_{jacket}\right) \tag{3.138}$$

where, U is the overall heat transfer coefficient, and A_{jacket} is the overall surface area available for heat transfer.

In contrast to using a balance on the jacket, in practice, it may be more convenient to describe the rate of heat transfer to the cooling jacket according to the overall mass flow of cooling fluid through the jacket, and the difference between the inlet and outlet temperatures of the jacket, thus eliminating the need for a second balance. According to this approach the overall heat transfer to the jacket can be approximated as:

$$\dot{Q}_{jacket} = \dot{m}_c\hat{C}_{p_c}\left(T_{jacket_{in}} - T_{jacket_{out}}\right) \tag{3.139}$$

where, $\dot{m}_c$ is the mass flow rate of cooling fluid, $\hat{C}_{p_c}$ is the heat capacity of the cooling fluid, and $T_{jacket_{in}}$ and $T_{jacket_{out}}$ are the measured temperatures at the inlet and outlet of the cooling jacket.

3.9 Summary of Model Assumptions

As with any model, many assumptions are made in order to make the formulation as simple as possible, without the loss of reality, and to maintain computational tractability. The following listing highlights the assumptions employed in the model development.

General Assumptions:

- Concentration or temperature gradients are not considered within the reaction medium (i.e. perfect mixing), thus ODE's were used to describe material and energy balances. In doing so, an instantaneous response would be observed in the simulation, to any reactant feed additions.
- All reactions are assumed to be 1^{st} order with respect to each reactant (i.e. monomer and radical react with a one-to-one dependence and the reaction is 2^{nd} order overall). This is the usual assumption with free-radical polymerization; however, others have considered other reaction orders with respect to impurities [171]. The choice to do so here was deemed unnecessary due to the lack of experimental evidence.

- Negligible pressure effects are assumed (i.e. vapour pressure in the reactor headspace is neglected). If the polymerization was carried out at high temperatures ($T > 80^oC$) then the influence of pressure might become important (i.e. amount of monomer in gaseous form increases, thus a higher reactor pressure is required to drive the monomer back into liquid form).

Nucleation Assumptions:

- Particle coagulation is not accounted for in the model.
- Radicals can only be captured from the aqueous phase once they reach a length of $j_{cr}/2$ (i.e. capturable for chains lengths in the range of $j_{cr}/2 \leq k < j_{cr}$).
- Collision theory (as opposed to diffusion theory) is assumed to adequately describe radical capture (i.e. capture $\propto$ surface area).
- Free-micellar area is assumed to be adequately described by taking the difference between the total micelle area that could be formed from all emulsifier and the total particle surface area (i.e. an adsorption isotherm was not used to account for the amount of emulsifier adsorbed on the particle surface).
- All particles are assumed to grow at the same rate, thus are considered to be monodisperse.

Kinetic Assumptions:

- Negligible diffusional limitations are assumed for propagation, initiation, and transfer reactions
- All monomer is consumed through propagation reactions (i.e. Long-Chain Approximation)
- No transfer to emulsifier or solvent is assumed to occur. Only transfer to monomer, polymer and chain transfer agent is considered.
- Radical reactivity depends only on the identity of the terminal monomer unit (i.e. penultimate reactions are not considered). As well, the length of the radical chain is assumed not to affect the reactivity.
- Reactions with impurities are independent of radical type and only dependent on the impurity itself.
- Desorption is assumed to only occur as a result of transfer to monomer (i.e. only monomeric radicals can desorb). Once a radical desorbs, propagation, termination, reaction with WSI, particle recapture, or micelle capture can occur. For desorbed radicals only, capture or recapture is assumed to occur regardless of the length of the radical (i.e. monomeric radicals can be captured). In making this assumption, radicals need not propagate in the aqueous phase until a length of $j_{cr}/2$ before capture.

Radical Balance Assumptions:

- The use of the stationary-state hypothesis for radicals is assumed applicable (i.e. $d[R^{\cdot}]/dt \approx 0$).
- Negligible reactor inflow or outflow of radicals is assumed
- No restrictions on $\bar{n}$ are assumed (i.e. $\bar{n}$ can be 0, 1, 2, ... and anything in between)

- A steady-balance is assumed to be adequate for calculating $\bar{n}$

Phase Partitioning Assumptions:

- Constant partition coefficients are assumed to be adequate for describing the partitioning of reaction ingredients between each phase in the reaction medium.
- An equilibrium is assumed to exist until the droplet phase disappears.

Molecular Weight Assumptions:

- The concentration of live radicals (in the particle phase) is considered negligible during the development of the molecular weight moment equations.
- Molecular weights in rubber systems (e.g. NBR, SBR) are controlled by transfer reactions (e.g. CTA, monomer, polymer). Termination reactions are considered to contribute to the molecular weight development, albeit only slightly in emulsion polymerization. For generality, termination reaction contributions were included in the moment equation development of this thesis.

3.10 Model Database

This section will discuss the kinetic, partitioning, and nucleation database used in support of the model. For the most part, physico-chemical characteristics, kinetic rate constants and other parameters were obtained from literature sources on AN, Bd, NBR, and SBR. Dube et al. [33] provide a detailed listing of the parameters used in their NBR model, and many of these parameters were used in the model of this work (at least as a starting point). Inevitably, adjustments were made to certain parameters in order to fit the model to literature data. A detailed discussion was given by Wong [190], Gugliotta et al. [61] and Vega et al. [171] on parameter adjustment for the cases of SBR and NBR, and following the advice given, a similar procedure was adopted in order to obtain reasonable estimates that were in the range of reported literature findings.

3.10.1 Kinetic Rate Constants

The only detailed modelling studies on the industrial production of NBR available in the open literature are those performed by Dube et al. [33], Vega et al. [171], and Rodriguez et al. [146]. Comparing the parameters used in each of these models can provide a relative range of values from which further refinement can be made. Table 3.4 compares the rate constants reported in the above papers along with the original literature source of the kinetic expressions. A few discrepancies in the reported values can be readily seen, more specifically, related to the values of $k_{p_{AA}}$, $k_{fm_{AA}}$, and $k_{fp_{AA}}$.

The homopropagation rate constant of acrylonitrile used by Vega et al. [171] (3.98×10^5 L/mol/min at 10^oC) is quite high compared to that used by Dube et al. [33] (1.51×10^4 L/mol/min at 10^oC). Garcia-Rubio et al. [56] show that the value used by Dube is adequate to predict the experimental data in SAN bulk copolymerization. Furthermore, McCarthy et al. [96] performed experiments on AN under seeded heterogeneous

conditions and suggested an approximate range for the propagation rate constant of 1.8×10^4 to 7.2×10^4 L/mol/min at 50^oC, which is in agreement with the value given by the Arrhenius expression used by Dube (7.5×10^4 L/mol/min at 50^oC). From the perspective of parameter sensitivity on the overall conversion, Dube suggested a parameter range of 1.5×10^4 to 1.5×10^5 at 10^oC. Based on the experimental findings mentioned above, the lower value used by Dube is believed to be a more reasonable choice than the higher value used by Vega. However, there is clearly considerable uncertainty attached to the estimate of $k_{p_{AA}}$, which warrants further investigation. In modelling an industrial reactor, a more thorough parameter sensitivity study, than what was done by Dube, should be carried out based on multiple process measurements (i.e. conversion, CPC, N_p, $\overline{MW}$) [141].

As a result of the relatively high AN propagation rate constant, the rate constant used by Vega for transfer to AN monomer from a radical ending in AN, $k_{fm_{AA}}$, is also quite high. This can be seen from the transfer constant, $C_{fm} = k_{fm_{AA}}/k_{p_{AA}}$, used to obtain the transfer rate constant estimate. Vega et al. also assume that transfer to monomer A or B is irrespective of the radical type that is transferring its activity (i.e. $k_{fm_{AA}} = k_{fm_{BA}}$ and $k_{fm_{BB}} = k_{fm_{AB}}$). On the contrary, Dube assumes that radicals only transfer to monomer of the same type (i.e. $k_{fm_{BA}} = 0$ and $k_{fm_{AB}} = 0$). This assumption was made to avoid introducing further uncertainly into the model. Performing simulations considering the assumption used by Vega, revealed an unnoticeable change in the process response; however, if radical desorption is considered a moderate decrease in $\bar{n}$ is noticed. A further discussion on these differences will be made in Chapter 4. The assumption made by Dube, will be followed in the model of this work.

The final discrepancy evident in Table 3.4, is the rate constant for transfer to an AN unit in dead polymer. Dube assumes that it would be more likely that transfer to polymer only occurs with Bd units in the polymer. This assumption was based on the findings of Garcia-Rubio et al. [56], who show that with an SAN system only linear chains are formed.

The rate constants that are probably the most uncertain are those for CTA and monomer-soluble impurity. Morton et al. [111] reported a transfer rate constant for butadiene radicals to t-dodecyl mercaptan that Wong [190] found to be too high for an SBR system. As a result, Wong modified Morton's rate constant by simply lowering it until the model corresponded to the molecular weight data (roughly six times lower). A similar approach was adopted in this study, and lowering the value given by Morton by a factor of 20 provided reasonable predictions. For transfer to mercaptan from AN radicals, a transfer constant was obtained by starting with the propagation rate constant $k_{p_{AA}}$ and adjusting it accordingly until a reasonably good fit to the experimental data of Vega et al. [171] was obtained. These modifications are summarized in Table 3.5. Establishing a reasonable rate constant estimate for monomer-soluble impurity was based on assuming a practical impurity concentration in the range of 20 ppm to 500 ppm and adjusting k_{fmsi} accordingly.

The polymer handbook lists numerous transfer constants ($C_{fcta} = k_{fcta}/k_p$) for various transfer agents at specific temperatures. A summary of C_{fcta} for tertiary-dodecyl mercaptan (t-DDM or $t-C_{12}$) and its counterpart n-dodecyl mercaptan (n-DDM) for monomer and copolymers of interest can be seen in Table 3.6.

Simulation studies for industrial NBR production by Vega et al. [171] show that the transfer constant

Table 3.4: Comparison of NBR kinetic rate constants

	Dube et al. [33]		Vega et al. [171]	
Parameter	**Value** [a]	**Source**	**Value** [b]	**Source**
$k_{p_{AA}}$	1.51×10^4	[56]	3.98×10^5	[14]
$k_{p_{BB}}$	4.77×10^2	[111]	5.30×10^2	[14]
$r_A = k_{p_{AA}}/k_{p_{AB}}$	0.05	[14]	0.03	[14]
$r_B = k_{p_{BB}}/k_{p_{BA}}$	0.35	[14]	0.30	[14]
$k_{fm_{AA}}$	0.22	[33]	2.00	[14]
$k_{fm_{BB}}$	0.049	[33]	0.01	[15, 190][c]
$k_{fm_{BA}}$	0	A[d]	$k_{fm_{AA}}$	A
$k_{fm_{AB}}$	0	A	$k_{fm_{BB}}$	A
$k_{fp_{AA}}$	0	A[e]	1.10	[14]
$k_{fp_{BB}}$	0.09	[15]	0.055	[190]
$k_{fp_{BA}}$	0	A	$k_{fp_{AA}}$	A
$k_{fp_{AB}}$	$k_{fp_{BB}}$	A	$k_{fp_{BB}}$	A
$k^{**}_{p_{AA}}$	0	A[f]	0	A
$k^{**}_{p_{BB}}$	9.68×10^{-3}	[18]	9.56×10^{-3}	[18]
$k^{**}_{p_{BA}}$	$k^{**}_{p_{AA}}$	A	$k^{**}_{p_{AA}}$	A
$k^{**}_{p_{AB}}$	$k^{**}_{p_{BB}}$	A	$k^{**}_{p_{BB}}$	A
$k_{t_{a_{AA}}}$	1.09×10^{12}[g]	[150]	-	-
k_{fcta_A}	7.74×10^{-1}	[33]	1.28×10^5	[14]
k_{fcta_B}	3.59×10^3	[111]	2.41×10^2	[171]
$k_{fmsi_{TBC}}$	6×10^6	[136]	-	-
$k_{z_{O_2}}$	1×10^7	[14]	-	-

[a] Evaluated at 10^oC from an Arrhenius expression (Appendix C)
[b] Given at 10^oC, No Arrhenius expression given
[c] Estimated from SBR data
[d] Assumption made, as no experimental value is available
[e] An AN or Bd radical is assumed not to transfer activity to an AN monomer
[f] AN has no internal double bonds
[g] The overall k_{t_a} is assumed to be equal to $k_{t_{AA_a}}$

($C_{f_{cta}}$) with a value of 0.32 at 10^oC adequately predicts number- and weight-average molecular weight when compared to experimental data. On the other hand, Uraneck and Burleigh [167] state that for an NBR system, initially with a AN/Bd ratio of 30/70, the transfer constant to t-dodecyl mercaptan is around 1.1. Taking into consideration this approximate range for C_{fcta}, appropriate adjustments were made (Table 3.5) in order that C_{fcta} was close to this range while providing a good fit to the experimental data of Vega et al. [171]. A comparison to experimental data is shown in Chapter 4.

Another source of uncertainty is the values of the reactivity ratios used. The polymer handbook lists a number of slightly different estimates for r_A and r_B, which all predict slightly different azeotropic compositions (i.e. $F_{AN} = f_{AN}$). This is evident from Figure 3.2, which reveals an azeotropic range of approximately 35 to 43% AN. As an added feature this figure also includes experimental data from Embree et al. [38] which are in agreement with the simulation profiles. The azeotropic composition can provide an indication

Table 3.5: CTA & impurity rate constant approximations

Parameter	Approximation	Source
k_{fcta_A}	$k_{p_{AA}}\beta$ [a]	A [b]
k_{fcta_B}	$k_{fcta_B}^{morton}/\alpha$ [c]	[190]
$k_{fmsi_{TBC}}$	δk_p [d]	[190]

[a] To fit the data of Vega et al. [171] $\beta = 20$ and $\alpha = 21$
[b] Approximated for a temperature of 10^oC
[c] Wong adjusted the value provided by Morton ($k_{fcta_B}^{morton}$) by lowering it by a factor of $\alpha = 6$
[d] For an NBR system, δ in the range of 0.0001-0.001 was reasonable (Wong used $k_{fmsi} = 0.25$ ($\delta \approx 0.0001$))

of the relative amounts of each monomer required in the system to minimize the compositional drift within the copolymer. Below the azeotrope, $F_{AN} > f_{AN}$, AN is incorporated into the copolymer more quickly than Bd, and when AN is completely consumed the cumulative copolymer composition will drift downwards as Bd is now the only monomer being incorporated into the growing polymer chain. Above the azeotrope, Bd is incorporated into the copolymer more quickly than AN, and the cumulative copolymer composition drifts upwards. To illustrate this behaviour, the NBR composition data from Embree et al. [38] were compared to model simulations. As shown in Figure 3.3, three different feed compositions are used to demonstrate composition drift. Despite the seemingly poor model fit the presence of compositional drift is undeniable.

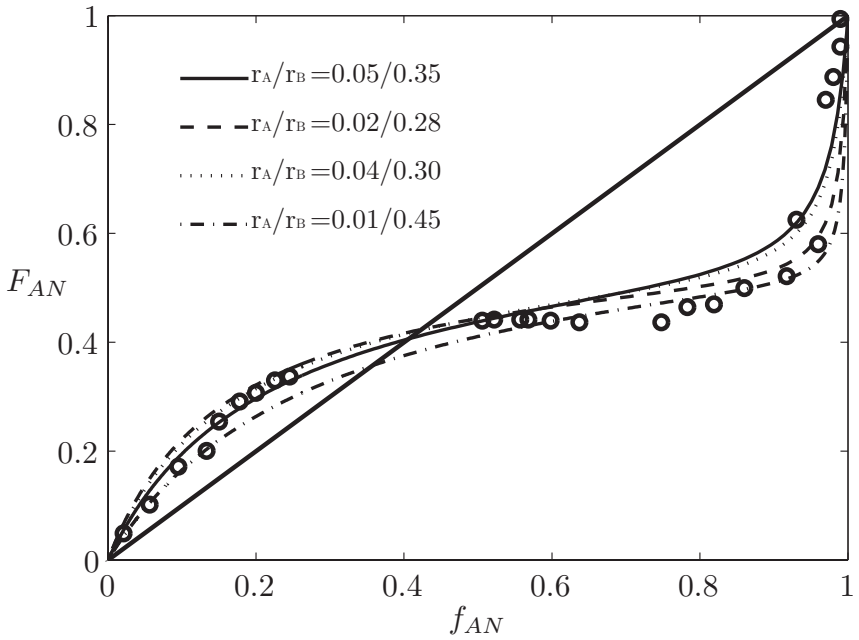

Figure 3.2: Instantaneous copolymer composition of AN as a function of the mole fraction of AN in the feed (i.e. particle phase) (Mayo-Lewis Equation)

Table 3.6: Transfer to CTA (mercaptan) coefficient comparison

Monomer/Polymer	$C_{fcta} = k_{fcta}/k_p$	**Temperature** (^oC)	**Source**
AN	0.73[a]	50	[14]
Bd	3.9 [b]	50	[111]
	0.65 [c]	50	[190]
Sty	0.69,1.3[b]	70,90	[14]
	18.7[d]	60	[13]
	0.1 [e]	60	[190]
NBR	1.1[f]	5	[167]
	1.4[g]	50	[167]
SBR	0.66[b]	5	[14]
	3.71,2.91,1.86[d]	30,50,70	[13]
SAN	0.84	50	[167]

[a] n-dodecanethiol ($n-C_{12}$ mercaptan)
[b] $C_{fcta} = 4.25 \times 10^{-2} \exp(2900/RT)$, where the CTA was $t-C_{12}$ mercaptan
[c] $C_{fcta} = 7.083 \times 10^{-3} \exp(2900/RT)$, where the CTA was $t-C_{12}$ mercaptan
[d] Solution polymerization
[e] $C_{fcta} = 1.288 \times 10^{-2} \exp(1400/RT)$
[f] $t-C_{12}$ mercaptan (Sulfole 120), note C_{fcta} increases with Bd composition
[g] AN/Bd charge of 20/80

3.10.2 Nucleation Parameters

Particle nucleation is a distinguishing characteristic of heterogeneous polymerization. Effective methods for tracking the nucleation and growth of particles are essential for predicting/monitoring not only the rate of polymerization and monomer conversion but also particle size characteristics. As previously mentioned, the approach to radical capture in this model (thesis) is based on collision theory, where the rate of capture is proportional to the surface area of the micelles and particles. Two parameters, ε and k_{cp}, are used to determine the rate of radical capture by micelles and particles. ε relates the rate of capture by particles to micelles, while k_{cp} is the rate constant for radical capture by particles and is normally a constant parameter, although it is possible to define it more generally as a function of temperature through an Arrhenius expression. However, in the case of low temperature polymerization, the influence of temperature is assumed to be negligible and is simply given as a constant, while ε is defined as:

$$\varepsilon = \frac{k_{cp}}{k_{cm}} \tag{3.140}$$

Thus, by specifying ε and k_{cp} one can determine k_{cm}. The rate of homogeneous nucleation is defined in a similar manner, where one parameter is used to set the initial rate. In this case μ is specified, and relates the initial rate of homogeneous nucleation (i.e. k_{h_o}) to the rate of radical capture by micelles (i.e. k_{cm}).

$$\mu = \frac{k_{h_o}}{k_{cm}} \tag{3.141}$$

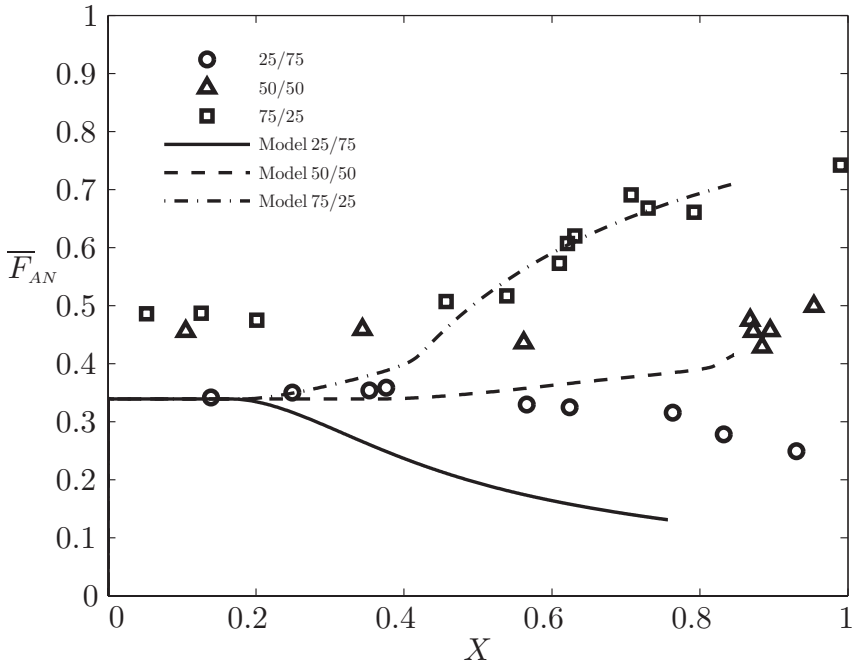

Figure 3.3: Cumulative copolymer composition of AN as a function of conversion

Upon combining Equations 3.140 and 3.141 and rearranging, k_{h_o} can be defined in terms of three specified parameters, shown as follows:

$$k_{h_o} = \frac{\mu}{\varepsilon} k_{cp} \tag{3.142}$$

Clearly, k_{h_o} is in direct proportion to μ, and as was found through simulation, the dominant factor controlling homogeneous nucleation was the magnitude of the parameter μ.

While μ is an important parameter for homogeneous nucleation, the parameters of greater influence on micellar nucleation are ε and k_{cp}. To shed some light on how sensitive nucleation is to these parameters, response surface plots were generated for a number of important model responses by varying both ε and k_{cp}. Simulations were performed using a batch reactor and all responses were recorded at a time of 300 minutes. Figures 3.4 and 3.5 illustrate the sensitivity of N_p, $\bar{n}$, and $\overline{d}_p$ to changes in ε and k_{cp}. As seen from each of these surface plots, the influence of k_{cp} is minimal compared to ε. As ε is decreased (i.e. k_{cm} increases) more particles are nucleated (i.e. higher N_p, lower $\bar{n}$, and $\overline{d}_p$), and all responses become more sensitive.

Table 3.7: Baseline nucleation parameters for micellar and homogeneous mechanisms

Parameter	**Approximation**
ε	4.839
k_{cp}	0.025
μ	550000 [a]

[a] Penlidis [136] cites a value of 0.55 for vinyl acetate, however 5.5×10^5 provides a better estimate of N_p^{hom} of approximately $10^{14}\#/L_w$

For an NBR system, using the radical concentration approach given in section 3.3, in order to obtain a number of particles per litre of water in the order of 10^{18} through micellar nucleation, ε is needed to be in the range of 4 to 8, while k_{cp} needed to be around 0.01 to 0.03 (Table 3.7). Note that there can be a strong correlation between ε and k_{cp} depending on their relative values. For example, if ε is increased then k_{cp}, in most cases, must be decreased in order to maintain a particular level of nucleation. In other words, if you increase both ε and k_{cp} together at the same rate then very little change in particle nucleation will be noticed, however, if you increase ε quicker than k_{cp} you are forcing more radicals to be captured by particles, and thus decreasing the rate of nucleation and overall number of particles.

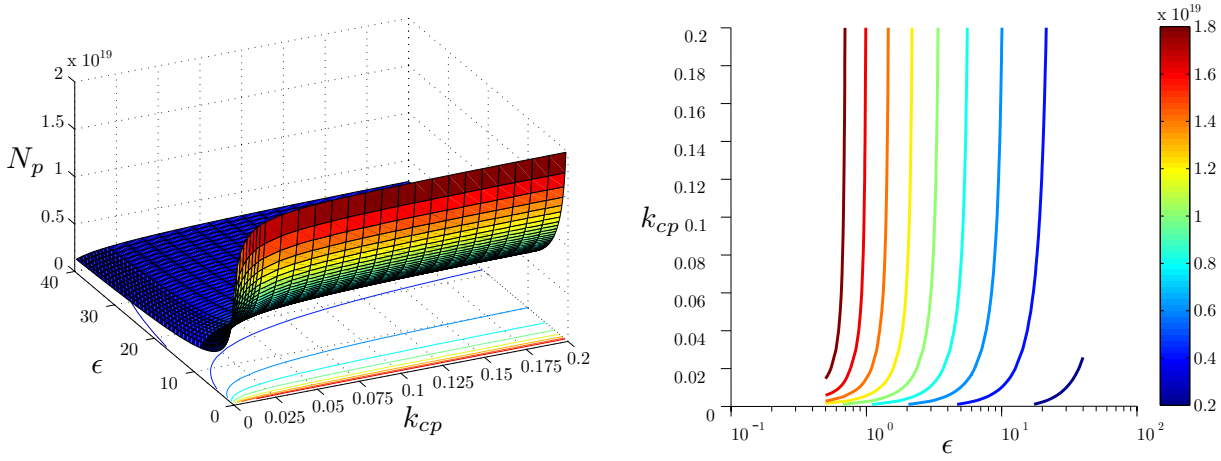

(a) (b)

Figure 3.4: Parameter sensitivity for ε & k_{cp} - influence on N_p

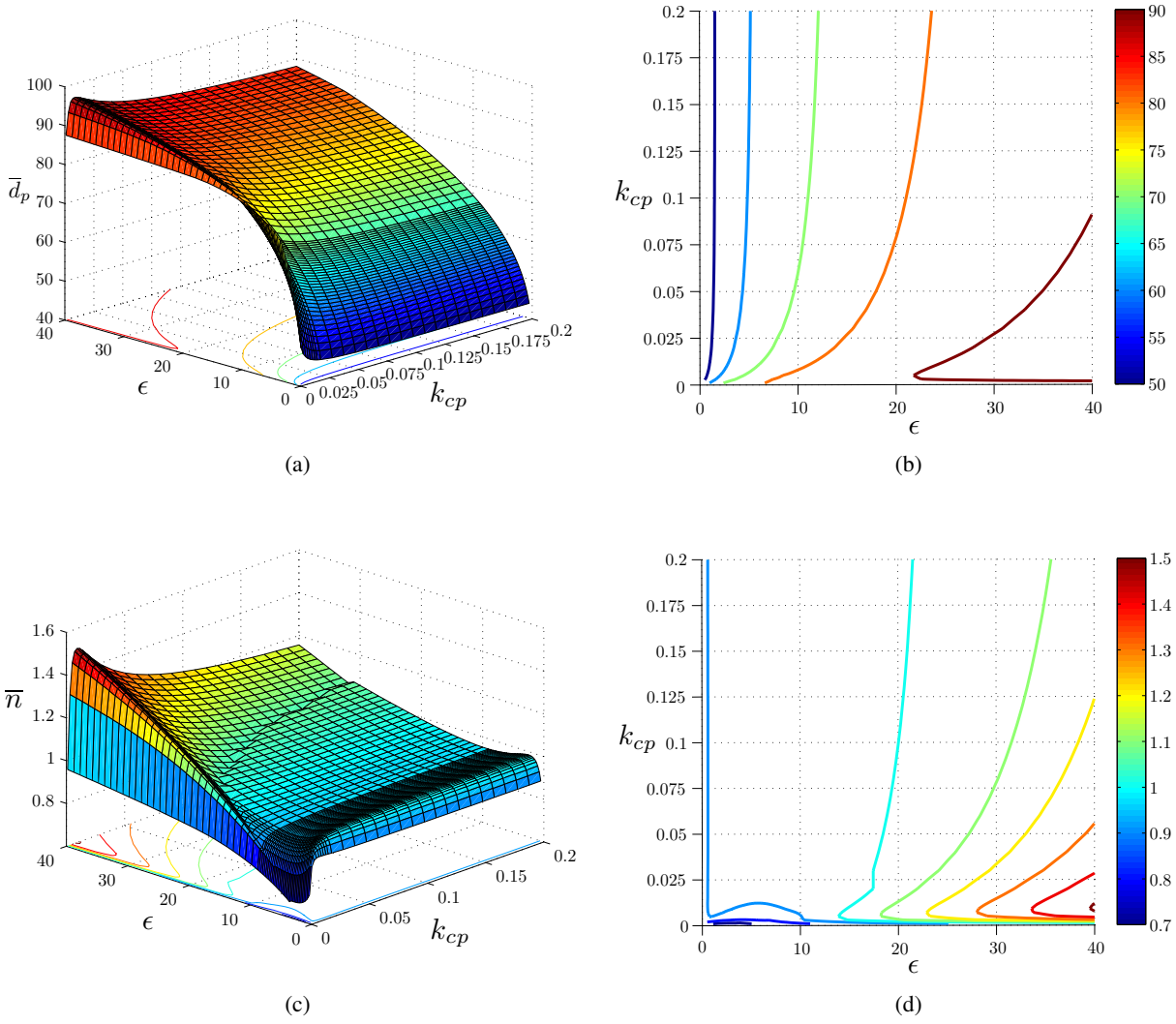

Figure 3.5: Parameter sensitivity for ε & k_{cp} - influence on $\overline{d}_p$ (top) & $\bar{n}$ (bottom)

Chapter 4

Model Validation, Simulation & Testing

In this chapter model simulations will be conducted in order to establish the general trends in the response variables using batch and CSTR reactors. Several model checks and base case simulation studies will be performed to show the influence of recipe ingredients (i.e. emulsifier, initiator and CTA reactor charges and inflow rates) on conversion, particle size/number, average radicals per particle, rate of polymerization and molecular weights/branching. Furthermore, the reader is referred to Appendix D for model checks on monomer partitioning and particle nucleation. Once the general trends are established, a comparison will be made to literature data for Bd and NBR in order to assess the model's validity and capability of predicting the general process response. Clearly, to obtain a good fit to the process data detailed parameter estimation is necessary; however, the objective here is not to go into detail on parameter estimation; instead minor parameter adjustments will be made in order to show that the model adequately predicts the general trends of the process outputs. It is believed that this procedure is a sufficient first step to showing model efficacy.

4.1 Model Trend Verification for NBR Simulations

This section will illustrate and discuss the general model response trends seen in batch and CSTR reactors. The purpose here is to verify that the model provides reasonable output predictions compared to theory and other similar emulsion systems (i.e. SBR). Different levels of the feed ingredients will be used to show the influence on the model response (i.e. conversion, number of particles, particle size, copolymer composition). In addition, the idea of radical desorption will be examined, as some investigators have suggested its importance in Bd systems [184]. Finally, several continuous reactor start-up procedures will be looked at and discussed.

4.1.1 Baseline Model Simulations

Perhaps the most important, and easiest to estimate on-line, process indicator is the conversion of the monomer feed. From the perspective of product characterization and identification the copolymer composition is a key indicator, while molecular weight and chain branching provide an indication of the final product quality, as well as information on the extent of gelation of the growing polymer mass. Conversion, copolymer composition, particle number and size, molecular weight, and branching frequency will all be shown in the following baseline figures in order to provide an illustration of the general model trends.

The recipes used for model demonstration are given in Table 4.1 for a batch reactor, while CSTR recipes were chosen with the same inlet feed compositions as the initial batch charge. The recipes shown below are representative of industrial NBR recipes and, in terms of the ingredients used, are quite similar to the SBR recipes discussed by Bovey et al. [13]. The ingredients K-oleate, Dresinate, and Tamol are emulsifiers, and KPS and PMHP are initiators.

Table 4.1: NBR base case batch recipes

Ingredient	**Recipe 1 (Cold)**[a]	**Recipe 2 (Hot)**
Acrylonitrile	32	28
Butadiene	68	72
Water	180	180
KPS [b]	-	0.25
PMHP [c]	0.223	-
Fe [d]	0.0056	-
SFS [e]	0.12	-
K-Oleate [f]	-	1.24
Dresinate [g]	1.25	-
Tamol [h]	2.85	2.85
Mercaptan	0.42	0.64
$[E]$ (mol/L)	0.0373	0.0371
$[I]_o$ (mol/L)	0.0065	0.0046
Temperature (^oC)	10	40

[a] parts per hundred monomer
[b] Potassium persulfate
[c] *para*-menthane hydroperoxide
[d] $FeSO_4 \cdot 7H_2O$
[e] Sodium formaldehyde sulfoxylate
[f] Potassium oleate
[g] Potassium soap of disproportionated rosin acids
[h] Dispersing agent - condensed polyarylsulfonic acid salt

The conversion-time history for cold NBR production and copolymer composition can be seen in Figure 4.1. The corresponding predictions for particle number and size, molecular weight, and chain branching are shown for both batch and CSTR reactors in Figures 4.2 and 4.3. Simulated polymer properties are tabulated in Table 4.2 for a conversion of 70%, which is roughly close to the typical final conversion used in an

industrial process.

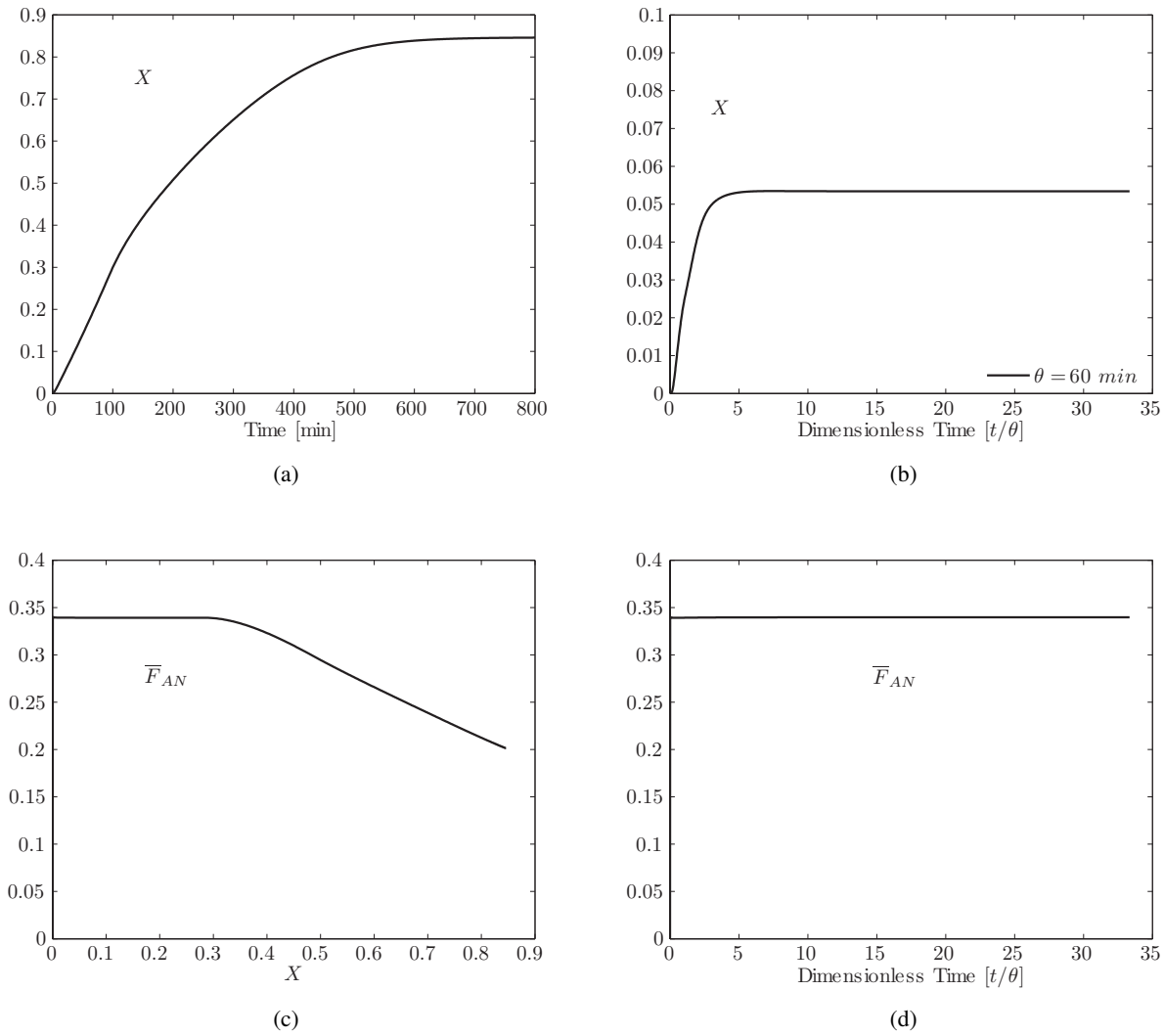

Figure 4.1: Batch (a,c) & continuous (b,d) reactor simulation - conversion and composition for cold NBR

In each of these figures, the simulations were performed excluding impurities. Impurities can significantly distort the reaction properties, and the purpose here is to establish a general idea of the typical trends before impurities are introduced. Conversion predictions for cold rubber production in a batch reactor, shown in Figure 4.1a, reveal a similar trajectory to those shown by Dube et al. [33] and Vega et al. [172] for NBR and Broadhead [15] for SBR. The reaction itself is quite slow, taking roughly 10 hours to reach 80 % conversion, which is typical for rubber production in a batch reactor. Similar predictions in a CSTR reveal a gradual increase in conversion until a steady-state is reached (roughly 4 hours to reach 5.4% conversion). For the profile shown in Figure 4.1b, the single CSTR reactor was initially filled with water and an overall mean residence time of 60 minutes was used, with one reactor in operation.

The cumulative copolymer composition (CCC), shown in Figure 4.1c for a batch reactor, remains con-

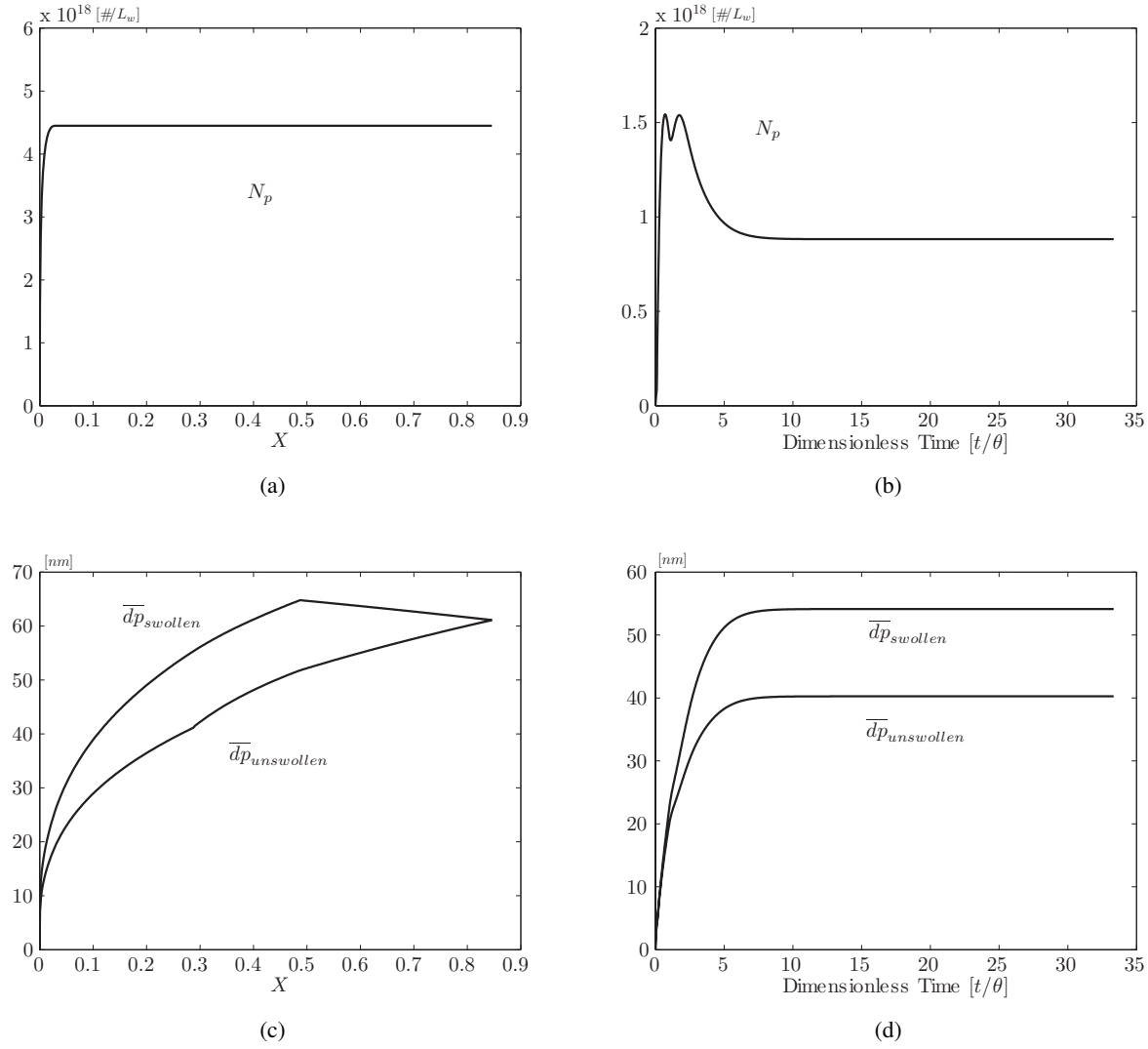

Figure 4.2: Batch (a,c) & continuous (b,d) - particle number & diameter for cold NBR

stant at approximately 34% AN until 30% conversion, beyond which it drifts to approximately 20% AN at 80% conversion. For a single CSTR, the conversion does not reach high enough levels for composition to show any drift; however, for a train of CSTR's the CCC can drift in a similar manner to the batch reactor if additional monomer is not fed along the train. Further details on reactor train simulations are shown in Chapter 5.

In general, composition drift is typical when one monomer is considerably more reactive than the other. In the case of AN/Bd, AN radicals are considerably more reactive than Bd radicals and propagate with AN or Bd monomer units at a much higher rate (i.e. $k_{p_{AA}} \gg k_{p_{BB}}$ & $k_{p_{AB}} \ggg k_{p_{BA}}$). Typical NBR recipes use a feed ratio of AN to Bd that is below the azeotropic composition (see Figure 3.2). As a result AN is incorporated into the copolymer at a much faster rate than Bd. Once AN is completely consumed the relative amount of AN in the copolymer decreases as more Bd is polymerized, thus the copolymer composition drifts. Factors

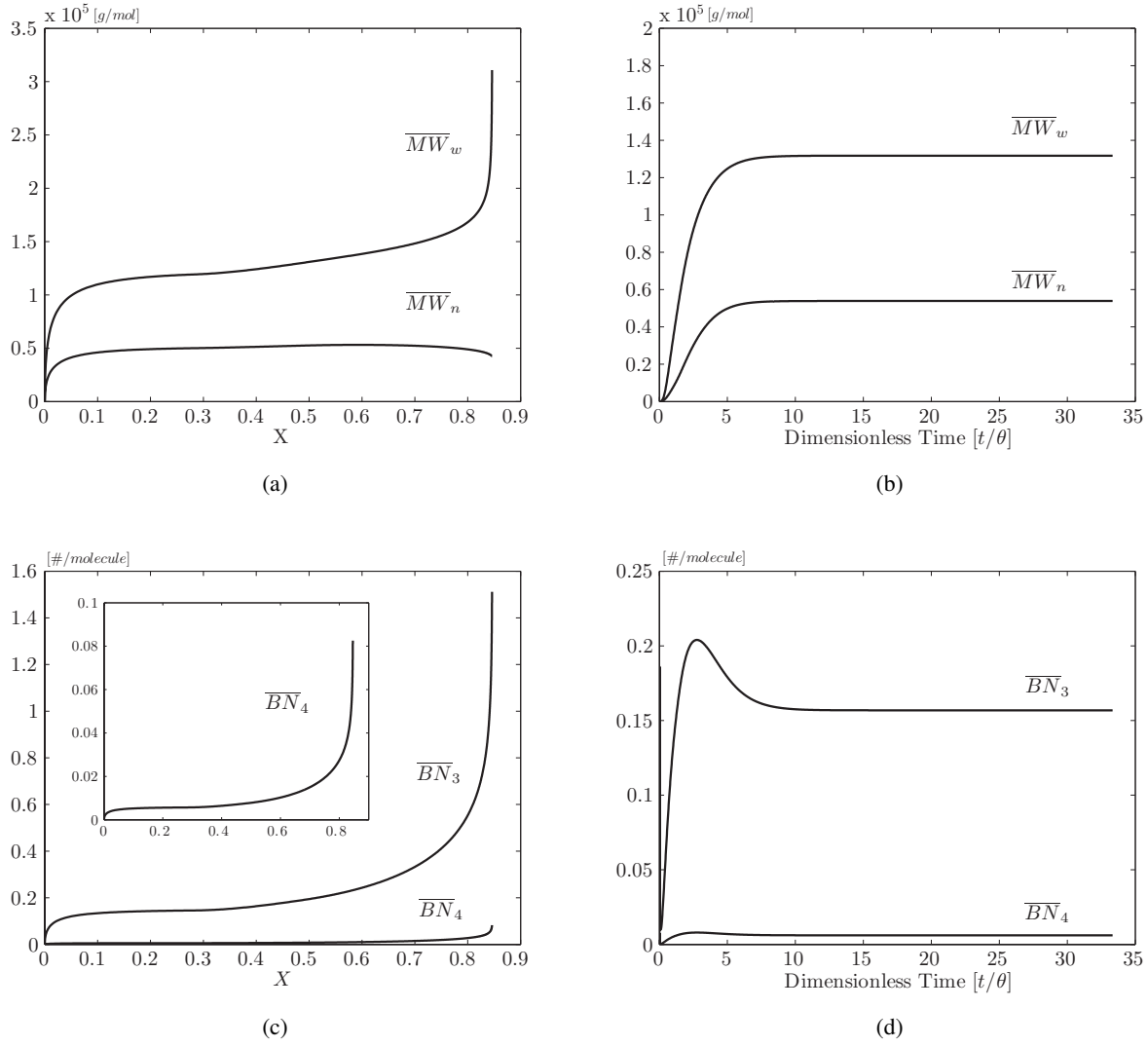

Figure 4.3: Batch (a,c) & continuous (b,d) - molecular weights & branching frequencies for cold NBR

influencing copolymer drift are the reactivity ratios and monomer phase partitioning. A comparison of CCC simulations using different reactivity ratios was previously shown in Figure 3.3, and revealed that reactivity ratio estimates clearly influenced the initial bound AN in the copolymer but had little influence on the onset of drift, which is more related to the initial feed composition ratio and the partitioning of monomer between each phase.

The number of particles per litre of water and the average particle diameter are shown in Figure 4.2 for batch and CSTR reactors. In a batch reactor, particle nucleation occurs very quickly, reaching a final number in less than 20 minutes, while in a CSTR nucleation is just as quick. A significant overshoot in the number of particles occurs initially, regardless of startup procedure, and then gradually N_p approaches steady-state. The time to reach steady-state is dependent on the reactor residence time, and typically decreases with residence time. For the example shown in Figure 4.2b, the number of particles reached a steady-state in

approximately 7 hours using a 1 hour residence time in a single CSTR. Besides the significant overshoot, a noticeable double peak is seen in the CSTR simulation. This behaviour is because of the particular reactor startup procedure used (e.g. the reactor initially full of water) and because of two different emulsifiers with differing critical micelle concentrations (CMC). Initially, the emulsifier concentration is below the CMC. As more emulsifier is fed the concentration increases above the CMC for one of the emulsifiers (i.e. the first peak), followed by the second emulsifier (i.e. the second peak). Particle diameters are shown for both swollen (monomer and polymer) and unswollen (polymer) particles. For the former, the final average diameter in a batch reactor is around 60 nm, while for a single CSTR the diameter is around 55 nm. Figure 4.2c also reveals a distinct decrease in diameter around 50% conversion, which occurs when the monomer droplets have disappeared and monomer in the particles is no longer replenished resulting in particle shrinkage due to monomer-polymer density differences.

Figure 4.3 provides predictions of average molecular weight and branching frequencies for batch and CSTR reactor simulations. The profiles shown here were generated using the CTA rate parameters specified in Table 3.5. In a batch reactor, the predictions for number and weight average molecular weight reveal a rapid increase within the first 5% conversion. Molecular weights remain fairly constant from 10% to 30% conversion, and then increase slightly from 30% to 80% conversion, at which point the weight-average molecular weight rapidly increases due to gelation. Typically, one would expect the number-average molecular weight to continually increase as conversion increases; however, the profile behaviour is highly dependent on the relative amount of CTA present and the reaction rate constant used. The choice of rate constant for this example was based on the molecular weight data shown by Vega et al. [171]. For a single CSTR, the molecular weight rapidly increases as the reactor is started up and reaches a steady-state value that is slightly above the molecular weights shown for a batch reactor at approximately the same conversion level. Detailed comparisons are shown between data and simulations in section 4.2. In a batch reactor, branching frequencies for tri- and tetra-functional branching increase rapidly within the first 5% conversion and remain fairly constant until above 80% conversion where significant branching and cross-linking occurs. A similar degree of branching is seen in a CSTR, along with a slight overshoot as the reactor starts up. The influence of the rate parameters on the molecular weight and branching frequency is discussed in detail in section 4.1.4.

Table 4.2: Summary of batch reactor simulation properties

Conversion	N_p $(\#/L_w)$ $(\times 10^{-18})$	$\overline{d}_p$ (nm)	$\overline{M}_n(g/mol)$ $(\times 10^{-6})$	$\overline{M}_w$ (g/mol) $(\times 10^{-6})$	PDI	$\overline{BN}_3$ $(\#/molecule)$	$\overline{BN}_4$ $(\#/molecule)$
70%	4.45	62.1	0.0433	0.1302	3.00	0.1593	0.0164
80%	4.45	61.6	0.0411	0.1352	3.29	0.2242	0.0231

To give some insight on the influence of the termination rate constant on the average number of radicals per particle, relevant profiles are shown in Figure 4.4. Initially, the termination rate constant remains constant while the particles are saturated with monomer, and once the droplets disappear the onset of diffusion-controlled termination is triggered. For the case shown in Figure 4.4a, k_t remains within the translational controlled region. As discussed in section 3.1.2, and repeated here for convenience, the termination rate

constant is defined through an empirical relation as follows [49, 136]:

$$k_t = k_{t_o} \exp(A_1 X + A_2 X^2 + A_3 X^3) \tag{4.1}$$

where, the parameters A_1, A_2 and A_3 were originally estimated by Friis and Hamielec [49] for a vinyl acetate system (Case I kinetics). Despite a completely different monomer system (i.e. Case II kinetics in our case), the parameter estimates were used for the NBR system and provided a reasonable profile for k_t. Clearly, a considerable amount of uncertainty is attached to these estimates, which warrants further review. Besides the expression given by Equation 4.1, numerous other empirical, semi-empirical, or theoretical expressions are used to model k_t. For example, Broadhead [15] used a semi-empirical expression based on free-volume theory to model k_t for an SBR system, which generated a similar profile to that shown in Figure 4.4a for NBR except that k_t began to flatten out (i.e. approach zero asymptotically) above 60% conversion. The flattening-out behaviour was more predominant as conversion increased beyond 80%, which indicates that the kinetics may be controlled by a reaction diffusion termination process (i.e. $k_t \propto k_p[M]$). This behaviour was not evident with NBR simulations which is most likely due to the parameter estimates used or the empirical expression itself. From an industrial perspective conversion is never allowed to proceed much higher then 70%, thus the present expression for k_t may be satisfactory; however, an interesting model extension would be to explore different empirical and semi-empirical expressions using industrial process data. At present, this is one particular aspect of the model that deserves another look.

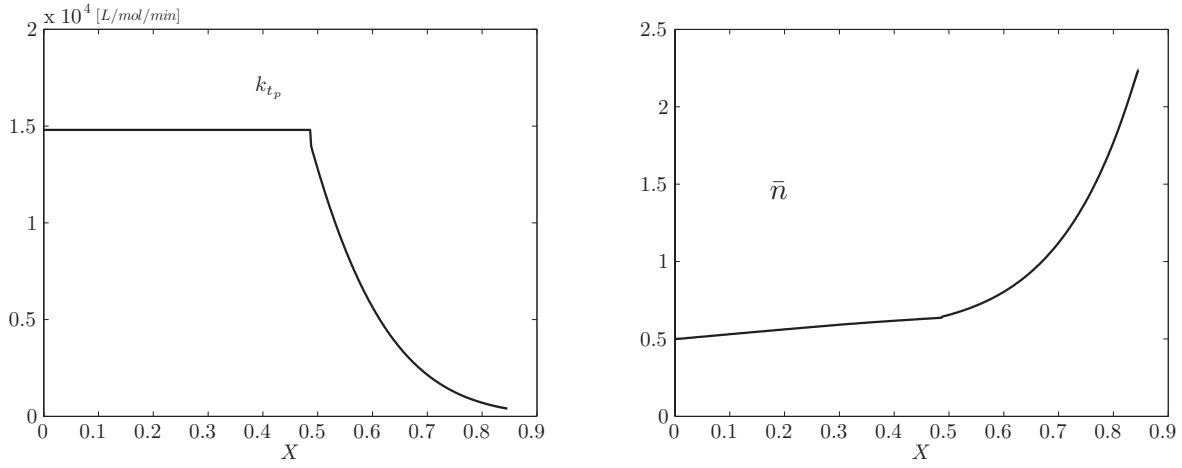

(a) (b)

Figure 4.4: Batch reactor simulation - average number of radicals per particle & termination rate constant for cold NBR

4.1.2 Influence of Emulsifier & Initiator on Particle Nucleation

In order to check the particle nucleation dependence on initiator and emulsifier concentration and to assess whether similar trends to those of Smith & Ewart could be observed, the model was simulated with several different levels of emulsifier and initiator. According to Smith & Ewart, the dependence of N_p on emulsifier and initiator concentrations is as follows:

$$N_p \propto [E]^{0.6} [I]_o^{0.4} \tag{4.2}$$

where, $[E]$ and $[I]_o$ are the initial concentrations of emulsifier and initiator charged to the reactor. The relative particle dependence on each of these ingredients can be determined by applying a logarithmic transformation, plotting N_p versus each ingredient, and looking at the slope of the resulting profile. Figure 4.5 displays each of these plots, and if one were to compare to the profiles of traditional Smith & Ewart dependencies a deviation would be evident. Both profiles show a nonlinear behaviour, with N_p increasing fairly linearly with emulsifier concentration, while N_p shows a quadratic dependence on initiator concentration with a fairly linear dependence up to a concentration of 0.01 mol/L. The behaviour seen by Smith & Ewart for a styrene system, which was further verified for an SBR system by Wong [190] and Broadhead [15], is not evident in an NBR system. This is most likely a result of the high water solubility of AN and significant homogeneous nucleation that is present.

In an attempt to further characterize the particle nucleation dependence on emulsifier and initiator concentration, a response surface plot was generated, as seen in Figures 4.5c and 4.5d. The trend is quite clear, as the emulsifier concentration is increased the particle number increases and as the initiator concentration is increased the particle number passes through a maximum. Based on these findings, recipe formulations can be tailored in order to achieve a desired number of particles.

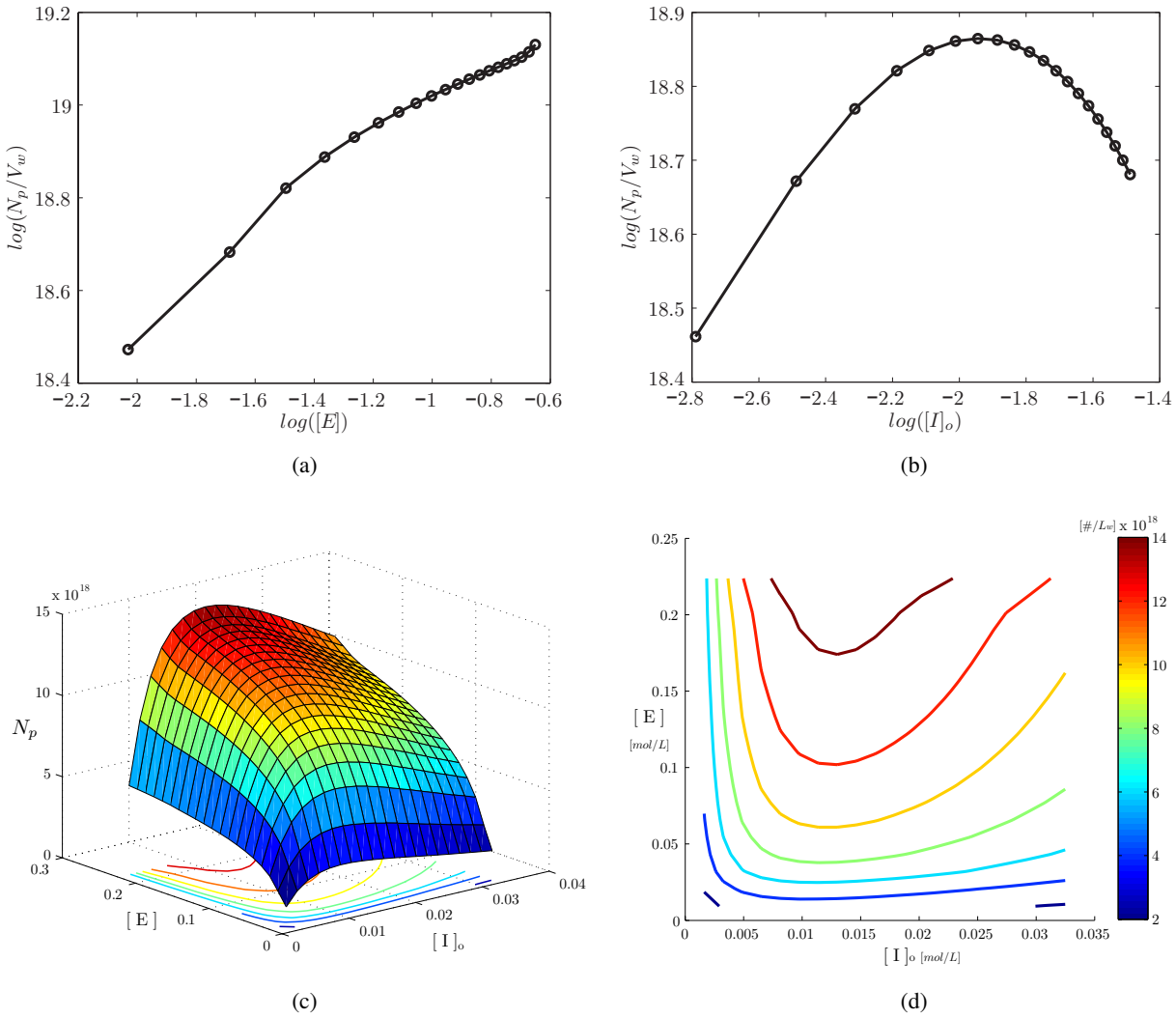

Figure 4.5: Batch reactor simulation - particle number for different levels of emulsifier and initiator

For a continuous reactor, the particle number dependence was assessed by varying the feed compositions of emulsifier and initiator independently as well as the mean residence time through adjustment of the total inlet flow rate to the reactor. Figure 4.6 demonstrates the influence of reactor residence time and different levels of emulsifier and initiator on the steady-state particle number. The baseline emulsifier and activator recipe (i.e. initiator, oxidizing agent, and reducing agent) used were set according to those specified in Table 4.1 for the cold recipe. The response of N_p to residence time at different levels of emulsifier and initiator is consistent with simulations for SBR shown by Kanetakis et al. [82], as well as with the experimental findings of Nomura et al. [122] for styrene. Clearly, there exist certain reactor operating conditions that provide a maximum number of particles, and with no surprise formal equations have been proposed that predict these optimal conditions [66, 120]. The point here is to point out that the current NBR model behaves according to the experimental findings of other similar systems (i.e. case II), and that by manipulating the residence

time of the first reactor in a train and the feed composition of emulsifier and initiator, more particles can be nucleated.

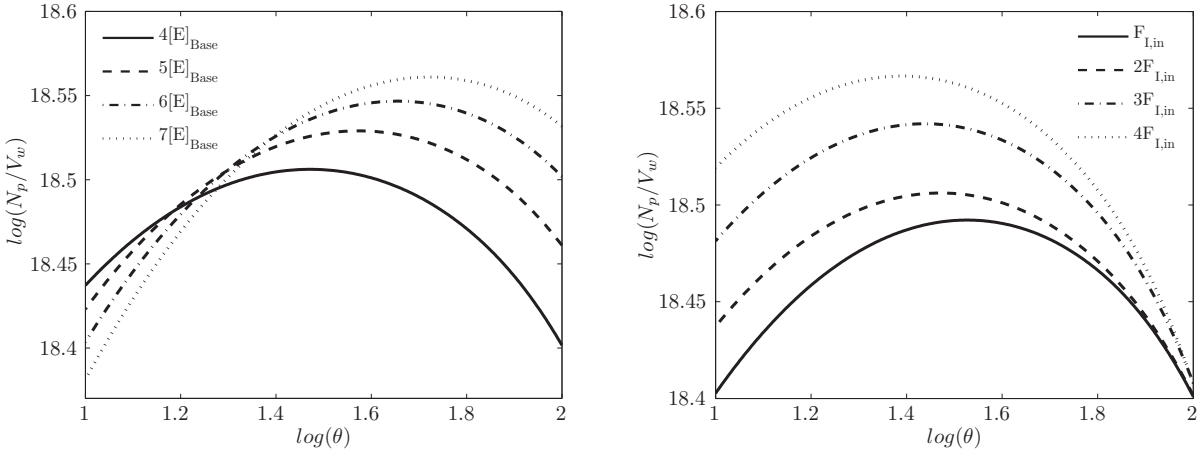

(a) (b)

Figure 4.6: Continuous reactor simulation - particle number versus mean residence time at different levels of emulsifier & initiator

4.1.3 Influence of Impurities on Polymerization Rate

Monomer Soluble Impurities

The effect of monomer and water soluble impurities on the polymerization rate, particle nucleation and growth has been shown in the literature to be quite pronounced [75, 139]. The objective here is to demonstrate the influence of impurities on the polymerization in both batch and continuous reactors. For the purpose of comparison, monomer and water impurities will be considered independently using several different impurity concentrations.

Considering first monomer impurities, the influence on conversion and polymerization rate is shown in Figures 4.7 and 4.8 for batch and continuous reactors. As the level of impurities is increased from 0 to 20 ppm, the polymerization rate is hindered at first and then sharply jumps above the base rate seen without impurities. This behaviour is reflected on the conversion (for the batch case) as the slope of the conversion profile is slightly higher throughout the course of polymerization with 20 ppm of impurity included (Figure 4.7a). Monomer impurities function by consuming radicals in the particle phase, and reducing $\bar{n}$ considerably until enough of the impurity is consumed to allow captured radicals to build up and polymerization to commence. Increasing the impurity concentration to 50, 100, and 200 ppm creates an increased induction at the beginning of polymerization and results in a much lower $\bar{n}$, which causes the rate to drop and prolongs the time to final conversion. In general, the polymerization reaction is rather slow and with the inclusion of impurities becomes even slower. As is shown in Figure 4.7d for a batch reactor, the impurity concentration can remain fairly constant with only a small amount of impurities. This lingering effect is clearly quite pronounced and can last over the course of polymerization. In a CSTR, monomer impurities function in a similar manner to a batch reactor, by hindering the onset of polymerization, after which the rate and conversion increase sharply coming to a final steady-state below the base conversion without impurities (Figure 4.8a).

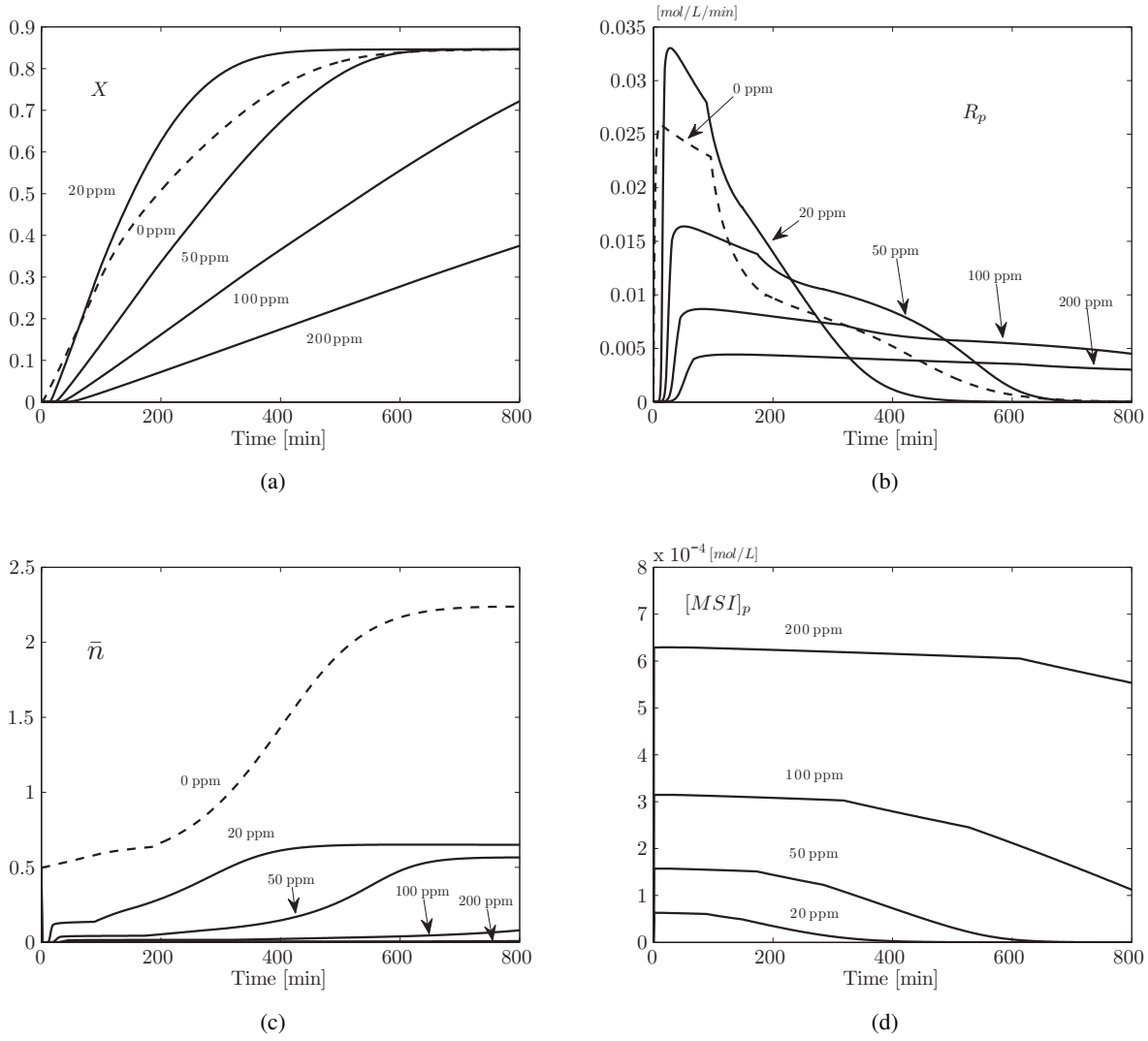

Figure 4.7: Batch reactor simulation - effect of $[MSI]$ on conversion & polymerization rate

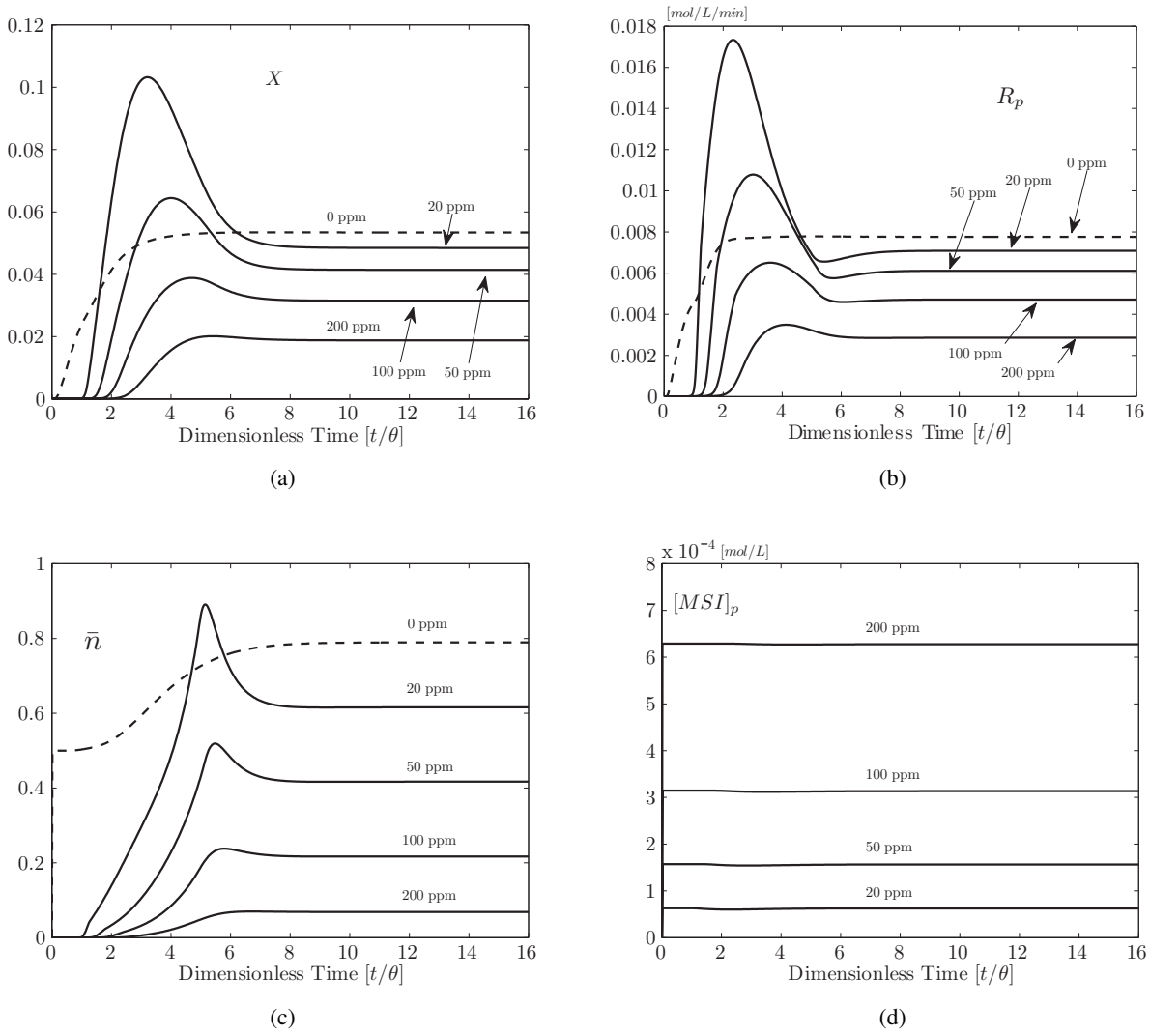

Figure 4.8: Continuous reactor simulation - effect of $[MSI]$ on conversion & polymerization rate

The effect of monomer impurities on particle number and size is shown in Figure 4.9 for batch and continuous reactors. In each case the general trends are similar to the batch case: as the impurity level is increased the number of particles increases and the average diameter decreases. This behaviour is a direct result of a prolonged nucleation period due to impurity inhibition. The profiles shown here are in good agreement with simulation and experimental results for a styrene system shown by Huo et al. [75]. An interesting behaviour is shown in Figure 4.9d for the transient response of N_p in a CSTR. As the impurity level is increased a significant and progressive burst in polymer particles is evident that considerably overshoots the steady-state value. These nucleation dynamics are reflected on $\overline{d}_p$ and $\bar{n}$, as seen by lower magnitudes initially when N_p is high, followed by a moderate spike when N_p descends below the steady-state, and finally decreasing back to their steady-state.

In order to assess the sensitivity of particle nucleation and monomer conversion to the monomer im-

purity rate constant, a base case of $k_{fmsi} = k_p$ was compared to upper and lower values of $k_{fmsi} = 5k_p$ and $k_{fmsi} = 0.1k_p$. Figure 4.10 demonstrates the influence of k_{fmsi} on key model responses. Lowering k_{fmsi} significantly below k_p allows monomer propagation to proceed along side radical consumption, thus only a minor induction period is seen after which conversion catches up to the impurity-free case quite quickly. Furthermore, the impurity concentration remains fairly high throughout polymerization, and initially builds up, since $k_{fmsi} \ll k_p$, before decreasing. The nucleation period is also shortened resulting in a small particle number and large average diameter. On the other hand, increasing the impurity rate constant above that for propagation causes radicals to preferentially react with impurities as opposed to monomer. This is evident from the long induction period and hindered conversion profile seen in Figure 4.10a. In addition, the nucleation period is now much longer, giving rise to more particles and an overall smaller diameter.

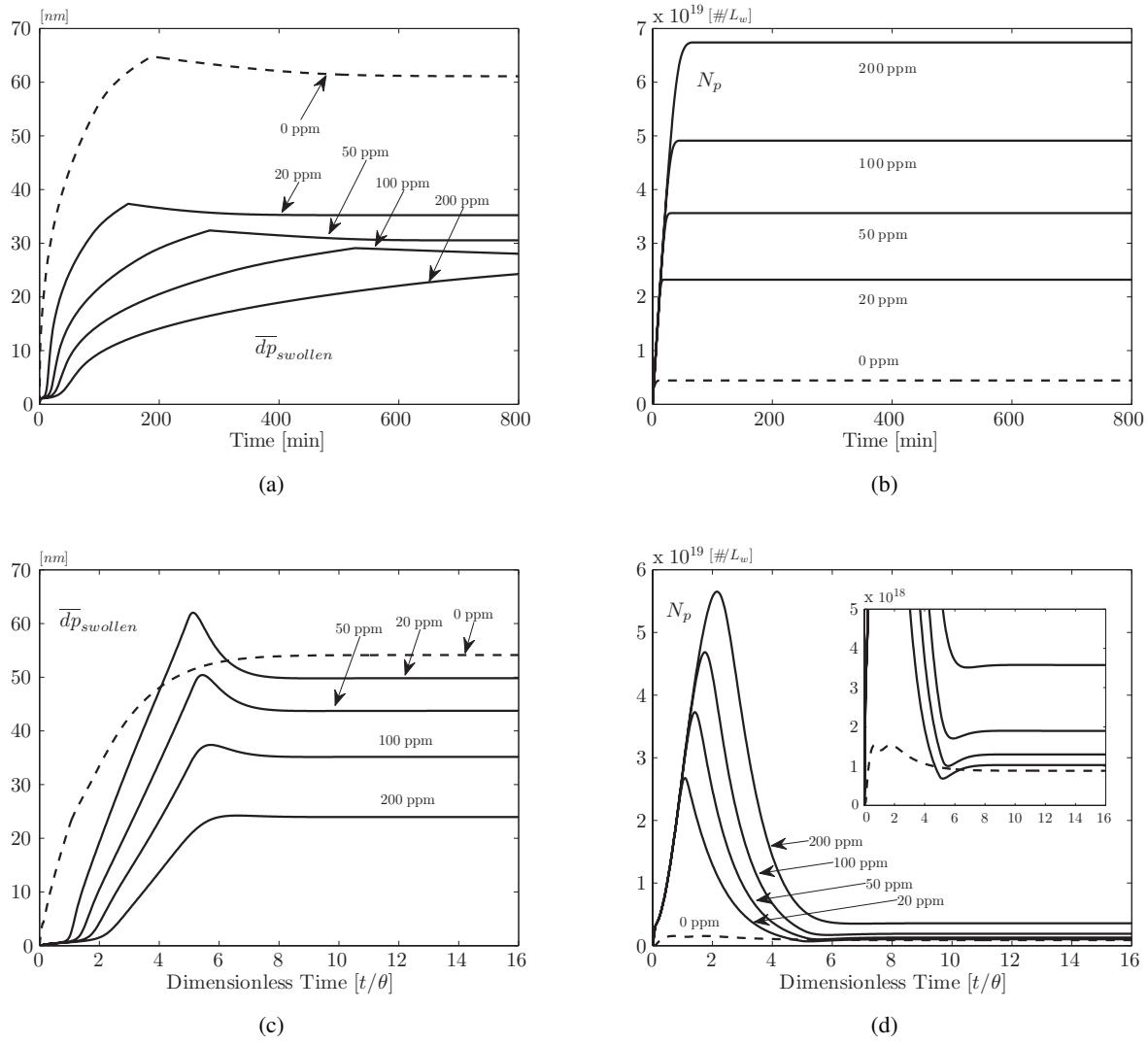

Figure 4.9: Batch (top) & CSTR (bottom) reactor simulation - effect of $[MSI]$ on particle number & diameter

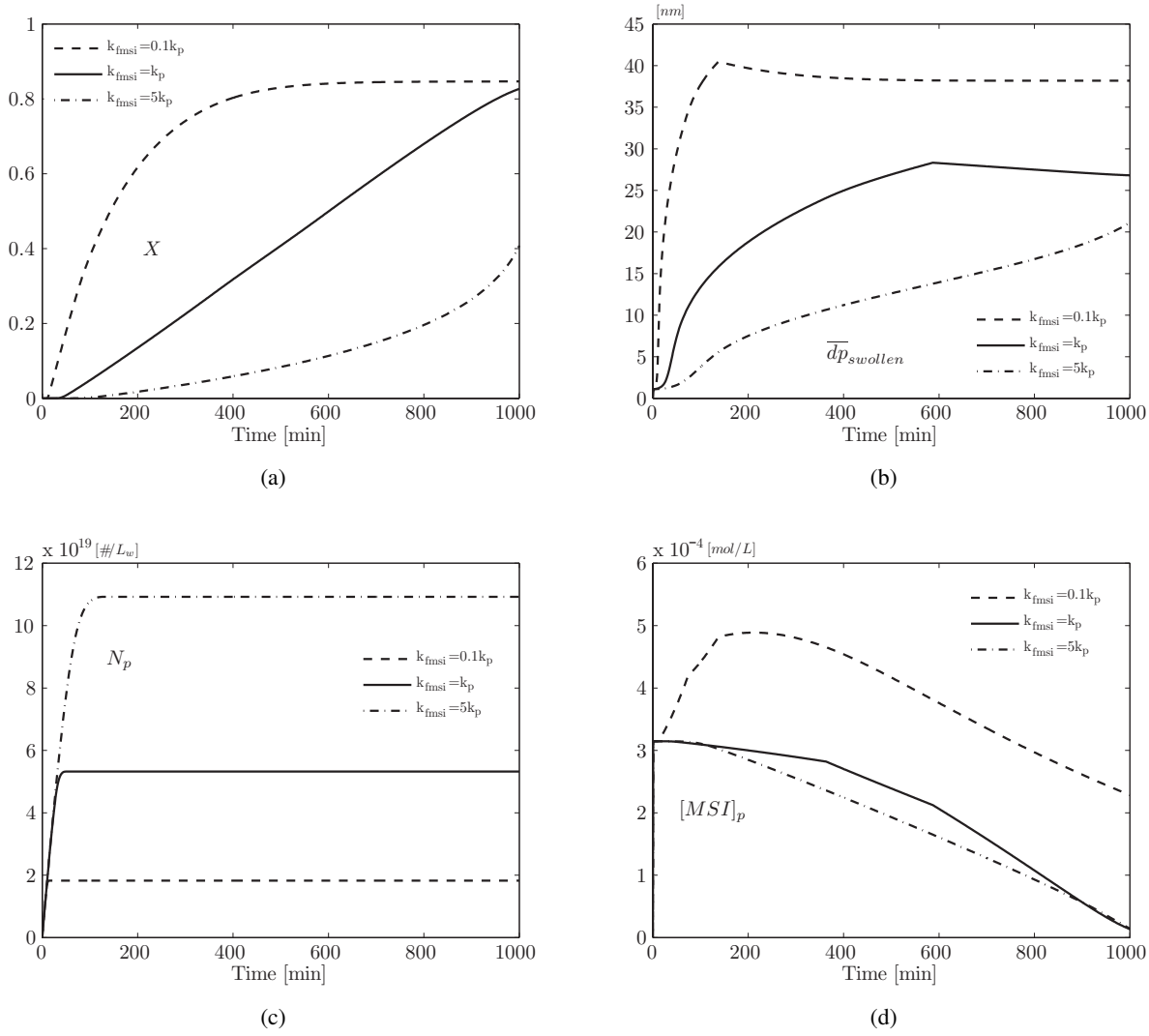

Figure 4.10: Batch reactor simulation - effect of k_{fmsi} for 100 ppm MSI

A summary of final latex properties in a batch reactor is provided in Table 4.3. Clearly seen is the influence of MSI's on particle nucleation; as $[MSI]$ increases N_p follows suit, while $\overline{d}_p$ decreases. The effect of impurities on the molecular properties does not appear to be of considerable significance.

Table 4.3: Influence of monomer soluble impurities on final polymer properties in a batch reactor

TBC [a] (ppm[b])	N_p $\times 10^{-18}$ $(\#/L_w)$	d_p (nm)	$\overline{MW}_n$ $\times 10^{-6}$ (g/mol)	$\overline{MW}_w$ $\times 10^{-6}$ (g/mol)	PDI	$\overline{BN}_3$ $(\#/molecule)$	$\overline{BN}_4$ $(\#/molecule)$
0	4.45	61.2	0.0446	0.2079	4.66	0.944	0.050
20	23.22	35.3	0.0439	0.2037	4.64	0.940	0.049
50	35.62	30.6	0.0443	0.2094	4.73	0.948	0.050
100	49.12	27.5	0.0441	0.2072	4.69	0.936	0.049
200	67.40	22.1	0.0432	0.1954	4.52	0.896	0.047

[a] t-butyl catechol

[b] parts per million monomer

Water Soluble Impurities

Depending on the reactivity of water soluble impurities, an induction period may be observed (during which the polymerization rate is reduced to almost zero), until all impurities have been consumed, or simply a considerably diminished polymerization rate may result throughout the entire polymerization. For demonstration within an NBR system, oxygen was used (which can be considered quite reactive) which acts by lowering the rate throughout the course of polymerization. The effect of several impurity levels on conversion and polymerization rate in a batch reactor can be seen in Figure 4.11. For a CSTR, the impurity influence is shown in Figure 4.12. In each case, batch or CSTR, increasing the level of impurities lowers the rate of polymerization, thus a greater reaction time is required to reach final conversion.

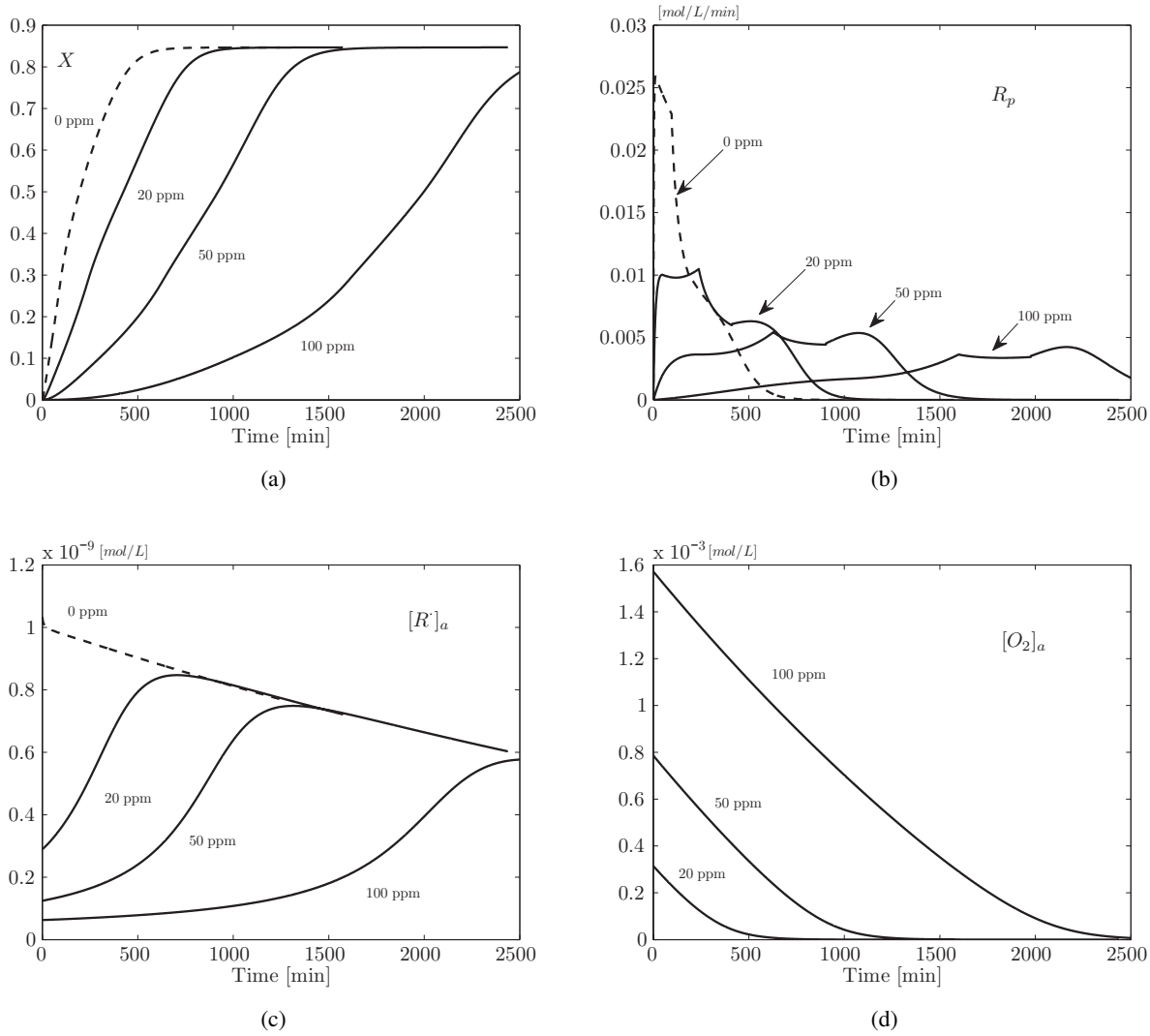

Figure 4.11: Batch reactor simulation - effect of $[WSI]$ on conversion & polymerization rate

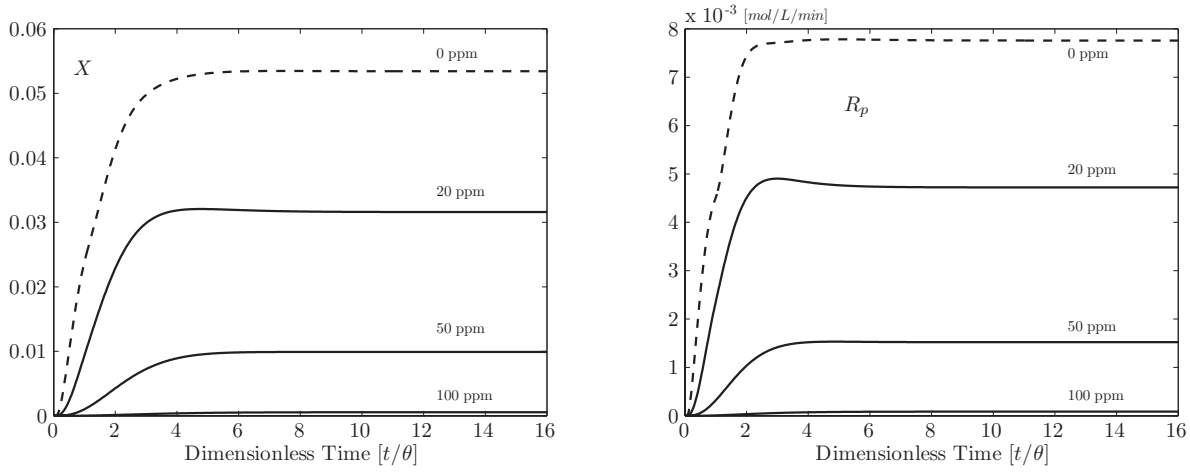

(a) (b)

Figure 4.12: Continuous reactor simulation - effect of $[WSI]$ on conversion & polymerization rate

The influence of WSI's on the final molecular properties was found to be minimal, which has been proven experimentally within the literature [75, 139]. Final molecular properties at different impurity levels for a batch reactor are summarized in Table 4.4. Note that the simulated final values for molecular weight and branching frequency were recorded once the system had reached a limiting final conversion and all the impurities had been consumed.

Table 4.4: Influence of water soluble impurities on final molecular properties in a batch reactor

O_2 [a] (ppm[b])	$\overline{MW}_n$ $\times 10^{-6}$ (g/mol)	$\overline{MW}_w$ $\times 10^{-6}$ (g/mol)	PDI	$\overline{BN}_3$ $(\#/molecule)$	$\overline{BN}_4$ $(\#/molecule)$
0	0.0446	0.2079	4.65	0.944	0.050
20	0.0454	0.2185	4.8	0.963	0.051
50	0.0458	0.2239	4.9	0.967	0.051
100	0.0460	0.2261	4.9	0.969	0.051

[a] Oxygen is used here for demonstration purposes
[b] parts per million monomer

4.1.4 Effect of CTA on Molecular Weight & Branching Frequency

In order to provide an idea of the influence of CTA on the molecular properties of the polymer in both batch and continuous reactors several simulation experiments will be performed that look at property sensitivity to both initial CTA concentration and the CTA rate constant. In order to assess the CTA level, the CTA transfer rate constants provided by Dube et al. [33] are used. The idea is to demonstrate the effect on $\overline{MW}_w$, $\overline{MW}_n$, $\overline{BN}_3$, and $\overline{BN}_4$. As well, the rate constants for transfer to polymer and internal double bond polymerization listed by Dube et al. are used.

The influence of CTA on each of the aforementioned molecular properties can be seen in Figure 4.13. Simulations were performed in a batch reactor using a cold NBR recipe with a base CTA concentration of 0.42 pphm. The initial charge concentration was increased in sequence up to four times the base concentration. As expected, when the concentration of CTA is increased molecular weight and branching frequency decrease. The effect of CTA on branching can be somewhat misleading, as CTA does not directly influence branching. Instead, CTA functions by creating more and shorter molecules through chain transfer, thus from an overall perspective the average number of branches per molecule decreases. Branching is more directly influenced by the rate of transfer to polymer and reaction with double bonds. Besides acting as a chain regulating agent, CTA has been found to be essential for efficient radical initiation in hot rubber recipes [167, 176, 180].

The rate constants for transfer to CTA (mercaptan) from AN and Bd radicals are not well known. A number of transfer constants were previously shown in Table 3.6, which were taken from the polymer handbook. Unfortunately, explicit rate constants in the form of an Arrhenius expression are not listed, instead the ratio $k_{fcta_i}/k_{p_{ii}}$ is given for a specific temperature. Though these estimates can provide a good starting point, further adjustment is usually required to fit experimental molecular weight data. In order to provide an idea of the sensitivity of molecule weight on each rate constant ($k_{fcta_{AN}}$, $k_{fcta_{Bd}}$), each parameter is adjusted by several different factors. Figures 4.14a and 4.14b demonstrate the influence of k_{fcta} on number- and weight-average molecular weight for transfer from AN radicals using three levels of k_{fcta}, while Figures 4.14c and 4.14d show similar responses to changes in k_{fcta} for Bd radicals. In each simulation base parameters of $k_{fcta_{AN}} = k_{p_{AN}}$ and $k_{fcta_{Bd}} = k^{morton}_{fcta_{Bd}}$ were used. For $k_{fcta_{AN}}$, levels of 10 and 100 times the base value were used, while maintaining the base value for $k_{fcta_{Bd}}$. Following this, $k_{fcta_{Bd}}$ was adjusted to a level of 10, 0.25, and 0.1 times the base value, while keeping $k_{fcta_{AN}}$ constant. As $k_{fcta_{AN}}$ is increased, the rate of CTA consumption by transfer from AN radicals increases and both $\overline{MW}_w$ and $\overline{MW}_n$ decrease initially until the concentration of AN in the particle starts to decline. At the highest level of $k_{fcta_{AN}}$, $\overline{MW}_w$ increases moderately after the AN droplets disappear, which is a result of a lower CTA concentration due to a higher consumption early on in the reaction. The molecular weight response appears to be much more sensitive to changes in $k_{fcta_{Bd}}$ than $k_{fcta_{AN}}$. Decreasing the base value of $k_{fcta_{Bd}}$ by 4 and 10 times, decreases the rate of consumption which results in a higher molecular weight. However, more interesting is the decline in molecular weight once AN in the particles starts to decrease. This indicates that the base parameter used for $k_{fcta_{AN}}$ is too low, thus allowing for higher molecular weights initially when the AN concentration is high. On the other hand, if $k_{fcta_{Bd}}$ is increased 10-fold, transfer from Bd radicals dominates and CTA is quickly

consumed; consequently, molecular weight increases, and as seen in Figure 4.14d, the sensitivity of $\overline{MW}_w$ is considerably more pronounced. In order to obtain reasonable profiles both $k_{fcta_{AN}}$ and $k_{fcta_{Bd}}$ probably need to be adjusted together.

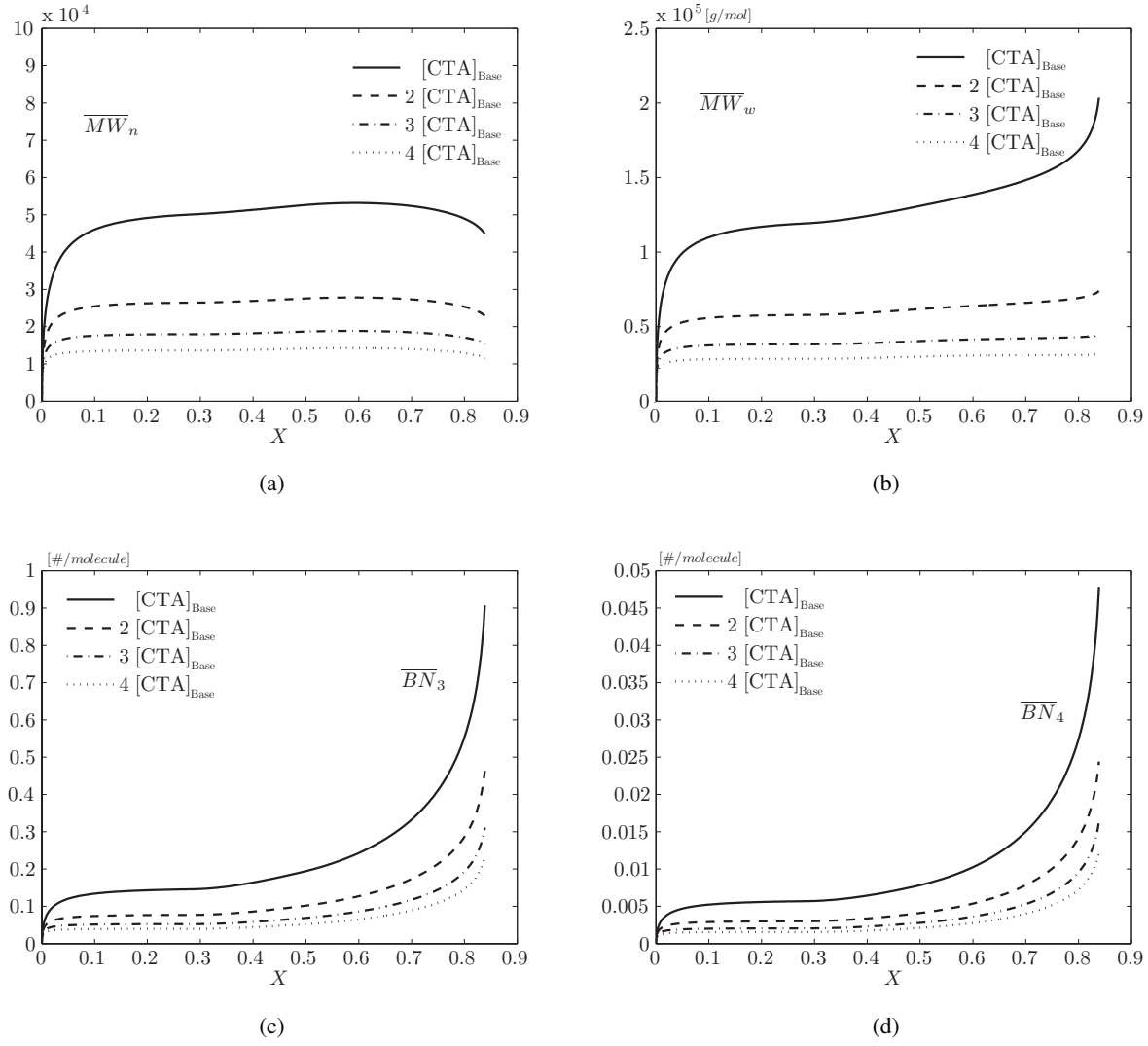

Figure 4.13: Batch reactor simulation - effect of $[CTA]$ on molecular weight and chain branching

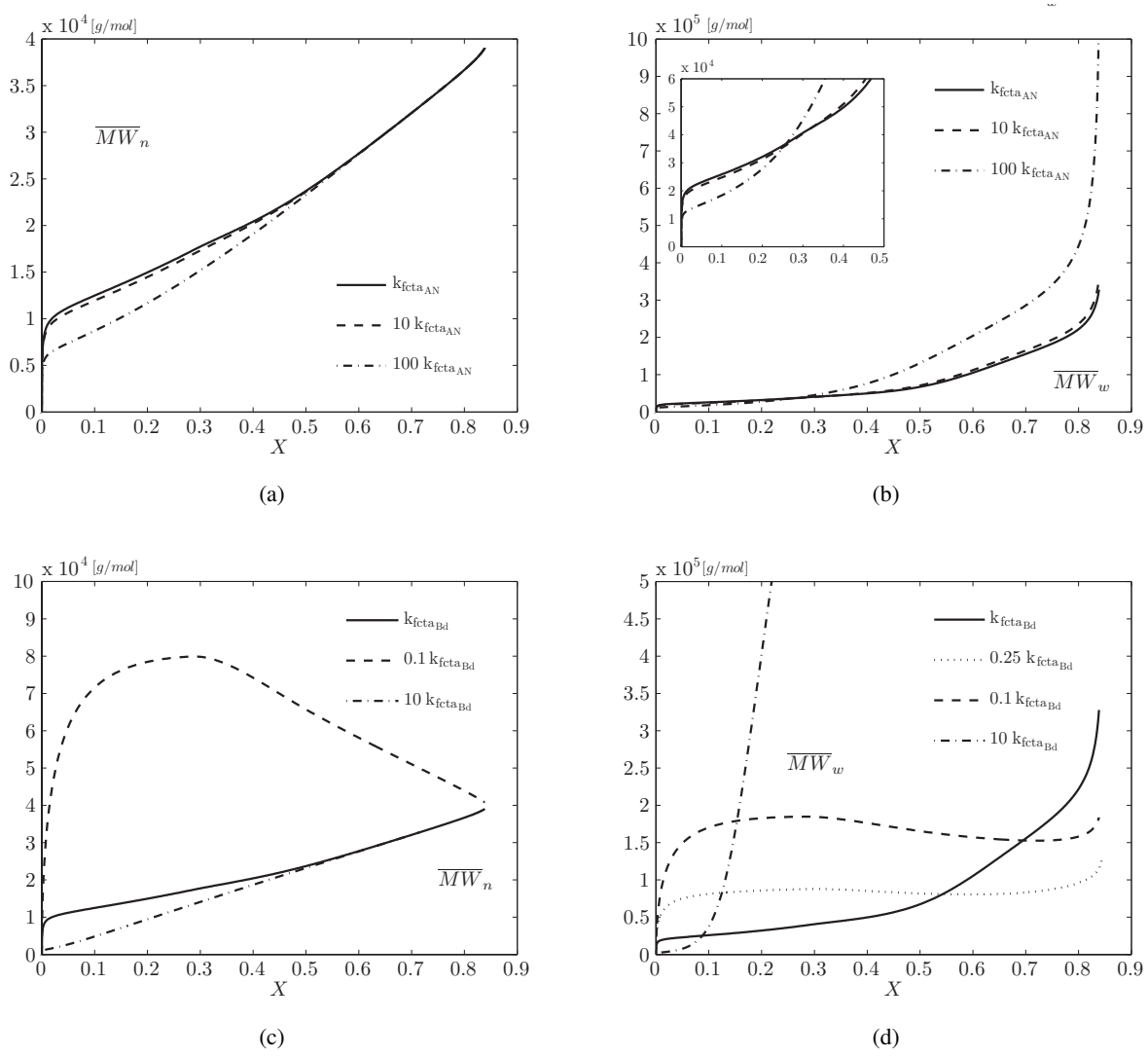

Figure 4.14: Batch reactor simulation - molecular weight sensitivity to k_{fcta}

4.1.5 Influence of Radical Desorption on Polymerization

Radical desorption in a Case II system (i.e. styrene, SBR, NBR) is negligible. If desorption were to occur the most probably route would be radical transfer to monomer followed by diffusion from the particle phase. In order to assess the influence of transfer to monomer, the models of Asua and Nomura are considered. First, Asua's model is used to assess the impact of desorption on conversion, polymerization rate and particle nucleation. Following this, both models are compared to each other, with respect to the influence on conversion and rate.

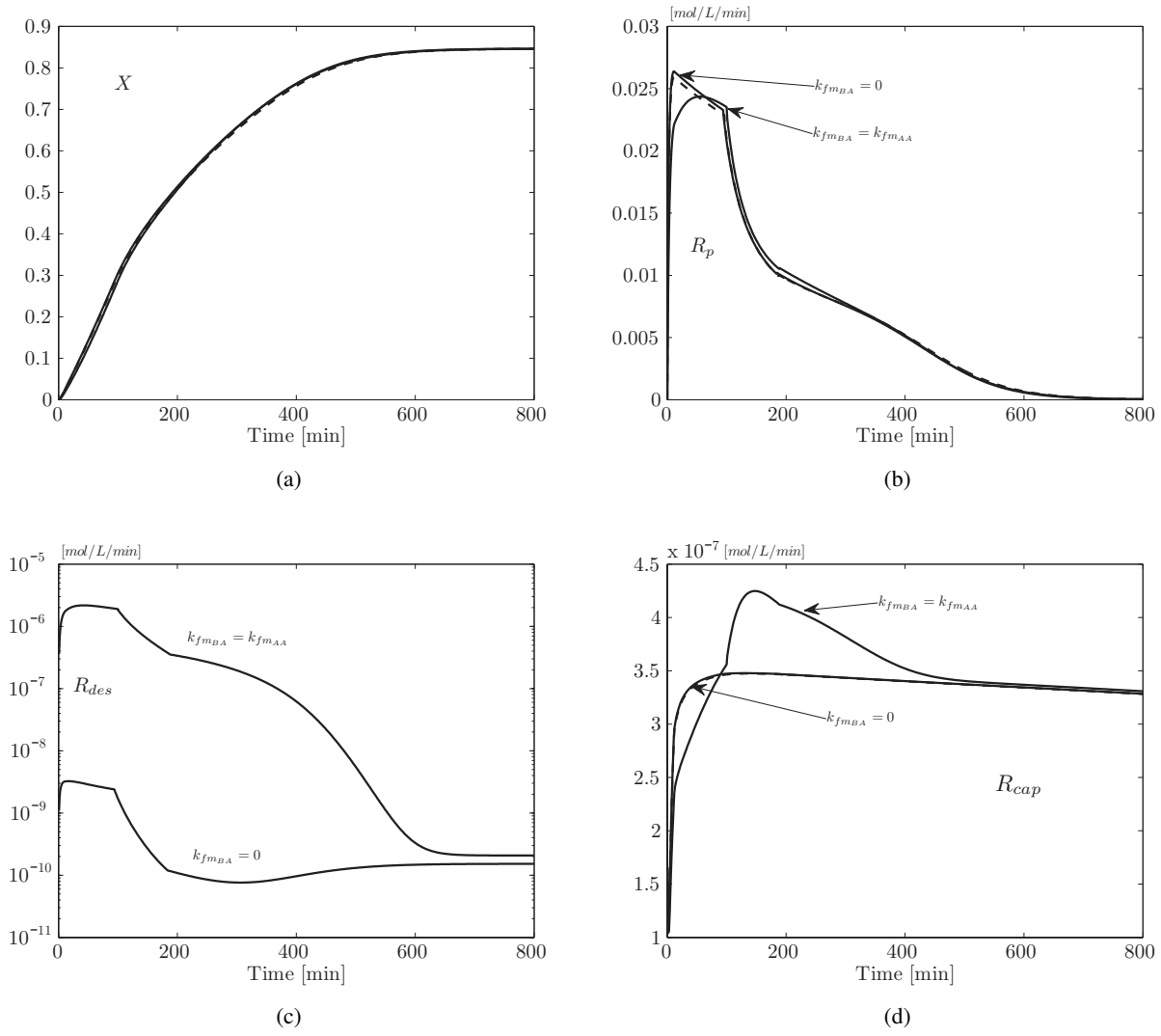

Figure 4.15: Batch reactor simulation - effect of R_{des} on conversion, polymerization rate, radical capture rate

Following Asua's approach, outlined in section 3.6, conversion and polymerization rate profiles for a batch reactor are shown in Figure 4.15. The transfer to monomer rate constants used were those listed by

Dube et al. [33] (Table 3.4). Furthermore, two different approximations were considered, the first assuming negligible transfer to unlike monomer ($k_{fm_{BA}} = 0$), and the second assuming transfer to unlike monomer equivalent to like monomer ($k_{fm_{BA}} = k_{fm_{AA}}$). From Figure 4.15a, the influence of desorption on conversion appears negligible, regardless of the approximation used. Similarly, the effect on polymerization rate is very minor (Figure 4.15b), with the second assumption having a greater influence, since the overall k_{fm} is larger than in the first assumption. The effect of each assumption is more pronounced when looking at the rate of desorption itself. Figure 4.15c depicts the desorption rate profile, which reveals that when assuming negligible transfer to unlike monomer a 10^3 order deficit in initial magnitude is present compared to assuming $k_{fm_{BA}} = k_{fm_{AA}}$ and $k_{fm_{AB}} = k_{fm_{BB}}$. In either case, as polymerization proceeds the rate of desorption remains relatively constant until AN is consumed after which the rate significantly decreases. This behaviour exemplifies the influence of AN on radical desorption, which is as expected due to the larger transfer to monomer rate constant and higher water solubility compared to Bd. Figure 4.15d adds further reprise to the influence of AN, as once AN droplets are depleted (i.e. AN in particle phase decreases) the rate of radical capture from the aqueous phase increases above that of radical desorption, which causes $\bar{n}$ to increase above 0.5. Profiles of $\bar{n}$ versus time are presented in Figure 4.16a, and as expected, as k_{fm} is increased $\bar{n}$ decreases. This behaviour is further seen in Figure 4.16b, using a so-called Hansen-Ugelstad plot, where $\bar{n}$ is plotted as a function of three dimensionless parameters α' (radical entry), m (radical desorption), and Y (aqueous phase radical termination). Typically, three regions can be identified in terms of α' that help to classify the kinetics of the system: $\alpha' < 10^{-3}$, $10^{-3} < \alpha' < 10^{-1}$, and $\alpha' > 10^{-1}$. For the first assumption mentioned above, $m \leq 10^{-3}$ which implies negligible desorption (region 1). As α' passes through region 2, k_{t_p} decreases increasing $\bar{n}$, and once α' reaches region 3 a burst in $\bar{n}$ occurs due to an even further decline in k_{t_p}. Considering the second assumption above, a similar behaviour is evident, albeit with a much higher rate of desorption (i.e. $m = 1$).

In the NBR simulations shown by Vega et al. [171], desorption is assumed to occur from transfer to AN, (i.e. $k_{fm_{BA}} = k_{fm_{AA}}$), and a much higher k_{fm} parameter is used. As a result, $\bar{n}$ was shown to remain fairly constant around 0.5. If one were to speculate, the results of Vega may be due to their parameter estimate for $k_{fm_{AA}}$ (i.e. too high), and the exclusion of diffusion-controlled termination within their model. Performing simulations using the model developed herein and the $k_{fm_{AA}}$ parameter used by Vega indicated that $\bar{n}$ remained slightly below 0.5 until around 80% were $\bar{n}$ increased sharply to around 2 due to diffusional limitations (i.e. k_t became small).

The influence of desorption on particle number and size can be seen in Figure 4.17. As radical desorption increases, from using assumption two (i.e. $k_{fm_{BA}} = k_{fm_{AA}}$) versus assumption one (i.e. $k_{fm_{BA}} = 0$), more particles are nucleated, which makes sense since more radicals are available for capture by micelles. Due to the increase in particle number, the average particle diameter decreases.

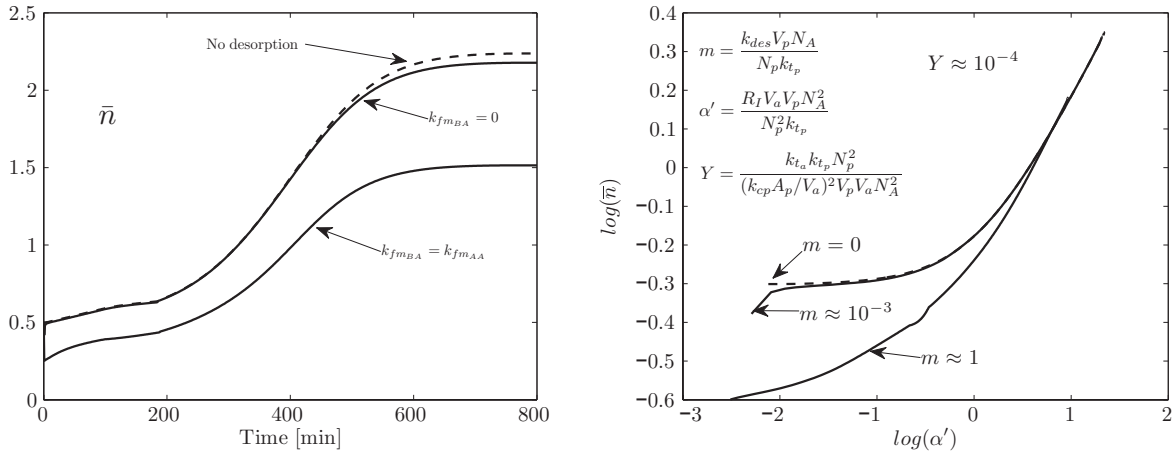

(a) (b)

Figure 4.16: Average number of radicals per particle as a function of α' and m

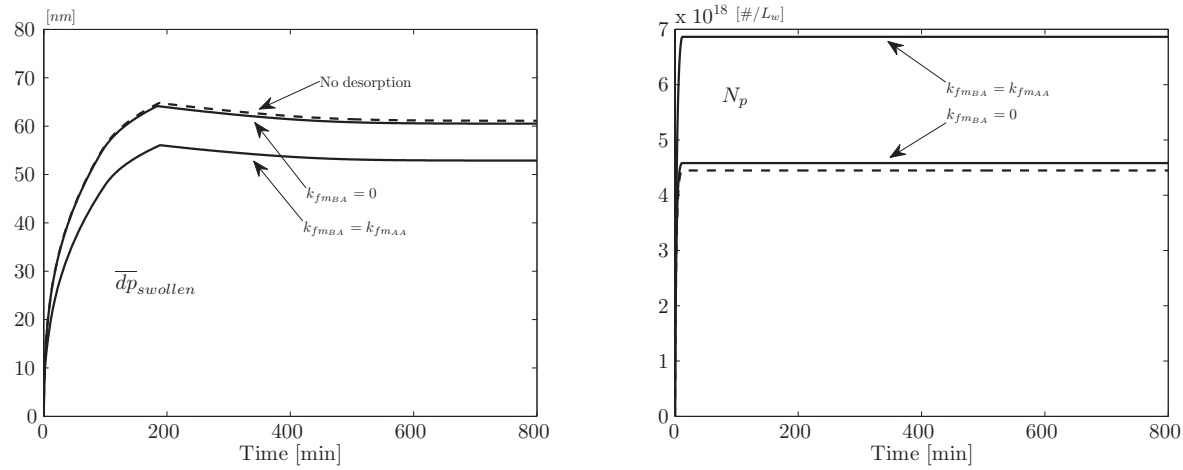

(a) (b)

Figure 4.17: Batch reactor simulation - effect of R_{des} on particle number & size

In order to assess how well the models of Nomura and Asua compare and to determine if any advantages exist from using either model, simulations were performed under identical conditions. The base case parameters listed by Dube et al. [33] were used and radical transfer to unlike monomer was assumed negligible (i.e. $k_{fm_{BA}} = 0$, and $k_{fm_{AB}} = 0$). As a result, the conversion and particle number profiles produced according to Nomura's approach were noticeably different from those of Asua's model, Figure 4.18. Nomura's model generates a larger initial desorption rate constant than Asua's model, as seen in Figure 4.18c, which quickly descends below Asua's model until AN droplets are depleted after which the two models produce similar estimates for k_{des}. The difference in each profile comes from the fundamental definitions of k_{des}, seen in Equations 3.99 and 3.102, where the rate of desorption is related to $K_o\bar{n}$ in Nomura's model and $K_o\beta$ in Asua's model. As can be seen in Figure 4.18f, the profiles of $\bar{n}$ and β are distinctly different, which clearly affects the k_{des} estimates produced from each model.

From the perspective of computational efficiency, Nomura's model requires significantly more computation time than Asua's model due to the iterative nature in determining $\bar{n}$ (i.e. k_{des} must first be guessed, $\bar{n}$ and k_{des} calculated and then $\bar{n}$ re-calculated (Equation 3.98), also refer to Appendix B).

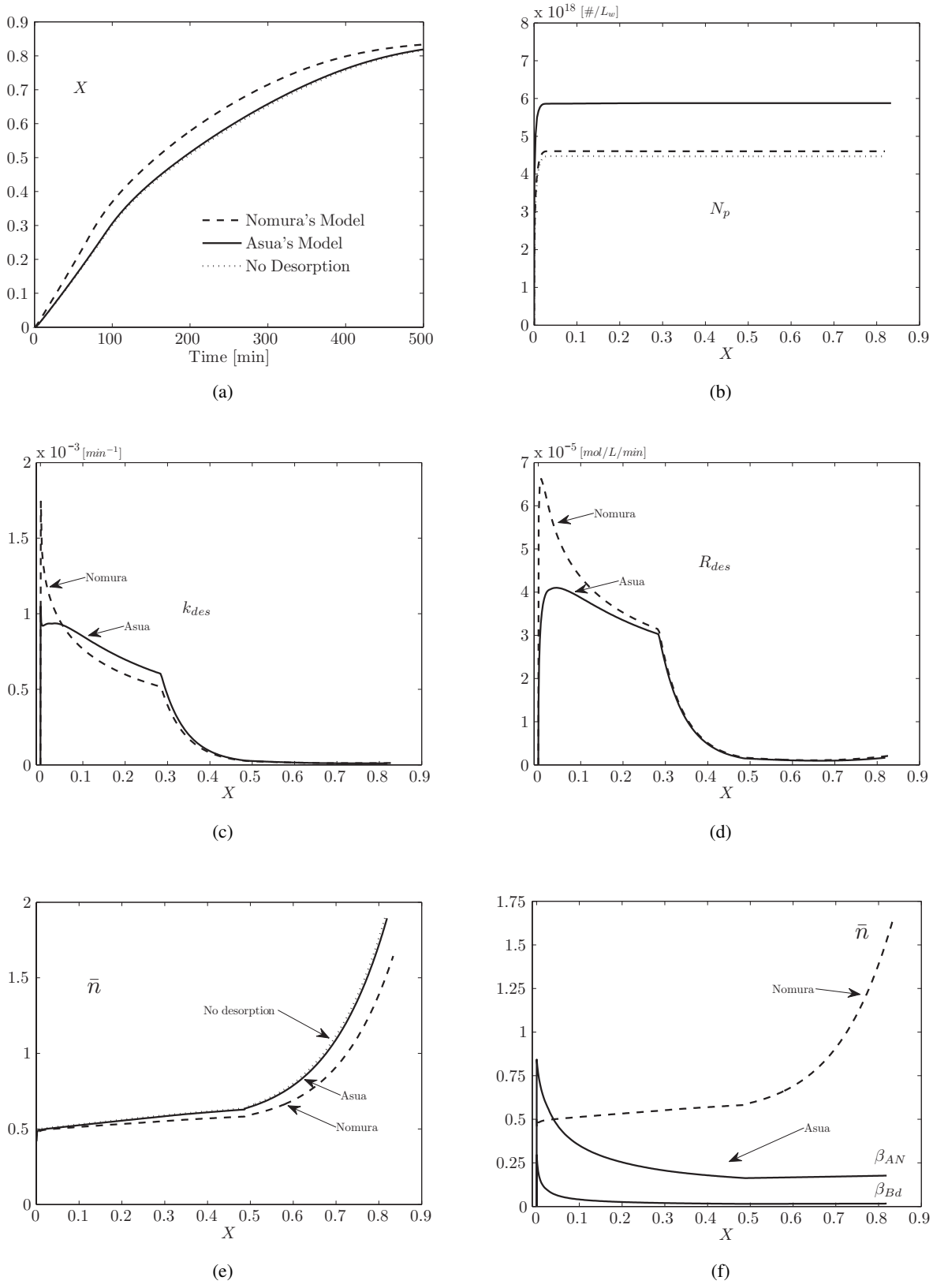

Figure 4.18: Batch reactor simulation - comparison of desorption models - conversion & desorption rate

4.1.6 Continuous Reactor Start-Up

In developing reactor operating and start-up procedures the use of a dynamic model can have great benefit. This section discusses start-up policies considering a single CSTR. To illustrate the transient behaviour typically seen upon reactor start-up, three different policies are used. The first assumes the reactor is initially full of water, the second considers the reactor initially full of the batch recipe (i.e. all ingredients charged as in batch operation), and in the third the reactor is initially empty before the flow of recipe is initialized. Upon start-up, all components are fed using a step input in the total inflow rate. The response variables assessed are conversion, $\bar{n}$, particle number and diameter, $\overline{MW}_w$, $\overline{MW}_n$, $\overline{BN}_3$, and $\overline{BN}_4$, as seen in Figures 4.19 and 4.20. Perhaps the most notable characteristic from each of these figures is that all variables eventually reach the same steady-state regardless of the start-up procedure used. Using the batch recipe, conversion, particle number, diameter and $\bar{n}$ all show an initial overshoot. The overshoot in conversion is due to the large initial burst in particle number, while the overshoot in diameter and $\bar{n}$ results from particle number dipping below its steady-state. The other two procedures (i.e. water, empty) seem to be slightly milder showing negligible overshoot in conversion, $\bar{n}$, and particle size. In an industrial reactor, large initial spikes in conversion and particle number could be substantially taxing on the reactor cooling system and therefore should be minimized. Perhaps the easiest method to do this is to start the reactor full of water. However, doing so requires considerably more time for the molecule properties to reach a steady-state (Figure 4.20). Thus, in a reactor train a large amount of waste would be generated due to off-spec product. The copolymer composition was found to be unaffected by the start-up policy and remained constant at its steady-state.

In order to assess the extent that mean residence time (θ) influences the steady-state solution, times of 30, 60 and 80 minutes were simulated. Figure 4.21 shows the effect of residence time on conversion and particle number using each of the aforementioned start-up polices. As θ is decreased to 30 min from the base case of 60 min, the steady-state conversion obviously decreases, since less time is spent in the reactor. On the other hand, when θ is increased to 80 min conversion increases. More interesting is the response of N_p, as decreasing θ increases N_p, while increasing θ decreases N_p. This behaviour was previously shown in Figure 4.6a, which clearly indicated the presence of an optimal residence time for maximizing N_p. Another observation from Figure 4.21 is that as θ is increased the steady-state solution requires a longer time to reach, which again makes perfect sense since the material remains in the reactor for a longer time.

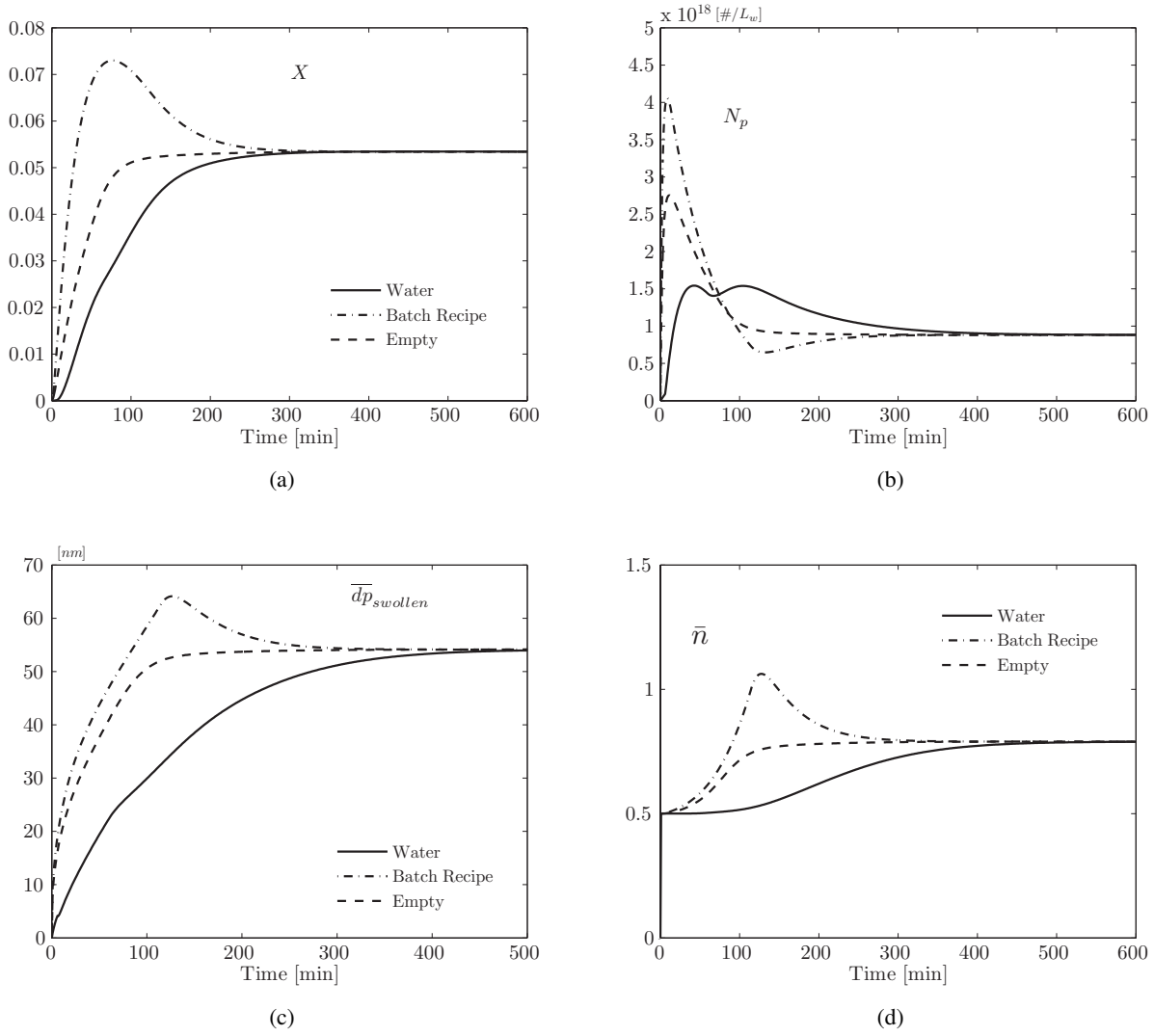

Figure 4.19: Continuous reactor simulation - start-up policies - conversion, particle number & diameter for $\theta = 60$ minutes

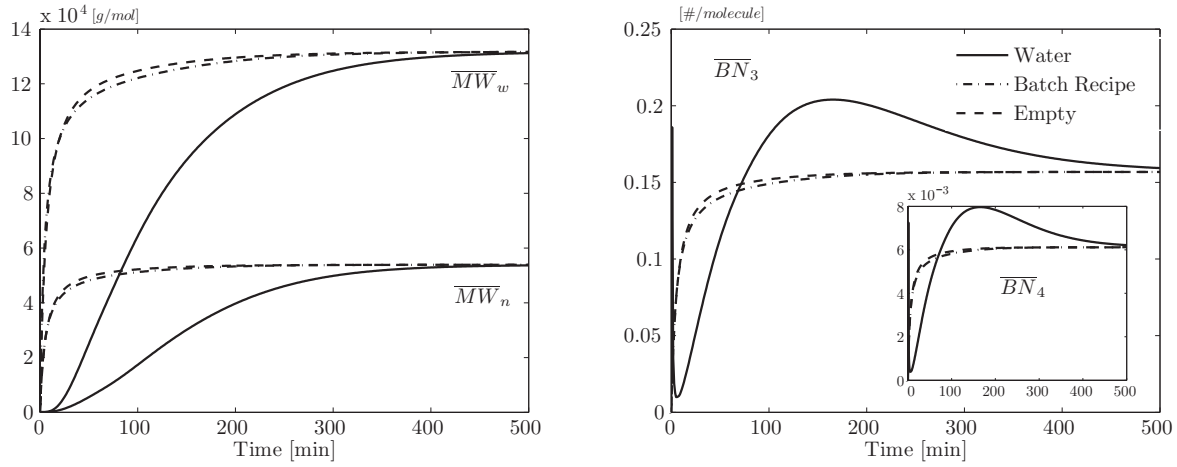

(a) (b)

Figure 4.20: Continuous reactor simulation - start-up policies - molecular weight & branching frequency for $\theta = 60$ minutes

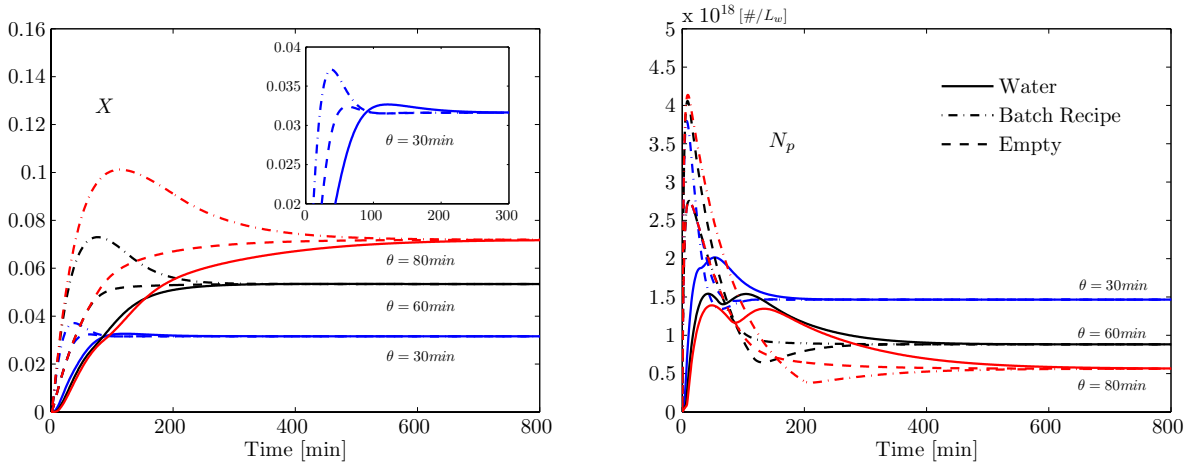

(a) (b)

Figure 4.21: Continuous reactor simulation - start-up policies - conversion & particle number for $\theta = 30, 60, 80$ minutes

4.2 Model Validation with Literature Data

In order to provide an idea of the validity of the model, comparisons are made to available experimental and process data for Bd and NBR. The first validation study was performed on NBR, using a limited amount of pilot plant data, previously shown by Dube et al. [33] and Vega et al. [171]. The next study focused on Bd alone, where the model was used to demonstrate emulsion homopolymerization of butadiene using various different levels of recipe ingredients (i.e. emulsifier & initiator). Weerts [184] provided an excellent source on the emulsion homopolymerization of Bd under laboratory conditions, while Pallaske et al. [133] provided information on a larger scale by performing pilot plant experiments. Further model reduction to AN homopolymerization was also considered, but at this point further investigation is required, as model predictions were not capable of accurately tracking conversion over the entire range. In each of the aforementioned sources all data were reported for a batch reactor.

4.2.1 Simulation of NBR Data

The presence of experimental or industrial data for NBR in the open literature is quite limited. After a thorough literature review, the only sources found were a series of papers from the Meira group [62, 146, 171, 172] who provide industrial batch/semibatch measurements for conversion, copolymer composition, particle number, and molecular weight, a paper by Dube et al. [33] on industrial batch reactor modelling that provides a limited amount of data on conversion, and a fairly old paper by Embree et al. [38] who provide a limited amount of data on copolymer composition. In what follows the model developed herein is compared to data from Vega et al. [171] and to previously unpublished data from Dube et al. [33].

Data of Vega et al. [171]

The experimental information of Vega et al. [171] was simulated in order to provide a qualitative check of the model. Exact details on the nature of the emulsifier (likely more than one) was not divulged in the recipe and for simulation purposes was assumed as specified in the base recipe of Table 4.1. In addition, *para*-menthane hydroperoxide (PMHP) was used in place of diisobutyl hydroperoxide (DIBHP) as the initiator in the simulations since more parameters were available (i.e. k_1 and k_2). This modification required that the initiator concentration be doubled from the original recipe as it was completely consumed before a monomer conversion of 60%, which was most likely a result of a lower reaction rate of DIBHP compared to PMHP. The remaining ingredients were the same as the base recipe and are presented in Table 4.5. Due to the industrial nature of the data the presence of impurities is certain. In the simulations performed by Vega et al., oxygen and vinylacetylene were assumed to be present and their simulation results compared well with the data. Model simulations shown here were performed considering oxygen and t-buyl catechol as water- and monomer-soluble impurities, and assuming negligible radical desorption. The type of monomer impurity is not that significant, more important is that the concentration used is reasonable (e.g. 50-300 ppm) and that the approximated rate constant yields a decent fit to the data.

Table 4.5: Cold NBR emulsion recipe in Vega et al. [171]

Ingredient	**Initial composition** [a]
Acrylonitrile	31
Butadiene	69
Water	180
Initiator [b]	0.0056
Oxidizing Agent [c]	0.0032
Reducing Agent [d]	0.067
Emulsifier [e]	3.72
t-Dodecyl Mercaptan	0.375
Temperature (^oC)	10

[a] parts per hundred monomer

[b] stated as diisobutyl hydroperoxide, however para-menthane hydroperoxide was used for simulation as more parameters were available

[c] $FeSO_4 \cdot 7H_2O$

[d] SFS

[e] Details on emulsifier type were not divulged, assumed as in Table 4.1 with 2.72 pphm Tamol, 1.0 pphm Dresinate

To fit the model to the data a few parameters needed to be adjusted from the base estimates listed by Dube et al. [33] (Table 3.4); as well initial impurity concentrations needed to be assumed. Since the purpose here was not to undertake a lengthy parameter estimation study, but rather to show that the model predicts reasonable trends, many of the parameters used were those previously cited by Dube. Notable adjustments were the impurity, CTA transfer and polymer transfer rate constants. Adjusting the impurity rate constants and concentrations allowed for a reasonable fit to the conversion data, while similar adjustments of the rate constants of CTA and transfer to polymer provided an acceptable fit to the molecular weight data. Particle number was the most difficult to fit using only adjustments in ε and impurity concentration, which is presumably a result of an inaccurate specification of emulsifier type and concentration in the simulation compared to what was originally used to generate the data. The corresponding adjusted parameters and assumed impurity concentrations are provided in Table 4.6. The results of the simulations are presented in Figures 4.22 and 4.23, while experimental and simulated final properties are compared in Table 4.7. For each property shown, simulation profiles compare well with the data revealing a reasonable trend, despite the measurement error associated with the data, the unknown recipe ingredients, and uncertain parameters used. Perhaps the only potentially significant discrepancy is seen from the copolymer composition profile, as the simulated composition drifts considerable more than the data yielding a 28% deviation in final composition. This observed deviation is most likely due to inaccurate estimates for the reactivity ratios or partition coefficients.

In closing, the model developed herein was able to predict the industrial data of Vega et al. [171] for conversion, composition, particle number and size, and molecular weight with only minor adjustments of a few parameters from the base estimates. Furthermore, if details on the emulsifiers used were provided and if a more involved parameter estimation study were carried out, an even closer fit to the data could easily be

Table 4.6: Model parameters used to fit data of Vega et al. [171]

Parameter	**Adjustment**
k_{fcta_A}	$20\ k_{p_{AA}}$
k_{fcta_B}	$k_{fcta_B}^{morton}/21$ [a]
$k_{fp_{AA}}$	0.3
$k_{fp_{BA}}$	$k_{fp_{AA}}$
$k_{z_{O_2}}$	6.67×10^6
k_{fmsi}	$0.001\ k_p$
ε	8.839
$[O_2]$ (pphm)	15
$[TBC]$ (pphm)	150

[a] $k_{fcta_B}^{morton}$ corresponds to the CTA transfer constant used by Morton et al. [111]

Table 4.7: Cold NBR emulsion final product properties - comparison between measurement and simulation results

Property	**Measured Value at** $t \approx 850min$ [a]	**Simulation Result**
x (%)	74.7	71.1
$\overline{F}_{AN}$ (-)	0.32	0.23
$N_p \times 10^{-18}$ $(\#/L_w)$	1.305	1.648
d_p (nm) [b]	83	80
$\overline{MW}_n$ (g/mol)	45400	60438
$\overline{MW}_w$ (g/mol)	214000	181970

[a] read off from provided figures in [171] for experiment 1
[b] unswollen diameter

obtained. However, the objective was simply to show reasonable model trends, which by the looks of each profile was clearly met.

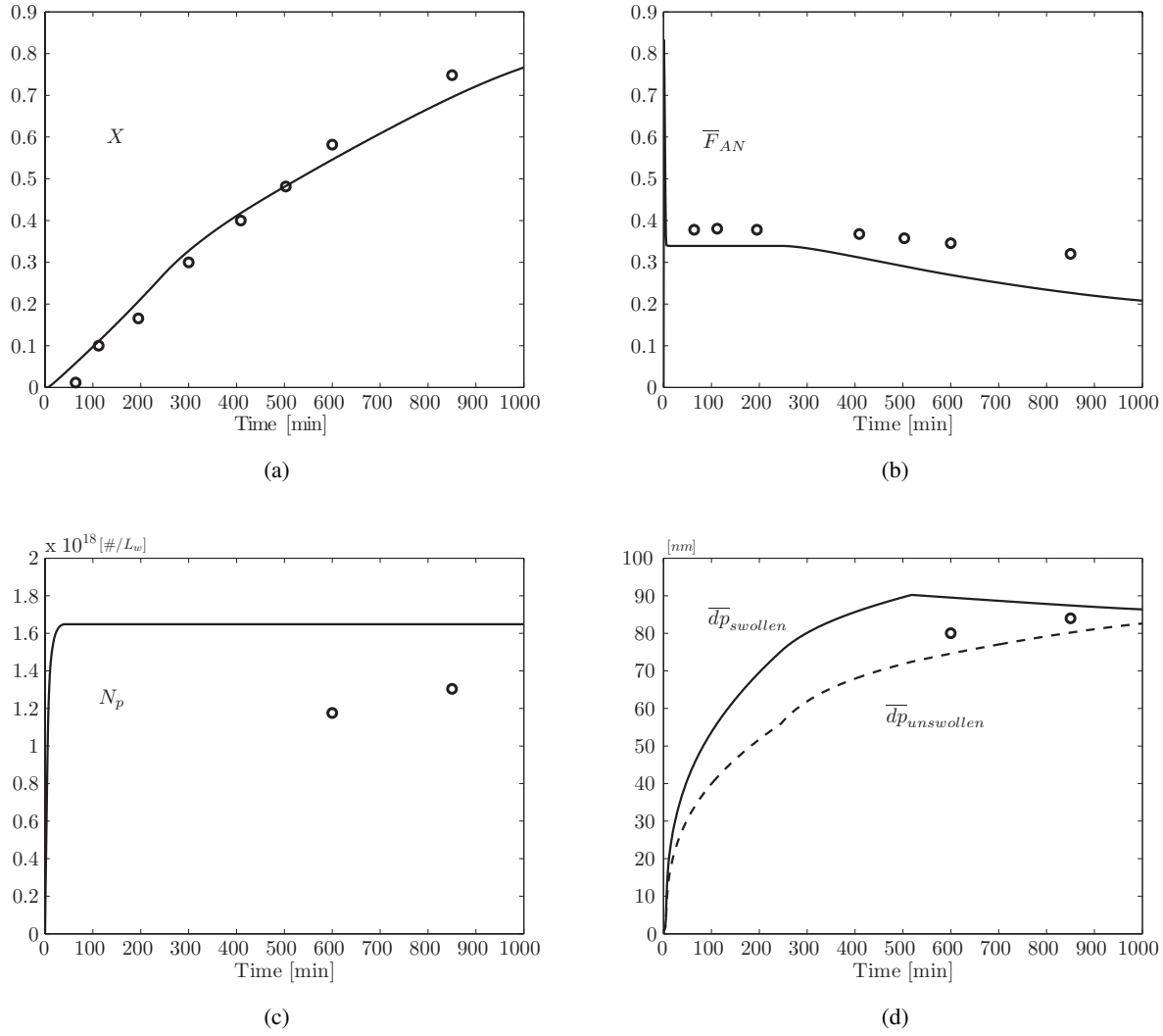

Figure 4.22: Batch reactor simulation - comparison to industrial data from Vega et al. [171] - conversion, copolymer composition, particle number & average diameter

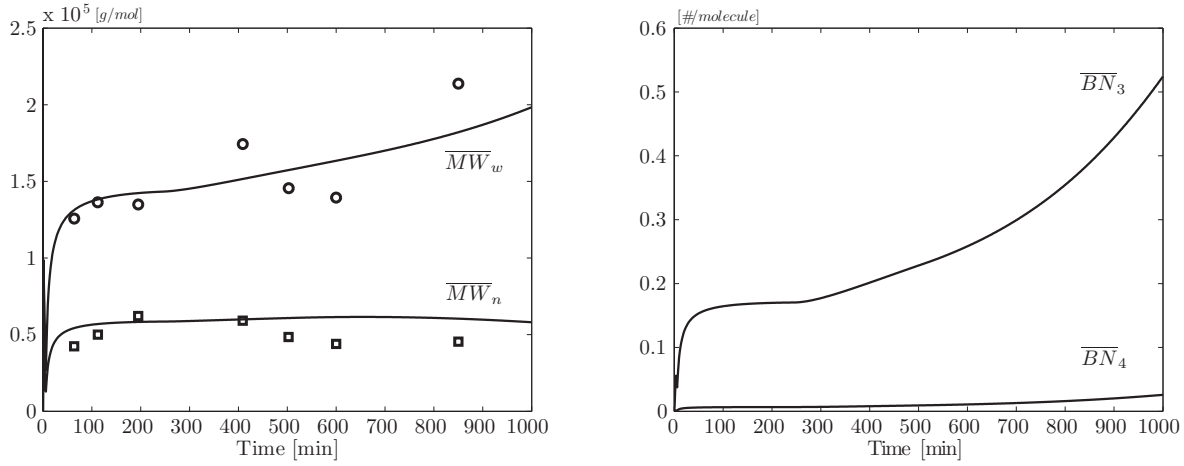

(a) (b)

Figure 4.23: Batch reactor simulation - comparison to industrial data from Vega et al. [171] - molecular weight & branching frequencies

Data from Dube et al. [33]

To install further confidence in the models predictive capabilities, comparisons to experimental data using two industrial hot NBR recipes were performed (Table 4.8). Measurements of percent solids and particle size are available from pilot plant experiments performed on PARACRIL NBR. A comparison between the model and data for the two recipes considered is shown in Figures 4.24 and 4.25. From the percent solids data it is quite clear that an induction period occurred at the beginning of the reaction when the samples were taken. Thus, to provide a decent model fit, impurities were assumed to be present, and by adjusting the relative concentrations (i.e. WSI & MSI) a reasonable fit to the data was obtained. The only parameters adjusted were the impurity reaction rate constants, as seen in Table 4.9. The remaining parameters used were left at their base values according to Tables 3.4 and 3.7.

The solids data for the first recipe, Figure 4.24a, reveals an induction period of approximately 150 minutes followed by a roughly linear increase; however, the model prediction reveals slightly more curvature in the profile trajectory. This discrepancy is possibly due to the emulsifier parameters used for the critical micelle concentration (CMC), surface coverage (S_a), and micelle radius (r_{mic}) for Daxad and Emersol. For the most part, these parameters were taken from Bovey et al. [13], however, r_{mic} and the CMC were assumed to be the same as those for Tamol. Such an assumption clearly influences the overall micellar surface area and consequently the particle nucleation period, which may account for the overly steep initial slope in the solids profile. In Figure 4.24c, model predictions for particle diameter seem to agree reasonably well with the experimental data, despite only having a limited data set. In the second recipe the solids prediction appears to follow the data more closely (Figure 4.25a); however, initially the profile is offset from the data which suggests that if the recipe specification was initially correct then possibly measurement error could be the culprit. Although this may be a possibility, it is difficult to be certain, as the experimental

Table 4.8: Hot NBR emulsion recipe (PARACRIL)

Ingredient	**Recipe 1**[a]	**Recipe 2**
Acrylonitrile	27.5	70
Butadiene	72.5	30
Water	180	120
Potassium Persulfate	0.25	0.25
Daxad [b]	2.85	2.0
Emersol [c]	1.16	2.0
Sulfole [d]	0.6	0.45
$[E]$ (mol/L)	0.0317	0.0566
$[I]_o$ (mol/L)	0.0046	0.0069
Temperature (^oC)	40	40

[a] Parts per hundred monomer
[b] Similar to Tamol (condensed polyarylsulfonic acid salt)
[c] Fatty acid soap (i.e. stearic/palmitic acid)
[d] Assumed similar to t-Dodecyl Mercaptan

and sampling methods were unknown. Beyond the first 150 minutes, the model tracks the data much more closely. Unfortunately, only a limited data set is available for particle diameter, which makes it difficult to draw any solid conclusions about the model prediction, other than to say the prediction is in the general area of the data. Furthermore, without more data on diameter, particle number, composition, and molecular weight it is difficult to assess the model fully.

Table 4.9: Model parameters used to fit data of Dube et al. [33]

Parameter	**Recipe 1**	**Recipe 2**
$k_{z_{O_2}}$	1×10^7	1×10^7
k_{fmsi}	0.0001 k_p	0.0001 k_p
$[O_2]$ (pphm)	50	27
$[TBC]$ (pphm)	500	200

Considering that only impurity effects were included and no parameter fitting was performed, the model was able to predict a reasonable response for percent solids and particle diameter that were in the general area of the pilot-plant data measurements.

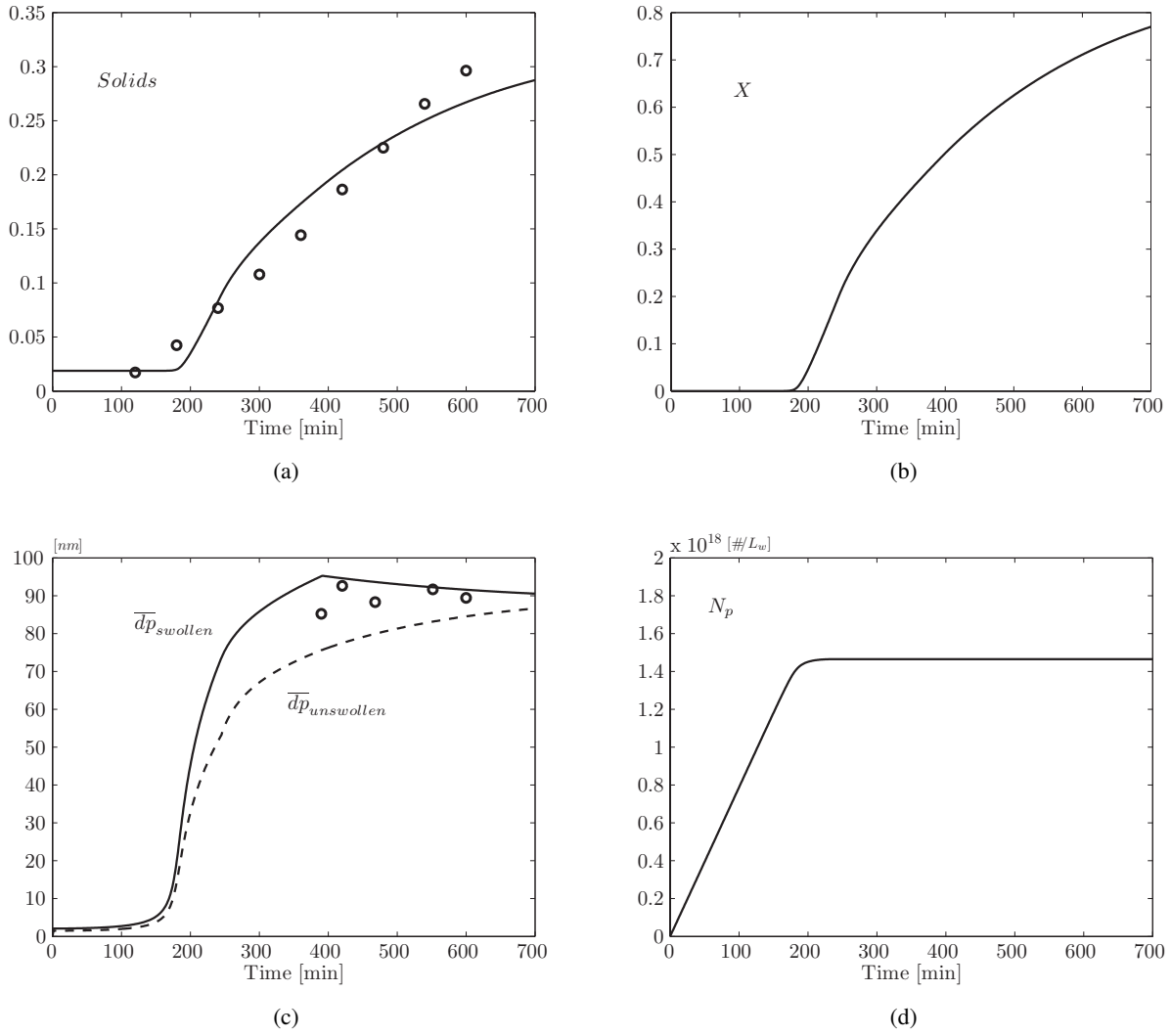

Figure 4.24: Batch reactor simulation - comparison to pilot plant data (recipe 1) - percent solids & particle diameter

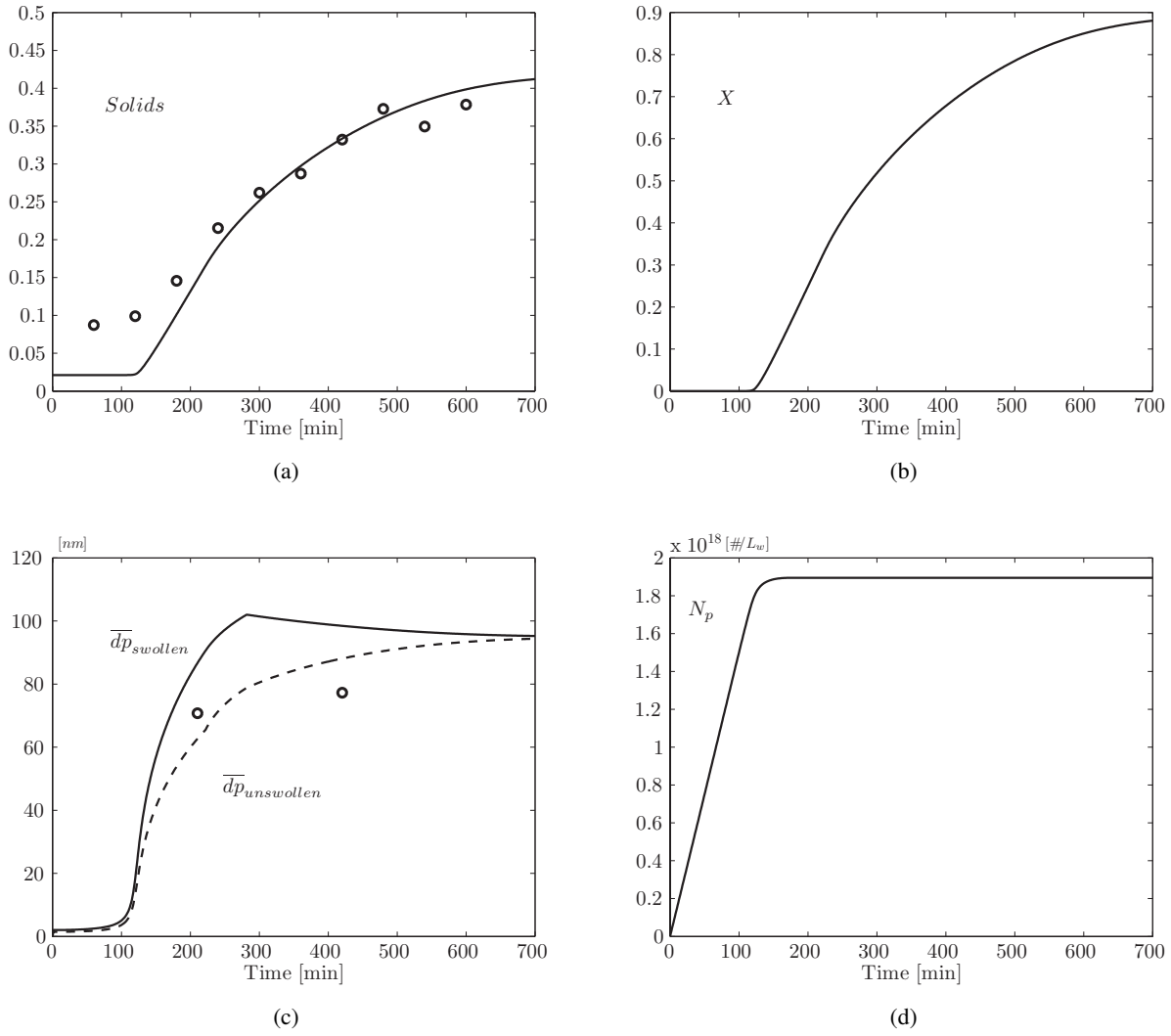

Figure 4.25: Batch reactor simulation - comparison to pilot plant data (recipe 2) - percent solids & particle diameter

4.2.2 Simulation of Emulsion Bd Data

Due to the limited amount of data on NBR and in an attempt to provide further comparison to experimental data, the model was reduced to simulate the emulsion homopolymerization of butadiene. Kinetic investigations have been performed by Weerts [184] on unseeded polymerization and by Verdurmen [174] on seeded polymerization. In each case, the focus of the work was to elucidate complex kinetic events within the system and to estimate the corresponding kinetic parameters (i.e. k_p, k_t, k_{fm}). In doing so, numerous measurements of conversion and particle size were taken, which are used here for model comparison. Further comparison is made to industrial pilot-plant data of Pallaske et al. [133], who provide measurements on conversion and particle size. Unfortunately no measurements on molecular weight are provided in either of the above mentioned sources, nor in any other available literature source.

Data of Weerts [184]

The first model comparison is made with the data from Weerts, where two different recipes are used. Table 4.10 shows the base recipes, and experimental data are available for different emulsifier and initiator levels, as well as different monomer to water ratios. Figure 4.26 presents conversion and particle size comparisons for recipe 1 using three different emulsifier levels, while Figure 4.27 presents similar comparisons on conversion for Recipe 2. For each simulation, the base kinetic parameters of Table C.2 were used. In order to provide a reasonable fit to data the nucleation parameter ε was adjusted 10-fold from its base value (Table 4.11). In addition, monomer and water impurities were not considered as the recipe was said to be purified and free of the typical impurities seen within industrial systems. This can be further seen by looking at the data and noticing that no induction period is evident. Keep in mind the objective here was not to fit the model to the data, but to show that the model predicts the general trends shown by the data using the base set of parameters.

Table 4.10: Butadiene emulsion recipe from Weerts [184]

Ingredient	**Recipe 1**[a]	**Recipe 2**
Butadiene	100	100
Water	230	230
Potassium Persulfate (KPS)	0.8	-
Sodium Persulfate (SPS)	-	0.7
Dresinate 214	7.6	-
Sodium Dodecyl Sulfate (SDS)	-	7.6
t-Dodecyl Mercaptan	0.7	0.7
$[E]$ (mol/L)	0.0997	0.1122
$[I]_o$ (mol/L)	0.0130	0.0128
Temperature (^oC)	40	40

[a] parts per hundred monomer

Conversion profiles for the first recipe reveal that the general trend is captured by the model, as the

emulsifier concentration (dresinate) is varied by 0.5 and 0.25 from its base value of 0.1 mol/L. Similar trends are seen for the second recipe using the emulsifier sodium dodecyl sulfate with the same base mass concentration and level variations as the first recipe. In the first recipe model predictions, Figure 4.26a, slightly underestimated the data for the base concentration, while when the emulsifier concentration was lowered the predictions increasingly overestimated the data. This behaviour is also seen from diameter-conversion comparisons in Figure 4.26b, where for the base emulsifier level model predictions overestimate the data (i.e. lower conversion and particle number, results in a larger average diameter), and when the concentration is lowered particle diameter is underestimated by the model. For the second recipe, model predictions shown in Figure 4.27a are much closer to the data for the base emulsifier concentration, and become progressively worse as the emulsifier concentration is decreased. Further comparison using different monomer-to-water ratios and keeping emulsifier concentration constant at the base value reveals an even closer fit to the experimental data (Figure 4.27b). The discrepancy between the data and model predictions when the emulsifier concentration is altered, suggests that further fine-tuning of ε may be necessary as the emulsifier concentration is decreased. Attempts to do so, revealed that indeed a better fit could be generated, however, by adjusting ε alone a decent fit over the entire conversion range was not possible, which suggests that further refinement of the emulsifier parameters (CMC, S_a, r_{mic}) or kinetic parameters (k_p, k_t, k_{fm}, etc.) is necessary.

Table 4.11: Model parameters used to fit the data of Weerts [184]

Parameter	**Recipe 1**	**Recipe 2**
ε	0.4839	0.4839
k_{cp}	0.025	0.025

In general, model predictions for conversion were able to follow the trends shown by the experimental data, although when the emulsifier concentration was varied further refinement of ε was required which at best only captured a portion of the conversion-time profile. Since ε represents the ratio of radical capture between particles and micelles it intimately affects particle formation, which in practice is based on emulsifier type and concentration.

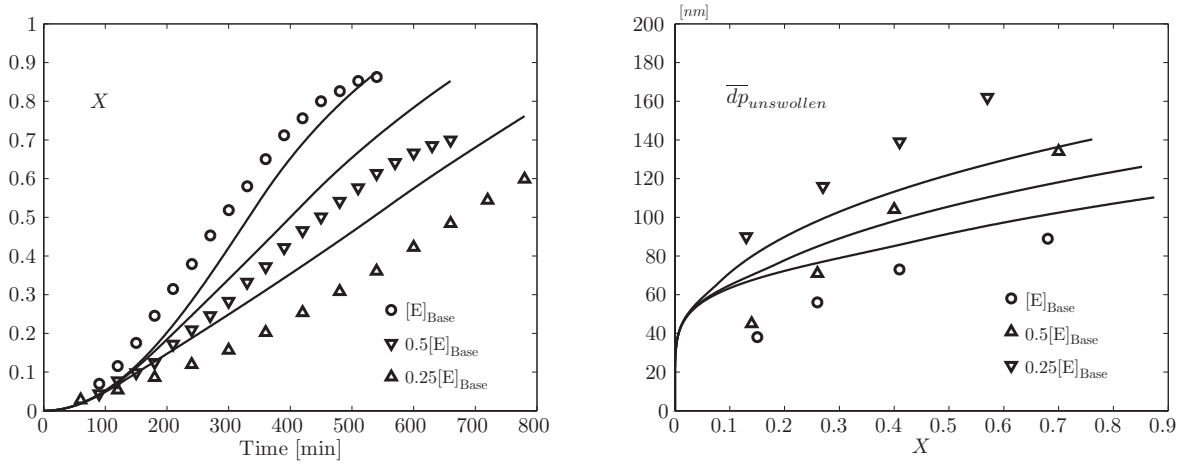

(a) (b)

Figure 4.26: Batch reactor simulation - comparison to experimental data of Weerts [184] (recipe 1) - conversion & particle diameter

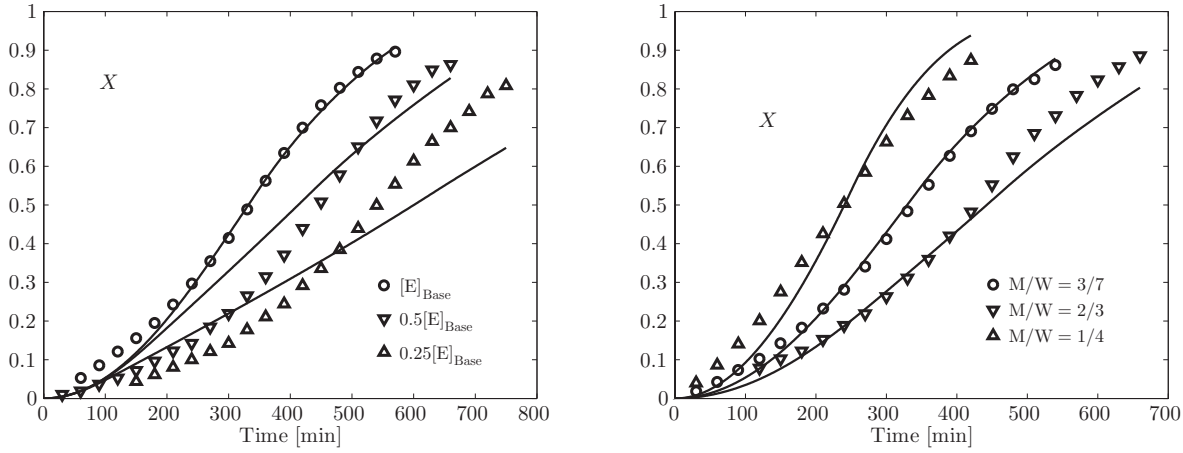

(a) (b)

Figure 4.27: Batch reactor simulation - comparison to experimental data of Weerts [184] (recipe 2) - conversion

Data of Pallaske et al. [133]

In what follows, conversion and particle size data are compared to simulation results for a batch reactor using three slightly different recipe formulations. The first recipe (see Table 4.12) used is considered a base formulation with typical emulsifier and initiator levels, the second uses a high emulsifier level, while in the third a low initiator and high emulsifier level are used. Each recipe is shown in Table 4.12, and in each case initiation occurred through a thermal decomposition reaction of persulfate.

Table 4.12: Industrial butadiene emulsion recipe from Pallaske et al. [133]

Ingredient	**Recipe 1**[a]	**Recipe 2**	**Recipe 3**
Butadiene	100	100	100
Water	168	168	168
Potassium Persulfate	0.328	0.328	0.058
Potassium Oleate	0.87	8.7	8.7
t-Dodecyl Mercaptan	0.7	0.7	0.7
$[E]$ (mol/L)	0.016	0.160	0.160
$[I]_o$ (mol/L)	0.0072	0.0072	0.0013
Temperature (^oC)	67.7	67.7	67.7

[a] parts per hundred monomer

For the first recipe, model/data comparisons are shown in Figure 4.28. In order to provide a rough fit to the data for conversion and particle size, monomer-soluble impurities were introduced into the simulation. It was quite evident from the induction period in the conversion data and the low initial particle diameter measurements that this was necessary. Figure 4.28a reveals a good model fit to conversion data beyond 350 minutes, while prior to this point a clear discrepancy is present due to the large induction caused by the impurities. Similarly, particle size is predicted quite well beyond 350 minutes and not so well early on. This behaviour suggests that perhaps too much MSI impurities were imposed; however, reducing the initial impurity level simply shifts the conversion profile to the left (i.e. smaller induction period), and increases the particle size profile above the data. Thus, this could indicate the presence of other influential factors (i.e. inaccurate monomer partitioning coefficients, or emulsifier parameters) which could distort the model prediction. In any event, it is difficult to speculate further without going into a parameter sensitivity/estimation study. As seen in Figures 4.29a and 4.29b, conversion predictions for the second and third recipe compare reasonable well with the experimental data over the entire reaction time. However, in each case the nucleation parameter ε had to be adjusted (Table 4.13), which was not unexpected since ε is highly correlated to emulsifier concentration. The presence of an induction period was not observed in the data, so impurities were not included in the simulation. Looking at the predictions for particle size (Figures 4.29c and 4.29d) reveals an overestimation by the model, which is due to a lower particle number prediction. As well, a distinct transition in the diameter profile is evident, which is a result of an extended particle nucleation period (i.e. stage I) due to a high initial concentration of free-emulsifier. Two approaches were considered to improve the particle size prediction; in the first, ε was decreased further which improved $\overline{d}_p$, however

the conversion prediction deteriorated. In the second, a small amount of MSI was added to the simulation and again the $\overline{d}_p$ prediction improved while the conversion prediction revealed a small induction period at first followed by a progressive increase that slightly overestimated the data. Based on these results, a more accurate fit to the conversion and particle size data could be achieved by careful adjustment of ε, k_{fmsi}, and the initial MSI concentration. However, manual adjustment of these parameters can be tedious, thus instead an optimization routine should be employed (i.e. parameter estimation).

Table 4.13: Model parameters used to fit the data of Pallaske et al. [133]

Parameter	**Recipe 1**	**Recipe 2**	**Recipe 3**
ε	0.4839	0.07839	0.1839
k_{cp}	0.025	0.025	0.025
k_{fmsi}	0.0001 k_p	-	-
$[TBC]$ (pphm)	200	-	-

Despite the noted discrepancies, the model was able to predict conversion and particle size reasonably well with only minor adjustments of a few parameters. Unfortunately, data was not available for particle number, which would aid in drawing further conclusions on particle nucleation and help in establishing better parameter estimates for ε and k_{cp}.

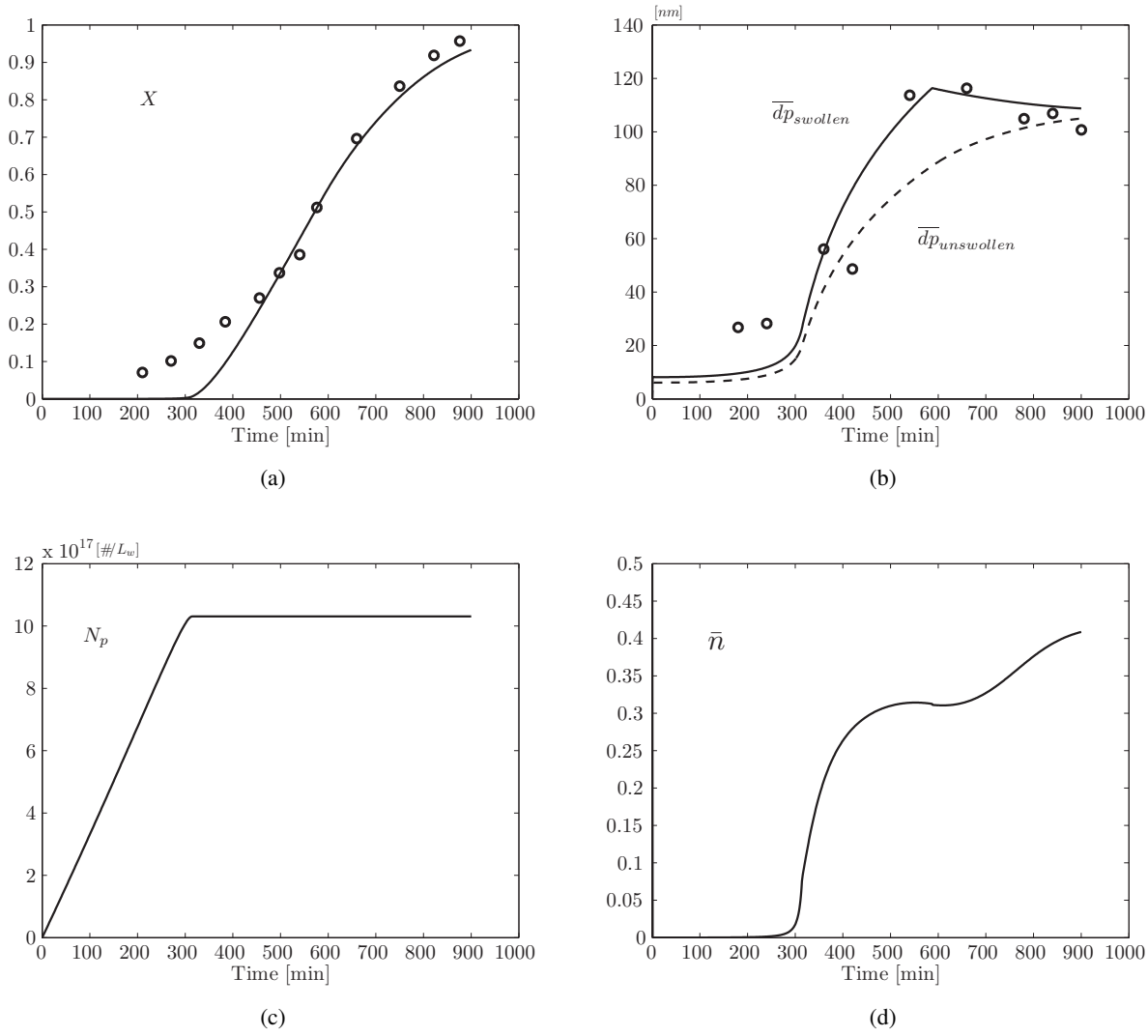

Figure 4.28: Batch reactor simulation - comparison to industrial data of Pallaske et al. [133] (recipe 1) - conversion and particle diameter

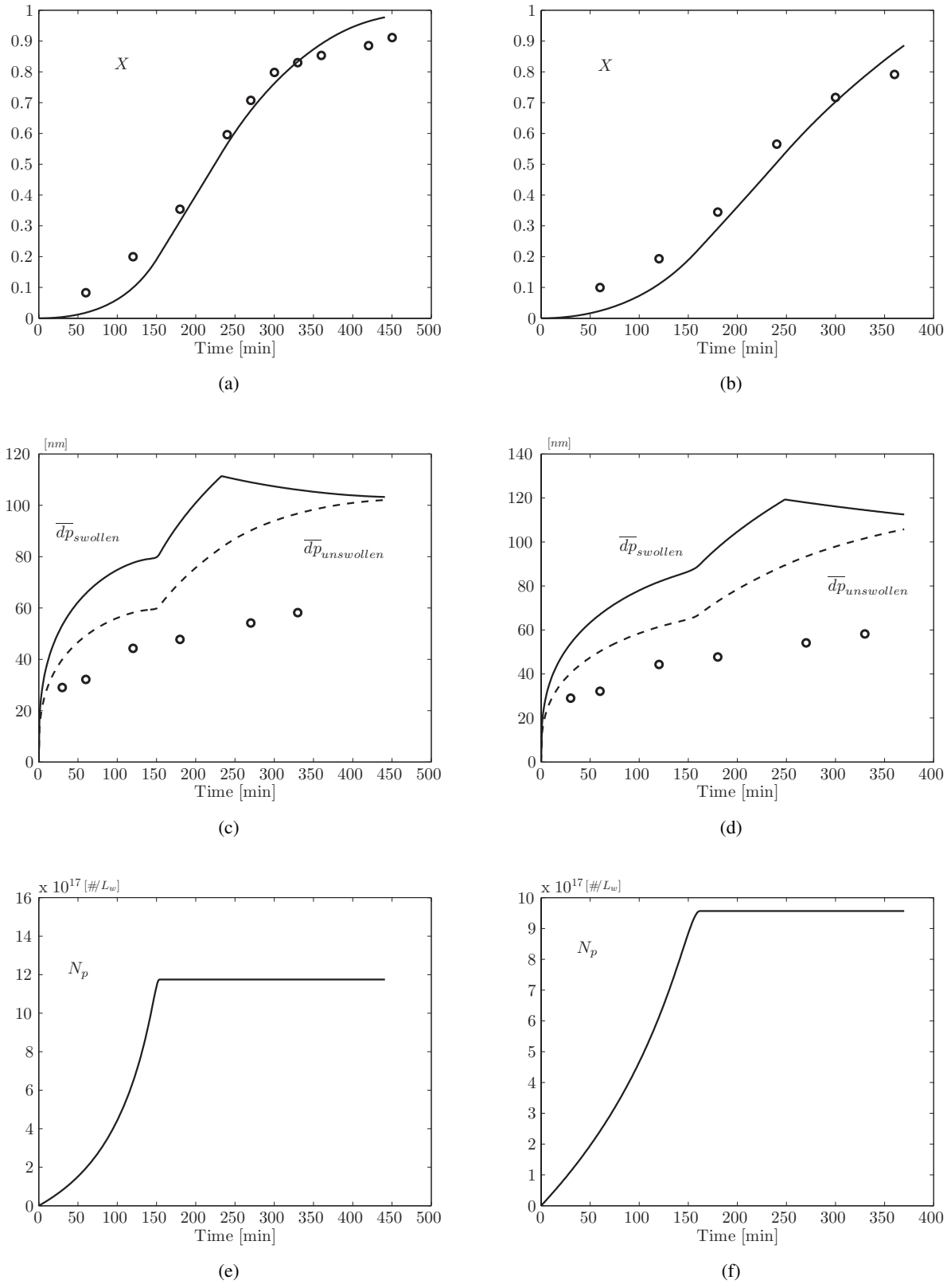

Figure 4.29: Batch reactor simulation - comparison to industrial data of Pallaske et al. [133] (recipes 2 & 3) - conversion and particle diameter

4.3 Concluding Remarks

This chapter has shown model simulation results for a batch and continuous reactor. The general model response was in agreement with previous modelling studies on SBR and NBR [16, 33, 171].

The effect of different levels of emulsifier and initiator on particle nucleation was demonstrated and revealed that particle number always increases with emulsifier concentration, while increasing the initiator concentration causes N_p to eventually pass through a maximum.

Monomer-soluble impurities were found to reduce $\bar{n}$, conversion, and particle size. Particle nucleation was prolonged causing a higher particle number, and as the concentration of impurity was increased, these effects were more pronounced. The effect on molecular properties was not as drastic as on conversion or particle nucleation. Radical consumption from water-soluble impurities was found to compete with micellar radical capture. All of these observed simulation trends were in agreement with previously shown (through simulation and experiment) trends by Penlidis [136].

The influence of radical desorption in an NBR system (i.e. case II) was found to be minimal, and highly dependent on the transfer to monomer rate constant (k_{fm}). Increasing the value of $k_{fm_{AA}}$ 10-fold according to the value used by Vega et al. [171] made little difference on the conversion profile and only seemed to influence N_p and $\bar{n}$, while having little influence on R_p (i.e. N_p increases and $\bar{n}$ decreases in a manner that does not affect R_p).

The model was successfully validated using an industrial NBR data set (i.e. X, $\overline{F}_{AN}$, d_p, $\overline{MW}_w$, and $\overline{MW}_n$) from Vega et al. [171]. Only slight discrepancies were observed due to possible differences in the parameters employed by the different groups. Additional comparisons to butadiene homopolymerization data revealed satisfactory model predictions; however, when the model was reduced to simulate acrylonitrile homopolymerizaton difficulties occurred in obtaining a reasonable conversion profile (i.e. high AN water solubility prevented conversion to proceed beyond 60% which was contradictory to the data of Tazawa et al. [159]). Nevertheless, the model was successful at simulating both NBR and Bd emulsion polymerization.

Chapter 5

Model Simulation Studies for a Train of Reactors

In this chapter the model developed and tested in Chapters 3 and 4 is put to use through a number of simulation studies on a train of continuous reactors. The first series of simulations performed focus on comparing batch and reactor train model predictions obtained using the same recipe. Next, a comparison is made between the model simulations of Minari et al. [105] and the model developed herein. Following this, the influence of impurities in a reactor train is investigated along with different reactor start-up policies within the train. The second aspect of this chapter presents simulation results related to controlling composition and molecular weight along the reactor train. In the final section of this chapter, strategies for maximizing polymer production are demonstrated.

5.1 Reactor Train Simulations

The benefit of using a dynamic model as opposed to a steady-state model to predict the evolution of properties in a continuous reactor train is that the affect of process upsets on the steady-state can be predicted and appropriately accounted for when designing reactor operating and control policies. Furthermore, numerous transient start-up and polymer grade change procedures can be studied through simulation, or the model could simply be used to monitor the process in real-time. Regardless of the model's intended use there are clearly more advantages to keeping the model in a dynamic form rather than in steady-state form. The purpose of this section is to demonstrate that simply feeding all recipe ingredients to the first reactor of the train without further additions often yields unacceptable or out-of-specification final properties. Comparisons are made between the batch reactor profiles and the steady-state reactor train profiles, as well as to similar simulation results on NBR found in the literature. In addition, the influence of impurities on polymer production in a reactor train is demonstrated, and the effects of different reactor start-up procedures are explored.

5.1.1 Baseline Simulations

To establish a sense of the dynamic behaviour of a long reactor train a baseline simulation was performed using 10 reactors each with a volume 20000 L, which is typical for the continuous production of NBR. A mean residence time of 60 minutes for each reactor is employed, which translates to a total volumetric inflow of 333 L/min into the first reactor. An identical recipe to the one used for a batch reactor was used for the continuous train, which can be seen in Table 5.1 under recipe 1. In addition, a mild reactor start-up procedure was used, where all reactors were initially full of water before material was fed to the first reactor. Dynamic solution profiles are presented for conversion, cumulative copolymer composition, particle number and size, molecular weight, and branching frequency. The model parameters used were as specified by Dube et al. [34] with modifications according to Tables 3.5 and 3.7. A comparison is made in Table 5.2 between the final latex properties of batch and continuous reactor train operation.

Simulation profiles for conversion, copolymer composition, particle number and size are presented in Figure 5.1, where Fiqures 5.1a and 5.1b depict the steady-state monomer and CTA additions into each reactor of the train. Operating the reactor train with a residence time of 60 minutes per reactor yields a gradual increase in conversion which reaches a steady-state of approximately 77% in the final reactor at around 26.6 hours. A similar time is required for copolymer composition, particle number and size, while the molecular properties (i.e. $\overline{MW}_n$, $\overline{MW}_w$, $\overline{BN}_3$, $\overline{BN}_4$) require approximately 30 hours to achieve steady-state in the final reactor (Figure 5.2). Copolymer composition begins to drift in the fourth reactor (Figure 5.1d), and the monomer droplet phase vanishes in the sixth reactor which is evident from a decrease in swollen particle diameter (Figure 5.1f). From Figure 5.1e it can be seen that particle nucleation occurs only in the first reactor followed by a long transient period where the steady-state is initially preceded by a large overshoot. The distinct "double-hump" in N_p in the first reactor is a result of the startup procedure and the use of two emulsifiers in the recipe which are initially below their critical micelle concentration. From Figure 5.2a the weight-average molecular weight appears to increase starting in the fifth reactor, while the number-average molecular weight (Figure 5.2b) remains fairly constant until the ninth reactor, where it begins to decrease slightly which is presumably a result of accumulated CTA in the final two reactors. Both tri- and tetra-functional chain branching frequency profiles (Figures 5.2c and 5.2d) reveal a sharp increase beyond the sixth reactor which indicates the onset of gel formation.

Figure 5.3 compares batch and steady-state reactor train profiles. In order to provide some insight on how latex properties in batch and reactor train compare, both profiles are superimposed in Figures 5.3a-f. Identical recipes are used, and each reactor in the train is initially full of water. The biggest difference between batch and reactor train profiles is seen in particle number and size (Figures 5.3c and 5.3d), where significantly more particles are nucleated in the batch reactor compared to the reactor train. As a result, the average particle diameter is larger in the reactor train. Further simulation revealed that to achieve a similar particle number in the reactor train to the batch reactor, the emulsifier concentration entering the first reactor would need to be at least ten times greater than the base recipe. Despite the particle number discrepancy, the copolymer composition, molecular weight and chain branching profiles reveal similar trends in both batch and reactor train. Note that the molecular properties are slightly higher in the batch reactor

since the conversion is higher compared to the steady-state CSTR conversion (i.e. higher conversion since more particles are nucleated). However, comparing both reaction modes (i.e. batch and CSTR train) at the same final conversion reveals a slightly higher weight-average molecular weight and tri-functional branching frequency for the CSTR train (see Table 5.2).

What has been shown in this section are dynamic and steady-state latex property profiles in a continuous reactor train. Based on the resulting simulations, in order to achieve similar latex properties in batch and reactor train a similar number of particles must be generated. Perhaps the most revealing aspect from the simulations shown is the need for composition, molecular weight and chain branching control over the course of the polymerization. In a similar manner to semi-batch policies used to control latex properties in a batch reactor, intermediate additions can be employed along a reactor train to minimize composition drift and to achieve a desired molecular weight. These aspects are explored further in section 5.2.

Table 5.1: NBR process recipes

Ingredient	**Batch Recipe**	**Continuous Recipe 1**	**Continuous Recipe 2**[a]
Acrylonitrile	32	32	31.4
Butadiene	68	68	68.6
Water	180	180	170.2
PMHP [b]	0.223	0.223	0.0096 [c]
Fe [d]	0.0056	0.0056	0.0096
SFS [e]	0.12	0.12	0.2
Dresinate [f]	1.25	1.25	3.49 [g]
Tamol [h]	2.85	2.85	-
Mercaptan	0.42	0.42	0.409
$q_{T_{in}}$ (L/min) [i]	-	333	321.7 [j]
Temperature (^oC)	10	10	10

[a] Recipe from Minari et al. [105]
[b] *para*-menthane hydroperoxide initiator
[c] The initiator had to be increased 3 times the value stated here in order to prevent premature depletion of initiator
[d] $FeSO_4 \cdot 7H_2O$
[e] Reducing agent
[f] Secondary emulsifier
[g] Emulsifiers were not specified by Minari et al. [105], thus were assumed here for simulation purposes
[h] Primary emulsifier
[i] Total inlet volumetric flow to the 1^{st} reactor
[j] An 8 reactor train with volume of 17473 L per reactor was used ($\theta = 54.3$ minutes)

Table 5.2: Final simulated properties for baseline batch and continuous processes

Property	**Batch Operation** [a]	**Continuous Operation 1** [b]
G^c (kg/min)	-	78.2
x $(\%)$	77.75	77.73
$N_p \times 10^{-18}$ $(\#/L_w)$	4.448	0.8813
d_p (nm)	61.8	98.9
$\overline{MW}_n$ (g/mol)	0.5014	0.4989
$\overline{MW}_w$ (g/mol)	1.6139	1.8429
PDI (-) [d]	3.22	3.69
$\overline{BN}_3$ $(\#/molecule)$	0.476	0.569
$\overline{BN}_4$ $(\#/molecule)$	0.023	0.028
$\overline{F}_{AN}$ (-)	0.2185	0.2174
$\Delta\overline{F}_{AN}$ $(\%)$ [e]	35.6	36 [f]

[a] All properties at 430 min in order to match steady-state (s.s.) CSTR conversion
[b] For a 10 reactor train
[c] Rate of polymer production
[d] Polydispersity ($\overline{MW}_w/\overline{MW}_n$)
[e] Percent drift in copolymer composition
[f] Percent drift from the 1^{st} to the final reactor

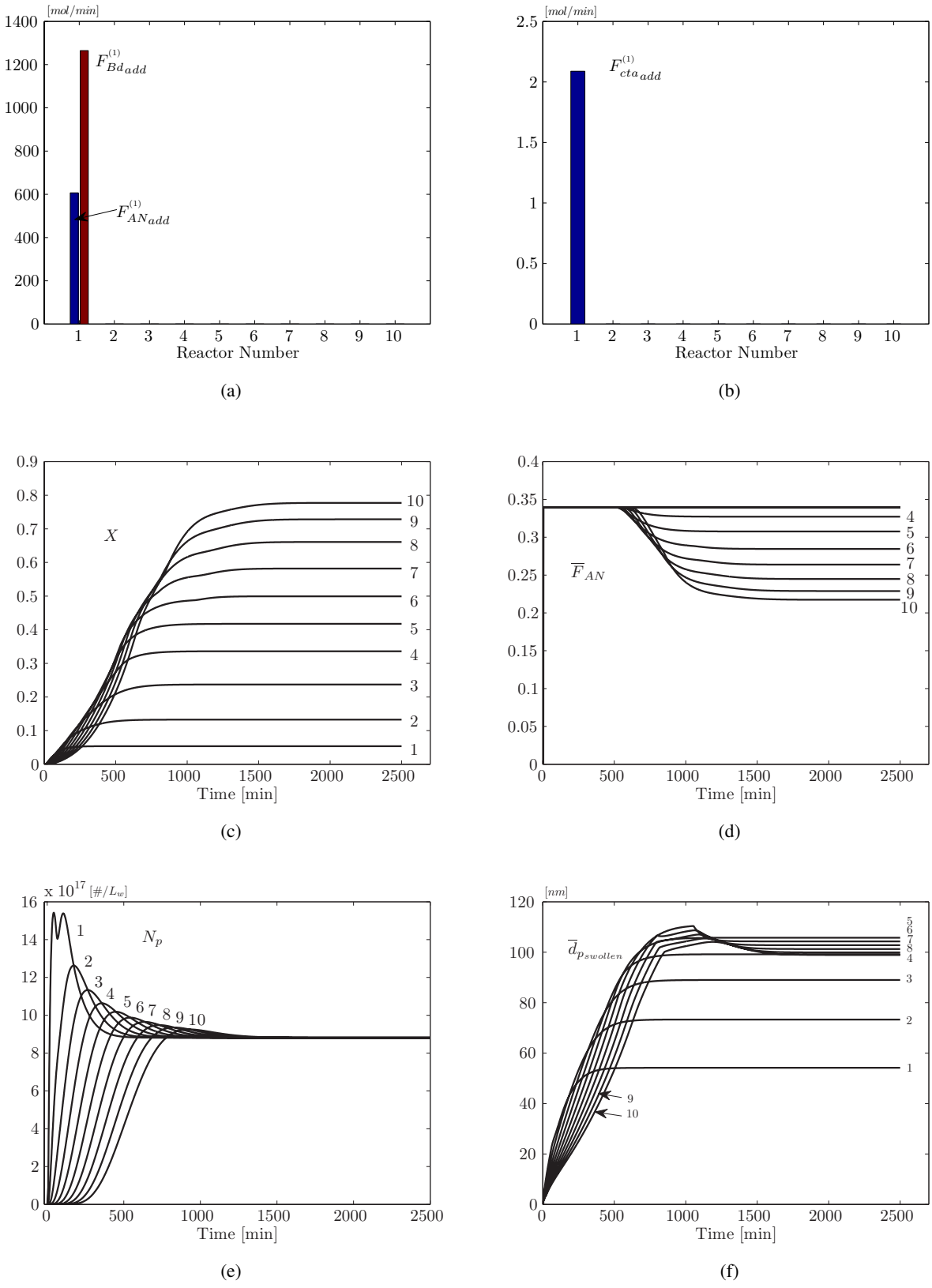

Figure 5.1: Continuous reactor train simulation - continuous recipe 1 - conversion, copolymer composition, particle number & diameter

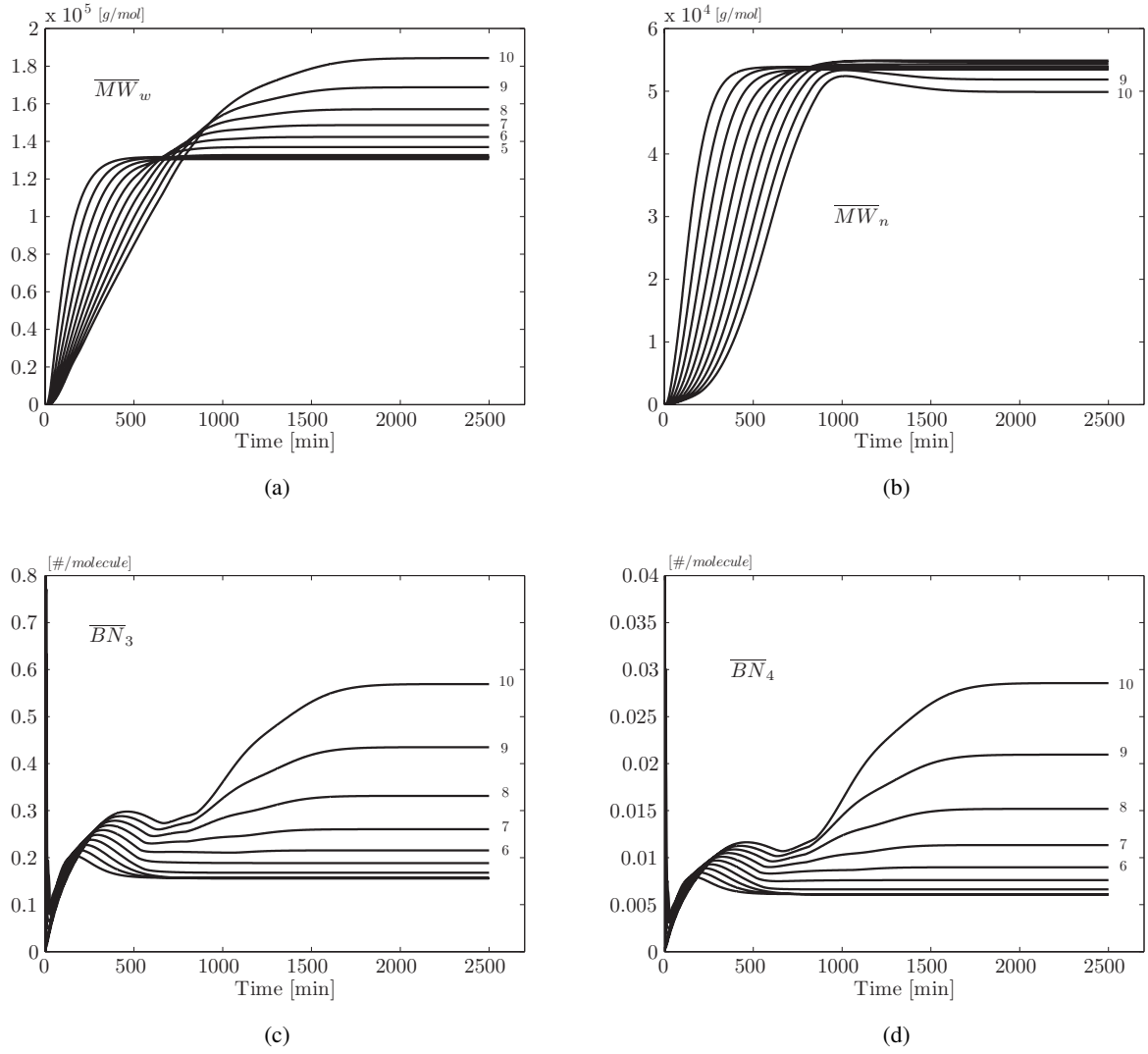

Figure 5.2: Continuous reactor train simulation - continuous recipe 1 - number-, weight-average molecular weights & tri-, tetra-functional branching frequencies

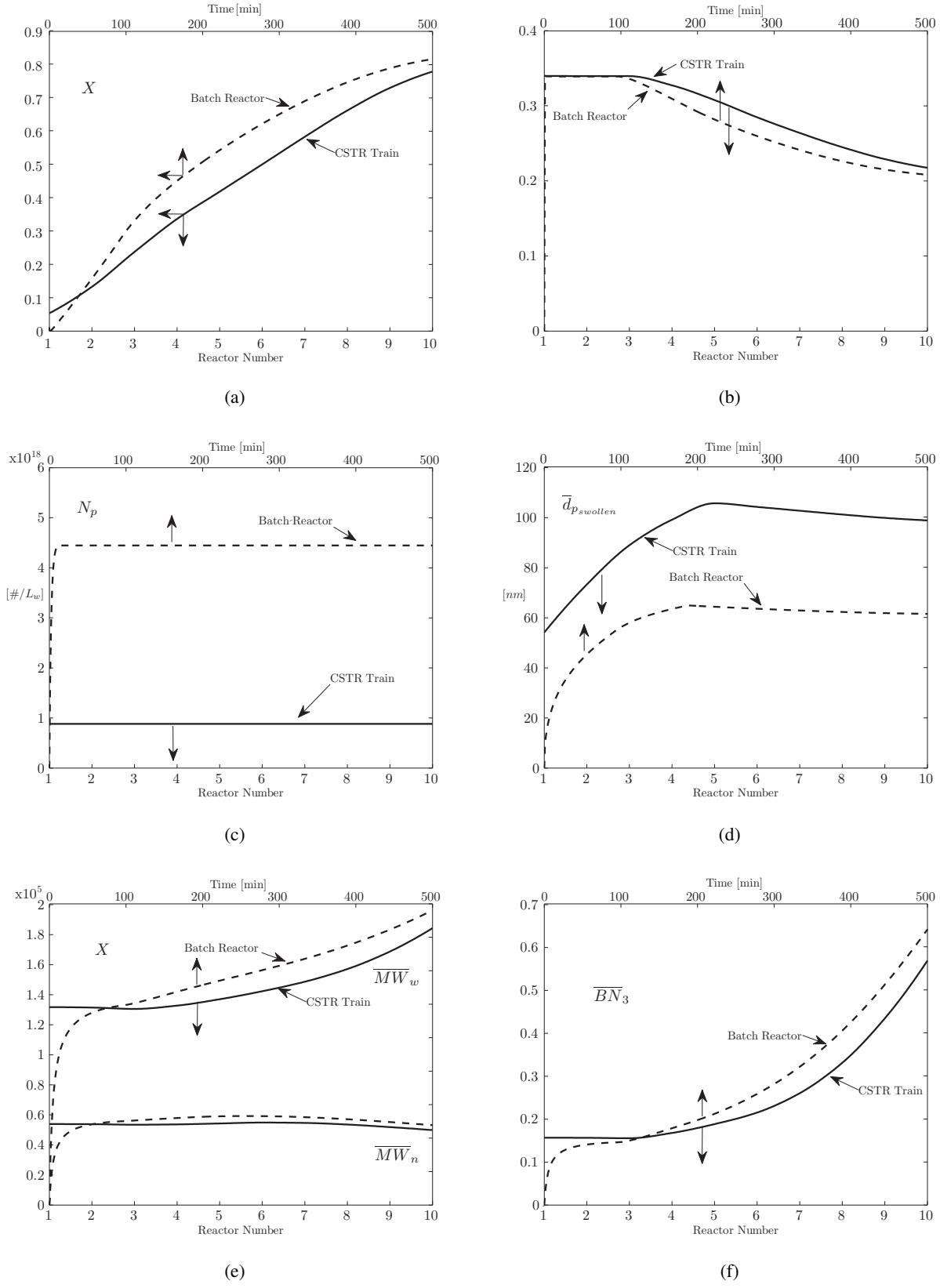

Figure 5.3: Comparison between batch and steady-state reactor train property profiles - conversion, CCC, particle number, diameter, molecular weight & branching frequencies

5.1.2 Comparison to Simulations of Minari et al.

The model developed herein is now compared to that used by Minari et al. [104, 105]. The purpose here is to simply show how well the proposed model compares in terms of the final properties when using the reactor operating conditions (i.e. residence time, reactor volume) and recipe of Minari. No attempt is made at this point to control composition or molecular properties through monomer or CTA addition policies. The recipe used is presented in Table 5.1 under the heading "continuous recipe 2". An 8 reactor train was employed with a mean residence time of 54 minutes per reactor and an individual reactor volume of 17473 litres. All recipe ingredients were fed to the first reactor. Since the specific emulsifier type was not specified by Minari, Dresinate was used and assumed to be the sole emulsifier present. As well, since PMHP was used in place of DIBHP as the initiator, the feed concentration had to be increased 3 times that of the base recipe (i.e. PMHP is more reactive than DIBHP and is consumed faster). In addition, to obtain a similar number of particles as Minari the nucleation parameter ε had to be reduced 10-fold (i.e. $\varepsilon = 0.4839$) from the value used in the baseline simulations.

A comparison between the simulation results reported by Minari et al. [105] and those generated from the model developed herein are presented in Table 5.3. The results shown are the steady-state latex properties in the final reactor (i.e. 8^{th} reactor). Considering that a number of unknowns are present with the recipe and parameters provided by Minari (i.e. unknown emulsifier type and no parameters presented) the model compares quite well. Without modifying any of the baseline parameters (except ε), the final conversion and rate of polymer production predicted by the present model were roughly 3% higher than those predicted by Minari; N_p was slightly lower resulting in a higher average diameter; both $\overline{MW}_n$ and $\overline{MW}_w$ were lower which was most likely due to differing chain transfer parameters; and $\overline{BN}_3$ was slightly higher again related to chain transfer parameters. In a similar manner to the baseline batch and CSTR simulation profiles, the cumulative copolymer composition reveals a significant drift of approximately 33% from the first to the last reactor in the train. This behaviour is strikingly different from that of Minari et al. who report only an 8% drift under normal operation (i.e. all ingredients fed to the 1^{st} reactor). Furthermore, using an identical monomer feed composition, the initial copolymer composition in the 1^{st} reactor was approximately 4% lower than that reported by Minari (i.e. 34% versus 37.8%). As previously mentioned in Chapter 4, the rather high initial composition and minimal drift reported by Minari, is most likely a result of different partition coefficient and reactivity ratio parameters. A possible explanation for the rather small composition drift is that the initially higher copolymer composition within the particle phase is closer to the azeotropic composition which results in a lesser rate of drift. Without data to corroborate the trends of Minari or to estimated the partition and reactivity parameters used in the present model more precisely, it is difficult to comment further on the drift or lack thereof seen between each model.

The resulting simulation profiles from the recipe of Minari can be seen in Figures 5.4 and 5.5. Compared to the baseline simulations, where 10 reactors were used, conversion is observed to progress along an 8 reactor train at a greater rate (Figure 5.4c). The reason for the increased rate is that more particles are generated in the first reactor than in the baseline simulations. This behaviour reveals that simply adding more reactors to the current reactor train will not necessarily increase polymer production. To increase

Table 5.3: Comparison of final simulated properties for the continuous process of Minari et al. [105]

Property	**Continuous Operation 2** [a]	**Results of Minari** [b]
G^c (kg/min)	75.6	72.2
x $(\%)$	75.5	72.7
$N_p \times 10^{-18}$ $(\#/L_w)$	2.18	2.48
d_p (nm)	74.8	69.5
$\overline{MW}_n$ (g/mol)	0.527	0.61
$\overline{MW}_w$ (g/mol)	1.834	2.10
PDI (-) [d]	3.48	3.44
$\overline{BN}_3$ $(\#/molecule)$	0.499	0.467
$\overline{BN}_4$ $(\#/molecule)$	0.024	- [e]
$\overline{F}_{AN}$ (-)	0.225	0.348
$\Delta\overline{F}_{AN}$ $(\%)$ [f]	33.7	8.5 [g]

[a] For an 8 reactor train according to the specifications of Minari

[b] Simulation results reported by Minari et al. [105] for normal s.s. operation where all ingredients are fed to the 1^{st} reactor

[c] Rate of polymer production

[d] Polydispersity $(\overline{MW}_w/\overline{MW}_n)$

[e] Not reported

[f] Percent drift in copolymer composition

[g] Based on an initial s.s. AN composition of 37.8% in the first reactor

production, better options are to determine an optimal reactor residence time for maximizing N_p (Figure 4.6) or to explore different reactor monomer feed policies. Only after exploring all feasible solutions for maximizing polymer production should extending the reactor train be considered. Further comments on this aspect and simulations are shown in section 5.3. The molecular properties progress in a similar manner to those shown for the baseline simulations; however, the smaller train experiences a shorter transient period (i.e. s.s. reached in 1300 min in the 8^{th} reactor versus 1600 min in the same reactor of the larger train) while at the same time achieving similar final properties. The reason for the shorter transient is a result of a smaller process time-constant (i.e. reactor residence time) which allows for faster process dynamics.

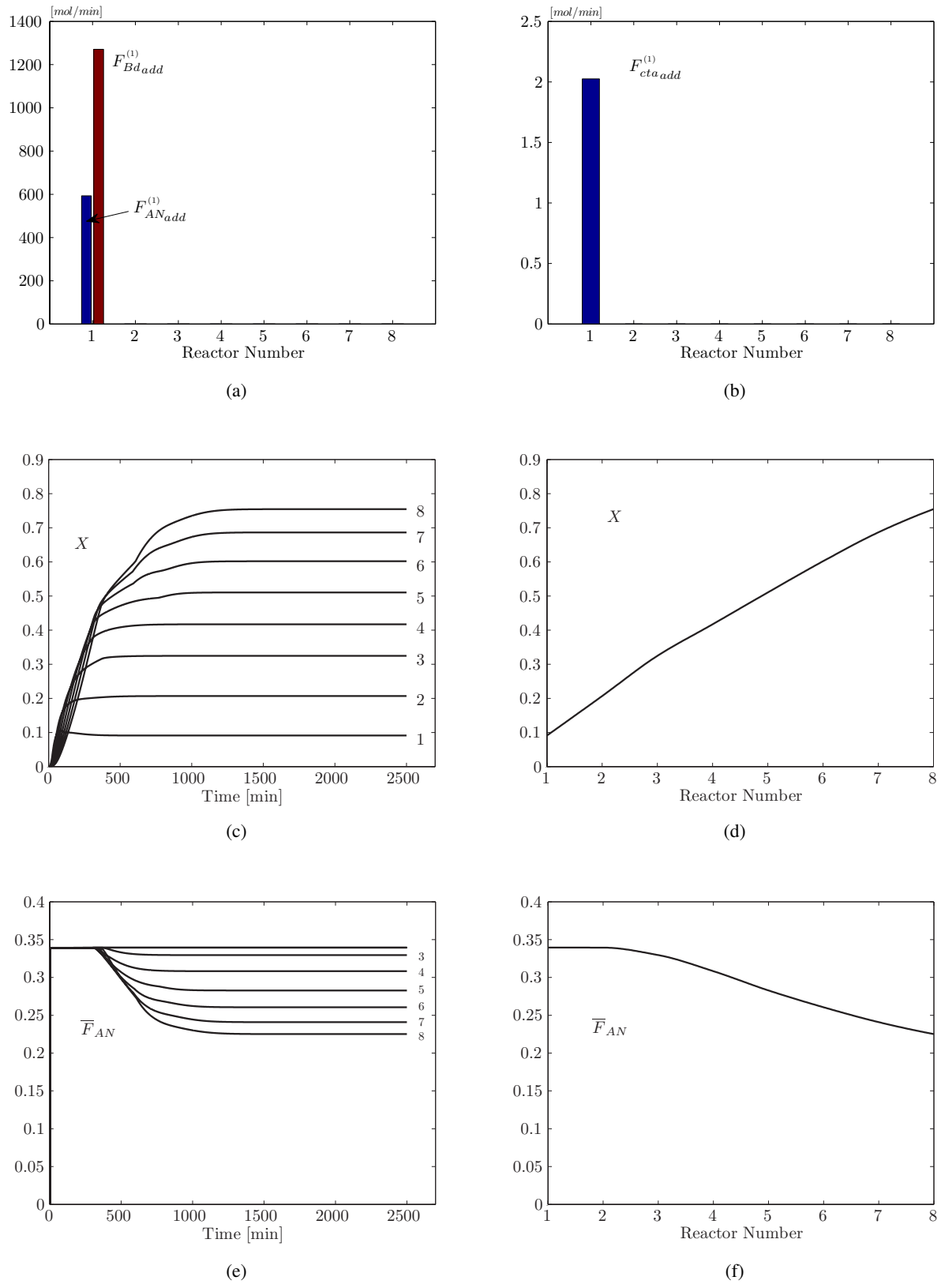

Figure 5.4: Continuous reactor train simulation - continuous recipe 2 - conversion & copolymer composition

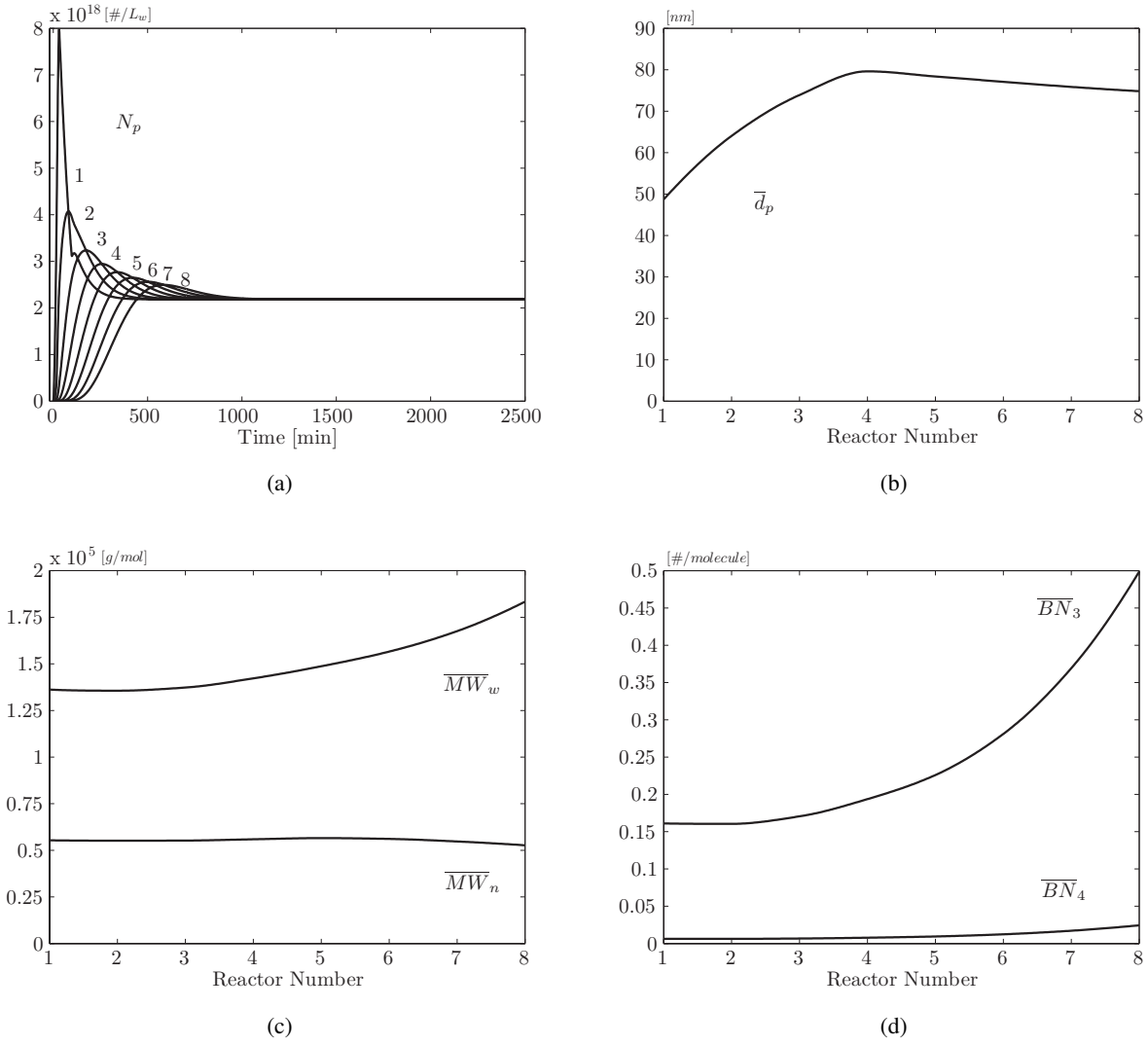

Figure 5.5: Continuous reactor train simulation - continuous recipe 2 - particle number, diameter, and molecular properties

5.1.3 Effect of Impurities in a Reactor Train

To provide some insight on the influence of impurities in a reactor train similar simulations were performed to those previously shown with a batch reactor in Chapter 4. Based on what was previously shown, it is known that monomer impurities prolong the nucleation time creating more particles, decrease the average particle size, and decrease the monomer conversion until all the impurity is consumed. On the other hand, water impurities scavenge radicals in the aqueous phase reducing the number of particle nucleated which in turn lowers the monomer conversion over the course of polymerization. What is shown in this section is the combined effect of both monomer- and water-soluble impurities on conversion, polymer production, particle number and average particle diameter.

A rather low monomer and water impurity concentration of 150 ppm and 20 ppm were used. The monomer impurity rate constant used is reported in Table 4.6, while the water impurity (i.e. oxygen) rate constant used was 1×10^7 L/mol/min. The steady-state latex properties can be seen in Figure 5.6. As expected, the monomer conversion is significantly reduced which inherently causes a lower rate of polymer production (if no additional monomer is fed along the train). Looking at Figure 5.6c reveals that the number of particles nucleated is reduced from the baseline simulation, which exemplifies the dominant influence of oxygen versus monomer impurities on particle nucleation. In an industrial reactor, the presence of oxygen is primary due to an unpurged reactor headspace. On the other hand, monomer impurities such as vinylacetylene enter the system with monomer feedstock (i.e. butadiene impurity), while TBC, which is added to the blow down drums as a stopping agent to hinder polymerization, re-enters the system from monomer recycle streams. From the perspective of maximizing polymer production (G_{pol}) using the least amount of reactors and recipe (i.e. emulsifier and initiator), it is important to carefully identify possible entry points and minimize the influence of impurities on production rate. From the simple example demonstrated here, one should note the potentially rate-hindering consequence of impurities and take the necessary precautions to limit the entry of large concentrations into system. Unfortunately, it is virtually impossible to remove all impurities from the system and as a result they should be considered as an integral component of the feed recipe. Considering impurities in this manner would allow one to develop an effective process model that accounts for various (usually unknown) radical scavenging reactions, and can adequately track the evolution of latex properties along the reactor train.

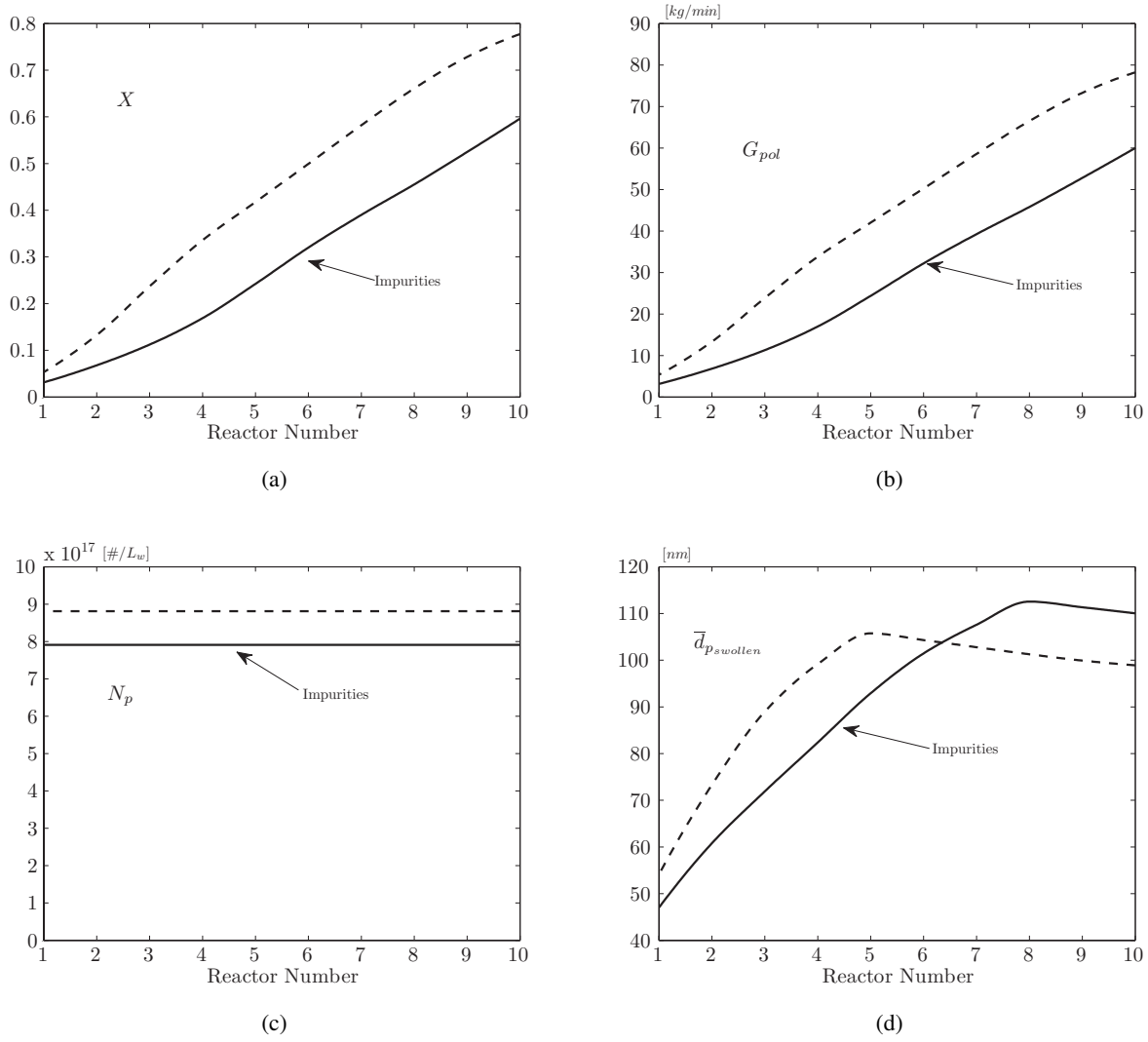

Figure 5.6: Continuous reactor train simulation - impurity effects - conversion, polymer production rate, particle number & diameter

5.1.4 Reactor Train Start-up Procedures

The dynamics of rubber systems (SBR and NBR) are in general quite sluggish and, depending on the startup procedure, can require some time to reach a steady-state. Thus, one approach to reducing the amount of off-spec material produced during reactor startup is to optimally design a policy that allows each reactor to reach a steady-state in each latex property as quickly as possible. A dynamic model can be quite useful to investigate such policies, and the purpose of the this section is to demonstrate two particular procedures; starting the reactor train up with each reactor full of water and second, each reactor empty where the reactor operates in semi-batch fashion until it overflows into a subsequent reactor. Clearly, these two approaches are not an optimal solution, but they demonstrate the typical open-loop response of the model.

In a similar manner to what was previously shown in Chapter 4, section 4.1.6, for a single CSTR, Figure 5.7 depicts transient profiles for conversion, particle number, average particle size and weight-average molecular weight using each of the aforementioned startup policies. Starting the reactor train full of water reveals a mild transition to the steady-state for each latex property compared to starting each reactor up empty. Both approaches eventual reach the same steady-state, with the water startup requiring significantly more time. Other possible approaches to startup are to initially charge all reactors with a pre-emulsified monomer solution (i.e. emulsifier, monomer, water) and then begin to feed in the activator and CTA. Simulations using this approach revealed a milder transient than starting the reactors empty with a much smaller burst in particle nucleation (i.e. much smaller heat release). All latex properties reached the same steady-state as the previous approaches, however, the transient behaviour was significantly less than either of the previous approaches and reached a steady-state in a similar time ($\sim$ 500 minutes) to the empty-startup approach. Note that only a 6 reactor train is used for demonstration purposes and the profiles for particle number are only shown for the first 4 reactors for the sake of clarity.

An important aspect to consider when designing a particular policy is the necessary cooling capacity. When starting the reactor empty a large spike in particle formation occurs which causes a spike in the polymerization rate creating a similar spike in the heat of reaction. As a result, the cooling system of the nucleating reactor (i.e. typically only the first reactor of train) must account for the possibility of large and potentially explosive spikes in heat generation.

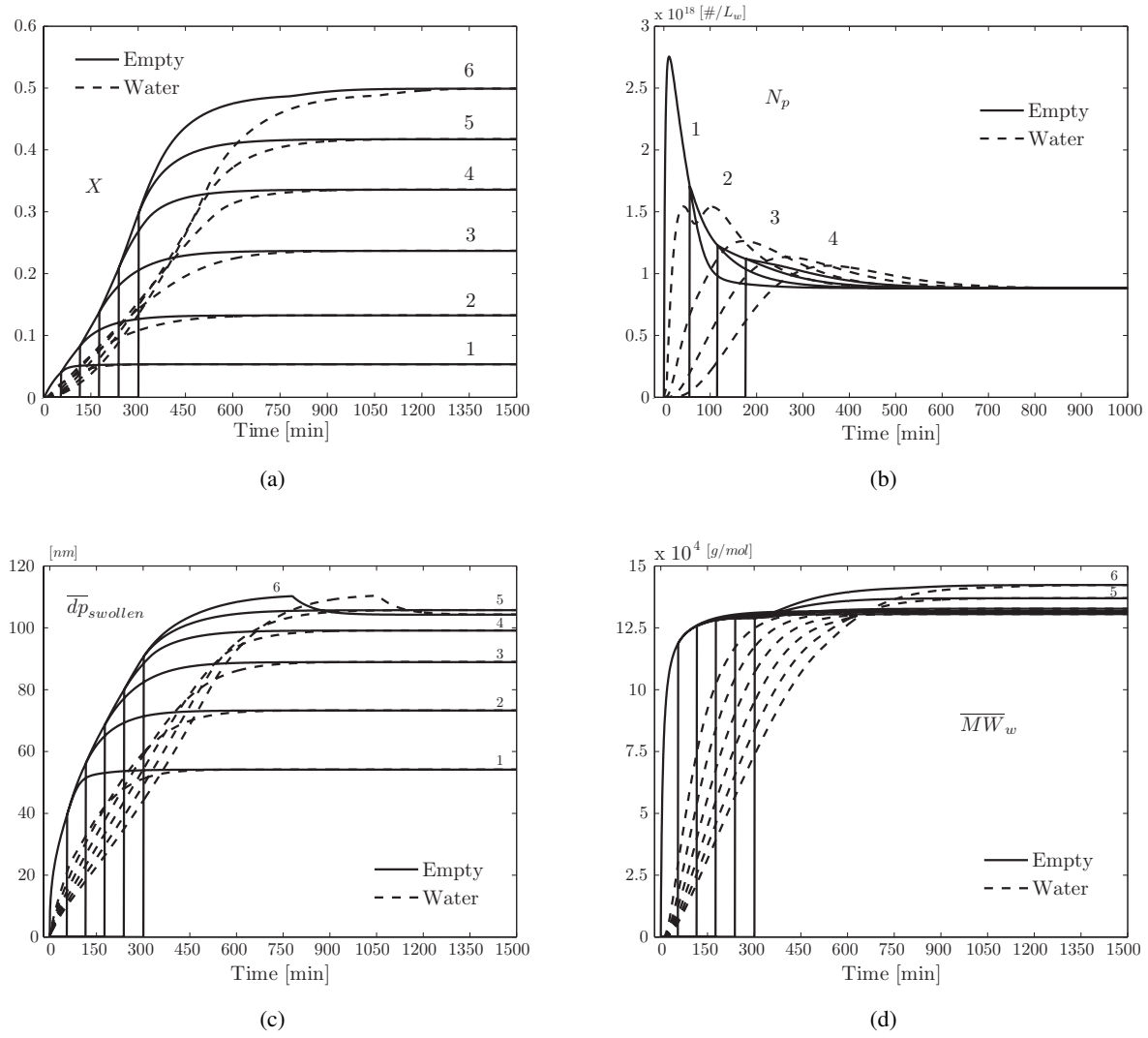

Figure 5.7: Continuous reactor train simulation - reactor startup (recipe 1, Table 5.1) - conversion, particle number, diameter & molecular weight

Note that the particle number shown in Figure 5.7b is plotted based on the average particle number per litre of water, and when starting the reactors up empty it might seem like more particles are initially formed compared to starting the reactor full of water. However, if plotted in terms of total particle number, this is in fact the opposite case, as the transient peaks are larger when starting the reactors full of water, hence the smaller average particle diameter for the water-startup case in Figure 5.7c.

5.2 Simulation Studies on Polymerization Optimization Scenarios

In this section optimization (and potentially control) policies are discussed for influencing copolymer composition, molecular weight, and particle size within a semi-batch or continuous reactor train. The objective here is to provide some insight on how the model developed herein can be used in a theoretical manner to investigate optimal operating policies. Several reactor train simulations are performed to show the influence of monomer, CTA, and emulsifier additions. The idea here is not to propose necessarily optimal feed flows, but instead to give an idea on how ingredient additions can influence the process response (i.e. $\overline{F}_{AN}$, $\overline{MW}_w$, N_p).

5.2.1 Copolymer Composition Control

In copolymer systems where one monomer is more reactive than the other and the feed ratio does not produce an azeotrope, the cumulative copolymer composition will drift as conversion increases. For example, if r_A and r_B represent the reactivity ratios of monomers A and B and if $r_A < 1$, $r_B < 1$, $r_A < r_B$, and the monomers are fed at a composition below the azeotrope (Figure 3.2), then the composition of A will drift downwards and that of B upwards. As a result, a heterogeneous polymer mixture is formed which can have inferior properties (mechanical, optical) than those originally specified. Composition drift occurs in batch reactors and in long trains of continuous reactors as conversion increases (i.e. $F_{AN} > f_{AN}$, from Figure 3.2). Note that for trains of CSTR's the steady-state copolymer composition will decrease in each successive reactor as AN is consumed. This deviation occurs because the flow of material through a reactor train follows the behaviour of a plug-flow reactor and at steady-state the reaction kinetics resemble those of a batch reactor. To circumvent this undesirable behaviour commercial technologies incorporate several controlled monomer additions within a batch process (i.e. semi-batch) or at specific points along the reactor train. Typically, the more reactive monomer is continually fed throughout the reaction so that composition remains fairly constant. For a batch reactor a number of different semi-batch control policies have been proposed that determine optimal monomer feed rates for minimizing composition drift [16, 34, 50, 67, 172], while for a continuous reactor train similar policies have been put forth that determine the optimal steady-state flow of monomer into each reactor along the train to maintain a desired composition [104].

Semi-batch policies for minimizing composition drift are typically based on maintaining a particular monomer ratio or concentration within the reactor. For example, to maintain a particular monomer ratio would require the adjustment of the more reactive monomer inflow so that the following constraint is met:

$$\frac{d}{dt}\left(\frac{N_A}{N_B}\right) = 0 \tag{5.1}$$

where N_A/N_B is the mole ratio required to maintain a particular composition. Equation 5.1 can be further reduced (i.e. through differentiation) to give:

$$\frac{dN_A}{dt} = \left(\frac{N_A}{N_B}\right)\frac{dN_B}{dt} \tag{5.2}$$

This policy is based on keeping the total molar ratio constant, however, when monomer is fairly soluble in the aqueous phase it is more appropriate to keep the molar ratio in the particle phase constant (i.e. $\alpha = N_{A_p}/N_{B_p}$). Using Equation 5.2, it is possible to derived an expression for the required optimal molar inflow of monomer A, $F_{A_{in}}$, (i.e. the more reactive monomer) [15]. Producing an optimal trajectory under the added complication of monomer phase partitioning prevents the derivation of an analytical solution and requires an iterative procedure of initially guessing $F_{A_{in}}$, solving the mass balance equations, checking the criteria of Equation 5.2, and updating $F_{A_{in}}$ if required [50].

Alternative to the aforementioned approach, is a policy that maintains a sufficiently low and constant particle phase monomer concentration to give a desired copolymer composition. In this approach, both monomer feeds (i.e. $F_{A_{in}}$ and $F_{B_{in}}$) are manipulated to maintain $[M_A]_p$ and $[M_B]_p$. Moreover, other policies are to feed monomer at a rate equivalent to the instantaneous copolymer composition (ICC), or at a rate to maintain a constant ratio between the rates of polymerization of each monomer [6]. Regardless of the exact approach, the objective is to minimize drift through the addition of monomer. Perhaps more important than the exact control approach, is to keep in mind the strain placed on the reactor cooling system and influence on the molecular weight (averages or distribution) that adding additional monomer may have. The later concern is often alleviated through simultaneously adding CTA to control the molecular weight.

More pertinent to the study at hand, is how to control copolymer composition in a continuous reactor train. Similar addition policies to those used for semi-batch reactors can be used, however it is often adequate to simply look at the steady-state consumption of monomer and define an appropriate additional feed rate of the more reactive monomer into each reactor. This approach was used by Minari et al. [104] for producing a desired (i.e. prespecified) steady-state copolymer composition. Their monomer inflow equation was based on writing a steady-state balance on total free and bound monomer and using the definition of the cumulative copolymer composition to form a combined expression for $F^{(r)}_{A_{in},add}$, which corresponds to the additional monomer that must be added as a side flow to reactor 'r' along the train. A derivation can be given as:

$$F^{(r-1)}_{A_{in}} + F^{(r)}_{A_{in},add} - F^{(r)}_{A} = R^{(r)}_{p_{A_p}} V^{(r)}_{p} + R^{(r)}_{p_{A_a}} V^{(r)}_{a} \tag{5.3}$$

$$F^{(r-1)}_{pol_{A_{in}}} - F^{(r)}_{pol_A} = -\left(R^{(r)}_{p_{A_p}} V^{(r)}_{p} + R^{(r)}_{p_{A_a}} V^{(r)}_{a} \right) \tag{5.4}$$

$$\overline{F}_A = \frac{N^{(r)}_{pol_A}}{N^{(r)}_{pol_A} + N^{(r)}_{pol_B}} \tag{5.5}$$

Using the above equations and similar balances on monomer B, a policy for monomer A can be written as:

$$F^{(r)}_{A_{in},add} = \left(F^{(r-1)}_{pol_{B_{in}}} + F^{(r-1)}_{B_{in}} - F^{(r)}_{B} + F^{(r)}_{B_{in},add} \right) \frac{\overline{F}_{A,d}}{1-\overline{F}_{A,d}} - \left(F^{(r-1)}_{pol_{A_{in}}} + F^{(r-1)}_{A_{in}} \right) + F^{(r)}_{A} \tag{5.6}$$

where $r = 1,\ldots,N_r$, and $F^{(r)}_{B_{in},add}$ is zero if the objective is to simply feed the more reactive monomer. Though stated in an explicit form, Equation 5.6 is solved through an iterative procedure where $F^{(r)}_{A_{in},add}$ is calculated, the polymerization model solved, the copolymer composition checked (i.e. $\overline{F}_{A,desired} \approx \overline{F}_{A,actual}$),

and the procedure repeated until convergence in composition and total volumetric outflow between each iteration.

Controlling the copolymer composition through the application of Equation 5.6 often suggests that monomer additions are necessary at many points along the train. However, in practice this may not be feasible due to limitations in the current infrastructure or the capital cost required to make the necessary upgrades. More realistic is to formulate a monomer addition policy with the added constraint of having only one or two addition points along the train. Such a policy would constitute a suboptimal solution, and is most easily realized through simulation. In what follows, several simulations are performed using a step input of monomer at select locations along the train in order to demonstrate the influence on copolymer composition.

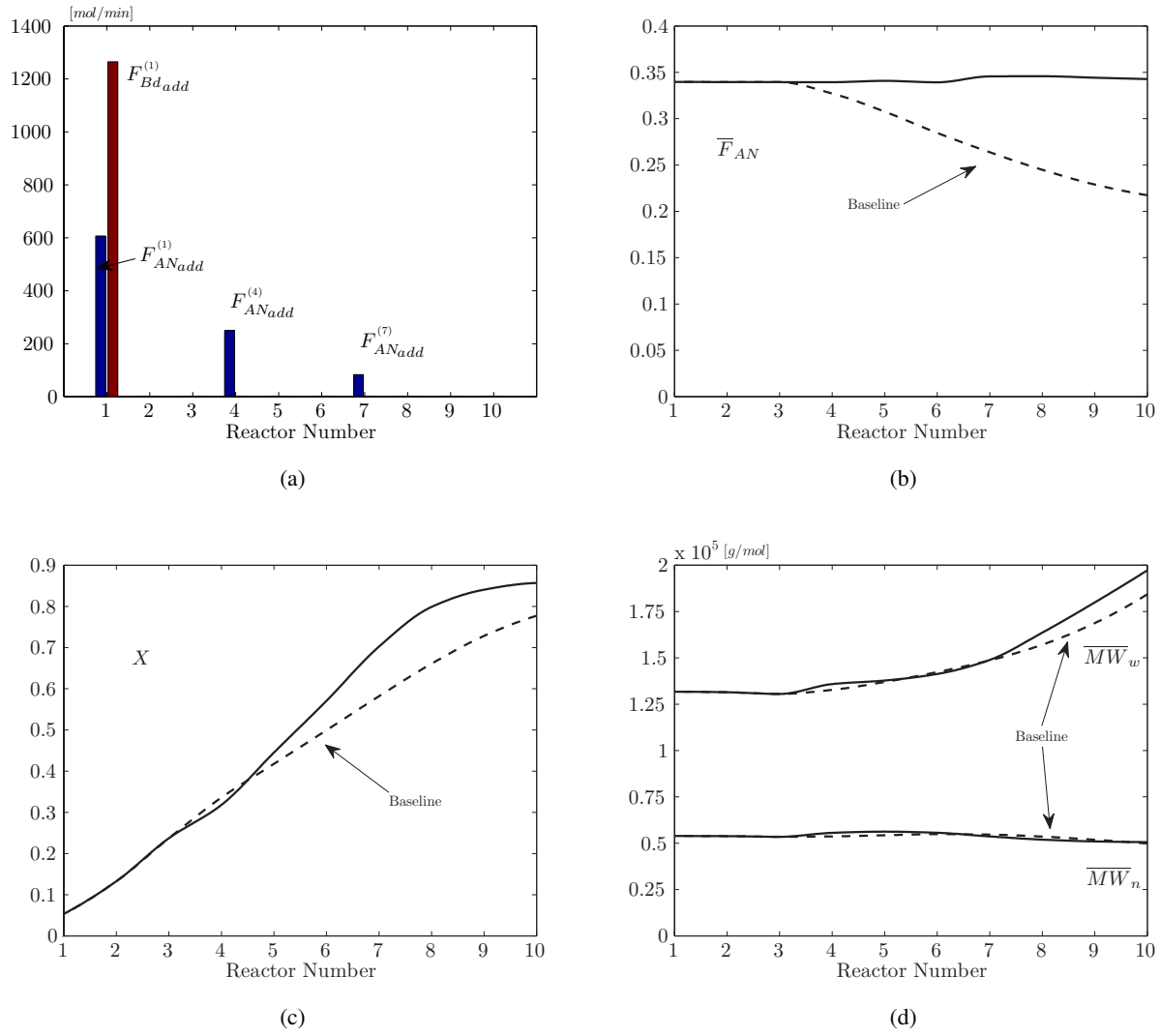

Figure 5.8: Continuous reactor train simulation - copolymer composition control

Figure 5.8b depicts the steady-state response of copolymer composition from a step input of AN at a

reaction time of 500 minutes into the fourth and seventh reactor of the train (Figure 5.8a). Using this policy the composition is capable of being maintained close to the initial feed composition ($\sim 34\%$). Conversion is observed to increase by 8% in the final reactor from the baseline simulation (Figure 5.8c), while the molecule weights and branching frequencies increase. A full listing of the final steady-state latex properties can be seen in Table 5.4. Note that the rate of polymer production increased by roughly 23% at a fixed particle number by introducing more of the higher reactive monomer to the system.

Table 5.4: Comparison of final simulated properties for the continuous process using AN additions to control $\overline{F}_{AN}$

Property	**Baseline**	**AN additions** [a]
G^b (kg/min)	101.4	78.2
x (%)	77.7	85.7
$N_p \times 10^{-18}$ $(\#/L_w)$	0.8813	0.8813
d_p (nm)	98.9	106.5
$\overline{MW}_n$ (g/mol)	0.499	0.506
$\overline{MW}_w$ (g/mol)	1.843	1.972
PDI (-) [c]	3.69	3.90
$\overline{BN}_3$ $(\#/molecule)$	0.569	0.869
$\overline{BN}_4$ $(\#/molecule)$	0.028	0.034
$\overline{F}_{AN}$ (-)	0.217	0.343
$\Delta\overline{F}_{AN}$ (%) [d]	36	0 [e]

[a] Steady-state simulation results for AN addition to reactors 4 and 7
[b] Rate of polymer production
[c] Polydispersity ($\overline{MW}_w/\overline{MW}_n$)
[d] Percent drift in copolymer composition
[e] Final composition was 0.3427, 0.0027 higher than in the first reactor

5.2.2 Molecular Weight and Chain Branching Control

The molecular properties of the latex are controlled through chain-transfer regulating agents (i.e. CTA). Increasing the concentration of CTA induces chain-transfer causing the average molecular weight (number- and weight-average) to decrease. These agents function only to promote chain-transfer and hopefully do not influence polymerization rate (i.e. particle number) or monomer conversion. The purpose of this section is to demonstrate the dynamic and steady-state molecular weight and branching frequency response to additions of CTA along the reactor train. Furthermore, the objective of the demonstration is to show how CTA can influence the molecular properties, but not necessarily to propose optimal feed policies to achieve a desired profile along the reactor train.

Due to the relatively small concentration of CTA compared to monomer in the recipe and the difficulty in evenly mixing such a small amount into the reaction mass, industrial control technologies typically feed both CTA and monomer to downstream reactors as a premixed solution [88]. Thus, with this in mind, simulations were performed by feeding CTA to the same reactors that monomer was fed to in the previous

example (Figure 5.8). Figure 5.9 presents dynamic and steady-state profiles for molecular weight and tri-functional branching frequency. Transfer agent was fed to reactors 4 and 7 as a step input which was applied at a reaction time of 1000 minutes (i.e. the time of droplet depletion and onset of diffusion-controlled termination). As expected, the molecular weight and branching frequencies decreased, where the weight-average molecular weight was observed to have a greater sensitivity to CTA additions (Figure 5.9c).

It is often desirable to control the molecular property profiles (dynamic and/or steady-state) along the reactor train. However, simultaneously obtaining a desired profile (i.e. optimal profile) for number- and weight-average molecular weight and tri- and tetra-functional branching frequencies can be a difficult task and it is easier to simply derive the required additional CTA feed rate in terms of either $\overline{MW}_n$, $\overline{MW}_w$, $\overline{BN}_3$, or $\overline{BN}_4$ [103]. When monomer additions are made to control the copolymer composition (i.e. additions of the more reactive monomer), simultaneous additions of CTA are often required to prevent deviations in the molecular properties (i.e. sudden transitions to higher molecular grades). Furthermore, similar CTA additions or re-distribution is necessary if the objective is to increase polymer productivity through distributing monomer between the first couple of reactors in the train (i.e. reduce the space occupied by the inert monomer droplet phase in each reactor). These concepts have been investigated on both NBR and SBR processes [82, 103, 105, 170] and are briefly demonstrated in section 5.3.

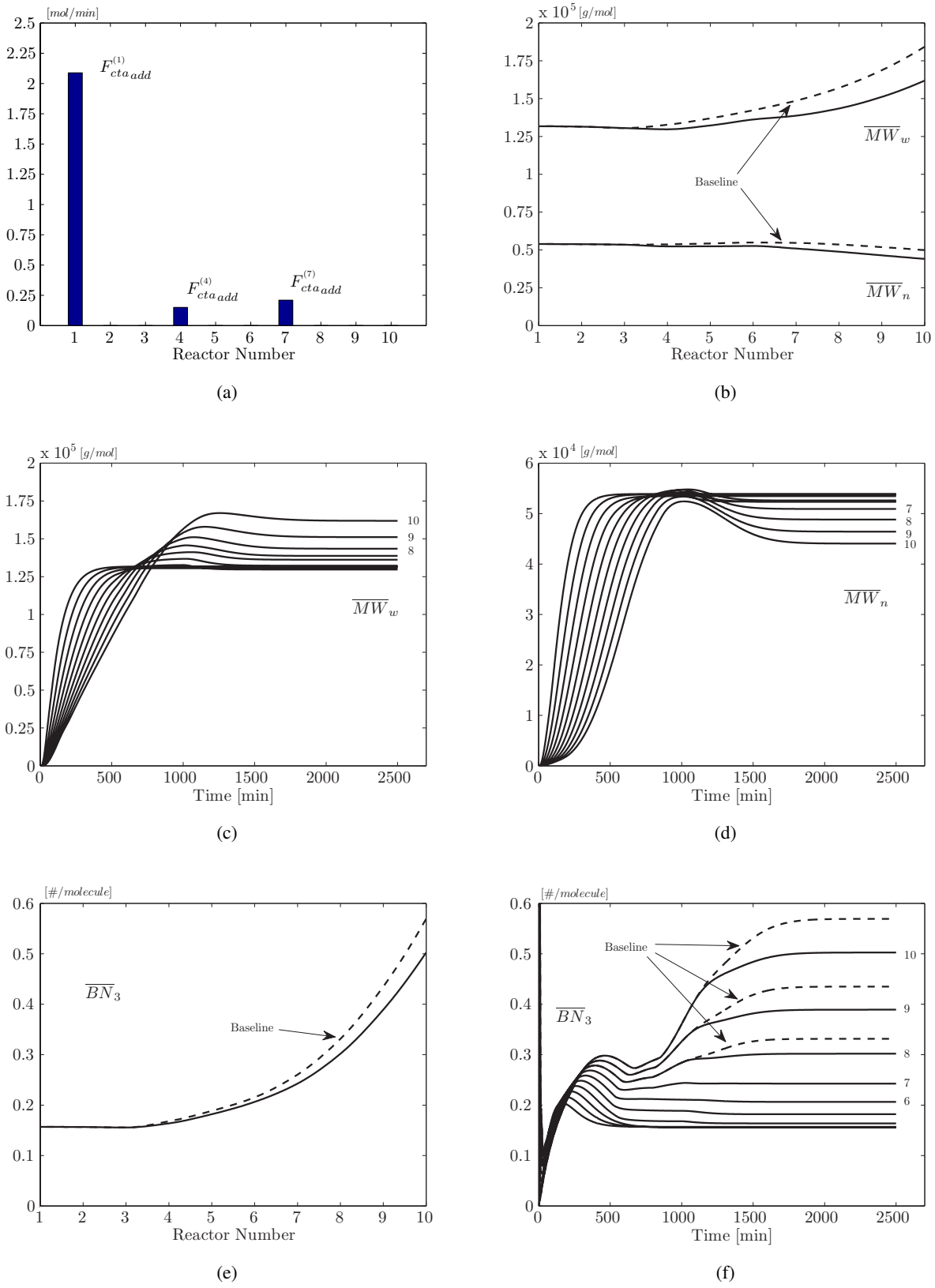

Figure 5.9: Continuous reactor train simulation - molecular weight control

5.2.3 Particle Size Control

Controlling the particle size distribution of the latex is typically of concern when the final product to be used is the latex itself (i.e. adhesives or paints). Though not of direct importance to an NBR system, it is interesting to see how one could influence the particle size distribution within a batch or CSTR reactor. Two approaches are to use a seed latex of a desired size, or to induce successive particle generations through feeding emulsifier to the reactor in semi-batch fashion. In the latter approach, custom particle size distributions (PSD) could be created (e.g. multimodal distributions) which can be used to impart certain properties on the resulting latex. In the case of this model, it suffices to show how the average particle number and size could be influenced by feeding additional emulsifier to the system.

The first simulation trial looks at the effect on particle size in a batch reactor from adding emulsifier (i.e. semi-batch addition) using intermittent pulses. The purpose here is to demonstrate how the particle nucleation period (i.e. stage I) could be extended to create more particles and broaden the size distribution. Figures 5.10a and 5.10b depict the feed profile used and the resulting free-emulsifier area available for particle nucleation. By adding emulsifier in successive pulses early on in the reaction (i.e. < 100 minutes), the particle number can be quickly built up (Figure 5.10c). As a result, the average particle diameter is decreased which reflects the broadening of the size distribution (i.e. lower mean value). In developing feed policies to achieve a desired particle number or size distribution it may be more convenient to first impose a desired profile in A_m and then to determine the required emulsifier feed rate to achieve this profile. This was the approach adopted by Penlidis [136] in developing emulsifier feed rate policies to control the PSD in vinyl acetate emulsion polymerization.

The second trial performed involved applying two successive pulse inputs of emulsifier feed to a continuous reactor. The purpose here was two-fold; first, to show the dynamic response of an input change, and second to inspire potential industrial methodologies for controlling particle size distribution, conversion and polymer production through an optimally designed emulsifier metering program (i.e. MPC applications [3]). Figures 5.11a and 5.11b reveal the effect of applying two 5 minute emulsifier pulses 400 minutes apart. Introducing a large spike in emulsifier concentration creates an abundance of free-emulsifier area which leads to a jump in particle number (i.e. new particle formation) followed by a gradual decrease back to the original steady-state (i.e. the pulse is finished). Applying a second pulse reveals the same behaviour, and looking at the resulting conversion and diameter predictions reveals an oscillating profile. Clearly, this is not a desirable behaviour as this can lead to considerable particle coagulation due to an inadequate stabilization of the particle surface area, and difficult temperature control due to the excessive heat release from new particle generations. A more appropriate emulsifier feed profile would be a step input (or a low feed rate), which would function to bring the particle number to a new steady-state within the continuous reactor and thus promote conversion and broaden the steady-state PSD along the reactor train.

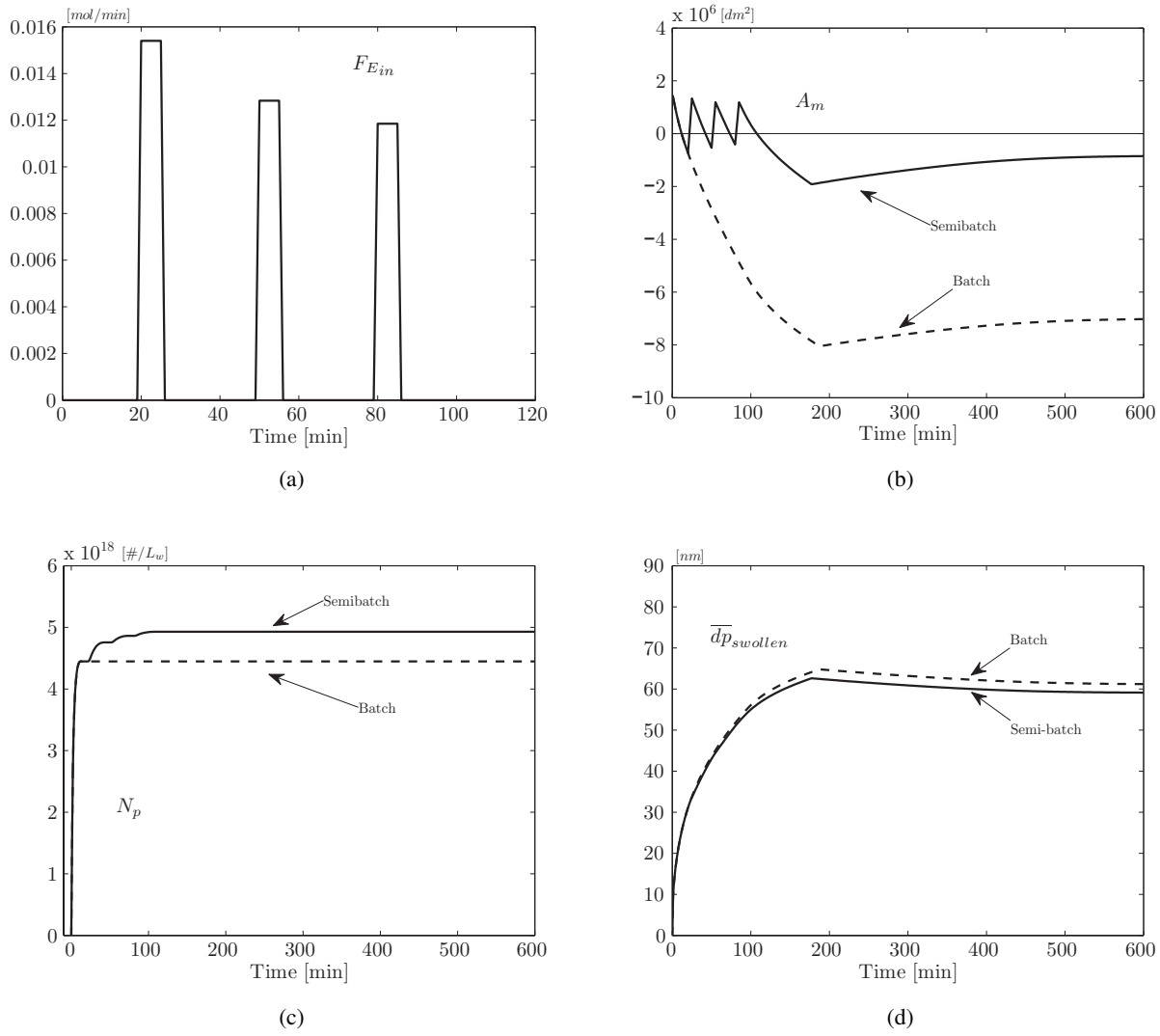

Figure 5.10: Semi-batch reactor simulation - particle size control through emulsifier additions

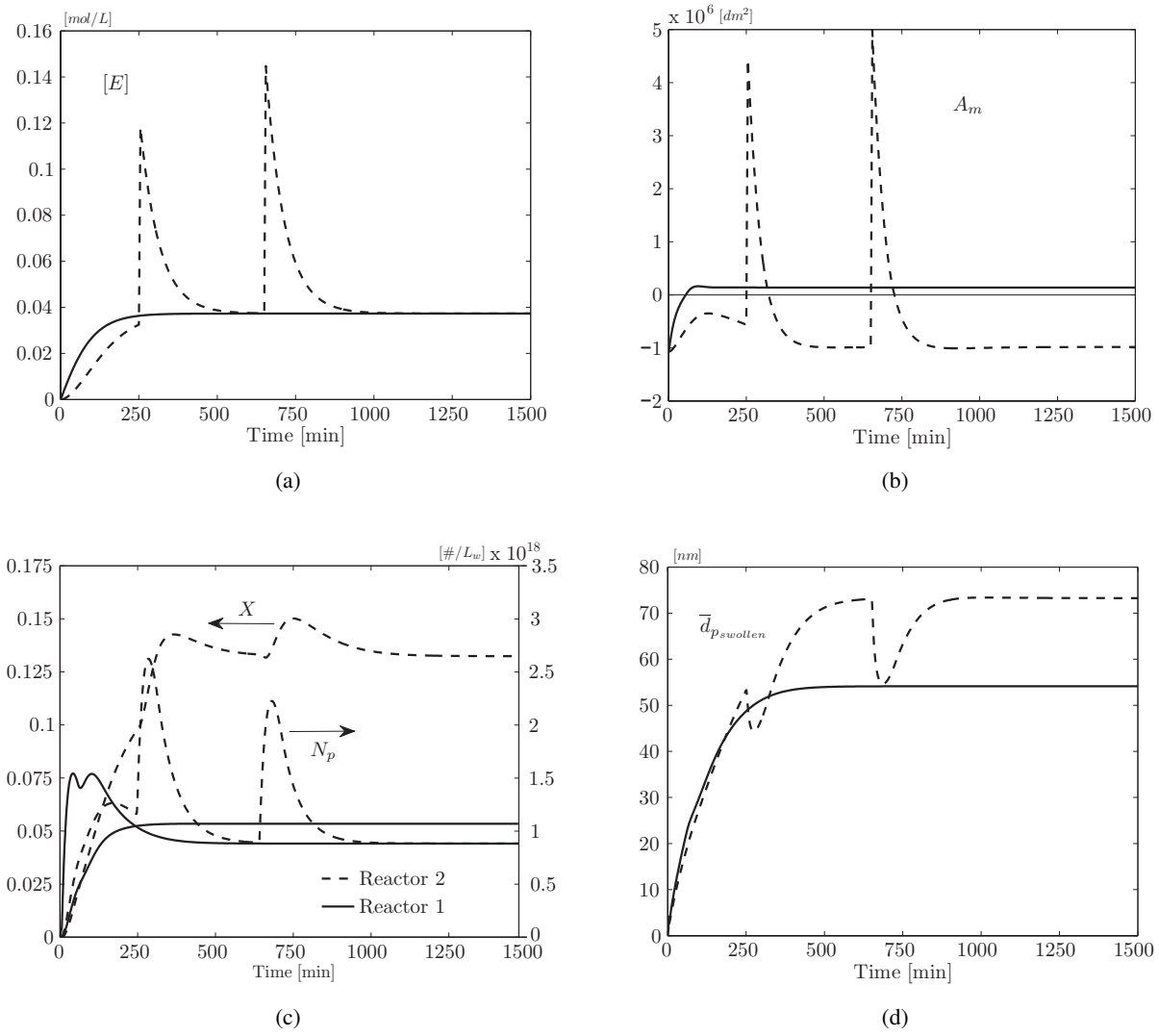

Figure 5.11: CSTR reactor simulation - effect of emulsifier pulse additions

5.3 Reactor Operation Studies for Maximizing Polymer Production

Obtaining the highest possible throughput from a continuous reactor train is a desirable goal for maximizing polymer production and utilizing the full capacity of the process unit operations. If a seed reactor is not used to set the particle number and size, then the first reactor of the train becomes the focal point of the process by acting as the nucleating reactor where the particle number is set. It is well known, and seen from previous simulations shown in this work, that increasing the number of particles nucleated increases the rate of polymerization (i.e. rate of conversion). Thus, in order to increase production it is advisable to maximize the number of particles nucleated in the first reactor, as long as it satisfies particle size (distribution) specs. Other possibilities are to dynamically program a particle formation profile through controlling the emulsifier feed into downstream reactors. However, as previously mentioned, this creates a broadening of the PSD and it may not be desirable for every grade.

Shown in this section is a potential strategy to maximize polymer production, whereby an optimal monomer feed split-ratio, reactor residence time, and particle number can be determined. For demonstration purposes, an arbitrary sub-optimal solution is presented which portrays the general idea of feeding monomer to the first few reactors of the train in order to minimize the inert droplet phase and to maximize polymer production.

5.3.1 Maximizing Particle Nucleation in the 1st Reactor

The first step to increasing polymer production is to increase the number of particles nucleated. Since nucleation typically only occurs in the first reactor of the train, this would result in an appropriate feed of ingredients to the first reactor so that N_p increases. Simulations were performed by specifying a total volumetric inflow and varying the split ratio between the first and downstream reactors. The composition of each monomer is maintained according to the recipe, while the flow of other ingredients is increased in proportion to the recipe so to maintain the total specified volumetric inflow and thus the residence time in the first reactor. Three different residence times were considered (50, 55 and 60 minutes) and the monomer was split between the first and downstream reactors using ratios between 100/0 and 60/40 (i.e. 60% in the first reactor and 40% distributed between downstream reactors). Form Figure 5.12a, profiles for the particle number versus the total volumetric flow of monomer can be seen, which reveal that the flow of monomer can be reduced from the normal steady-state while maintaining the same steady-state particle number. Furthermore, the profiles reveal that the particle number can be increased using a split ratio between 72/28 and 62/38, irrespective of the residence time. The realization that particle number increases by decreasing the monomer flow results from introducing more emulsifier and initiator (among other recipe ingredients) into the reactor to maintain the desired residence time. When selecting a split ratio to increase the particle number it is also important to look at the influence on other latex properties, in particular cumulative copolymer composition. Figure 5.12b, depicts a similar plot to Figure 5.12a for copolymer composition. An interesting observation is that the same range of ratios used to increase particle number also decreases copolymer composition, which is of course undesirable. Thus, a compromise must be made between increasing particle number in the first

reactor and maintaining a desired composition. The strict adherence to a desired composition within the first reactor of a possible 8 or 10 in the train, is often of little significance if the composition is adequately maintained in subsequent reactors in order to achieve the desired final composition in the final reactor. This being said, composition can be sacrificed for a higher N_p, if AN is properly fed (i.e. optimally) into subsequent reactors to achieve a desired final composition. These ideas are further explored in the following section.

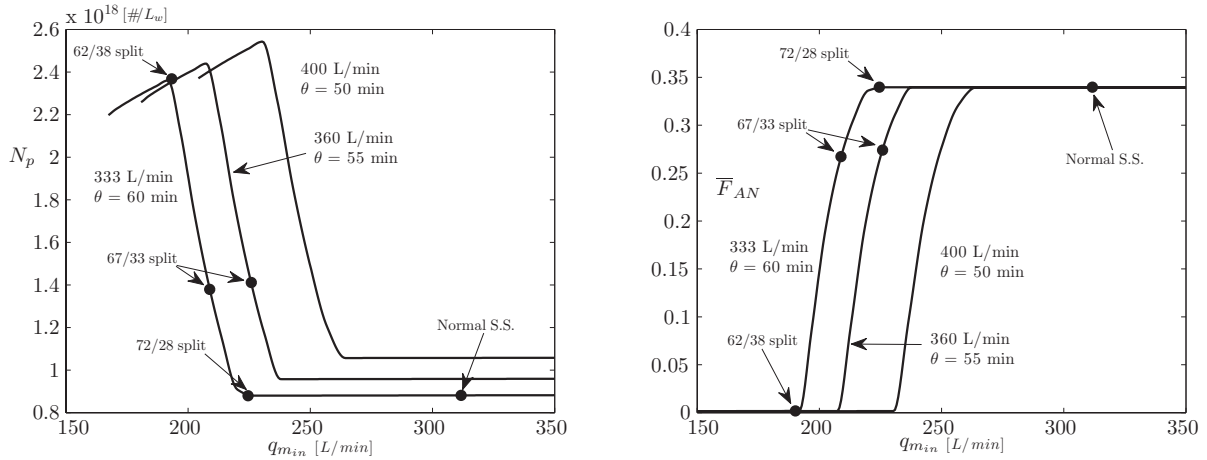

Figure 5.12: Continuous reactor train simulation - maximizing particle nucleation in the 1^{st} reactor

5.3.2 Splitting Feed Streams Between 1st & Downstream Reactors

Using the ideas of selecting an appropriate split ratio for the first reactor presented in the previous section, this section looks at the split ratio effect and subsequent re-entry of the monomer diverted to downstream reactors on the entire train. The purpose of splitting the monomer feed has two main benefits; as previously shown, the first is to increase N_p, while the second not so obvious goal is to reduce the volume occupied by the inert monomer droplet phase and to increase the monomer uptake within the polymer particles within the first few reactors of the train. The central goal here is to increase the rate of polymer production.

Performing simulations using a residence time of 60 minutes, a split ratio of 72/28 and evenly distributing the diverted 28% into the 2^{nd}, 3^{rd} and 4^{th} reactors revealed a decrease in polymer production from the baseline simulations indicated in Figure 5.12 as the normal steady-state. Furthermore, simply increasing the amount of diverted monomer to downstream reactors (i.e. point 67/33 at $\theta = 60$ min) did not increase polymer production, regardless of the amount of the diverted monomer fed into the 2^{nd}, 3^{rd} and 4^{th} reactors. It was found that in order to increase production a combination of increased particle number, additional AN to reduce composition drift, an appropriate monomer split ratio (i.e. 67% of total recipe monomer fed to the 1^{st} reactor), and optimally selected residence time (i.e. optimal in the sense of providing maximum particle nucleation) was required. For example, as seen in Figure 5.12a, operating the 1_{st} reactor of the train using a

monomer inflow of 230 L/min (i.e. monomer split ratio of 67/33) and total inflow of 360 L/min (i.e. $\theta = 55$ min) one is able to increase particle nucleation rate and reduce the volume of the monomer droplet phase compared to operating at the normal steady-state.

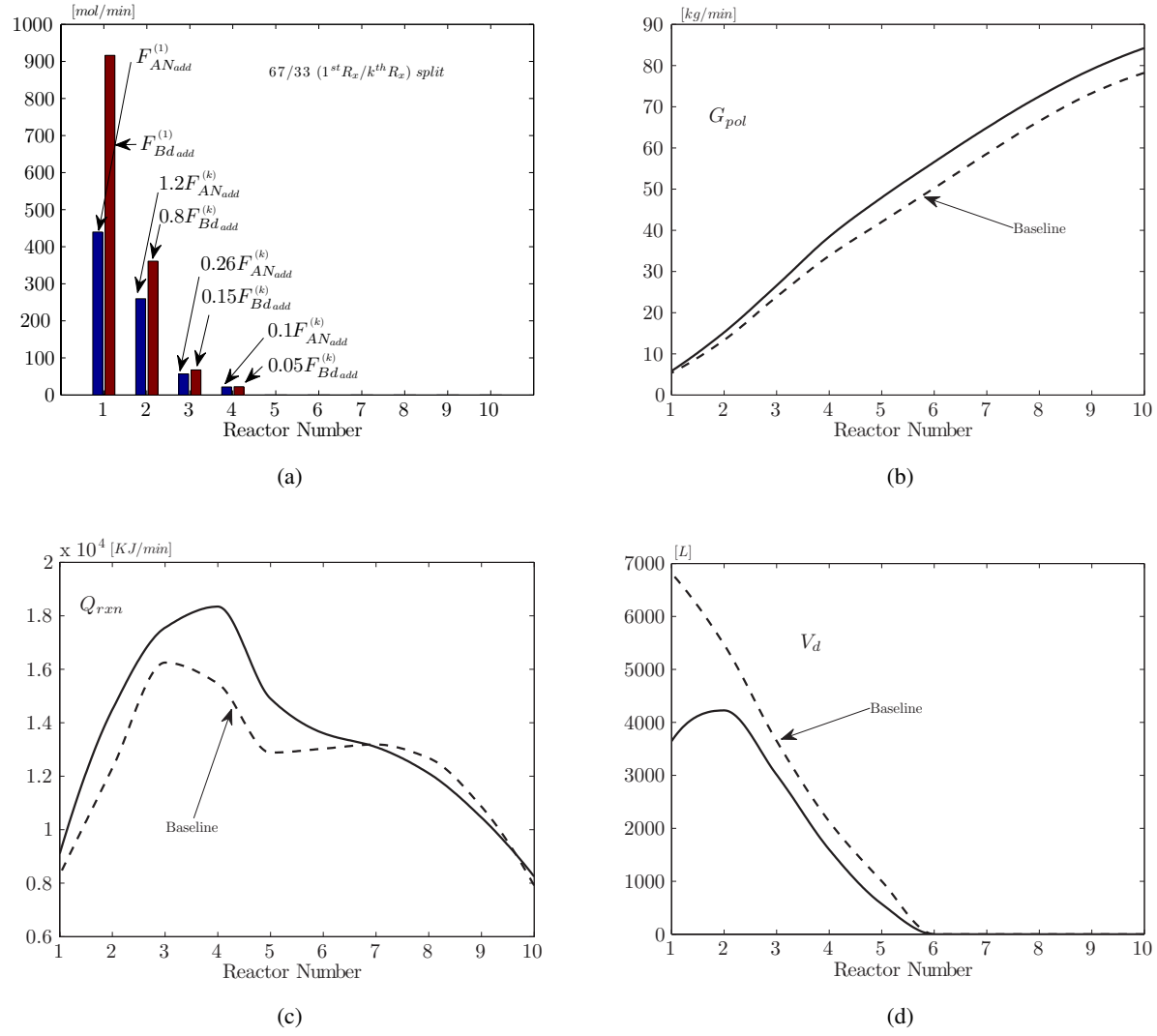

Figure 5.13: Continuous reactor train simulation - monomer feed policies for maximizing polymer production

Figures 5.13 and 5.14 reveal steady-state latex properties using a split ratio of 67/33, a residence time of 55 minutes in the 1^{st} reactor and a feed policy of diverted monomer according to Figure 5.13a. Note that this policy was set arbitrarily using 80%, 15% and 5% of the diverted monomer into the 2^{nd}, 3^{rd} and 4^{th} reactors. Furthermore, additional AN was introduced into the same reactors according to the percentages of 50%, 75% and 100% on top of the base feed rates. Note that diverting monomer into downstream reactors clearly decreases the residence time (e.g. θ in the 10^{th} reactor was found to be slightly higher than 50 minutes). From Figure 5.13b it can be seen that, according to this operating policy, the rate of polymer

production is increased by approximately 6 kg/min from the baseline simulation. Also apparent from Figure 5.13d is that the inert droplet phase was reduced and in fact disappeared 400 minutes sooner in the 6^{th} reactor than the baseline simulation. The cost of reducing the inert droplet phase is apparent from Figure 5.13c, where the heat duty within the first few reactors is increased. This places additional strain on the reactor cooling system and must be accounted for in the design of the heat exchanger. The effect of the operating strategy on conversion, particle number, copolymer composition and molecular weight can be seen in Figures 5.14a-d. Conversion is slightly decreased from the baseline simulation since more monomer was added to the system. Particle number is increased for the reasons previously stated. Composition is initially lower than the baseline simulation and remains off target of the desired 34% within each reactor of the train, which signifies that additional AN is required. The number- and weight-average molecular weights were significantly lower than the baseline simulation, which was due to a higher initial flow of CTA into the first reactor of the train. The initial flow of CTA was increased in order to maintain the residence time (i.e. CTA, initiator, emulsifier, and water were all increased in proportion to fill the void from diverting monomer flow from the 1^{st} reactor); however, in hindsight such a policy (i.e. increasing CTA flow) may be undesirable and perhaps keeping the CTA in proportion to the monomer being fed to the first reactor and feeding into subsequent reactors as needed would be a better policy. At this point, such a policy has not been investigated, and would be related to the molecular weight control policies previously discussed in section 5.2.2.

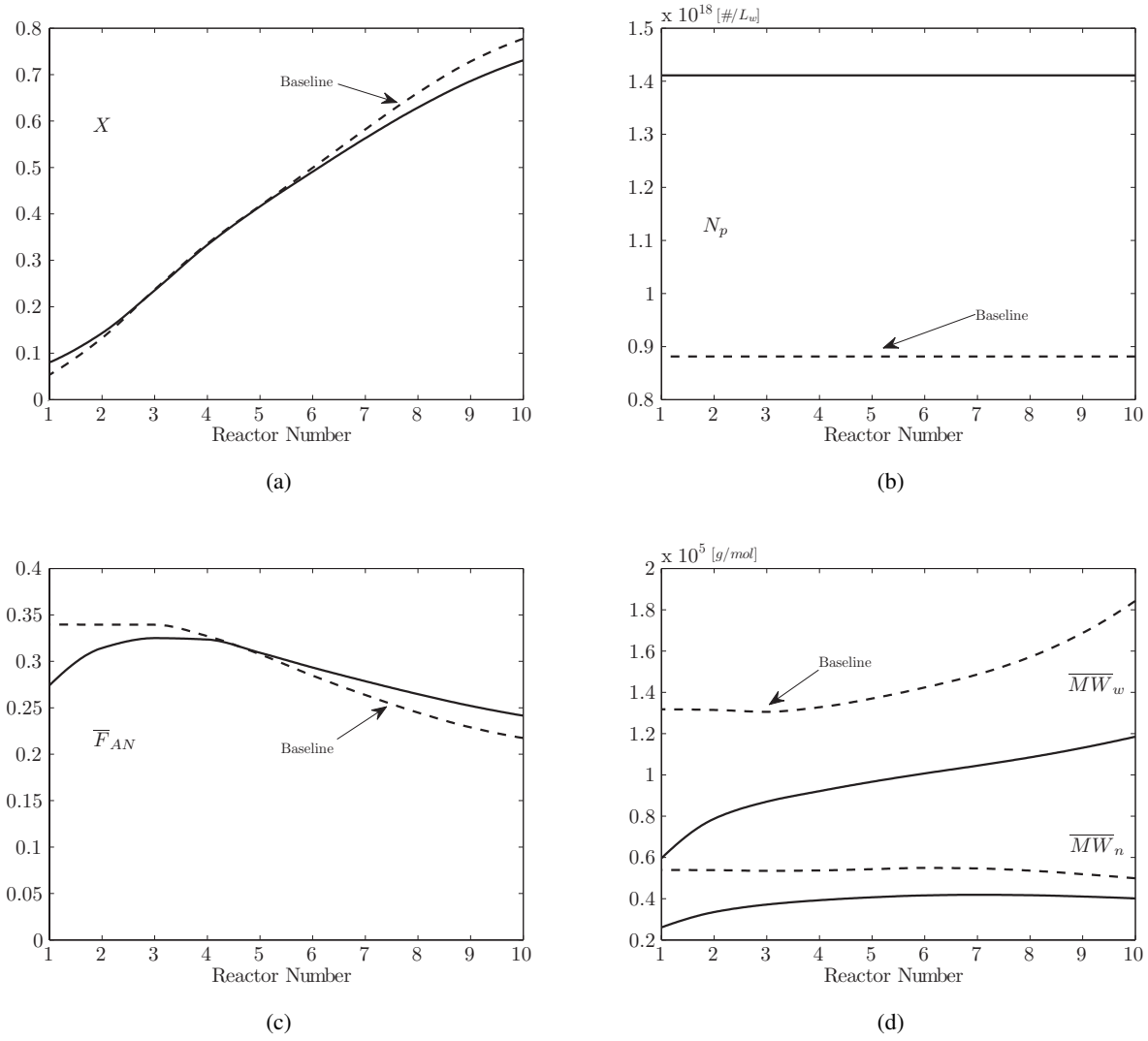

Figure 5.14: Continuous reactor train simulation - monomer feed policies for maximizing polymer production - resulting latex properties

In closing, the example shown here has revealed that the rate of polymer production can be increased without increasing the reactor train capacity (i.e. adding additional reactors) through increasing particle nucleation in the 1^{st} reactor, minimizing the amount of inert monomer being passed along to each reactor in the train (i.e. operating in stage III of emulsion polymerization without droplets present as early in the train as possible), and adding additional AN on top of the diverted monomer streams. In fact without the addition of AN, polymer productivity was not increased, and an extension to what is shown here would be to maintain the composition constant at a desired value in each reactor and note the increase in productivity. As shown in section 5.2.1, such a policy would certainly increase productivity even more than what was shown here using a sub-optimal example (i.e. composition drift was not controlled).

5.4 Concluding Remarks

This chapter demonstrated the use of the model to track latex properties over time in a train of continuous reactors. Comparisons were made to an NBR model found within the literature and, from the perspective of simulation, revealed similar results. The influence of impurities within a reactor train was found to be quite detrimental to the overall polymer production rate which forced an immediate decrease of the steady-state conversion and particle number, while the molecular properties were only effected in later reactors of the train.

Several case studies on the influence of monomer, CTA, and emulsifier additions on copolymer composition, molecular weight, chain branching, and particle nucleation were demonstrated and revealed the potential for the application of optimal feed policies to control or impose a desired response in the final polymer properties. If the intended goal is to control copolymer composition through the addition of the more reactive monomer (i.e. AN), then molecular weight must be simultaneously controlled though CTA additions. On the other hand if the goal is to increase polymer production, first particle nucleation should be maximized in the first reactor through an appropriate monomer feed split ratio followed by additions of AN and CTA to prevent composition drift and to maintain a desired molecular weight. If the goal is to increase or broaden the PSD, then emulsifier feed policies should be devised so not to cause rapid pulses in the behaviour of the free-emulsifier area which in turn would create oscillations in final latex properties (i.e. a steady-state would never be reached).

Chapter 6

Concluding Remarks, Recommendations & Future Work

This chapter provides some concluding remarks with respect to the model development and validity compared to reported industrial data. The general simulation trends are reiterated, as well as suggestions to improve copolymer composition and molecular weight control. In addition, a number of recommendations are made to improve and fine-tune the proposed model. Finally, some comments are made on future model applications.

6.1 General Summary/Contributions

A dynamic model capable of simulating batch, semi-batch, continuous, and trains of continuous reactors has been developed for the emulsion copolymerization of acrylonitrile/butadiene. The model is defined in terms of ordinary differential equations that track the moles, number of particles, volume, temperature, and molecular weight moments over time. Both homogeneous and micellar particle nucleation mechanisms are considered, which are based on a collision theory approach to radical capture. An empirical expression is used for diffusion-controlled radical termination, as opposed to free-volume theory. Model outputs of interest are conversion, cumulative copolymer composition (i.e. bound AN), average particle diameter, number- and weight-average molecular weight, and tri- and tetra-functional branch frequencies. A monodisperse particle size distribution has been assumed.

Industrial NBR and butadiene emulsion batch data were compared to model simulations and revealed good results considering that all of the parameters where taken from the literature. Monomer and water soluble impurities were found to have a profound impact on model predictions, and were a necessary aspect to model in order to obtain a good fit to industrial data. Baseline model simulations revealed that composition, molecular weight, and chain branching need to be controlled either within batch or reactor train operation. For a batch reactor, the composition can be controlled through semi-batch additions of AN, either through

a number of pulses or a step flow into the reactor. Similarly, for a continuous reactor train, several AN additions along the train are necessary to maintain a fairly constant composition. In order to control molecule weight and chain branching, CTA additions are necessary along the reactor train. Simulation of the model revealed that adequate composition and molecular weight control can be obtained by a constant side flow AN and CTA in the fourth and seventh reactors.

The work presented here has attempted to provide a detailed mechanistic mathematical model that can be used to model industrial rubber production in batch, semi-batch, and continuous reactors. The object was to provide further insight on the modelling aspect as opposed to the numerous potential model uses (i.e. control policies, controller design (IMC, MPC), etc.), on top of what has previously been reported for SBR and NBR systems [16, 33, 61, 146, 171].

6.2 Concluding Remarks

The following remarks can be stated with respect to the work performed and the accomplishments made during this thesis work.

- A model to predict the evolution of latex properties for NBR (i.e. conversion, polymer production rate, average particle size, average molecular weight and branching frequencies) in batch, semi-batch, and continuous reactors has been developed and shown to compare well with process data for a batch reactor published in the literature [171].
- Only limited NBR data was available in the literature to test the model against. As a result the model was reduced to each monomer and tested for the homopolymer case. For the case of Bd, the model was able to adequately track two different sets of literature data [133, 184].
- Simulation studies on a train of continuous reactors proved to be comparable to those preformed by Minari et al. [105]. The copolymer composition was able to be adequately controlled (i.e. drift prevention) by adding AN into select downstream reactors. For example, using the baseline recipe, adding AN to reactors 4 and 7 proved to be adequate for maintaining a relatively constant composition. The effect of adding CTA along the reactor train revealed that the molecular properties could be influenced without affecting other properties (i.e. conversion, rate, particle number, etc.).
- A number of influential parameters were found to affect model predictions. Model outputs were found to be quite sensitive to particle nucleation parameters ε and k_{cp} when $\varepsilon < 10$ and $k_{cp} < 0.05$, and these parameters may require careful adjustment when changing the level of emulsifier or initiator in the recipe.
- It is believed that the fundamental rate constants for propagation and termination are in good order. However, effective implementation of the model to commercial processes will require extensive parameter estimation, in particular, species partition coefficients, transfer to CTA and impurity rate constants.

In closing, the objective of this thesis work was to present a detailed mechanistic mathematical model that could be used as a precursor for an industrial process implementation to predict average latex properties of nitrile-butadiene rubber. It is believed that a base model has been adequately developed and demonstrated and the next stage of the project is to move forward with more rigorous model testing and parameter estimation studies using process/pilot plant data.

6.3 Recommendations

From the perspective of model development and the techniques used to capture various physicochemical phenomena, the following recommendations for further explorations are offered.

- The model developed herein uses a monodisperse approximation (i.e. all particles are the same size at any given time "t"), thus an extension of the model would be to incorporate methods for capturing particle size polydispersity, which would be present due to different particle nucleation times predominantly seen over long periods of nucleation. There is a substantial amount of literature discussing various techniques to model the particle size distribution (e.g. full solution of population balances, age-distribution analysis, or residence-time analogy); however, a first approach for an NBR system might be to adopt an age-distribution analysis previously used for SBR by Broadhead et al. [16] and Gugliotta et al. [61]. Further details on this approach, among others, can be found in Penlidis [136].
- Alternative methods to capture diffusion-controlled termination should be incorporated into the model and compared to the empirical approach currently being used. For example, Broadhead [15] uses free-volume theory (FVT) for an SBR system. Although FVT contains more parameters, those used by Broadhead for SBR could initially be employed to test the NBR model.
- Though diffusion-controlled propagation is not suspected to have a significant influence in the particle phase for an NBR system (i.e. low to medium solids content and $T > T_{glass}$), it may be worth to explore semi-empirical or free-volume expressions for k_p [53, 68] especially for hot rubber production were the solid content is typically much higher than in the cold rubber process.
- The approach adopted in this work for particle nucleation was based on collision theory. An alternative method, that may be useful for an NBR system, is a diffusion-based approach to radical capture. Techniques on this method have been shown by Gao and Penlidis [53] as well as in some recent publications by the Gilbert group [2, 156, 191].
- For an industrial model, species partitioning using constant partition coefficients is probably the most computationally efficient approach to establish different phase concentrations and perhaps is the only approach for determining the concentration of lesser species such as initiator, CTA, impurities, etc. However, an interesting study would be to incorporate the thermodynamic approach for monomer partitioning, previously discussed in Chapter 3. Such an approach has been implemented for an SBR system with good results by Gugliotta et al. [61], however, the draw back is the number of additional parameters introduced into the model, which for an NBR system are not readily available in the

literature compared to other more common systems (i.e. styrene-butyl acrylate, styrene-methacrylate [60]). Recent studies have been published on an emulsion acrylonitrile-styrene system that report many of the necessary parameters [92, 132], while for butadiene some of these parameters can be found in the polymer handbook [14].

- In order to test and provide further comparison to experimental data, the model was reduced to simulate emulsion Bd homopolymerization and proved to be quite successful at tracking conversion and particle size. When a similar study was performed for AN homopolymerization and compared to the data of Tazawa et al. [159], it was realized that conversion could only be partially tracked as a limiting value of 65% was encountered, while according to the experimental data of Tazawa conversion can proceed up to 90% before reaching a limiting value. The reason behind this observed discrepancy is due the how the model handles the partitioning of AN between the aqueous and particle phase. When the limiting value of 65% was reached AN was depleted from particle and droplet phases, while it remained in abundance in the aqueous phase around its solubility limit. Simply forcing more AN back into the particle phase (i.e. empirically) did not improve the fit of the model to the data. It is recommended that further investigation be given to improve the model for predicting emulsion AN homopolymerization. Perhaps employing better values for the partition coefficients or the thermodynamic partitioning approach may provide an improved model prediction.

- Besides what has previously been shown by Dube et al. [33] and the limited studies on select parameters shown herein, an in-depth multiresponse parameter sensitivity study has not yet been performed. Such a study will be invaluable when deciding on how to effectively sample process data to achieve reliable parameter estimates (i.e. partition coefficients, reactivity ratios). It is recommended that a sensitivity study be carried out, and a good starting point is the proposed methodology of Polic et al. [141]. The sensitivity approach used by Polic looks at gradient based responses of the process outputs to changes in select parameters. This can be quite computationally intensive and the software "CVODES" within the SUNDIALS package is recommended. An another informative study is shown in Flores et al. [43].

- An interesting extension to the work of Minari et al. [104, 105], who demonstrated that in order to achieve desired composition and molecular properties, AN and CTA must be fed into virtually each reactor of train, would be to formulate an optimization problem that restricts the number of allowable reactors available to receive additional ingredient feed streams. This would constitute a more realistic scenario since only two or three addition streams are typically used in practice. As well, restricting AN and CTA additions to the same feed points would make for a more practical solution since industrial operations usually premix monomer and CTA before feeding to the reactor train.

- A final recommendation is on the model development platform. In this work all coding was performed in the MATLAB programming environment using the SUNDIALS solver package. The choice of MATLAB allowed for a fast model development time compared to conventional languages such as C++, visual basic or FORTRAN. However, a typical downside to MATLAB is the lengthy computational time required to solve large system models and the lack of prepackaged 'robust' optimization

solvers to handle dynamic optimization formulations. If optimization and control are to be easily studied with minimal coding effort, it is recommended that the model be redeveloped using gPROMS which is better suited to handle large complex system modelling, optimization, control, and parameter estimation problems. Recent literature that used a combination of gPROMS and SIMULINK for real-time emulsion polymerization control (i.e. on-line control) has proved to be a very practical approach to quickly implementing a model-based controller on an industrial platform (i.e. in conjunction with a DCS) [3], and should be considered for future model development and control studies.

6.4 Future Work

Optimal reactor operation and control strategies are essential for process improvement (i.e. improved product reproducibility, waste minimization, and safety). Numerous articles are available on optimal semi-continuous and continuous strategies for achieving desired latex properties [6, 26, 50, 104, 170, 172] and efficient process control methodologies [27, 84, 86, 114, 115, 182]. With a sound model in place these strategies can be explored and applied in useful ways. The following list highlights some of these applications and points to various literature sources that provide further insight.

- A relevant extension of this thesis work is to demonstrate optimal policies for controlling latex properties, as previously described in Chapter 5 through sub-optimal model demonstrations and in the work of Minari et al. [104, 105], who explore optimal reactor train policies for composition and molecular weight control.
- A second area of interest is to demonstrate and implement practical on-line reactor control strategies through a model-based controller. Limited literature is available on NBR reactor control (i.e. closed-loop control) and the goal here would be to apply available methods to an NBR system that have been previously demonstrated on other systems.
- In addition to on-line control methods, off-line control scenarios are also of interest in order to develop efficient strategies for minimizing process upsets during polymer grade transition [103, 106, 170], and to present possible control and design options for selecting an optimal control structure to ease the grade transition in a reactor train [7].

Immediate future considerations are to update the model to allow for optimal semi-continuous and continuous operating policies to be studied.

References

[1] J. A. Abusleme and E. Giannetti. Emulsion polymerization: Improved methods for solving the smith-ewart equations in the unsteady state. *Macromolecules*, 24:4281–4285, 1991.

[2] B. Alhamad, J. A. Romagnoli, and V. G. Gomes. Advanced modelling and optimal operating strategy in emulsion copolymerization: Application to styrene/mma system. *Chemical Engineering Science*, 60(10):2795–2813, 2005.

[3] B. Alhamad, J. A. Romagnoli, and V. G. Gomes. On-line multi-variable predictive control of molar mass and particle size distributions in free-radical emulsion copolymerization. *Chemical Engineering Science*, 60:6596–6606, 2005.

[4] H. M. Andersen and Jr S. I. Proctor. Redox kinetics of peroxydisulfate-iron-sulfoxylate system. *Journal of Polymer Science: Part A: General Papers*, 3(6):2343–2366, 1965.

[5] P. D. Armitage, J. C. DeLaCal, and J. M. Asua. Improved methods for solving monomer partitioning in emulsion copolymer systems. *Journal of Applied Polymer Science*, 51(12):1985–1990, 1994.

[6] G. Arzamendi and J. M. Asua. Monomer addition policies for copolymer composition control in semicontinuous emulsion copolymerization. *Journal of Applied Polymer Science*, 38(11):2019–2036, 1989.

[7] M. Asteasuain, A. Bandoni, C. Sarmoria, and A. Brandolin. Simultaneuous process and control system design for grade transition in styrene polymerization. *Chemical Engineering Science*, 61: 3362–3378, 2006.

[8] J. M. Asua, E. D. Sudol, and M. S. El-Aasser. Radical desorption in emulsion polymerization. *Journal of Polymer Science: Part A: Polymer Chemistry*, 27:3903–3913, 1989.

[9] M. J. Ballard, R. G. Gilbert, and D. H. Napper. Improved methods for solving the smith-ewart equations in the steady state. *Journal of Polymer Science: Polymer Letters Edition*, 19:533–537, 1981.

[10] M. J. Barandiaran, J. C. del la Cal, and J. M. Asua. Emulsion polymerization. In J. M. Asua, editor, *Polymer Reation Engineering*, chapter 6, pages 233–272. Blackwell Publishing, 2007.

[11] B. Barclay, A. Penlidis, and J. Gao. Modelling and simulation of complex aspects of multicomponent emulsion polymerization. *Polymer Reaction Engineering*, 11(4):737–814, 2003.

[12] L. Boguslavsky, S. Baruch, and S. Margel. Synthesis and characterization of polyacrylonitrile nanoparticles by dispersion/emulsion polymerization process. *Journal of Colloid and Interface Science*, 289:71–85, 2005.

[13] F. A. Bovey, I. M. Kolthoff, A. I. Medalia, and E. J. Meehan. *Emulsion Polymerization*. Interscience Publishers, 1955.

[14] J. Brandrup, E. H. Immergut, E. A. Grulke, A. Abe, and D. R. Bloch, editors. *Polymer Handbook*. John Wiley & Sons, 4th edition edition, 1999.

[15] T. O. Broadhead. Dynamic modelling of the emulsion copolymerization of styrene/butadiene. Master's thesis, McMaster University, Department of Chemical Engineering, 1984.

[16] T. O. Broadhead, A. E. Hamielec, and J. F. MacGregor. Dynamic modelling of the batch, semi-batch and continuous production of styrene/butadiene copolymers by emulsion polymerization. *Die Makromolekulare Chemie*, 10(S19851):105–128, 1985.

[17] G. M. Burnett, G. G. Cameron, and P. L. Thorat. Copolymerization of styrene and butadiene in emulsion. i. composition of the latex particles. *Journal of Polymer Science: Part A-1*, 8:3235–3442, 1970.

[18] G. M. Burnett, G. G. Cameron, and P. L. Thorat. Copolymerization of styrene and butadiene in emulsion. 11. relative rates of crosslinking and propagation. *Journal of Polymer Science: Part A-1*, 8:3443–3453, 1970.

[19] G. M. Burnett, G. G. Cameron, and P. L. Thorat. Copolymerization of styrene and butadiene in emulsion. 111. crosslinking studies by partial conversion properties. *Journal of Polymer Science: Part A-1*, 8:3455–3460, 1970.

[20] E. Casella, O. Araujo, and R. Giudici. Mathematical modeling of batch emulsion copolymerization processes. *Polymer Reaction Engineering*, 11(4):869–910, 2003.

[21] S. A. Chen and H. W. Wu. Emulsion polymerization: Theory of particle size distribution in copolymerization system. *Journal of Polymer Science Part A: Polymer Chemistry*, 26(6):1487–1506, 1988.

[22] F. S. Dainton and R. S. Eaton. The polymerization of acrylonitrile in aqueous solution. part III. the ferric ion photosensitized reaction at 15, 25, 30, and $50^o c$. *Journal of Polymer Science*, 39(135): 313–320, 1959.

[23] F. S. Dainton and D. G. L. James. The polymerization of acrylonitrile in aqueous solution. part II. the reaction photosensitized by Fe^{3+}, $Fe^{3+}OH^-$, Fe^{2+}, and I^- ions. *Journal of Polymer Science*, 39 (135):299–312, 1959.

[24] F. S. Dainton and P. H. Seaman. The polymerization of acrylonitrile in aqueous solution. part I. the reaction catalyzed by fenton's reagent at $25^o c$. *Journal of Polymer Science*, 39(135):279–297, 1959.

[25] F. S. Dainton, P. H. Seaman, D. G. L. James, and R. S. Eaton. The polymerization of acrylonitrile in aqueous solution. *Journal of Polymer Science*, 34(127):209–228, 1959.

[26] C.M. daSilva and E.C. Biscaia. Multi-objective dynamic optimization of semi-batch polymerization processes. *Macromolecular Symposia*, 206:291–306, 2004.

[27] I. S. De Buruaga, P. D. Armitage, J. R. Leiza, and J. M. Asua. Nonlinear control for maximum production rate of latexes of well-defined polymer composition. *Industrial & Engineering Chemistry Research*, 36(10):4243–4254, 1997.

[28] S. Deibert and F. Bandermann. Rate coefficients of the free-radical polymerization of 1,3-butadiene. *Die Makromolekulare Chemie*, 194:3287–3299, 1993.

[29] S. Deibert, F. Bandermann, J. Schweer, and J. Sarnecki. Propagation rate coefficient of free-radical polymerization of 1,3-butadiene. *Die Makromolekulare Chemie, Rapid Communications*, 13(7):351–355, 1992.

[30] M. M. Denn. *Process Modeling*. Pitman Publishing, 1986.

[31] E. P. Dougherty. The scope dynamic model for emulsion polymerization i. theory. *Journal of Applied Polymer Science*, 32:3051–3078, 1986.

[32] Eugene P. Dougherty. The scope dynamic model for emulsion polymerization ii. comparison with experiment and applications. *Journal of Applied Polymer Science*, 32:3079–3095, 1986.

[33] M. A. Dube, A. Penlidis, R. K. Mutha, and W. R. Cluett. Mathematical modeling of emulsion copolymerization of acrylonitrile/butadiene. *Industrial & Engineering Chemistry Research*, 35(12):4434–4448, 1996.

[34] M. A. Dube, J. B. P. Soares, A. Penlidis, and A. E. Hamielec. Mathematical modeling of multicomponent chain-growth polymerizations in batch, semibatch, and continuous reactors: A review. *Industrial & Engineering Chemistry Research*, 36(4):966–1015, 1997.

[35] A. S. Dunn. Harkins, Smith-Ewart and related theories. In P. A. Lovell and M. S. El-Aasser, editors, *Emulsion Polymerization and Emulsion Polymers*, chapter 4. John Wiley & Sons, 1997.

[36] E. E. Elbing, S. J. McCarty, B. A. W. Coller, I. R. Wilson, and D. F. Sangster. Acrylonitrile polymerization from aqueous solution. the role of particle area. *Journal of the Chemical Society. Faraday transactions I*, 83:657–663, 1987.

[37] E. E. Elbing, W. K. Tan, C. J. Lyons, B. A. W. Coller, and I. R. Wilson. Acrylonitrile polymerization from aqueous solution. the role of surfactants. *Journal of the Chemical Society. Faraday transactions I*, 83:645–655, 1987.

[38] W. H. Embree, J. M. Mitchell, and H. L. Williams. Compositional heterogeneity of butadiene-acrylonitrile copolymers prepared in emulsion at $5^o c$. *Canadian Journal of Chemistry*, 29:253–269, 1951.

[39] P. J. Feeny, D. H. Napper, and R. G. Gilbert. Coagulative nucleation and particle size distributions in emulsion polymerization. *Macromolecules*, 17:2520–2529, 1984.

[40] A. P. Filho, O. Araujo, R. Giudici, and C. Sayer. Batch and semicontinuous styreneŰbutadiene emulsion copolymerization reactions. *Macromolecular Symposia*, 243(1):114–122, 2006.

[41] R. M. Fitch. Latex particle nucleation and growth. In D. R. Bassett, editor, *Emulsion Polymers and Emulsion Polymerization*, 165, chapter 1, pages 1–29. American Chemical Society, 1981.

[42] R. M. Fitch and C. Tsai. Polymer colloids: Particle formation in non-micellar systems. *Polymer Letters*, 8:703–710, 1970.

[43] A. Flores, E. Saldivar, and R. Guerrero. Dynamic modelling, nonlinear parameter fitting and sensitivity analysis of a living free-radical polymerization reactor. In S. P. Asprey and S. Maccietto, editors, *Dynamic Model Development: Methods, Theory and Applications*, volume 16 of *Computer-Aided Chemical Engineering*, pages 21–39. Elsevier, 2003.

[44] K. Fontenot and F. J. Schork. Simulations of mini/macro emulsion polymerizations i. development of the model. *Polymer Reaction Engineering*, 1(1):75–108, 1992.

[45] J. Forcada and J. M. Asua. Modeling of unseeded emulsion copolymerization of styrene and methyl methacrylate. *Journal of Polymer Science, Part A: Polymer Chemistry*, 28(5):987–1009, 1990.

[46] J. Forcada and J. M. Asua. Emulsion copolymerization of styrene and methyl methacrylate. ii. molecular weights. *Journal of Polymer Science, Part A: Polymer Chemistry*, 29:1231–1242, 1991.

[47] M. Fortuny, C. Graillat, and T. F. McKenna. A new technique for the experimental measurement of monomer partition coefficients. *Macromolecular Chemisty and Physics*, 205:1309–1319, 2004.

[48] M. Fortuny, C. Graillat, T. F. McKenna, P. H. H. Araujo, and J. C. Pinto. Modeling the nucleation stage during batch emulsion polymerization. *AIChE Journal*, 51(9):2521–2533, 2005.

[49] N. Friis and A. E. Hamielec. Kinetics of vinyl-chloride and vinyl-acetate emulsion polymerization. *Journal of Applied Polymer Science*, 19(1):97–113, 1975.

[50] T. Fujisawa and A. Penlidis. Copolymer composition control policies: Characteristics and applications. *Journal of Macromolecular Science. Part A: Pure and Applied Chemistry*, 45:115–132, 2008.

[51] J. Gao. *Advances in Mathematical Modelling of Multicomponent Free-Radical Polymerizations in Bulk, Solution and Emulsion*. PhD thesis, University of Waterloo, Department of Chemical Engineering, 1999.

[52] J. Gao and A. Penlidis. A comprehensive simulator/database package for bulk/solution free-radical terpolymerizations. *Macromolecular Chemistry and Physics*, 201(11):1176 –1184, 2000.

[53] J. Gao and A. Penlidis. Mathematical modeling and computer simulator/database for emulsion polymerizations. *Progress in Polymer Science*, 27(3):403–535, 2002.

[54] J. Gao and A. Penlidis. A comprehensive simulator/database package for reviewing free-radical homopolymerizations. *Journal of Macromolecular Science-Reviews in Macromolecular Chemistry and Physics*, C36(2):199–404, 1996.

[55] J. Gao and A. Penlidis. A comprehensive simulator database package for reviewing free-radical copolymerizations. *Journal of Macromolecular Science-Reviews in Macromolecular Chemistry and Physics*, C38(4):651–780, 1998.

[56] L. H. Garcia-Rubio, M. G. Lord, J. F. MacGregor, and A. E. Hamielec. Bulk copolymerization of styrene and acrylonitrile: Experimental kinetics and mathematical modelling. *Polymer*, 26(13): 2001–2013, 1985.

[57] E. Giannetti. Comprehensive theory of particle growth in the smith-ewart interval ii of emulsion polymerization systems. *Macromolecules*, 23(22):4748–4759, 1990.

[58] R. G. Gilbert. *Emulsion Polymerization: A Mechanistic Approach*. Academic Press, 1986.

[59] R. G. Gilbert. Modelling rates, particle size distributions and molar mass distributions. In P. A. Lovell and M. S. El-Aasser, editors, *Emulsion Polymerization and Emulsion Polymers*, chapter 5. Jon Wiley & Sons, 1997.

[60] L. M. Gugliotta, G. Arzamendi, and J. M. Asua. Choice of monomer partition model in mathematical modeling of emulsion copolymerization systems. *Journal of Applied Polymer Science*, 55(7):1017–1039, 1995.

[61] L. M. Gugliotta, M. C. Brandolini, J. R. Vega, E. O. Iturralde, J. L. Azum, and G. R. Meira. Dynamic model of a continuous emulsion copolymerization of styrene and butadiene. *Polymer Reaction Engineering*, 3(3):201–233, 1995.

[62] L. M. Gugliotta, J. R. Vega, C. E. Antonione, and G. R. Meira. Emulsion copolymerization of acrylonitrile and butadiene in an industrial batch reactor. estimation of conversion and polymer quality from on-line energy measurements. *Polymer Reaction Engineering*, 7(4):531–552, 1999.

[63] J. Guillot. Kinetics and thermodynamic aspects of emulsion copolymerization. acrylonitrile-styrene copolymerization. *Acta Polymerica*, 32:593–600, 1981.

[64] A. Guyot. Features of emulsion copolymerization of acrylonitrile. In K. H. Reichert and W. Geiseler, editors, *Polymer Reaction Engineering: Influence of Reaction Engineering on Polymer Properties*, pages 287–312. Hanser Publishers, 1983.

[65] A. Guyot, J. Guillot, C. Graillat, and M. F. Llauro. Controlled composition in emulsion copolymerization application to butadiene-acrylonitrile copolymers. *Journal of Macromolecular Science - Chemistry*, A21(6-7):683–699, 1984.

[66] A. E. Hamielec and J. F. MacGregor. Latex reactor principles: Design, operation, and control. In I. Piirma, editor, *Emulsion Polymerization*, chapter 9. Academic Press, 1982.

[67] A. E. Hamielec and J. F. MacGregor. Modelling copolymerizations - control of composition, chain microstructure, molecular weight distribution, long chain branching and crosslinking. In K. H. Reichert and W. Geiseler, editors, *Polymer Reaction Engineering: Influence of Reaction Engineering on Polymer Properties*, pages 22–71. Hanser Publishers, 1983.

[68] A. E. Hamielec, J. F. MacGregor, and A. Penlidis. Multicomponent free-radical polymerization in batch, semibatch and continuous reactors. *Makromolekulare Chemie - Macromolecular Symposia*, 10:521–570, 1987.

[69] F. K. Hansen. Is there life beyond micelles? Mechanisms of latex particle nucleation. In E. S. Daniels, E. D. Sudol, and M. S. El-Aasser, editors, *Polymer Latexes: Preparation Characterization, and Applications*, 492, chapter 2, pages 16–27. American Chemical Society, 1992.

[70] F. K. Hansen and J. Ugelstad. Particle nucleation in emulsion polymerization. i. theory for homogeneous nucleation. *Journal of Polymer Science: Part A: Polymer Chemistry*, 16(8):1953–1979, 1978.

[71] F. K. Hansen and J. Ugelstad. Particle formation mechanisms. In I Piirma, editor, *Emulsion Polymerization*, chapter 2, pages 51–92. Academic Press, 1982.

[72] W. D. Harkins. General theory of mechanism of emulsion polymerization. *American Chemical Society - Journal*, 69(6):1428–1444, 1947.

[73] E. J. Hoffman. Kinetic modelling of emulsion polymerization of styrene and acrylonitrile. Master's thesis, McMaster University, Department of Chemical Engineering, 1984.

[74] W. Hofmann. Nitrile rubber. *Rubber Chemistry and Technology*, 37(2.2):1–252, 1967.

[75] B. P. Huo, J. D. Campbell, A. Penlidis, J. F. MacGregor, and A. E. Hamielec. Effect of impurities of emulsion polymerization: Case II kinetics. *Journal of Applied Polymer Science*, 35(8):2009–2021, 1988.

[76] R. A. Hutchinson and A. Penlidis. Free-radical polymerization: Homogeneous systems. In J. M. Asua, editor, *Polymer Reation Engineering*, chapter 3, pages 118–174. Blackwell Publishing, 2007.

[77] P. D. Iedema and N. H. Kolhapure. Matematical methods. In T. Meyer and J. Keurentjes, editors, *Handbook of Polymer Reation Engineering*, chapter 9, pages 431–532. Wiley-VCH, 2005.

[78] C. D. Immanuel, C. F. Cordeiro, S. S. Sundaram, E. S. Meadows, T. J. Crowley, and F. J. Doyle. Modeling of particle size distribution in emuslion co-polymerization: Conparison with experimental data and parametric sensitivity studies. *Computers and Chemical Engineering*, 26:1133–1152, 2002.

[79] Z Izumi. Emulsion polymerization of acrylonitrile. part ii. mechanism of emulsion polymerization of acrylonitrile. *Journal of Polymer Science Part A-1: Polymer Chemistry*, 5(3):469–480, 1967.

[80] Z. Izumi, H. Kiuchi, and M. Watanabe. Emulsion polymerization of acrylonitrile. part i. role and effect of emulsifiers in the emulsion polymerization of acrylonitrile. *Journal of Polymer Science Part A-1: Polymer Chemistry*, 5(3):455–468, 1967.

[81] J. Kanetakis. Simulation of styrene/butadiene rubber production in a continuous stirred tank reactor train: Modelling of particle size distributions. Master's thesis, McMaster University, Department of Chemical Engineering, 1983.

[82] J. Kanetakis, F. Y. C. Wong, A. E. Hamielec, and J. F. Macgregor. Steady-state modeling of a latex reactor train for the production of styrene-butadiene rubber. *Chemical Engineering Communications*, 35(1-6):123–140, 1985.

[83] C. Kiparissides, J. F. MacGregor, and A. E. Hamielec. Continuous emulsion polymerization. modeling oscillations in vinyl acetate polymerization. *Journal of Applied Polymer Science*, 23(2):401–418, 1979.

[84] C. Kiparissides, E. Papadopoulos, and J. Morris. Real-time optimization and model-based control of polymer reactors. In R. Berber, editor, *Methods of Model Based Process Control*, pages 495–529. Kluwer Academic Publishers, 1995.

[85] H. Kiuchi. Polymerization of acrylonitrile in aqueuous systems. vii. mechanism of the emulsion polymerization of acrylonitrile. *KoL gyoL kagaku zasshi*, 68(5-8):1604–1609, 1965.

[86] J. R. Leiza and J.M. Asua. Emulsion copolymerisation: Process strategies and morphology. In J.M. Asua, editor, *Polymeric Dispersions: Principles and Applications*, pages 363–378. Kluwer Academic Publishers, 1997.

[87] J. R. Leiza and J. Meuldijk. Emulsion copolymerisation: Process strategies and morphology. In A. Van Herk, editor, *Chemistry and Technology of Emulsion Polymerisation*, chapter 4, pages 79–110. Blackwell Publishing, 2005.

[88] J. R. Leiza and J. C. Pinto. Control of polymerization reactors. In J. M. Asua, editor, *Polymer Reation Engineering*, chapter 8, pages 315–361. Blackwell Publishing, 2007.

[89] B. Li and B. W. Brooks. Prediction of the average number of radicals per particle for emulsion polymerization. *Journal of Polymer Science Part A: Polymer Chemistry*, 31(9):2397–2402, 1993.

[90] G. Lichti, R. G. Gilbert, and D. H. Napper. The growth of polymer colloids. *Journal of Polymer Science: Polymer Chemistry Edition*, 15:1957–1971, 1977.

[91] C. C. Lin, H. C. Ku, and W. Y. Chiu. Simulation model for the emulsion copolymerization of acrylonitrile and styrene in azeotropic composition. *Journal of Applied Polymer Science*, 26:1327–1342, 1981.

[92] X. Liu, M. Nomura, and K. Fujita. Thermodynamic correlation of partial and saturation swelling of styrene-acrylonitrile copolymer particles by styrene and acrylonitrile monomers. *Journal of Applied Polymer Science*, 64(5):931–939, 1997.

[93] D. Mackey and A. H. Jorgensen. Nitrile rubber. In *Kirk-Othmer Encyclopedia of Chemical Technology*. John Wiley & Sons, 2001.

[94] I. A. Maxwell, J. Kurja, G. H. J. Van Doremaele, and A. L. German. Thermodynamics of swelling of latex particles with two monomers. *Die Makromolekulare Chemie*, 193(8):2065–2080, 1992.

[95] I. A. Maxwell, J. Kurja, G. H. J. Van Doremaele, A. L. German, and B. R. Morrison. Partial swelling of latex particles with monomers. *Die Makromolekulare Chemie*, 193(8):2049–2063, 1992.

[96] S. J. McCarthy, E. E. Elbing, I. R. Wilson, R. G. Gilbert, D. H. Napper, and D. F. Sangster. Seeded heterogeneous polymerization polymerization of acrylonitrile. *Macromolecules*, 19:2440–2448, 1986.

[97] R. N. Mead and G. W. Poehlein. Emulsion copolymerization of styrene-methyl acrylate and styrene-acrylonitrile in continuous stirred-tank reactors. 1. *Industrial & Engineering Chemistry Research*, 27 (12):2283–2293, 1988.

[98] R. N. Mead and G. W. Poehlein. Emulsion copolymerization of styrene-methyl acrylate and styrene-acrylonitrile in continuous stirred tank reactors. 2. aqueous-phase polymerization and radical capture. *Industrial & Engineering Chemistry Research*, 28(1):51–57, 1989.

[99] E. S. Meadows, T. J. Crowley, C. D. Immanuel, and F. J. Doyle. Nonisothermal modeling and sensitivity studies for batch and semibatch emulsion polymerization of styrene. *Industrial & Engineering Chemistry Research*, 42(3):555–567, 2003.

[100] E.J. Meehan. Variation of monomer pressure with degree og conversion in emulsion polymerization of butadiene and butadiene-styrene. *Journal of American Chemical Society*, 71:628–633, 1949.

[101] K. W. Min and W. H. Ray. On the mathematical modeling of emulsion polymerization reactors. *Journal of Macromolecular Science: Reviews in Macromolecular Chemistry*, C11(2):177–255, 1974.

[102] K. W. Min and W. H. Ray. Computer simulation of batch emulsion polymerization reactors through a detailed mathematical model. *Journal of Applied Polymer Science*, 22(1):89–112, 1978.

[103] R. J. Minari, L. M. Gugliotta, J. R. Vega, and G. R. Meira. Continuous emulsion styrene-butadiene rubber (sbr) process: Computer simulation study for increasing production and for reducing transients between steady states. *Industrial & Engineering Chemistry Research*, 45(1):245–257, 2006.

[104] R. J. Minari, L. M. Gugliotta, J. R. Vega, and G. R. Meira. Emulsion copolymerization of acrylonitrile and butadiene in a train of cstrs. intermediate addition policies for improving the product quality. *Latin American Applied Research*, 36(4):301–308, 2006.

[105] R. J. Minari, L. M. Gugliotta, J. R. Vega, and G. R. Meira. Continuous emulsion copolymerization of acrylonitrile and butadiene: Computer simulation study for improving the rubber quality and increasing production. *Computers and Chemical Engineering*, 31(9):1073–1080, 2007.

[106] R. J. Minari, L. M. Gugliotta, J. R. Vega, and G. R. Meira. Continuous emulsion copolymerization of acrylonitrile and butadiene: Simulation study for reducing transients during changes of grade. *Industrial & Engineering Chemistry Research*, 46:7677–7683, 2007.

[107] B. S. Minhas. *Emulsion Polymerization of Butadiene*. PhD thesis, University of Ottawa, Department of Chemical Engineering, 1983.

[108] B. R. Morrison, I. A. Maxwell, R. G. Gilbert, and D. H. Napper. Testing nucleation models for emulsion-polymerization systems. In E. S. Daniels, E. D. Sudol, and M. S. El-Aasser, editors, *Polymer Latexes: Preparation Characterization, and Applications*, 492, chapter 3, pages 28–44. American Chemical Society, 1992.

[109] M. Morton and W. E. Gibbs. The emulsion polymerization of 2,3-dimethylbutadiene-1,3. *Journal of Polymer Science: Part A*, 1:2679–2695, 1963.

[110] M. Morton, P.P Salatiello, and H. Landfield. Absolute propagation rates in emulsion polymerization i. butadiene in mutual system. *Journal of Polymer Science*, 8(1):111–121, 1952.

[111] M. Morton, P.P Salatiello, and H. Landfield. Absolute propagation rates in emulsion polymerization ii. butadiene in hydroperoxide-polyamine systems. *Journal of Polymer Science*, 8(2):215–224, 1952.

[112] M. Morton, S. Kaizerman, and W. Altier. Swelling of latex particles. *Journal of Colloid and Interface Science*, 9:300–312, 1954.

[113] R. K. Mutha. *Nonlinear Estimation and Control: Applications to Polymer Reactors*. PhD thesis, University of Toronto, 1996.

[114] R. K. Mutha, W. R. Cluett, and A. Penlidis. Nonlinear model-based predictive control of control nonaffine systems. *Automatica*, 33(5):907–913, 1997.

[115] R. K. Mutha, W. R. Cluett, and A. Penlidis. A new multirate-measurement-based estimator: Emulsion copolymerization batch reactor case study. *Industrial & Engineering Chemistry Research*, 36(4): 1036–1047, 1997.

[116] R. Nishida, G. W. Poehlein, and F. J. Schork. Polymerization of acrylonitrile in continuous stirred-tank reactors. *Polymer Reaction Engineering*, 3(4):397–420, 1995.

[117] L. F. J. Noel, I. A. Maxwell, and A. L. German. Partial swelling of latex particles by two monomers. *Macromolecules*, 26:2911–2918, 1993.

[118] L. F. J. Noel, J. M. A. M. Van Zon, I. A. Maxwell, and A. L. German. Prediction of polymer composition in batch emulsion copolymerization. *Journal of Polymer Science: Part A: Polymer Chemistry*, 32(6):1009–1026, 1994.

[119] M. Nomura. Kinetics and mechanisms of emulsion polymerization. *Journal of Industrial and Engineering Chemistry*, 10(7):1182–1216, 2004.

[120] M. Nomura. On the optimal reactor type and operation for continuous emulsion polymerization. In D. R. Bassett, editor, *Emulsion Polymers and Emulsion Polymerization*, 165, chapter 6, pages 121–143. American Chemical Society, 1981.

[121] M. Nomura. Desorption and reabsorption of free radicals in emulsion polymerization. In I. Piirma, editor, *Emulsion Polymerization*, chapter 5. Academic Press, 1982.

[122] M. Nomura, H. Kojima, M. Harada, W. Eguchi, and S. Nagata. Continuous flow operation in emulsion polymerization of styrene. *Journal of Applied Polymer Science*, 15(3):675–691, 1971.

[123] M. Nomura, M. Kubo, and K. Fujita. Kinetics of emulsion copolymerization. iii. prediction of the average number of radicals per particle in an emulsion copolymerization system. *Journal of Applied Polymer Science*, 28(9):2767–2776, 1983.

[124] M. Nomura, I. Horie, M. Kubo, and K. Fujita. Kinetics and mechanism of emulsion copolymerization. iv. kinetic modeling of emulsion copolymerization of styreneand methyl methacrylate. *Journal of Applied Polymer Science*, 37:1029–1050, 1989.

[125] M. Nomura, H. Tobita, and K. Suzuki. Emulsion polymerization: Kinetic and mechanistic aspects. In M. Okubo and A. Butte, editors, *Polymer Particles*, volume 175 of *Advances in Polymer Science*, pages 1–128. Springer, 2005.

[126] S. Omi, K. Kushibiki, M. Negishi, and M. Iso. A generalized computer modeling of semi-batch n-component emulsion copolymerization system and its applications. *Zairyo Gijutsu*, 3(9):426–441, 1985.

[127] S. Omi, M. Negishi, and M. Kushibiki, K.and Iso. Experimental and modelling study of semi-continuous emulsion copolymerization of styrene and acrylonitrile. *Die Makromolekulare Chemie*, 10(S19851):149–158, 1985.

[128] S. Omi, M. Negishi, M. Fujitake, and M. Iso. Semi-batch operation of acrylonitrile emulsion polymerization. *Zairyo Gijutsu*, 4(3):130–140, 1986.

[129] S. Omi, K. Kushibiki, and M. Iso. The computer modeling of multicomponent, semi-batch emulsion copolymerization. *Polmer Engineering and Science*, 27(6):470–482, 1987.

[130] R. J. Orr and L. Breitman. Molecular areas of soaps at the surface of latex particles. *Canadian Journal of Chemistry*, 38:668–680, 1960.

[131] J. T. O'Toole. Kinetics of emulsion polymerization. *Journal of Applied Polymer Science*, 9(4):1291–1297, 1965.

[132] V. M. Ovando-Mendina, E. Mendizabal, and R. D. Peralta. Kinetic modeling of microemulsion copolymerization. *Polymer Bulletin*, 54:129–140, 2005.

[133] U. Pallaske, A. Schmidt, and K. H. Ott. General mathematical model for simulation of dynamic behavior of emulsion polymerization. In K. H. Reichert and W. Geiseler, editors, *Polymer Reaction Engineering: Emulsion Polymerization, High Conversion Polymerization, Polycondensation*, 2nd Berlin International Workshop on Polymer Reaction Engineering, pages 19–39. Huthig and Wepf, 1986.

[134] M. J. Park, M. T. Dokucu, and F. J. Doyle. Modeling and sensitivity analysis of particle size distribution and chain length distribution in a semibatch emulsion copolymerization reactor. *Macromolecular Theory and Simulations*, 14:474–490, 2005.

[135] A. Penlidis. Emulsion polymerization industrial course notes. Technical report, University of Waterloo, 2007.

[136] A. Penlidis. *Polymer Reactor Design. Optimization and Control in Latex Production Technology*. PhD thesis, McMaster University, Department of Chemical Engineering, 1986.

[137] A. Penlidis and M. A. Dube. Mathematical modelling and simulation of industrial emulsion copolymerization reactors. Technical report, University of Waterloo, 1990.

[138] A. Penlidis, J. F. MacGregor, and A. E. Hamielec. Mathematical modeling of emulsion polymerization reactors: A population balance approach. *Journal of Coatings Technology*, 58(737):49–60, 1986.

[139] A. Penlidis, J. F. MacGregor, and A. E. Hamielec. Effect of impurities on emulsion polymerization: Case I kinetics. *Journal of Applied Polymer Science*, 35(8):2023–2038, 1988.

[140] I. Y. Poddubny and M. A. Rabinerzon. Regulation of molecular weight distribution in the polymerization of butadiene-styrene and butadiene-nitrile rubbers. *Journal of Applied Polymer Science*, 9(7): 2527–2536, 1965.

[141] A. L. Polic, L. M. F. Lona, T. A. Duever, and A. Penlidis. A protocol for the estimation of parameters in process models: Case studies with polymerization scenarios. *Macromolecular Theory and Simulations*, 13(2):115–132, 2004.

[142] J. B. Rawlings and J. G. Ekerdt. *Chemical Reactor Analysis and Design Fundamentals*. Nob Hill Publishing, 2004.

[143] J. B. Rawlings and W. H. Ray. Modeling of batch and continuous emulsion polymerization reactors. part i: Model formulation and sensitivity to parameters. *Polymer Engineering and Science*, 28(5): 237–256, 1988.

[144] J. B. Rawlings and W. H. Ray. Modeling of batch and continuous emulsion polymerization reactors. part ii: Comparison with experimental data from continuous stirred tank reactors. *Polymer Engineering and Science*, 28(5):257–274, 1988.

[145] J. R. Richards, J. P. Congalidis, and R. G. Gilbert. Mathematical modeling of emulsion copolymerization reactors. *Journal of Applied Polymer Science*, 37(9):2727–2756, 1989.

[146] V. I. Rodriguez, D. A. Estenoz, L. M. Gugliotta, and G. R. Meira. Emulsion copolymerization of acrylonitrile and butadiene. calculation of the detailed macromolecular structure. *International Journal of Polymeric Materials*, 51(6):511–527, 2002.

[147] C. P. Roe. Surface chemistry aspects of emulsion polymerization. *Industrial & Engineering Chemistry*, 60(9):20–33, 1968.

[148] E. Saldivar and W. H. Ray. Mathematical modeling of emulsion copolymerization reactors: Experimental validation and application to complex systems. *Industrial & Engineering Chemistry Research*, 36(4):1322–1336, 1997.

[149] E. Saldivar, P. Dafniotis, and W. H. Ray. Mathematical modeling of emulsion copolymerization reactors. i. model formulation and application to reactors operating with micellar nucleation. *Journal of Macromolecular Science - Reviews in Macromolecular Chemistry and Physics*, C38(2):207–325, 1998.

[150] S. Sarkar, M. S. Adhikari, M. Banerjee, and R. S. Konar. Persulfate initiated aqueous polymerization of acrylonitrile at 50-degrees-c in an inert atmosphere of nitrogen gas. *Journal of Applied Polymer Science*, 36(8):1865–1876, 1988.

[151] H. A. S. Schoonbrood, M. A. T. Van Den Boom, A. L. German, and J. Hutovic. Multimonomer partitioning in latex systems with moderately water-soluble monomers. *Journal of Polymer Science: Part A: Polymer Chemistry*, 32:2311–2325, 1994.

[152] F. J. Schork, Y. Luo, W. Smulders, J. P. Russum, A. Butte, and K. Fontenot. Miniemulsion polymerization. In *Polymer Particles*, volume 175 of *Advances in Polymer Science*, pages 129–255. Springer, 2005.

[153] O. K. Shvetsov. Synthesis of acrylonitrile copolymer dispersions. *Acta Polymerica*, 37(9):573–577, 1986.

[154] W. V. Smith and R. H. Ewart. Kinetics of emulsion polymerization. *Journal of Chemical Physics*, 16 (6):592–599, 1948.

[155] Z. Song and G. W. Poehlein. Particle formation in emulsion polymerization: Particle number at steady state. *Journal of Macromolecular Science - Chemistry*, A25(12):1587–1632, 1988.

[156] M. H. Srour, V. G. Gomes, and J. A. Romagnoli. Online inferential product attribute estimation for optimal operation of emulsion terpolymerisation: Application to styrene/mma/ma. *Chemical Engineering Science*, 62(16):4420–4438, 2007.

[157] W. H. Stockmayer. Note on the kinetics of emulsion polymerization. *Journal of Polymer Science*, 24 (106):314–317, 1957.

[158] A G. Storti, S. Carrà, M. Morbidelli, and G. Vita. Kinetics of multimonomer emulsion polymerization. the pseudo-homopolymerization approach. *Journal of Applied Polymer Science*, 37(9):2443–2467, 1989.

[159] A. Tazawa, S. Omi, and H. Kubota. The rate of emulsion polymerization of acrylonitrile. *Journal of Chemical Engineering of Japan*, 5(1):44–50, 1972.

[160] S. C. Thickett and R. G. Gilbert. Emulsion polymerization: State of the art in kinetics and mechanisms. *Polymer*, 48:6965–6991, 2007.

[161] W. M. Thomas and R.L. Webb. Propagation rate in acrylonitrile polymerization. *Journal of Polymer Science*, 25:124–125, 1957.

[162] W. M. Thomas, E. H. Gleason, and G. Mino. Acrylonitrile polymerization in aqueous suspension. *Journal of Polymer Science*, 24:43–56, 1957.

[163] M. Uchida. Emulsion polymerization of acrylonitrile. *KoL gyoL kagaku zasshi*, 60(7-12):484–488, 1957.

[164] M. Uchida. Influence of additions of inhibitors to emulsion polymerization of acrylonitrile. *KoL gyoL kagaku zasshi*, 60(7-12):768–773, 1957.

[165] J. Ugelstad and F. K. Hansen. Kinetics and mechanism of emulsion polymerization. *Rubber Chemistry and Technology*, 49(3):536–609, 1976.

[166] J. Ugelstad, P. C. Mork, H. R. Mfutakamba, E. Soleimany, I. Nordhuus, R. Schmid, A. Berge, T. Ellingsen, O. Aune, and K. Nustad. Thermodynamics of swelling pf polymer, oligomer and polymer-oligomer particles. preparation and application of monodisperse polymer particles. In G. W. Poehlein, R. H. Ottewill, and J. W. Goodwin, editors, *Science and Technology of Polymer Colloids*, volume 1 of *NATO ASI on Polymer Colloids*, pages 51–99. Martinus Nijhoff Publishers, 1983.

[167] C. A. Uraneck and J. E. Burleigh. Modification of butadiene-acrylonitrile and styrene-acrylonitrile copolymerizations in emulsion systems. *Journal of Applied Polymer Science*, 12(5):1075–1095, 1968.

[168] H. M. Vale and T. F. McKenna. Modeling particle size distribution in emulsion polymerization reactors. *Progress in Polymer Science*, 30(10):1019–1048, 2005.

[169] E. Vanzo, R. H. Marchessault, and V. Stannett. The solubility and swelling of latex particles. *Journal of Colloid Science*, 20:62–71, 1965.

[170] J. R. Vega, L. M. Gugliotta, M. C. Brandolini, and G. R. Meira. Steady-state optimization in a continuous emulsion copolymerization of styrene and butadiene. *Latin American Applied Research*, 25:207–214, 1995.

[171] J. R. Vega, L. M. Gugliotta, R. O. Bielsa, M. C. Brandolini, and G. R. Meira. Emulsion copolymerization of acrylonitrile and butadiene. mathematical model of an industrial reactor. *Industrial & Engineering Chemistry Research*, 36(4):1238–1246, 1997.

[172] J. R. Vega, L. M. Gugliotta, and G. R. Meira. Emulsion copolymerization of acrylonitrile and butadiene. semibatch strategies for controlling molecular structure on the basis of calorimetric measurements. *Polymer Reaction Engineering*, 10(1-2):59–82, 2002.

[173] J. R. Vega, L. M. Gugliotta, and G. R. Meira. Emulsion copolymerization of acrylonitrile and butadiene in an industrial reactor. mathematical modeling, estimation, and control of polymer quality variables on the basis of calorimetric measurements. *Latin American Applied Research*, 33(2):115–122, 2003.

[174] E. M. Verdurmen. *Particle Nucleation and Growth in Butadiene Emulsion Polymerization*. Ph.d. thesis, Technische Universiteit Eindhoven, Eindhoven, The Netherlands, 1993.

[175] E. M. Verdurmen, E. H. Dohmen, J. M. Verstegen, I. A. Maxwell, A. L. German, and R. G. Gilbert. Seeded emulsion polymerization of butadiene. 1. the propagation rate coefficient. *Macromolecules*, 26:268–275, 1993.

[176] E. M. Verdurmen, J. M. Geurts, J. M. Verstegen, I. A. Maxwell, and A. L. German. Seeded emulsion polymerization of butadiene. 2. effects of persulfate and tert-dodecyl mercaptan. *Macromolecules*, 26:6289–6298, 1993.

[177] E. M. Verdurmen, A. L. German, E. D. Sudol, and R. G. Gilbert. Particle growth in butadiene emulsion polymerization, 2. gamma radiolysis. *Macromolecular Chemistry and Physics*, 195(2): 635–640, 1994.

[178] E. M. Verdurmen, J. M. Geurts, and A. L. German. Particle growth in butadiene emulsion polymerization, 1. the use of fremy salt as aqueous radical scavenger. *Macromolecular Chemistry and Physics*, 195(2):621–633, 1994.

[179] E. M. Verdurmen, J. M. Geurts, and A. L. German. Particle growth in butadiene emulsion polymerization, 3. radical adsorption and desorption rate coefficients. *Macromolecular Chemistry and Physics*, 195(2):641–645, 1994.

[180] E. M. Verdurmen, J. M. Verstegen, and A. L. German. Particle growth in butadiene emulsion polymerization, 4. the promoting effect of mercaptans. *Macromolecular Chemistry and Physics*, 195(2): 647–659, 1994.

[181] J. Vialle, J. Guillot, and A. Guyot. Acrylonitrile copolymerizations. iv. butadiene copolymerization. *Rubber Chemistry and Technology*, 45(6):1546–1553, 1972.

[182] R.A.M. Vieira, M. Embirucu, C. Sayer, J.C. Pinto, and E.L. Lima. Control strategies for complex chemical processes. applications in polymerization processes. *Computers and Chemical Engineering*, 27:1307–1327, 2003.

[183] F. T. Wall, R. W. Powers, G. D. Sands, and G. S. Stent. Properties of polymers as functions of conversion. iv. composition studies of rubber-like copolymers. *Journal of the American Chemical Society*, 70(3):1031–1037, 1948.

[184] P. A. Weerts. *Emulsion Polymerization of Butadiene, A Kinetic Study*. Ph.d. thesis, Technische Universiteit Eindhoven, Eindhoven, The Netherlands, 1990.

[185] P. A. Weerts, J. L. M. van der Loos, and A. L. German. Emulsion polymerization of butadiene, 1. the effect of initiator and emulsifier concentration. *Die Makromolekulare Chemie*, 190(4):777–788, 1989.

[186] P. A. Weerts, J. L. M. van der Loos, and A. L. German. Emulsion polymerization of butadiene, 2. polymerizations with sodium dodecyl sulfate. *Die Makromolekulare Chemie*, 191(11):2615–2630, 1990.

[187] P. A. Weerts, A. L. German, and R. G. Gilbert. Kinetic aspects of the emulsion polymerization of butadiene. *Macromolecules*, 24:1622–1628, 1991.

[188] P. A. Weerts, J. L. M. van der Loos, and A. L. German. Emulsion polymerization of butadiene, 3. kinetic effects of stirring conditions and monomer/water ratio. *Die Makromolekulare Chemie*, 192 (9):1993–2008, 1991.

[189] P. A. Weerts, J. L. M. van der Loos, and A. L. German. Emulsion polymerization of butadiene, 4. effect of thiols. *Die Makromolekulare Chemie*, 192(9):2009–2019, 1991.

[190] F. Y. C. Wong. Steady-state modelling of a low temperature styrene-butadiene latex reactor train. Master's thesis, McMaster University, Department of Chemical Engineering, 1984.

[191] J. Zeaiter, J. A. Romagnoli, G. W. Barton, V. G. Gomes, B. S. Hawkett, and R. G. Gilbert. Operation of semi-batch emulsion polymerisation reactors: Modelling, validation and effect of operating conditions. *Chemical Engineering Science*, 57(15):2955–2969, 2002.

[192] M. Zubitur, P. D. Armitage, S. Ben Amor, J. R. Leiza, and J. M. Asua. Mathematical modeling of multimonomer (vinylic, divinylic, acidic) emulsion copolymerization systems. *Polymer Reaction Engineering*, 11(4):627–662, 2003.

[193] M. Zubitur, S. Ben Amor, C. Bauer, B. Amram, M. Agnely, J. R. Leiza, and J. M. Asua. Multimonomer emulsion copolymerization in presence of inhibitors. *Chemical Engineering Journal*, 98 (3):183–198, 2004.

Appendices

Appendix A

Detailed Process Model Development

This Appendix lists all the reactions, reaction rates, rate constants, mass balances, energy balances, and model outputs considered in the modelling of emulsion copolymerization of AN/Bd.

Reaction Mechanism, Rate Constant & Rate Development

In developing rate expressions, all reactions are assumed to have a first order dependence on each species. The pseudo-rate constant method is employed to capture information from both monomers. Particle phase termination is the only reaction considered to be diffusion-controlled.

Redox & Thermal Initiation:
The following mechanism is an example of initiation using a persulfate based initiator.

$$S_2O_8^{2-} + Fe^{2+} \xrightarrow{k_1} SO_4^{-\cdot} + Fe^{3+} + SO_4^{2-} \tag{A.1}$$

$$Fe^{3+} + SFS \xrightarrow{k_2} Fe^{2+} + SFS^{+} \tag{A.2}$$

$$SO_4^{-\cdot} + M_j \xrightarrow{k'_{p_{ja}}} R^{\cdot}_{1,j} \tag{A.3}$$

$$S_2O_8^{2-} \xrightarrow{k_d} 2SO_4^{-\cdot} \tag{A.4}$$

Rate constants in the above reactions are expressed using an Arrhenius expression (Equation A.5). Since the reactions take place in the aqueous phase, diffusional limitations do not arise, and therefore are not considered in the model.

$$k_i = A_i \exp\left(-E_i/RT\right) \tag{A.5}$$

The overall rate of initiation, considering both redox and thermal mechanisms, is:

$$R_I = k_1 \left[I\right]_a \left[Fe^{2+}\right]_a + 2fk_d \left[I\right]_a \tag{A.6}$$

where, f is the initiator efficiency.

The reaction rates (consumption/generation) for the initiation species are:

$$R_{I_c} = k_1 [I]_a \left[Fe^{2+}\right]_a + k_d [I]_a \quad (A.7)$$

$$R_{RA} = k_2 [RA]_a \left[Fe^{3+}\right]_a \quad (A.8)$$

$$R_{Fe^{2+}} = k_1 [I]_a \left[Fe^{2+}\right]_a - k_2 [RA]_a \left[Fe^{3+}\right]_a \quad (A.9)$$

$$R_{Fe^{3+}} = -R_{Fe^{2+}} \quad (A.10)$$

Propagation:

$$R^{\cdot}_{n,i} + M_j \xrightarrow{k_{p_{ij}}} R^{\cdot}_{n+1,j} \quad (A.11)$$

The individual rate constants for each monomer are given by an Arrhenius expression, the cross-propagation constants are described through reactivity ratios, and the overall propagation rate constant is given by a pseudo rate constant expression.

$$k_p = \sum_i^N \sum_j^N k_{p_{ij}} \phi_i^{\cdot} f_j \quad (A.12)$$

The overall rate of polymerization (assuming long-chain approximations I/II) can be determined using the above rate constant and the following equation:

$$R_{p_k} = k_{p_k} [M]_k [R^{\cdot}]_k \quad (A.13)$$

where, k designates the phase (aqueous or particle) that polymerization takes place. Alternatively, the polymerization rate for each monomer can be written as follows:

$$R_{p_{j_k}} = [R^{\cdot}]_k [M]_k f_{j_k} \sum_i^N \left(k_{p_{ij}} \phi_i^{\cdot}\right) \quad (A.14)$$

where the monomer and radical mole fractions are defined as:

$$f_{i_k} = \frac{[M_i]_k}{\sum_j^N [M_j]_k} \quad (A.15)$$

$$\phi_{i_k}^{\cdot} = \frac{\sum_{\substack{j \\ j \neq i}}^N k_{p_{ji_k}} f_{i_k}}{\sum_{\substack{i \\ i \neq j}}^N \sum_{\substack{j \\ j \neq i}}^N k_{p_{ji_k}} f_{i_k}} \quad (A.16)$$

Termination:

$$R^{\cdot}_{n,i} + R^{\cdot}_{m,j} \xrightarrow{k_t} P_{(m+n)} \text{ or } P_n + P_m \quad (A.17)$$

The overall termination rate constant can be expressed using the following empirical expression:

$$k_t = k_{t_o} \exp(A_1 X + A_2 X^2 + A_3 X^3) \quad (A.18)$$

$$X = \begin{cases} x_c & \text{if } V_d > 0 \\ x & \text{otherwise} \end{cases} \quad (A.19)$$

The overall chemically-controlled rate constant, k_{t_o}, can be expressed using a pseudo rate constant that combines each monomer; however, for this particular investigation a constant value of 90000 was found to be

adequate. The rate constant for termination by disproportionation is determined by assuming a portion of the overall rate constant towards disproportionation. Considering that both combination and disproportionation combine to give total termination, k_{tc} can be obtained by subtracting k_{td} from k_t.

$$k_{td} = \gamma k_t \tag{A.20}$$
$$k_{tc} = (1-\gamma)k_t \tag{A.21}$$

Transfer to Chain-transfer Agent (CTA):

$$R^{\cdot}_{n,i} + (CTA \sim H)_j \xrightarrow{k_{fcta_j}} P_{n,i} + CTA^{\cdot}_j \tag{A.22}$$

The overall pseudo rate constant for CTA i is:

$$k_{fcta_i} = \sum_j^N k_{fcta_j} \phi^{\cdot}_j \tag{A.23}$$

Chain-transfer agent is assumed only to partition between monomer and particle phase, and is only consumed in the particle phase. The rate of consumption is:

$$R_{cta_i} = k_{cta_{i_p}} [CTA_i]_p [R^{\cdot}]_p \tag{A.24}$$

Transfer to Monomer:

$$R^{\cdot}_{n,i} + M_j \xrightarrow{k_{fm_{ij}}} P_{n,i} + M^{\cdot}_j \tag{A.25}$$

$$k_{fm} = \sum_i^N \sum_j^N k_{fm_{ij}} \phi^{\cdot}_i f_j \tag{A.26}$$

Transfer to Polymer:

$$R^{\cdot}_{n,i} + P_{m,j} \xrightarrow{k_{fp_{ij}}} P_{n,i} + R^{\cdot}_{m,j} \tag{A.27}$$

$$k_{fp} = \sum_i^N \sum_j^N k_{fp_{ij}} \phi^{\cdot}_i \overline{F}_j \tag{A.28}$$

Reaction with Water-soluble Impurities (WSI):

$$R^{\cdot}_{n,i} + Z_j \xrightarrow{k_{z_{ij}}} P_i \tag{A.29}$$

$$k_z = \sum_i^N k_{z_{i_a}} \phi^{\cdot}_{i_a} \tag{A.30}$$

The consumption of WSI's occurs only in the aqueous phase. The rate is given as follows:

$$R_{z_i} = k_{z_{i_a}} [Z_i]_a [R^{\cdot}]_a \tag{A.31}$$

Reaction with Monomer-soluble Impurity (MSI):

$$R^{\cdot}_{n,i} + MSI_j \xrightarrow{k_{fmsi_{ij}}} P_i \tag{A.32}$$

$$k_{fmsi} = \sum_{i}^{N} k_{fmsi_i} \phi_i^{\cdot} \tag{A.33}$$

The consumption of MSI's occurs only in the particle phase. The rate is given as follows:

$$R_{msi_i} = k_{fmsi_{ip}} \left[MSI_i\right]_p \left[R^{\cdot}\right]_p \tag{A.34}$$

Reaction with Terminal Double Bonds:

$$R_{n,i}^{\cdot} + P_m^{t=} \xrightarrow{k^*_{p_{ij}}} R_{n+m,i}^{\cdot} \tag{A.35}$$

$$k_p^* = \sum_{i}^{N} \sum_{j}^{N} k^*_{p_{ij}} \phi_i^{\cdot} \overline{F}_j \tag{A.36}$$

Note, reactions with terminal double bonds are not considered to occur in NBR/SBR systems, and the development here is given as a formality.

Reaction with Internal Double Bonds:

$$R_{n,i}^{\cdot} + P_m^{i=} \xrightarrow{k^{**}_{p_{ij}}} R_{n+m,i}^{\cdot} \tag{A.37}$$

$$k_p^{**} = \sum_{i}^{N} \sum_{j}^{N} k^{**}_{p_{ij}} \phi_i^{\cdot} \overline{F}_j \tag{A.38}$$

The rates of radical absorption and desorption from the particle phase are necessary in order to establish the radical concentration in the respective phases. The rates of absorption and desorption are as follows:
Capture by Micelles:

$$R_{cm} = k_{cm} A_m \left[R^{\cdot}\right]_a^{mic} / V_a \tag{A.39}$$

Capture by Particles:

$$R_{cp} = k_{cp} A_p \left[R^{\cdot}\right]_a^{par} / V_a \tag{A.40}$$

Radical Desorption:

$$R_{des} = \frac{k_{des} N_p \overline{n}}{N_A V_a} \tag{A.41}$$

Recaptured Desorbed Radicals by Micelles:

$$R_{des}^{mic} = R_{des} \left(\frac{A_m}{A_m + \varepsilon A_p} \right) \tag{A.42}$$

Note Equation A.42 represents the rate of capture of desorbed radicals by micelles and is used in Equation A.91 when defining the rate of particle formation by micellar nucleation [137].

Model Outputs

Model outputs are conversion, bound AN, particle size, percent solids, molecular weight, and branching frequency. Some of these, along with other useful variables, are defined as follows:

Conversion (mass basis):

$$X = \sum_{i}^{N} \left(\frac{N_{pol_i} MW_{m_i}}{\sum_{i}^{N} \left(N_{pol_i} + N_{m_i} \right) MW_{m_i}} \right) \tag{A.43}$$

Cumulative copolymer composition (CCC) (mole basis):

$$\overline{F}_i = \frac{N_{pol_i}}{\sum_{j}^{N} N_{pol_j}} \tag{A.44}$$

Instantaneous copolymer composition (ICC):
The total ICC can be calculated based on the rate of polymerization of monomer i in all phases divided by the total rate of polymerization of all monomers in all phases.

$$F_i = \frac{\sum_{k}^{P} R_{p_{i_k}} V_k}{\sum_{i}^{N} \sum_{k}^{P} R_{p_{i_k}} V_k} \tag{A.45}$$

Alternatively, the ICC for each monomer i, assuming only two monomers in each phase k, can be calculated using the Mayo-Lewis equation as follows:

$$F_{i_k} = \frac{r_{i_k} f_{i_k}^2 + f_{1_k} f_{2_k}}{r_{1_k} f_{1_k}^2 + 2 f_{1_k} f_{2_k} + r_{2_k} f_{2_k}^2} \tag{A.46}$$

Total Particle Surface Area:

$$A_p = \left(36 \pi N_p\right)^{1/3} V_p^{2/3} \tag{A.47}$$

Total Free Micelle Surface Area:

$$A_m = \sum_{i}^{N} \left(S_{a_i} \left([S_i]_a - CMC \right) V_a N_A \right) - A_p \tag{A.48}$$

*Monodisperse **Swollen** Particle Diameter:*

$$d_p = \left(\frac{6 V_p}{\pi N_p} \right)^{1/3} \tag{A.49}$$

*Monodisperse **Un-swollen** Particle Diameter:*

$$d_p = \left(\frac{6 V_p \phi_p^p}{\pi N_p} \right)^{1/3} \tag{A.50}$$

Percent Solids

$$Solids = \left(\frac{M_{pol}}{M_T} \right) \times 100 \tag{A.51}$$

where, the mass of total polymer M_{pol} and total mass of reaction species M_T are:

$$M_{pol} = \sum M_{pol_i} \tag{A.52}$$

$$M_T = \sum M_{m_i} + \sum M_{pol_i} + M_s + \sum M_{emul_i} \tag{A.53}$$

Note that M_s and M_{emul_i} represent the mass of water (i.e. solvent) and emulsifier in the system.

Monomer Concentration

The monomer concentration, $[M_i]_k$, in each phase k where $k = p,d,a$, can be calculated from the corresponding volume fractions. These fractions are determined from an appropriate partitioning method, and are defined as follows:

$$\phi_i^k = \frac{V_i^k}{V_k} \tag{A.54}$$

Once these fractions are determined, the monomer concentrations in each phase k can be calculated through a simple relation, as follows:

$$[M_i]_k = \phi_i^k \frac{MW_i}{\rho_i} \tag{A.55}$$

The constant partition coefficient method can be used to determine the volume fractions. The general idea is as follows:

1. Rearrange the partition coefficient describing monomer partitioning between aqueous and particle phases in order to express moles of monomer in the particle phase.

$$K_i^{a/p} = \frac{\phi_i^a}{\phi_i^p} = \frac{[M_i]_a}{[M_i]_p} = \frac{N_i^a/V_a}{N_i^p/V_p} \tag{A.56}$$

$$N_i^p = \frac{N_i^a V_p}{K_i^{a/p} V_a} \tag{A.57}$$

2. Define the number of moles of monomer dissolved in the aqueous phase (N_i^a) and total moles of monomer in the system through differential equations.

$$\frac{dN_i}{dt} = F_{i_{in}} - F_i - \left(R_{p_{i_p}} V_p + R_{p_{i_a}} V_a\right) \tag{A.58}$$

$$\frac{dN_i^a}{dt} = F_{i_{a_{in}}} - F_{i_a} - \eta \tag{A.59}$$

$$\eta = \begin{cases} 0 & \text{if } V_d > 0 \\ R_{p_{i_a}} V_a & \text{otherwise} \end{cases}$$

3. Determine the moles of monomer in the droplet phase by taking the difference between the total moles, moles in the aqueous phase, and moles in the particle phase.

$$N_i^d = N_i - N_i^a - N_i^p \tag{A.60}$$

4. When $N_i^d \leq 0$, recalculate the moles of monomer in the particle phase by taking the difference between total monomer in the system and moles in the aqueous phase.

$$N_i^p = N_i - N_i^a \tag{A.61}$$

Note that to implement the above procedure into a computer program several checks will be required to determine when the droplets disappear. This can be accomplished with a boolean variable that flags true when

the droplets disappear and a persistent (global) variable that stores the time when the droplets disappear. Using an extra variable to track the time when the droplet phase disappears makes it possible to reset the flag variable when the ODE solver backtracks in time if the error criteria are not met. Further details on this algorithm, as well as an algorithm for the thermodynamic approach, can be found in Appendix B.

Initiator/Emulsifier/Impurity Concentrations

The concentration of lesser species within each phase of the system is determined through a partitioning coefficient approach that is based on parameters estimated from experimental or process data. In general, the concentration of species i in phase k can be determined according to the following expression:

$$[i]_k = \frac{N_i}{V_p K_i^{p/k} + V_d K_i^{d/k} + V_a K_i^{a/k}} \tag{A.62}$$

where, N_i is the total number of moles of species i in the system, and k represents p, d, or a for particle, droplet, or aqueous phase. Note that in this development, $K_i^{k/k}$ is always one.

For the model developed in this work, it is assumed that initiator, oxidizing/reducing agents, water-soluble impurity, and emulsifier all reside in the aqueous phase and are insoluble in all other phases. Under this assumption Equation A.62 could be restated for aqueous phase components as follows:

$$[i]_a = \frac{N_i}{V_a} \tag{A.63}$$

where,

$$K_i^{p/a} \approx 0 \tag{A.64}$$

$$K_i^{d/a} \approx 0 \tag{A.65}$$

$$K_i^{a/a} = 1 \tag{A.66}$$

On the other hand, monomer-soluble impurity and CTA are assume to be soluble only in the organic phase. Thus, partitioning is between the particle and droplet phases. For the particle phase, the concentration can be given as follows:

$$[i]_p = \frac{N_i}{V_p + V_d K_i^{d/p}} \tag{A.67}$$

Radical Concentrations

Aqueous Phase Radical Concentration

In order to determine the concentration of radicals in the aqueous phase a population balance must be written on all radicals entering and leaving. As mentioned in Chapter 3, differential equations can be written to account for all radicals of different chain lengths, and by applying the steady-state hypothesis (SSH) an overall value for the concentration is obtained by summing up all radicals of length k. In general, this can be written as:

$$[R^{\cdot}]_a = [R^{\cdot}_{in}]_a + \sum_{i=1}^{N} \sum_{k=1}^{jcr-1} \left[R^{\cdot}_{k,i}\right]_a \tag{A.68}$$

The concentration of radicals of length k for each monomer i can be obtained according to the following equations [33, 34, 137].

$$[R^{\cdot}_{in}]_a = \frac{R_I}{\sum_i^N k'_{p_{ia}}[M_i]_a + \sum_i^{N_z} k_{z_i}[Z_i]_a}$$

if $k = 1$

$$\left[R^{\cdot}_{1,i}\right]_a = \frac{R_{des} + k'_{p_{ia}}[R^{\cdot}_{in}]_a[M_i]_a}{\sum_j^N k_{p_{ija}}\left[M_j\right]_a + k_{t_a}[R^{\cdot}]_a + \sum_i^{N_z} k_{z_i}[Z_i]_a}$$

elseif $2 \leq k \leq j_{cr}/2$

$$\left[R^{\cdot}_{k,i}\right]_a = \frac{\left(\sum_j^N k_{p_{jia}}\left[R^{\cdot}_{k-1,j}\right]_a\right)[M_i]_a}{\sum_j^N k_{p_{ija}}\left[M_j\right]_a + k_{t_a}[R^{\cdot}]_a + \sum_i^{N_z} k_{z_i}[Z_i]_a}$$

elseif $(j_{cr}/2+1) \leq k \leq (j_{cr}-1)$

$$\left[R^{\cdot}_{k,i}\right]_a = \frac{\left(\sum_j^N k_{p_{jia}}\left[R^{\cdot}_{k-1,j}\right]_a\right)[M_i]_a}{\sum_j^N k_{p_{ija}}\left[M_j\right]_a + k_{t_a}[R^{\cdot}]_a + \sum_i^{N_z} k_{z_i}[Z_i]_a + k_{cm}A_m/V_a + k_{cp}A_p/V_a}$$

else

$$\left[R^{\cdot}_{j_{cr},i}\right]_a = \frac{\left(\sum_j^N k_{p_{ji}}\left[R^{\cdot}_{j_{cr}-1,j}\right]_a\right)[M_i]_a}{k_{cm}A_m/V_a + k_{cp}A_p/V_a}$$

The concentration of radicals that may be captured or undergo homogeneous nucleation can be written as follows [33, 34]:

$$[R^{\cdot}]_a^{cap} = [R^{\cdot}]_a^{mic} + [R^{\cdot}]_a^{par} \tag{A.69}$$

$$[R^{\cdot}]_a^{mic} = \sum_i^N \left(\sum_{k=j_{cr}/2+1}^{j_{cr}-1} \left[R^{\cdot}_{k,i}\right]_a \left(\frac{A_m}{A_m + \varepsilon A_p}\right) + \left[R^{\cdot}_{j_{cr},i}\right]_a \left(\frac{A_m}{A_m + \varepsilon A_p + \mu H}\right) \right) \tag{A.70}$$

$$[R^{\cdot}]_a^{par} = \sum_i^N \left(\sum_{k=j_{cr}/2+1}^{j_{cr}-1} \left[R^{\cdot}_{k,i}\right]_a \left(\frac{\varepsilon A_p}{A_m + \varepsilon A_p}\right) + \left[R^{\cdot}_{j_{cr},i}\right]_a \left(\frac{\varepsilon A_p}{A_m + \varepsilon A_p + \mu H}\right) \right) \tag{A.71}$$

$$[R^{\cdot}]_a^{hom} = \sum_i^N \left[R^{\cdot}_{j_{cr},i}\right]_a \left(\frac{\mu H}{A_m + \varepsilon A_p + \mu H}\right) \tag{A.72}$$

$$H = \begin{cases} \left(1 - \frac{LA_p}{4V_a}\right) V_a & \text{if } LA_p < 4V_a \\ 0 & \text{otherwise} \end{cases} \tag{A.73}$$

An alternative to summing up individual radical chains of length k to determine the total radical concentra-

tion, is to perform an overall balance on $[R^{\cdot}]_a$.

$$\frac{d[R^{\cdot}]_a}{dt} = (R_I + \rho_{des}) - k_{t_a}[R^{\cdot}]_a^2 - \left(\sum_i^{N_z} k_{z_i}[Z_i]_a + k_{cm}A_m/V_a + k_{cp}A_p/V_a + k_h\right)[R^{\cdot}]_a \tag{A.74}$$

Applying the steady-state hypothesis generates a quadratic equation (Equation A.75) that can easily be solved; however, using such an approach does not capture radical chain-length behaviour, the number of radicals captured, or the number of radicals that undergo homogeneous nucleation. Therefore when determining the rate of nucleation (micellar or homogeneous) the overall concentration is used to approximate the actual concentrations of radicals that may be capturable or capable of undergoing homogeneous nucleation. As found out through simulation, this can overestimate the actual rates of nucleation which results in a higher estimate of the number of particles nucleated.

$$[R^{\cdot}]_a = \frac{-b + \sqrt{b^2 + 4k_{t_a}(R_I + R_{des})}}{2k_{t_a}} \tag{A.75}$$

$$b = \left(\sum_i^{N_z} k_{z_i}[Z_i]_a + k_{cm}A_m/V_a + k_{cp}A_p/V_a + k_h\right) \tag{A.76}$$

Particle Phase Radical Concentration

The concentration of radicals in the particle phase can be written as:

$$[R^{\cdot}]_p = \frac{\bar{n}N_p}{V_p N_A} \tag{A.77}$$

Average Number of Radicals per Particle

The average number of radicals per particle can be calculated from the following equation:

$$\bar{n} = \cfrac{\alpha}{p + \cfrac{2\alpha}{p+1+\cfrac{2\alpha}{p+2+\cdots}}} \tag{A.78}$$

where, p and α are dimensionless group terms that are related to radical loss and gain from the particles. They are defined based on previous definitions by Penlidis and Dube [137] as follows:

$$p = \frac{\left(k_{des} + k_{fmsi_p}[MSI]_p\right)V_p N_A}{k_{t_p}N_p} \tag{A.79}$$

$$\alpha = \frac{k_{cp}A_p\left([R^{\cdot}]_a^{par} + [R^{\cdot}]_a^{des}\right)V_p N_A^2}{k_{t_p}N_p^2} \tag{A.80}$$

A detailed algorithm for computer implementation can be found in Appendix B.

Particle Phase Radical Desorption

Radical desorption can occur when small radicals diffuse out of the particle phase. The overall rate of radical desorption (in $mol/L/min$) can be stated as follows:

$$R_{des} = k_{des}\left[R^{\cdot}\right]_p \tag{A.81}$$

where, k_{des} is the rate coefficient for desorption (in $1/min$). As discussed in Chapter 3, many expressions have been proposed to describe k_{des}; however, the ones compared in this work were those of Nomura [121] and Asua et al. [8] (see Figure 4.18). Typically, desorption occurs as a result of transfer reactions. For an NBR/SBR system, only transfer to monomer may be a possible route for radical desorption.

According to Nomura, the total desorption rate constant k_{des}, neglecting transfer to CTA, can be defined as:

$$k_{des} = \sum_{i}^{N} k_{des_i} \tag{A.82}$$

where, the individual radical (i) desorption coefficients (k_{des_i}) are:

$$k_{des_i} = k_{fm_i}\left[M_i\right]_p \left(\frac{K_{o_i}}{K_{o_i}\bar{n} + \sum_j^N k_{p_{ij}}\left[M_j\right]_p}\right) \tag{A.83}$$

$$k_{fm_i} = \sum_{j}^{N} k_{fm_{ji}}\phi_j^{\cdot} \tag{A.84}$$

The rate of diffusion of radicals i out of a particle (K_{o_i}), used above in Equation A.83, can be defined as:

$$K_{o_i} = \frac{12D_{w_i}}{m_{d_i}d_p^2\delta_i} \tag{A.85}$$

where, δ_i can be defined as:

$$\delta_i = \left(1 + \frac{2D_{w_i}}{m_{d_i}D_{p_i}}\right)^{-1} \tag{A.86}$$

$$m_{d_i} = \left(K_i^{a/p}\right)^{-1} \tag{A.87}$$

A similar expression for k_{des} was put forth by Asua, which can be defined as:

$$k_{des_i} = k_{fm_i}\left[M_i\right]_p \left(\frac{K_{o_i}}{\beta_i K_{o_i} + \sum_j^N k_{p_j}\left[M_j\right]_p}\right) \tag{A.88}$$

where, β_i is the probability that a desorbed monomeric radical of type i reacts in the aqueous phase by propagation or termination, and can be defined as:

$$\beta_i = \frac{k_{p_{a_{ij}}}\left[M_j\right]_a + k_{t_a}\left[R^{\cdot}\right]_a}{k_{p_{a_{ij}}}\left[M_j\right]_a + k_{t_a}\left[R^{\cdot}\right]_a + \sum_j^{Nz} k_{z_j}\left[Z_j\right]_a + k_{cm}A_m/V_a + k_{cp}A_p/V_a} \tag{A.89}$$

Note that in the above expression it is assumed that desorbed monomeric radicals can be recaptured, hence the inclusion of terms $k_{cm}A_m/V_a$ and $k_{cp}A_p/V_a$ in the denominator.

Using Equation A.41 for R_{des}, the total concentration of desorbed monomeric radicals in the aqueous phase that may potentially be recaptured by particles can be calculate by the following equation:

$$[R^{\cdot}]_a^{des} = \frac{R_{des}}{k_{cp} A_p / V_a} \tag{A.90}$$

This, relation is needed when determining the average number of radicals per particle ($\bar{n}$).

Particle Nucleation

Rate of Micellar Nucleation

The rate of micellar nucleation can be defined as follows:

$$R_{mic} = \left(R_{des}^{mic} + \frac{k_{cm} [R^{\cdot}]_a^{mic}}{r_{mic}} \right) N_A \tag{A.91}$$

where, R_{des}^{mic} was previously defined in Equation A.42.

Rate of Homogeneous Nucleation

The rate expression used in this work, and as defined by Dube et al. [34], can be expressed using a homogeneous rate coefficient (k_h) as follows:

$$R_{hom} = k_h [R^{\cdot}]_a^{hom} N_A \tag{A.92}$$

If the emulsifier concentration is above the CMC, then both micellar and homogeneous nucleation occur simultaneously. In this case, micellar nucleation will significantly dominate (e.g. $\sim 10^{18}\#/L_w$) and homogeneous nucleation will appear to have no effect on particle formation (e.g. $\sim 10^{14}\#/L_w$). On the other hand, if the emulsifier concentration is initially below the CMC and more emulsifier is gradually fed to the reactor, then homogeneous nucleation will dominate initially. This subtle difference can significantly influence the prediction of the overall number of particles (N_p), since if homogeneous nucleation was not considered, no particles would be generated until the emulsifier concentration increased beyond the CMC, which would result in an lower estimate of N_p.

Another expression used by Dube et al. [33], was developed based on the original work of Hansen and Ugelstad [70], who defined R_{hom} as follows:

$$\begin{aligned} R_{hom} &= k_{p_a} [M]_a \left[R^{\cdot}_{j_{cr}-1} \right]_a N_A \\ &= \sum_i^N \sum_j^N k_{p_{ij_a}} \phi^{\cdot}_{i_a} f_{j_a} [M]_a \left[R^{\cdot}_{j_{cr}-1} \right]_a N_A \\ &= \sum_i^N \sum_j^N k_{p_{ij_a}} [M_j]_a \left[R^{\cdot}_{j_{cr}-1,i} \right]_a N_A \end{aligned} \tag{A.93}$$

For the AN/Bd system, the above development was further refined by assuming that radicals are not captured

until $j_{cr}/2$. The following expression can be given:

$$R_{hom} = \left(k_{p_{ABa}} \left(\left[R^{\cdot}_{j_{cr}/2,A} \right]_a + \sum_{k=j_{cr}/2+1}^{j_{cr}-1} \left[R^{\cdot}_{k,A} \right]_a \right) + k_{p_{BBa}} \left[R^{\cdot}_{j_{cr}/2,B} \right]_a \right) [M_B]_a N_A + k_{p_{AAa}} \left[R^{\cdot}_{j_{cr}-1,A} \right]_a [M_A]_a N_A \quad \text{(A.94)}$$

Unfortunately, this expression does not provide as much freedom to adjust the amount of homogeneous nucleation occurring, when compared to Equation A.92. This is due to the parameter μ ($\mu = k_{h_o}/k_{cm}$) available in Equation A.92, which can be adjusted until a reasonable amount of particles are formed by homogeneous nucleation. Thus, using Equation A.94 can result in a prediction of N_p^{hom} that is abnormally high relative to N_p^{mic}. In fact, N_p^{hom} was found to be of the same order of magnitude as N_p^{mic} when Equation A.94 was used in place of Equation A.92 in this work. The numerical results of course depend on the specific parameter values used in these equations.

Moment Generation Rates

As described in Chapter 3, the rates of moment generation, on a mole basis, for V_pQ_o, V_pQ_1, and V_pQ_2, can be defined as follows:

$$R_{V_pQ_o} = \left(\tau + \frac{\beta}{2} - C_{p^{**}} \frac{V_pQ_1}{V_p [M]_p} - C_{p^*} \frac{V_pQ_o}{V_p [M]_p} \right) k_p [M]_p [R^{\cdot}]_p \quad \text{(A.95)}$$

$$R_{V_pQ_1} = \gamma k_p [M]_p [R^{\cdot}]_p \quad \text{(A.96)}$$

$$R_{V_pQ_2} = \left(\gamma + 2 \left(1 + \frac{C_{p^*} V_pQ_1 + C_{p^{**}} V_pQ_2}{V_p [M]_p} \right) \frac{\xi}{\lambda} + \beta \left(\frac{\xi}{\lambda} \right)^2 \right) k_p [M]_p [R^{\cdot}]_p \quad \text{(A.97)}$$

Note, the units of V_pQ_i are moles since each moment, Q_i, is in terms of concentration (mol/L).

Similarly, for chain branching, the state is $V_pQ_o\overline{BN}_i$, and the rates are defined as:

$$R_{V_pQ_o\overline{BN}_3} = \left(\frac{C_{fp} V_pQ_1}{V_p} + \frac{C_p^* V_pQ_o}{V_p} \right) k_p [R^{\cdot}]_p \quad \text{(A.98)}$$

$$R_{V_pQ_o\overline{BN}_4} = \frac{C_p^{**} V_pQ_1}{V_p} k_p [R^{\cdot}]_p \quad \text{(A.99)}$$

Average Molecular Weights & Branching Frequencies

The number- and weight-average molecular weights can be determined from the state variables V_pQ_i, as follows:

$$\overline{M}_n = \frac{V_pQ_1}{V_pQ_o} M_{eff} \quad \text{(A.100)}$$

$$\overline{M}_n = \frac{V_pQ_2}{V_pQ_1} M_{eff} \quad \text{(A.101)}$$

where, M_{eff} is the effective molecular weight of the monomers in the system, determined by weighting the individual monomer molecular weights by the cumulative copolymer composition, as follows:

$$M_{eff} = \sum_{i}^{N} MW_{m_i} \overline{F}_i \tag{A.102}$$

The average branching frequencies for tri- and tetra-functional branching can be determined directly from the state variables, $V_p Q_o$ and $V_p Q_o \overline{BN}_i$, as follows:

$$\overline{BN}_3 = \frac{V_p Q_o \overline{BN}_3}{V_p Q_o} \tag{A.103}$$

$$\overline{BN}_4 = \frac{V_p Q_o \overline{BN}_4}{V_p Q_o} \tag{A.104}$$

Reactor Balances (Material/Energy)

Balances can be written assuming a lumped parameter system (i.e. no gradients exist and all variables are only a function of time). In subsequent development, all ingredients are assumed to enter the reactor and react without any delay (i.e. no reaction delay due to mixing).

Mole Balances

Material balances were performed on a mole basis. This section lists all mole balances used in the model.

Initiator:

$$\frac{dN_{I_j}}{dt} = F_{I_{j_{in}}} - F_{I_j} - R_{I_{c_j}} V_a \tag{A.105}$$

Reducing Agent:

$$\frac{dN_{RA_j}}{dt} = F_{RA_{j_{in}}} - F_{RA_j} - R_{RA_j} V_a \tag{A.106}$$

Oxidizing Agent (Iron-Fe):

$$\frac{dN_{Fe}}{dt} = F_{Fe_{in}} - F_{Fe} \tag{A.107}$$

$$\frac{dN_{Fe^{2+}}}{dt} = F_{Fe^{2+}_{in}} - F_{Fe^{2+}} - R_{Fe^{2+}} V_a \tag{A.108}$$

$$\frac{dN_{Fe^{3+}}}{dt} = F_{Fe^{3+}_{in}} - F_{Fe^{3+}} - R_{Fe^{3+}} V_a \tag{A.109}$$

Monomer:

$$\frac{dN_{m_j}}{dt} = F_{m_{j_{in}}} - F_{m_j} - \left(R_{p_{j_p}} V_p + R_{p_{j_a}} V_a \right) \tag{A.110}$$

Bound Monomer:

$$\frac{dN_{pol_j}}{dt} = F_{pol_{j_{in}}} - F_{pol_j} + \left(R_{p_{j_p}} V_p + R_{p_{j_a}} V_a \right) \tag{A.111}$$

Solvent (water):

$$\frac{dN_s}{dt} = F_{s_{in}} - F_s \tag{A.112}$$

Emulsifier:

$$\frac{dN_{em_j}}{dt} = F_{em_{j_{in}}} - F_{em_j} \tag{A.113}$$

Water-soluble Impurities (WSI):

$$\frac{dN_{z_j}}{dt} = F_{z_{j_{in}}} - F_{z_j} - R_{z_{ja}} V_a \tag{A.114}$$

Monomer-soluble Impurities (MSI):

$$\frac{dN_{msi_j}}{dt} = F_{msi_{j_{in}}} - F_{msi_j} - R_{msi_{jp}} V_p \tag{A.115}$$

Chain-transfer Agent (CTA):

$$\frac{dN_{cta_j}}{dt} = F_{cta_{j_{in}}} - F_{cta_j} - R_{cta_{jp}} V_p \tag{A.116}$$

where, j corresponds to multiple components of initiator, emulsifier, CTA, monomer, etc.

Total Particle Balance

An overall balance on the number of particles (N_p expressed in # of particles) can be written as:

$$\frac{dN_p}{dt} = F_{p_{in}} - F_p + (R_{mic} + R_{hom}) V_a \tag{A.117}$$

Moment Balances

In a similar manner to the mole balances above, the generation of each moment, $V_p Q_i$, can be defined as:

$$\frac{d(V_p Q_o)}{dt} = F_{(V_p Q_o)_{in}} - F_{V_p Q_o} + R_{V_p Q_o} V_p \tag{A.118}$$

$$\frac{d(V_p Q_1)}{dt} = F_{(V_p Q_1)_{in}} - F_{V_p Q_1} + R_{V_p Q_1} V_p \tag{A.119}$$

$$\frac{d(V_p Q_2)}{dt} = F_{(V_p Q_2)_{in}} - F_{V_p Q_2} + R_{V_p Q_2} V_p \tag{A.120}$$

For each branching frequency, the balances are defined as:

$$\frac{d\left(V_p Q_o \overline{BN}_3\right)}{dt} = F_{\left(V_p Q_o \overline{BN}_3\right)_{in}} - F_{V_p Q_o \overline{BN}_3} + R_{V_p Q_o \overline{BN}_3} V_p \tag{A.121}$$

$$\frac{d\left(V_p Q_o \overline{BN}_4\right)}{dt} = F_{\left(V_p Q_o \overline{BN}_4\right)_{in}} - F_{V_p Q_o \overline{BN}_4} + R_{V_p Q_o \overline{BN}_4} V_p \tag{A.122}$$

Phase Volumes

The change in volume of the growing particles can be described by considering the average increase in polymer within the particle phase. Assuming a constant monomer density (i.e. $\rho \neq f(T)$ and overall particle phase inlet/outlet flows experience negligible density differences), an overall mass balance can be written

for the polymer in the system and further reduced to describe the change in average volume. The change in overall polymer volume can be defined as:

$$\frac{dV_{pol}}{dt} = q_{pol_{in}} - q_{pol} + \frac{\sum_i^N MW_{m_i}\left(R_{p_{i_a}}V_a + R_{p_{i_p}}V_p\right)}{\rho_p} \tag{A.123}$$

where, the first two terms account for the flow of polymer in and out of the reactor, and the third term considers the overall change in volume due to polymerization.

In order to account for the overall change in the particle phase volume (i.e. polymer and monomer), Equation A.123 can be divided by the volume fraction of polymer to particle volume (ϕ_p^p). Following this approach, the total particle phase volume can be described in two regimes: the first, when monomer droplets exist, thus allowing for a monomer saturated particle; the second, when droplets disappear, causing the particles to shrink due the consumption of monomer and the relative density difference between monomer and polymer. The overall average particle phase volume can be written according to the two regimes as follows:

$$\frac{dV_p}{dt} = q_{p_{in}} - q_p + growth \tag{A.124}$$

$$growth = \begin{cases} \sum_i^N \frac{MW_{m_i}\left(R_{p_{i_a}}V_a + R_{p_{i_p}}V_p\right)}{\phi_p^p \rho_p} & \text{if } V_d > 0 \\ \sum_i^N \frac{MW_{m_i}R_{p_{i_a}}V_a}{\rho_p} + \sum_i^N MW_{m_i}R_{p_{i_p}}V_p\left(\frac{1}{\rho_{m_i}} - \frac{1}{\rho_p}\right) & \text{otherwise} \end{cases} \tag{A.125}$$

The relative contribution of polymerization in the aqueous phase (i.e. $R_{p_{i_a}}V_a$) compared to the particle phase (i.e. $R_{p_{i_p}}V_p$) to the overall particle phase volume seen in Equation A.125 has been shown through simulation to be insignificant despite the relatively high water solubility of AN. However, the inclusion of $R_{p_{i_a}}V_a$ provides an important contribution when a CSTR initially contains just water and micelles are not present, thus kick-starting particle formation when the emulsifier concentration is below the CMC. For generality, $R_{p_{i_a}}V_a$ was included regardless of the reactor type and operation mode.

Energy Balance

Derivations of energy balances can be found in numerous books on reactor engineering and process control. The formulation that will be provided here is based on a liquid phase reaction with no consideration for vapour pressure of monomer in the reactor head space. A similar approach was taken by Broadhead [15]. Besides the usual assumptions made for a liquid phase reaction, the following additional assumptions were made in deriving the balance on the reactor:

1. All latent heat effects were ignored
2. The only sensible heat effects considered were those from water, monomer, and polymer
3. The heat of reaction was set as the heat of polymerization
4. The heat capacity is independent of temperature changes
5. No temperature gradients exist within the reactor or cooling jacket
6. Negligible heat of polymerization in the aqueous phase
7. The reactor was assumed to be cylindrical in shape and heat only transfers through the reactor walls

8. The area for heat transfer can be approximated as:

$$A_{jacket} = 2\pi rh = \frac{2V_R}{r} \tag{A.126}$$

9. The overall heat transfer coefficient is approximated as a lumped constant

Based on these assumptions, the following balance can be written:

$$\frac{dH}{dt} = \sum_i^N F_{i_{in}} \overline{H}_{i_{in}} - \sum_i^n F_i \overline{H}_i + Q_{Rx} - Q_{jacket} - Q_{loss} \tag{A.127}$$

$$\frac{d\left(\sum_i^N m_i \hat{C}_{p_i} T\right)}{dt} = \sum_i^N F_{i_{in}} \overline{C}_{p_i} (T_{in} - T_{ref}) - \sum_i^n F_i \overline{C}_{p_i} (T - T_{ref}) + Q_{Rx} - Q_{jacket} - Q_{loss} \tag{A.128}$$

$$\sum_i^N m_i \hat{C}_{p_i} \frac{dT}{dt} = \sum_i^N F_{i_{in}} \overline{C}_{p_i} (T_{in} - T) + Q_{Rx} - Q_{jacket} - Q_{loss} \tag{A.129}$$

$$Q_{Rx} = \sum_i^N R_p V_p (-\Delta H_{p_i}) \tag{A.130}$$

$$Q_{jacket} = UA_j (T - T_j) \tag{A.131}$$

$$Q_{loss} \approx 0 \tag{A.132}$$

where, the heat of polymerization (in units of J/mol) can be calculated as:

$$\Delta H_p(T) = \Delta H_p(T_{ref}) + \sum_i^n H_{i,out} - \sum_i^n H_{i,in} \tag{A.133}$$

$$H_i = \int_{T_{ref}}^{T} C_{p_i} dT \approx C_{p_i} (T - T_{ref}) \tag{A.134}$$

Considering monomers AN and Bd, and copolymer, the heat of polymerization can be expanded according to the following equation:

$$\sum_i^n (-\Delta H_{p_i}(T)) R_{p_i} V_p = \sum_i^n -\Delta H_{p_i}(T_{ref}) R_{p_i} V_p - \sum_i^n R_{p_i} V_p C_{p_p} (T - T_{ref}) + \sum_i^n R_{p_i} V_p C_{p_i} (T - T_{ref}) \tag{A.135}$$

In a similar manner to the reactor, a balance can be developed for the cooling jacket.

$$m_w \hat{C}_{p_w} \frac{dT_j}{dt} = F_{j_{in}} \overline{C}_{p_w} (T_{j_{in}} - T_j) + Q_{jacket} - Q_{loss} \tag{A.136}$$

Flow Rates

The flow rates (molar and volumetric) of species entering and leaving the reactor are defined under the assumption of ideal mixing and a constant reactor overflow.

Entry Flow Rates

Depending on how the model is to be used, two slightly different methods for determining the flow of material into the reactor can be developed. In the first, one could simply specify mass or volumetric flow rates from which the necessary molar flow rates could be calculated for use in the mole balances. In the second approach, one could specify an overall volumetric flow of all species entering the reactor and the mass fraction of each species in the overall inflow stream. From an industrial perspective, the first method is probably of greater convenience, as flow readings can easily be obtained for each individual flow stream. For simulation purposes, the second method is of more convenience and easier to use from the perspective of maintaining a desire recipe composition in the inflow stream and a reasonably constant reactor residence time. The results shown in this thesis were based on the second approach.

According to the second method, if all streams entering the reactor are envisioned as one and the corresponding mass fractions of each specie are specified along with the total volumetric flow of material entering the reactor, then the individual volume fractions and resulting volumetric and molar flow rates can be determined as follow:

$$\phi_{i_{in}} = \frac{\omega_{i_{in}}/\rho_i}{\sum_j^{N_c} \omega_{j_{in}}/\rho_j} \tag{A.137}$$

$$q_{i_{in}} = \phi_{i_{in}} q_{T_{in}} \tag{A.138}$$

$$F_{i_{in}} = q_{i_{in}} \frac{\rho_i}{MW_i} \tag{A.139}$$

where, $\omega_{i_{in}}$ is the mass fraction of species i in the feed stream.

Using the specified total volumetric flow rate of material entering the reactor and the total volume of reactor contents (i.e. $V_T = V_R$ at overflow), the average residence time can be determined as follows:

$$\theta = \frac{V_T}{q_{T_{in}}} \tag{A.140}$$

Note that if the reactor is started up empty, the residence time is clearly undefined until the reactor overflows, and must be handled accordingly in the computer program (i.e. run model in semi-batch mode until reactor starts to overflow and then begin to calculate θ). As well, the above development only applies for the first reactor if a train of reactors is used, as all subsequent reactors in the train would take the previous reactors outflows as inflows.

Exit Flow Rates

In order to determine the flow of species out of the reactor, the overall volumetric flow rate is first determined, and the individual volume fractions of each phase calculated. Using these two variables, the individual phase flow rates can be determined and further used to calculate the molar flow rates of each species out of the reactor.

The total volumetric flow of material out of the reactor, at overflow, can be defined as:

$$q_T = q_{T_{in}} - shrinkage \tag{A.141}$$

where, the shrinkage term accounts for the overall volume shrinkage due to polymerization, and can be

defined as:

$$shrinkage = \sum_{i}^{N} MW_{m_i} \left(R_{p_{i_a}} V_a + R_{p_{i_p}} V_p \right) \left(\frac{1}{\rho_{m_i}} - \frac{1}{\rho_p} \right) \tag{A.142}$$

The volume fraction and volumetric outflow of each phase k can be defined as:

$$\phi_k = \frac{V_k}{V_T} \tag{A.143}$$

$$q_k = \phi_k q_T \tag{A.144}$$

where, V_T is the total volume of the reactor contents, and can be calculated by summing up the volume occupied by each individual component in the reactor. Upon reactor overflow, the total volume can be set to the reactor volume.

In general, the total molar flow of each component out of the reactor can be determined as follows:

$$F_i = \sum_{k}^{P} [i]_k q_k \tag{A.145}$$

In some cases, it may be more convenient to define the above flow rates as:

$$F_i = \left(\frac{N_i}{V_T} \right) q_T \tag{A.146}$$

For all the species considered in the model of this work, the following molar flow rates can be defined:

$$F_I = [I]_a q_a \tag{A.147}$$

$$F_{RA} = [RA]_a q_a \tag{A.148}$$

$$F_{Fe^{2+}} = \left[Fe^{2+}\right]_a q_a \tag{A.149}$$

$$F_{Fe} = [Fe]_a q_a \tag{A.150}$$

$$F_{m_i} = [M_i]_d q_d + [M_i]_a q_a + [M_i]_p q_p \tag{A.151}$$

$$F_{pol_i} = [P_i]_a q_a + [P_i]_p q_p \tag{A.152}$$

$$F_{em_i} = [EM_i] q_T \tag{A.153}$$

$$F_{z_i} = [Z_i]_a q_a \tag{A.154}$$

$$F_{msi_i} = [MSI_i]_p q_p \tag{A.155}$$

$$F_{cta_i} = [CTA_i]_p q_p \tag{A.156}$$

$$F_p = N_p \frac{q_p}{V_p} \tag{A.157}$$

For a reactor train the outflows from reactor i are set equal to the inflows to reactor $i+1$. If any additional species are introduced as a sideflow to the reactor they are accounted for accordingly. This can be represented as follows:

$$F^i_{j_{in}} = F^{i-1}_j \tag{A.158}$$

where the index i represents the reactor number (note that i begins at 2). In terms of computer implemen-

tation, the outflows are stored in a vector at 1 minute increments and when solving the next reactor in the train the inflows are set according to the previously stored vector. Since the step size taken by the solver will in general be unknown, an interpolation is performed to determine the correct flow rates for the current simulation time used.

Appendix B

Detailed Algorithms for Computational Implementation

This Appendix discusses computer implementation aspects as well as provides potentially useful algorithms for implementing monomer partitioning and calculating the average number of radicals. A detailed step-by-step algorithm is not explicitly given, instead a general overview of the steps required is provided.

Comments on the Computer implementation of the Model

The model was implemented in the MATLAB programming environment. The only internal MATLAB toolbox used was the SPLINE command, which was used to determine the appropriate input flow rates of each species (i.e. output flow rates from the previous reactor in the train) for the corresponding time step taken by the ODE solver. Note the inputs existed as a time vector (i.e. each element of the vector corresponded to the flow rate at 1 minute intervals) and a spline was fit so that an accurate interpolation could be made. The SUNDIALS numerical package was used to solve the model, as it was found to be more robust than any of the prepackaged MATLAB solvers. This package is written in C and comes with a MATLAB interface (i.e. pre-written mex files).

The following lists potentially useful suggestions that were found essential to the model development in this work.

- When introducing the recipe into a full reactor (CSTR or semi-batch) it was necessary to ramp all inflow rates for roughly 1 or 2 minutes until the full step was reached. Doing so, prevented the solver from returning a convergence error. Due to the slow dynamics of the system this had no significant effect on the solution profiles.
- To ease the initial numerical solution for each reactor in a long train it was found that a small delay (typically only 1 to 10 minutes) had to be placed on the start of the integration routine for downstream reactors (i.e. beyond reactor 5). For example, if a delay of 5 minutes was used on the 6^{th} reactor in the train then the solver would be initialized at 5 minutes using the appropriate inflow rate corresponding to 5 minutes flowing out of the previous reactor.
- If a reactor was started up empty it was necessary to place a step input in the inflow rates starting from time zero.

- The absolute and relative tolerances for the solver had to be carefully selected for the solver routine to function properly. An acceptable relative tolerance was found to be between 10^{-5} and 10^{-4} while the absolute tolerance had to be selected based on the desired accuracy of each state variable. Clearly, for a smaller reactor the tolerances would need to be tighter than for a larger reactor since the state variable would be much smaller in magnitude.
- To ease the numerical solution, a scaling factor (down) was introduced for the number of particles state N_p, equal to $\times 10^{16}$.

Species Partitioning Algorithms

Monomer Partitioning as per Dube et al. [33], Penlidis and Dube [137]

if $V_d > 0$

$$\frac{dN^a_{m_i}}{dt} = F_{m_{i_a},in} - F_{m_{i_a}}$$

else

$$\frac{dN^a_{m_i}}{dt} = F_{m_{i_a},in} - F_{m_{i_a}} - R_{p_{i_a}} V_a$$

---

calculate

$$N^p_{m_i} = \frac{N^a_{m_i}/V_a}{K^{a/p}_{m_i}/V_p}$$

---

if flag = true

$$N^d_{m_i} = N_{m_i} - N^a_{m_i} - N^p_{m_i}$$

if $N^d_{m_i} < 0$
set $N^d_{m_i} = 0$
set flag = false
set t_d = current time

elseif flag = false **and** $t_d <$ current time

set $N^d_{m_i} = 0$
set $N^p_{m_i} = N_{m_i} - N^a_{m_i}$

elseif flag = false **and** $t_d >$ current time

$$N^d_{m_i} = N_{m_i} - N^a_{m_i} - N^p_{m_i}$$

if $N^d_{m_i} < 0$
set $N^d_{m_i} = 0$
reset t_d = current time
else
set flag = true

Monomer Partitioning as per Armitage et al. [5], Gao [51], Gao and Penlidis [53]

Rearrange:

$$\left(\frac{\Delta G}{RT}\right)_j^p = \left(\frac{\Delta G}{RT}\right)_j^d \longrightarrow D_j$$

$$\left(\frac{\Delta G}{RT}\right)_j^a = \left(\frac{\Delta G}{RT}\right)_j^p \longrightarrow P_j$$

Guess: ϕ_p^p, V_d, V_a
Loop: until convergence in V_p, V_d & V_a

$$D_j = \exp\left(\begin{array}{l}(1-m_{ij})\,\phi_{m_i}^p + \phi_p^p + \chi_{ji}\left(\phi_{m_i}^p\right)^2 + \chi_{jp}\left(\phi_p^p\right)^2 \\ +\phi_{m_i}^p\phi_p^p\left(\chi_{ji}+\chi_{jp}+\chi_{ip}m_{ji}\right) + \frac{2\sigma_j\overline{V}_j}{r_pRT} \\ -(1-m_{ij})\,\phi_{m_i}^d + \chi_{ji}\left(\phi_{m_i}^d\right)^2\end{array}\right)$$

$$P_j = \exp\left(\begin{array}{l}(1-m_{ij})\,\phi_{m_i}^p + \phi_p^p + \chi_{ji}\left(\phi_{m_i}^p\right)^2 + \chi_{jp}\left(\phi_p^p\right)^2 \\ +\phi_{m_i}^p\phi_p^p\left(\chi_{ji}+\chi_{jp}+\chi_{ip}m_{ji}\right) + \frac{2\sigma_j\overline{V}_j}{r_pRT}\end{array}\right)$$

$$V_{m_i}^p = \frac{V_{m_i}}{\frac{V_d\phi_p^p D_j}{V_{pol}} + 1 + \frac{V_a\phi_p^p\phi_{m_i,sat}^a P_j}{V_{pol}}}$$

$$V_p = \sum_i^N V_{m_i}^p + V_{pol}$$

$$V_{m_i}^d = V_d D_j \phi_{m_i}^p$$

$$V_d = \sum_i^N V_{m_i}^d$$

$$V_{m_i}^a = V_a\phi_{m_i,sat}^a P_j \phi_{m_i}^p$$

$$V_a = \sum_i^N V_{m_i}^a + V_w$$

Re-calculate the volume fractions: based on converged values

$$\frac{\phi_{m_i}^d}{\phi_{m_i}^a} = \frac{V_{m_i}^d/V_d}{V_{m_i}^a/V_a}$$

$$\frac{\phi_{m_i}^a}{\phi_{m_i}^p} = \frac{V_{m_i}^a/V_a}{V_{m_i}^p/V_p}$$

Average Radicals per Particle

The average number of radicals per particle is calculated according to Equation A.78 where the total aqueous phase radical concentration ($[R^{\cdot}]$), concentration of potentially capturable radicals $\left([R^{\cdot}]^{par}, [R^{\cdot}]^{mic}\right)$ and concentration of potentially recapturable desorbed radicals $\left([R^{\cdot}]^{des}\right)$ must first be determined (see equations mentioned in the insert below). A brief algorithm is as follows:

Guess: $\bar{n}$, ε
Loop: until convergence in $\bar{n}$ (i.e. $\varepsilon <$ tolerance)

Calculate: k_{des},R_{des} from Equation A.83 or A.88
set: Total radical concentration to initiator radical concentration

$$[R^{\cdot}] = [R^{\cdot}]_{initiator}$$

Loop: for $k = 1$ to $j_{cr} - 1$ to calculate $[R^{\cdot}]_k$ and update the total radical concentration $[R^{\cdot}]$ at each iteration
Calculate: $[R^{\cdot}]_{j_{cr}}$,$[R^{\cdot}]^{par}$,$[R^{\cdot}]^{mic}$,$[R^{\cdot}]^{hom}$,$[R^{\cdot}]^{des}$ from Equations A.71,A.70,A.72, and A.90.
Calculate: $\bar{n}$ from Equation A.78
Re-calculate: k_{des} if Nomura's approach is used (i.e. Equation A.83)
Re-calculate: $\bar{n}$
Calculate: error (note if Normura approach is not used or if desorption is not considered only one iteration is necessary)
$\varepsilon = (\bar{n}_{new} - \bar{n}_{old}) / \bar{n}_{new}$

Appendix C

Detailed Listing of Model Parameters

This section provides a list of the database gathered from various literature sources for the physical and chemical properties of the species involved.

- *Monomer:* Acrylonitrile (AN), Butadiene (Bd)
- *Emulsifier:* Dresinate, Tamol, Sodium Oleate, Potassium Oleate, Sodium Dodecyl Sulfate (SDS)
- *Initiator: para*-Menthane Hydroperoxide (PMHP), Potassium Persulfate (KPS)
- *Reducing Agent:* Sodium Formaldehyde Sulfoxylate (SFS)
- *Transfer Agent: tert*-Dodecyl Mercaptan
- *Monomer Impurity: tert*-Butyl Catechol (TBC)
- *Water Impurity:* Oxygen, Hydroquinone

Many of the values listed below were taken from the Watpoly Simulator/Database package [51–55] and the paper on NBR of Dube et al. [33]. The symbols are defined in the Nomenclature of this thesis; however, in some instances referring to the articles above may provide a clearer explanation.

Table C.1: Acrylonitrile database items

Item	Value	Unit
MW_m	53.06	g/mol
ρ_m	$0.835549232 - 0.001382856 \times T(^\circ C)$	kg/L
ρ_p	$1.18 - 0.00131 \times T(^\circ C)$	kg/L
ζ	8.4896	$g/100gH_2O$
δ_m	332.275	$\left(cal/dm^3\right)^{1/2}$
δ_p	403.35	$\left(cal/dm^3\right)^{1/2}$
σ_p	0.0001945	cal/dm^2
Cp_m	430	$cal/kg/K$
Cp_p	301	$cal/kg/K$
ΔH_p	-17800	cal/mol
T_{g_m}	190	K
T_{g_p}	377	K
$k_{p_{AA_p}}$	$6.282 \times 10^9 \exp(-7278.38/RT)$	$L/mol/min$
$k_{to_{AA_p}}$	$2.5 \times 10^{12} \exp(-4000/RT)$	$L/mol/min$
$k_{to_{AA_a}}$	1×10^{12}	$L/mol/min$
$k_{fm_{AA_p}}$	$6.545586731 \times 10^7 \exp(-10972.36526/RT)$	$L/mol/min$
$k_{fp_{AA_p}}$	0	$L/mol/min$
$k^*_{p_{AA_p}}$	0	$L/mol/min$
$k^{**}_{p_{AA_p}}$	0	$L/mol/min$
$K_m^{d/a}$	1.53833	-
$K_m^{a/p}$	0.75	-
j_{cr_m}	30	#
x_{c_m}	0.41	-
D_{w_m}	5×10^{-7}	dm^2/min
D_{po_m}	1×10^{-7}	dm^2/min
δ	0.001	L/g
lo_m	6.2	
lj_m	5.85	
Sn_m	1200	-
K_3	$0.831 \exp(7980/RT)$	-
m	0.5	-
n	1.75	-
A	0.95	-
$V_{f_{cr}}$	$5.33 \exp(-3060/RT)$	-
B	0.5	-
α_m	0.001	$1/K$
α_p	0.00048	$1/K$

Table C.2: Butadiene database items

Item	Value	Unit
MW_m	54.09	g/mol
ρ_m	$0.645950704 - 0.001270986 \times T(^\circ C)$	kg/L
ρ_p	$0.891357143 - 0.000025714 \times T(^\circ C)$	kg/L
ζ	0.081135	$g/100gH_2O$
δ_m	224.092	$\left(cal/dm^3\right)^{1/2}$
δ_p	250.451	$\left(cal/dm^3\right)^{1/2}$
σ_p	0.0009556	cal/dm^2
Cp_m	426	$cal/kg/K$
Cp_p	350	$cal/kg/K$
ΔH_p	-20895	cal/mol
Tg_m	108	K
Tg_p	223	K
$k_{p_{BB_p}}$	$7.2 \times 10^9 \exp(-9300/RT)$	$L/mol/min$
$k_{to_{BB_p}}$	8×10^8	$L/mol/min$
$k_{to_{BB_a}}$	$1.48 \times 10^{12} \exp(-2382/RT)$	$L/mol/min$
$k_{fm_{BB_p}}$	$5.277997052 \times 10^8 \exp(-12993.98433/RT)$	$L/mol/min$
$k_{fp_{BB_p}}$	$3.96951 \times 10^8 \exp(-12470.6/RT)$	$L/mol/min$
$k^*_{p_{BB_p}}$	0	$L/mol/min$
$k^{**}_{p_{BB_p}}$	$8.1 \times 10^8 \exp(-14150/RT)$	$L/mol/min$
$K_m^{d/a}$	655.58	-
$K_m^{a/p}$	0.0025	-
j_{cr_m}	5	#
x_{c_m}	0.55	-
D_{w_m}	1.2×10^{-12}	dm^2/min
D_{po_m}	1.2×10^{-9}	dm^2/min
δ	0.001	L/g
lo_m	6	
lj_m	6.5	
Sn_m	1200	-
K_3	5000	-
m	0.5	-
n	1.75	-
A	0.15	-
$V_{f_{cr}}$	0.05	-
B	1	-
α_m	0.001	$1/K$
α_p	0.00048	$1/K$

Table C.3: AN/Bd copolymer database items

Item	Value	Unit
r_{AN}	0.05	-
r_{Bd}	0.35	-
ϕ_{wall}	1	-
δ_p	292.556	$\left(cal/dm^3\right)^{1/2}$
x_{c_p}	0.48	-
$k_{fm_{AB_p}}$	0	$L/mol/min$
$k_{fm_{BA_p}}$	0	$L/mol/min$
$k_{fp_{AB_p}}$	$3.96951 \times 10^8 \exp\left(-12470.6/RT\right)$	$L/mol/min$
$k_{fp_{BA_p}}$	0	$L/mol/min$
$k^*_{p_{AB_p}}$	0	$L/mol/min$
$k^*_{p_{BA_p}}$	0	$L/mol/min$
$k^{**}_{p_{AB_p}}$	$8.1 \times 10^8 \exp\left(-14150/RT\right)$	$L/mol/min$
$k^{**}_{p_{BA_p}}$	0	$L/mol/min$

Table C.4: Water database items

Item	Value	Unit
MW_s	18.02	g/mol
ρ_{em}	1	kg/L
Tg_s	118	K
Cp_s	400	$cal/kg/K$

Table C.5: Dresinate database items

Item	Value	Unit
MW_{em}	324.44	g/mol
ρ_{em}	0.95	kg/L
CMC	0.001	mol/L
S_a	4.37×10^{-17}	$dm^2/molecule$
r_{mic}	7.5×10^{-8}	dm

Table C.6: Tamol database items

Item	Value	Unit
MW_{em}	800	g/mol
ρ_{em}	1.15	kg/L
CMC	0.009	mol/L
S_a	6.0943×10^{-17}	$dm^2/molecule$
r_{mic}	7.5×10^{-8}	dm

Table C.7: Sodium Oleate database items

Item	Value	Unit
MW_{em}	304.45	g/mol
ρ_{em}	0.95	kg/L
CMC	0.001	mol/L
S_a	4.37×10^{-17}	$dm^2/molecule$
r_{mic}	7.5×10^{-8}	dm

Table C.8: Hydroquinone database items

Item	Value	Unit
MW_z	110.11	g/mol
ρ_z	1.3	kg/L
k_z	$1.33 \times 10^8 \exp(-4353/RT)$	$L/mol/min$

Table C.9: Dissolved oxygen database items

Item	Value	Unit
MW_z	31.9988	g/mol
ρ_z	0.029	kg/L
k_z	1×10^7	$L/mol/min$

Table C.10: *para*-Menthane hydroperoxide database items

Item	Value	Unit
MW_I	172.267	g/mol
ρ_I	0.91	kg/L
k_d	$2.8 \times 10^{18} \exp(-33500/RT)$	$L/mol/min$
f	0.7	-

Table C.11: Potassium persulfate database items

Item	Value	Unit
MW_I	270.32	g/mol
ρ_I	1.3	kg/L
k_d	$1.524 \times 10^{18} \exp(-33320/RT)$	$L/mol/min$
f	0.7	-

Table C.12: *tert*-Dodecyl mercaptan database items

Item	Value	Unit
MW_{cta}	202.4	g/mol
ρ_I	0.859	kg/L
k_{fcta_A}	$1.141505444 \times 10^8 \exp(-10603.67497/RT)$	$L/mol/min$
k_{fcta_B}	$3.06 \times 10^8 \exp(-6400/RT)$	$L/mol/min$
$K_{cta}^{d/p}$	1.5	-

Table C.13: *tert*-Butyl catechol database items

Item	Value	Unit
MW_{msi}	166.22	g/mol
ρ_{msi}	1.05	kg/L
k_{fmsi_A}	6×10^3	$L/mol/min$
$K_{msi}^{d/p}$	1.5	-

Table C.14: Sodium formaldehyde sulfoxylate database items

Item	Value	Unit
MW_{RA}	154.11[a]	g/mol
ρ_{RA}	1.75	kg/L
${k_2}^b$	2.5	$L/mol/min$
${k_2}^c$	64.68	$L/mol/min$

[a] SFS Dihydrate - $CH_3NaO_3S \cdot 2H_2O$
[b] PMHP
[c] KPS

Table C.15: Ferrous sulfate database items

Item	Value	Unit
MW_{OA}	278.11[a]	g/mol
ρ_{OA}	1	kg/L
${k_1}^b$	$3.78 \times 10^{11} \exp(-11100/RT)$	$L/mol/min$
${k_1}^c$	2.82	$L/mol/min$

[a] Ferrous Sulfate Heptahydrate - $FeSO_4 \cdot 7H_2O$
[b] PMHP
[c] KPS

Appendix D

Model Troubleshooting & Trend Verification

This Appendix provides additional simulation profiles on other underlying variables within the model. To better understand how the monomer is partitioned between each phase, profiles are presented for concentration and volume. To provide further insight on the contribution to particle nucleation from homogeneous and micellar methods, individual profiles are shown for each mechanism. The sensitivity of particle nucleation to the critical chain length parameter (j_{cr}) is also investigated. Furthermore, dynamic and steady-state solution profiles for $\bar{n}$ for the baseline recipe (Table 5.1) are shown for a 10 reactor train.

Batch/CSTR Simulation Profiles

Monomer Partitioning

Using similar plots shown by Gao and Penlidis [53], Figure D.1 depicts batch reactor profiles for the volume of each phase, volume of each monomer in each phase, monomer concentration in each phase, and the ratio of the volume AN over Bd in the droplet phase versus the polymer particle phase. From each of these plots it is clear that a significant amount of AN resides dissolved in the aqueous phase and that the AN droplets disappear sooner than Bd droplets. From the perspective of simulation, once each monomer droplet type (i.e. AN or Bd) is consumed, the corresponding monomer volume in the particle phase begins to deplete as the system is no longer considered to be at equilibrium. An important partitioning characteristic seen in many copolymer systems is that the ratio of each monomer volume in the droplet phase (V^d_{AN}/V^d_{Bd}) is nearly equal to the ratio in the particle phase (V^p_{AN}/V^p_{Bd}). For a system where one of the monomers is considerably more water-soluble (i.e. AN), then the ratio comparison should be made accounting for the dissolved monomer according to $\left(V^d_{AN}+V^a_{AN}\right)/\left(V^d_{Bd}+V^a_{Bd}\right)$ versus $\left(V^p_{AN}/V^p_{Bd}\right)$. Profiles for each ratio can be seen in Figure D.1d and are plotted up until the AN droplets disappear. A clear offset is apparent between each ratio where the droplet-aqueous phase ratio is approximately 0.1 units greater than the particle phase ratio. Theory suggests that these two ratios should be in closer relation, which further suggests that the solubility (ζ_{AN}) used for AN may be slightly too high or that the partitioning coefficient ($K^{a/p}_{AN}$) may need to be adjusted.

To give further insight on the phase volumes and monomer concentrations in a reactor train and to ensure that the model was functioning properly, volume and concentration profiles were plotted in Figure D.2. For constant overflow reactors the total reaction volume remained equal to the reactor volume, while

the aqueous, particle, and droplet phases passed through a transient period before reaching their steady-state. For the sake of space, profiles for the 1^{st}, 4^{th}, 6^{th} and 10^{th} reactors are only shown. Note that the droplet phase first disappears in the 6^{th} reactor at around 16.7 hours and for subsequent reactors disappears sooner.

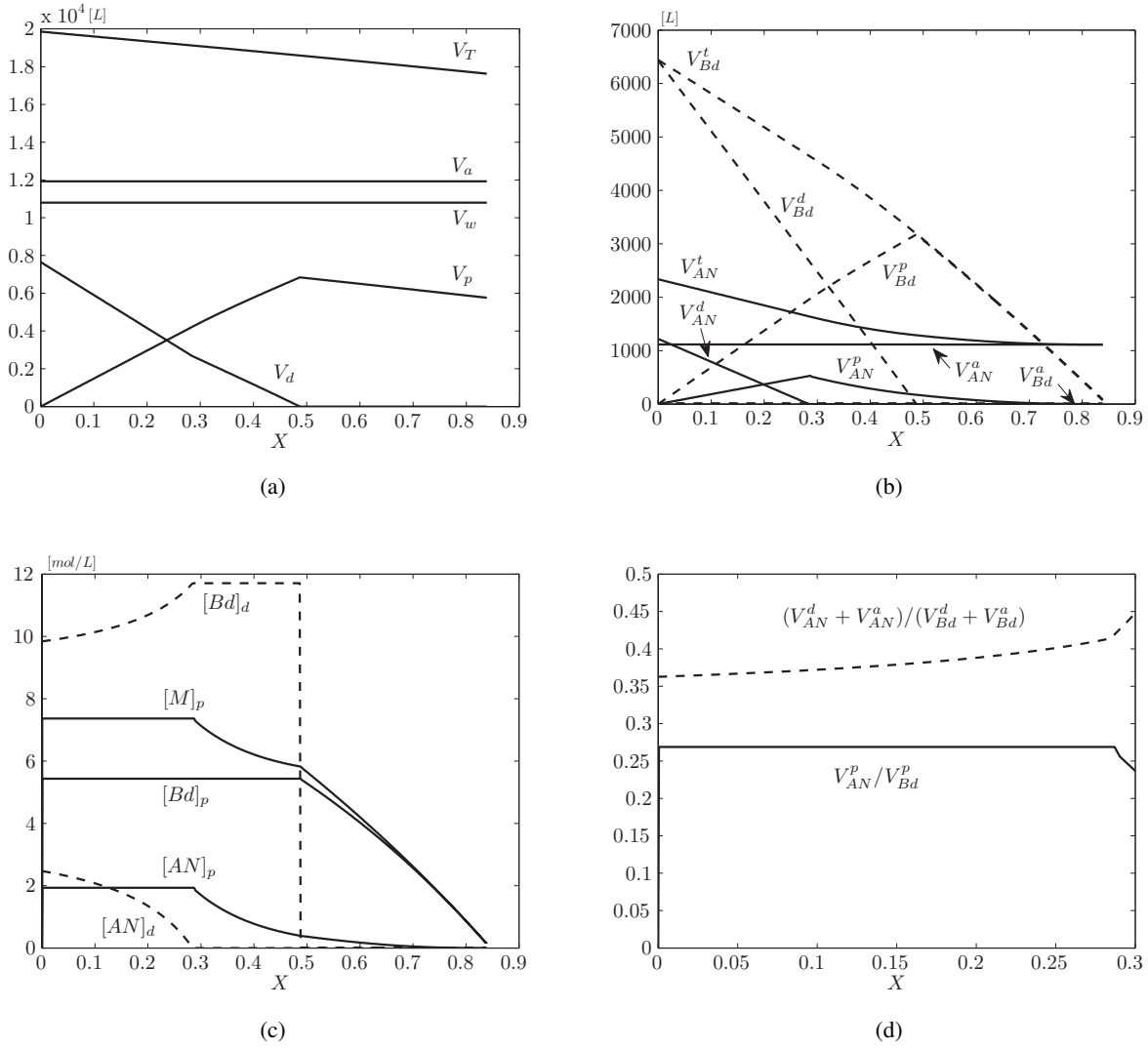

Figure D.1: Batch simulation - phase/monomer volumes & concentrations

Particle Nucleation

The contribution to the total particle number in a batch reactor from homogeneous and micellar nucleation mechanisms can be seen from Figure D.3b. For fairly water-soluble monomers such as AN, homogeneous nucleation is considered to be substantial, but still several orders of magnitude less than micellar nucleation. The value of N_p^{hom} was adjusted by increasing the parameter μ until an acceptable order of around 10^{14} $\#/L_w$ was obtained [53]. Compared to the magnitude of micellar nucleation, homogeneous nucleation would seem insignificant. However, the inclusion of homogeneous nucleation is crucial to the model and can be more

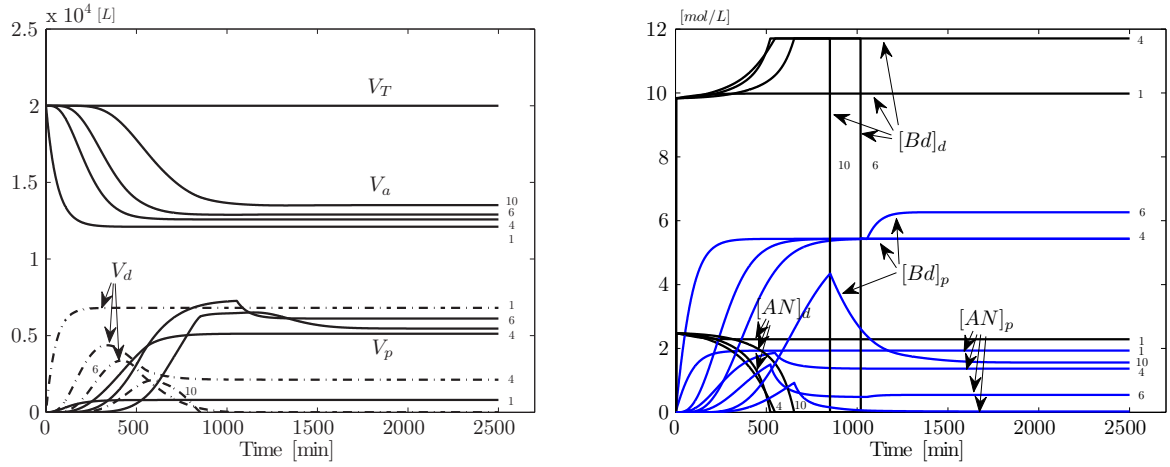

(a) (b)

Figure D.2: CSTR Train Simulation - phase/monomer volumes & concentrations

appreciated when a continuous reactor is used and started up full of water where the emulsifier concentration is initially below the CMC (i.e. no micellar nucleation). Furthermore, the inclusion of homogeneous nucleation is necessary in order to properly account for the aqueous phase radical concentration.

To test the particle response (homogeneous and micellar) to changes in the critical oligomeric chain length (j_{cr}) of AN terminal units, the parameter $j_{cr_{AN}}$ was varied around the accepted literature value of 30 units. Figure D.4 depicts particle number from homogeneous and micellar mechanisms for $j_{cr_{AN}}$ ranging from 20 to 45 in increments of 5 units. As $j_{cr_{AN}}$ is increased, radicals are allowed to grow longer thus reducing the number that participate in homogeneous nucleation. In the case of micellar nucleation, the criteria specified to signal the start of radical capture was $j_{cr}/2$, thus increasing $j_{cr_{AN}}$ increases the time before micellar nucleation initiates and thus decreases the number of particles formed.

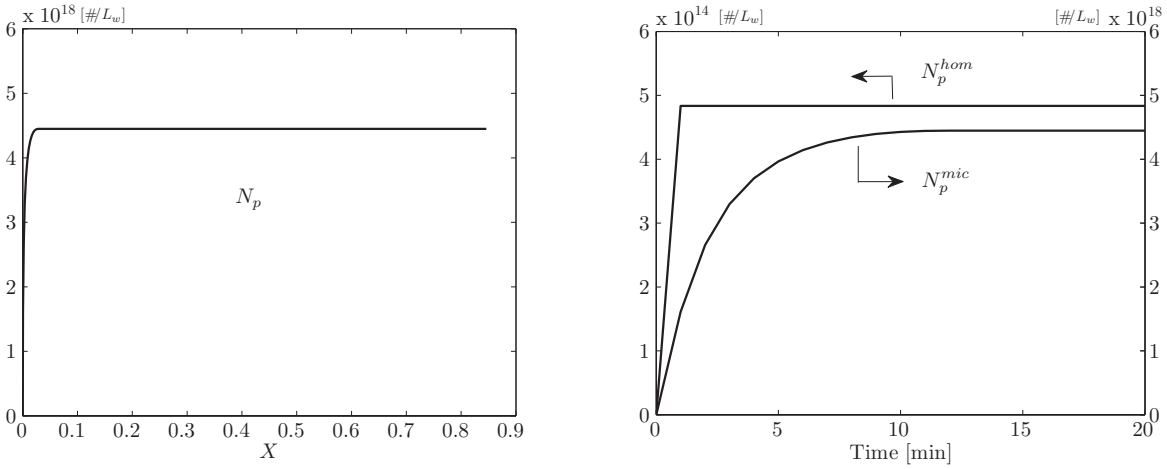

(a) (b)

Figure D.3: Batch Simulation - number of particles via homogeneous & micellar nucleation

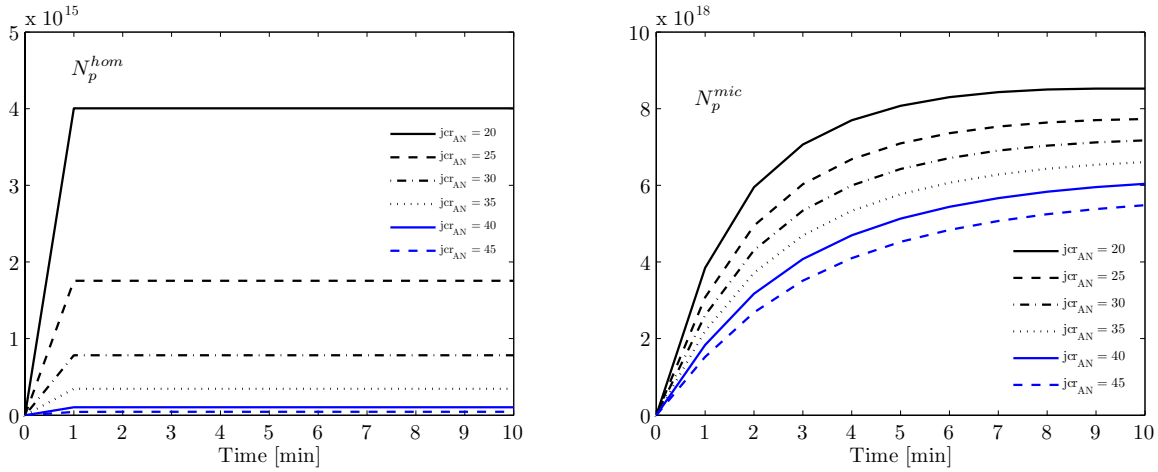

(a) (b)

Figure D.4: Batch simulation - number of particles via homogeneous & micellar nucleation - sensitivity to j_{cr}

To give a perspective of the evolution of $\bar{n}$ (Smith & Ewart steady-state equation) along the reactor train, both dynamic and steady-state profiles are plotted in Figure D.5. From the dynamic profile, a pronounced jump in $\bar{n}$ is seen starting in the 6^{th} reactor (small jump) and progressing to larger jumps in subsequent reactors. The onset of this observed behaviour is due to the monomer droplets disappearing and initialization of diffusion-controlled termination. An average number of radicals per particle in the range of 3 to 6 is quite high. The simulation results shown where $\bar{n}$ climbs beyond 3 are most likely a result of an insufficient amount of CTA in the last few reactors of the train (i.e. high molecular weights and chain entanglements) and/or a low value of k_t due to diffusion-controlled termination (i.e. maybe the parameters in Equation 3.42 need adjusting to allow for a lower rate of decline in k_t, which would delay the rapid increase in $\bar{n}$). In the case of batch NBR production with a final conversion of 80%, $\bar{n}$ was not observed to increase beyond 3. Barclay et al. [11] explored several different copolymer systems (e.g. Sty/MMA, Sty/MA, Sty/BA, BA/MMA) under batch and semi-batch operation and in each case $\bar{n}$ remained below 3 until high conversion levels where $\bar{n}$ rapidly increased due to the gel effect. The results shown in Figure D.5 for a reactor train where a high value of $\bar{n}$ is evident around 60% conversion would seem unrealistic, and should be revisited once information becomes available for continuous NBR production (i.e. data sampled from along the entire train).

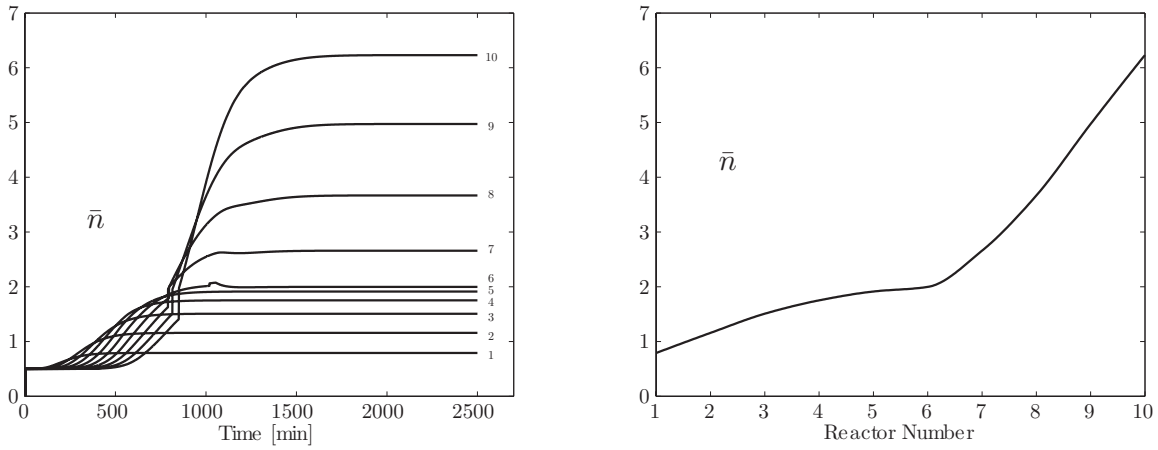

(a) (b)

Figure D.5: CSTR train simulation - average number of radicals per particle